Variable-Density Groundwater Flow beneath the Wind-Tidal Flats of Padre Island

by

Joel Daniel Stevens, B.S.

Thesis

Presented to the Faculty of the Graduate School of

The University of Texas at Austin

in Partial Fulfillment

of the Requirements

for the Degree of

Master of Science in Geological Sciences

The University of Texas at Austin

May 2007

Variable-Density Groundwater Flow beneath the Wind-Tidal Flats of Padre Island

Approved by
Supervising Committee:

_____

_____

_____

Dedication

I dedicate this work to my wonderful wife, Lindsay, and my son, Jackson.

Acknowledgements

I would like to acknowledge my advisor, Jack Sharp, for his guidance and comments during this study. I would like to acknowledge the Geology Foundation and their donors for their generous support. I would also like to recognize Advanced Geosciences Inc. for their willingness to take me on as an intern and graciously allow use of their equipment during field work. I would like to thank the UT Hydrogeology Boot Camp of 2005 for helping me install several of the wells and collect core samples. Lindsay Stevens, Terence Garner and Tom Fenstemaker all deserve special thanks for their support and help in the field.

May 2007

Abstract

Variable-Density Groundwater Flow beneath the Wind-Tidal Flats of Padre Island

Joel Daniel Stevens, M.S.GeoSci

The University of Texas at Austin, 2007

Supervisor: John M. Sharp, Jr.

Field evidence for density-driven free convection, a potentially important groundwater transport process, has been examined at Padre Island National Seashore to determine if this phenomenon can develop under natural environmental conditions. Hitherto, this process had not been conclusively detected or measured in field scale hydrogeology. Field methods, including nested monitoring wells and time-lapse 3-D resistivity surveys, reveal evidence of variable-density groundwater flow in the wind-tidal flats. Evaporative concentration of groundwater near the water table resulted in unstable inverted density gradients, reduced groundwater levels, and reduced hydraulic gradients. These factors allowed plumes of dense fluid to migrate downward into less dense fluid which were observed in monitoring wells and 3-D resistivity surveys. This shows that the development and flow of variable-density fluids in groundwater can be detected and monitored through field techniques. It demonstrates that the development of density inversions may overcome the dissipating forces of dispersion and diffusion to create a sufficiently large unstable gradient to induce free convection.

Table of Contents

List of Tables

List of Figures

Chapter 1 Introduction

This project is motivated by the complex problems associated with fluids of varying density in groundwater environments. There is much to learn about variable-density fluid mixing, plume effects, and rates of mixing and flow. In addition, the scale of these processes needs study. These topics have applications in a broad spectrum of geologic problems ranging from dolomitization to transport of dense non-aqueous phase liquids. This project investigates variable-density fluid flow in natural groundwater environments to understand these processes. The density-varying influence in this case is groundwater of varying salinity.

1.1 PROJECT SCOPE

This project addresses some of the problems associated with variable-density fluid flow such as salinity variation development, mixing, plume effects, flow rates, and scale. It is hypothesized that natural groundwater environments are conducive to fluid mixing of waters with differing densities through plume development and migration. This mixing of fluids of varying density through buoyancy and displacement by contrasting plumes is termed density-driven free convection.

Many laboratory and computer experiments (Horton and Rogers, 1945; Lapwood, 1948; Wooding, 1957; Elder, 1967a,b; Schneider, 1963; Schincariol and Schwartz, 1990; Oostrom et al. 1992a,b; Hassanizadeh and Leijnse, 1995; Wooding et al., 1997a,b; Simmons et al., 1999; Pearl et al., 1993; Oltean et al., 1994; Diersch and Kolditz, 2002; Oswald and Kinzelbach, 2004; and Shi, 2005) have demonstrated density-driven free convection can develop in simulated environments. However, few field investigations have investigated this process in the natural environment and have not shown conclusive

evidence (Amdurer and Land, 1982; Allison and Barnes, 1985; Bowler, 1986; Duffy and Al-Hassan, 1988; Land, 1991; Tyler et al., 1997; Fan et al., 1997; and Leising et al., 1995). Therefore, problems such as field scale issues, geology, and climate need to be addressed.

This thesis describes a field study to determine whether density-driven free convection exists in a natural groundwater environment. A significant issue is whether a large inverted density gradient, or denser fluid overlying less dense fluid, can develop in a natural environment without diffusion impeding such development. Can density inversions develop and can they develop to a threshold where density-driven free convection can occur and dominate fluid flow? These problems and questions are addressed through field hydrogeology methods and electrical resistivity geophysical methods.

Opening the door to field studies of density-driven free convection and creating a methodology to monitor and evaluate dense-solute transport would allow greater precision in mapping groundwater movement. This could help forecast groundwater contaminant transport and predict saltwater intrusion in coastal environments. Furthermore, the confirmation of density-driven free convection in the field would require the re-evaluation of contamination plume models that only account for diffusion and hydrodynamic dispersion. Therefore, a natural groundwater environment should be analyzed to determine the parameters that allow the development and flow of density-driven free convection.

Using Padre Island as a research site, it is examined whether density-driven free convection occurs in this groundwater environment, and which combination of topographic, climatic, and geologic conditions promote such free convection. Also

included in this analysis is whether or not the Rayleigh Number, a dimensionless value of fluid instability, appropriately measures the threshold of instability in a natural system.

1.2 PREVIOUS STUDIES ON DENSITY-DRIVEN FREE CONVECTION

Density-driven free convection in porous media has been researched extensively through laboratory sand tank experiments and analytical and numerical models to find that it is the process by which buoyant forces control fluid movement rather than hydraulically driven forced convection (Diersch and Kolditz, 2002; Elder, 1967b; Frolkovic and Schepper, 2001; Gebhart et al., 1988; Nield and Bejan, 1999; Sharp, et al., 2001; Simmons et al., 2001; Tyler et al., 1997; and Wooding, et al., 1997a,b). This occurs because in a porous medium, dense fluid (saline water) overlying less-dense fluid (freshwater) is unstable. This instability drives the saltwater to descend into the freshwater and the less-dense freshwater to ascend into the saline layer. Rather than moving in a circular convection pattern, plumes, or fingers, mix the saline and freshwater until reaching equilibrium. A visual depiction of this process is captured in Simmons and others (2001) experiment seen in Figure 1.

The plumes associated with density-driven free convection make the potential ramifications of the process so important. The plumes inherent to free convection allow more solute mixing at a faster rate than diffusion alone and spread solutes over a greater distance (Simmons et al., 2001). Because density-driven free convection allows more efficient solute spreading across greater distances than diffusion, it may serve an important role in solute transport of the following natural and anthropogenic fluid systems in which density contrasts exist: seawater intrusion, infiltration of leachates from waste disposal sites, DNAPL flow and transport, infiltration through hydrophobic soils, flow through salt formations in high-level nuclear waste disposal sites, dolomitization by

seepage reflux, hydrocarbon migration and entrapment mechanisms, diagenesis of sedimentary basins, groundwater processes beneath playas and playa lakes, heat and fluid flow in geothermal systems as well as design of saline (and irrigation) water disposal basins (Simmons, et al., 2001 and Diersch and Kolditz, 2002).

The initiation or onset of free convection is commonly evaluated in the laboratory using the Rayleigh Number to examine the ratio of buoyancy-driven forces (causing flow) to viscous forces (resisting flow). The Rayeigh Number was named after Lord Rayleigh (John Strutt), who conducted early experiments on convection cells (Rayleigh, 1916). Helpful reviews of Rayleigh Numbers can be found in publications by Holzbecher (1998), Nield (1968 and 1990), and Nield and Bejan (1999). The Rayleigh Number (Ra or N_{Ra}) is a dimensionless number which gives a threshold above which, the system is unstable and free convection occurs and, below which, diffusion dominates. For an infinite, horizontal, uniform porous layer with no flow and constant temperature boundaries, the critical Rayleigh Number is $4\pi^2$ (Lapwood, 1948). A mixed convection version (Simmons and Narayan, 1997) of the Rayleigh Number equation is used for this study to take into account the effects of hydraulic forces. This Rayleigh Number equation for mixed convection is empirically defined by:

$$Ra = \frac{U_c H}{D_o} = \frac{gk\beta\Delta CH}{\theta\nu_o D_o} = \frac{Buoyancy + Gravitational\ Driving\ Forces}{Diffusion + Dispersion\ (viscous\ resistance\ and\ dispersive\ dissipation)} \quad (1)$$

where

U_c = convective velocity
H = thickness of the porous layer
D_0 = molecular diffusivity
g = acceleration due to gravity
k = intrinsic permeability
$\beta = \rho_0^{-1}(\partial\rho / \partial C)$ = linear expansion coefficient
ΔC = concentration difference by mass fraction
θ = aquifer porosity
$\nu_0 = \mu_0 / \rho_0$ = kinematic viscosity of the fluid
ρ_o = initial fluid density
μ_0 = fluid viscosity

Detailed explanations of free convection theory and reviews are found in several publications including Bear (1988), Bejan (1984), Cheng (1978), Combarnous and Borries (1975), Diersh and Kolditz (2002), Gebhart et al. (1988), Holzbecher (1998), Nield and Bejan (1999), and Tien and Vafai (1990). Prior to 1960, research in free convection focused on geophysical and geothermal problems. With the development of computers, numerical analysis and modeling of free convection became increasingly important. Research and applications of free convection also became diverse. Pioneering work by Horton and Rogers (1945) and Lapwood (1948) researched convection in saturated porous media of infinite horizontal extent to determine instability criteria. The first numerical computations of two-dimensional convection processes in porous media were conducted by Wooding in 1957. Primary laboratory work by Elder (1967a,b) and Schneider (1963) using Hele-Shaw cells furthered research of free convection with computations of multi-cellular thermal convection currents in two-dimensions. Recent research focuses on comparison of laboratory experiments with numerical results in two-dimensions (Schincariol and Schwartz, 1990; Oostrom et al. 1992a,b; Hassanizadeh and Leijnse, 1995; Wooding et al., 1997a,b; and Simmons et al., 1999) and three-dimesions (Pearl et al., 1993; Oltean et al., 1994; Diersch and Kolditz, 2002; Oswald and Kinzelbach, 2004; and Shi, 2005) to establish benchmark models. Still many problems remain. Diersh and Kolditz (2002) question the reliability and applicability of numerical models for variable-density situations at the scale of real world problems. Oswald and Kinzelbach (2004) suggest that a numerical model be compared to a known and well documented field situation to benchmark the models. However, they lament that such a

field case “does not exist” due to the complexities of field scale issues such as heterogeneity.

Research of density-driven free convection in the field has indeed been difficult and limited due to field-scale issues. Allison and Barnes (1985), Bowler (1986), Duffy and Al-Hassan (1988), Land (1991), and Tyler et al. (1997) examined salt budgets of playa lakes and found salt losses that could not be accounted for. They suggested that downward transport of brines through playa sediments may explain the salt loss. Fan et al. (1997) found surface water derived oxygen and hydrogen isotopes in subsurface brine of playa sediments and suggested density-driven free convection as the mechanism for their transport. Leising et al. (1995) used free convective processes to explain alteration of sediments in closed basins. In basins with hydraulic conductivities greater than 10^{-7} m/s, volcanic sediments had metasomatized or been altered by brine water. However, in basins where sediments had a hydraulic conductivity of 10^{-8} m/s or less, metasomatism of sediments was not evident. Amdurer and Land (1982) used seepage reflux or free convection and precipitation of algal micrite to explain manometric data and lack of gypsum in sediments below the wind-tidal flats at Padre Island, Texas. Wood (2002) notes that playas of the Southern High Plains contribute approximately 90% of groundwater recharge to the High Plains Aquifer demonstrating the hydraulic importance of playas and underlying aquifers. The above studies cite circumstantial evidence for density-driven free convection and do not explicitly measure the development and fluid flow caused by free convection. Despite its importance to groundwater solute transport, no study known to the author has monitored or detected density-driven free convection in the field. Therefore, a field study is warranted to determine how field scale problems influence density-driven free convection development and flow.

1.3 FIELD LOCATION SELECTION AND DESCRIPTION

The selection of a field study location was based on geologic and environmental conditions that would be suitable for the development of density-driven free convection. In addition, a field site was sought that had the simplest scenario with the least amount of outside influences analogous to the laboratory and computer simulations of density-driven free convection in porous media. The most important field conditions are hypothesized to be: physical mechanisms that induce contrasting salinity gradients and small hydraulic gradients. Physical mechanisms for inverse density stratification in the shallow groundwater zone may include: intense evaporation, inundation of saline flood waters, or dissolution of evaporites by infiltrated or recharge water. Ambient hydraulic gradients would need to be minimal to reduce the hydraulically-induced mixing influences of advection and dispersion. For the shallow subsurface, a flat topography with a mimicking water table would facilitate a small hydraulic gradient. Under these conditions, it is hypothesized that density-driven free convection has potential to occur.

Few locations could meet all criteria and still be feasible to conduct field research. Playas and sabkhas are naturally occurring environments where free convection has been explicitly or implicitly studied. The wind-tidal flats of Padre Island are similar to playa and sabkha environments and can be used for density-driven free convection research. In addition to being a potential location for free convection research; Padre Island is relatively close to The University of Texas at Austin; the National Park Service and Padre Island National Seashore staff encourage research conducted onsite; and previous years of field training through The University of Texas Hydrogeology Field Camp (UTHFC) and general graduate student research add familiarly of hydrogeologic conditions.

1.3.1 Padre Island Geology

Field research of density-driven free convection was conducted on North Padre Island, Texas within the Padre Island National Seashore. Padre Island is a barrier island in the Texas Coastal Plain bounded on the west by Laguna Madre and on the east by the Gulf of Mexico (see Figure 2). The island can be divided into five general environments: a sand and shell beach, a stable ridge of fore-island dunes, vegetated flats, shifting back-island dunes, and plains of wind-tidal flats (Boylan, 1986; Wiese and White, 1980)(see Figure 3). Two field study sites, one at Bird Island Basin and another 30 km south at Yarborough Pass, are located in the wind-tidal flats (see Figure 4).

The development of the Texas Gulf Coast, including Padre Island, began during the last Pleistocene glacial-interglacial cycle approximately 18,000 bp. A detailed stratigraphy and geologic history of this period is presented by Paine (1991) and a brief history of the development of Padre Island is presented by Wiese and White (1980) and are summarized below. During the last glaciation or low stand, sea level was approximately 90 to 160 m below current mean sea level (MSL). This resulted in rapidly down-cutting streams that formed incised valleys and transported large amounts of sediment approximately 80 km southeast of the current seashore (see Figure 5). By about 5,000 bp, glacial melt water brought sea levels to within 5 meters of MSL. As sea level continued to increase, the incised stream valleys became bays and estuaries. Between 1,000 and 3,000 bp, sea levels reached current MSL and shorelines began to develop sand bars from previous deltaic sediments and stream deposits. Through longshore currents, aggradation, and eolian processes, the sand bars began to merge, forming barrier islands. Padre Island continues to be reshaped by longshore currents, active waves, strong wind

and periodic hurricanes which also constantly sort and rework sediment resulting in exceptionally clean sediment of similar grain size.

The barrier island complex of Padre Island has sand deposits ranging in thickness from 10 to 12 meters near the research sites (Fisk, 1959; Shafer and Baker, 1973; Boylan, 1986) (see Figures 6 and 7). Sieve analyses (UTHFC, 2003; Boylan, 1986; Davis, 1978) of these sands show a trend from well sorted medium to fine sand sediments of the beach and fore-island dunes to fine to very fine sand, silt and clay in the barrier flat and wind-tidal flat provinces. Underlying the Holocene sediments is the Pleistocene age Beaumont Clay, which is an approximately two-hundred-meter-thick fluvial/deltaic deposit composed of predominantly clay with varying degrees of sand and silt (Sellards et al., 1933 and Paine, 1991).

1.3.2 Aquifer Characteristics

Shafer and Baker (1973), Baker (1979), and Carr et al. (1985) describe the barrier island complex as a minor alluvial aquifer. The Holocene barrier island complex generally yield small quantities (6.3×10^{-4} to 1.26×10^{-3} m^3/sec) (Shafer, 1968) of brackish water to shallow wells on Padre Island.

Pump tests in shallow wells conducted by Berkebile et al. (2001) found hydraulic conductivities of 7.5×10^{-5} m/sec. Slug tests by Boylan (1986) found a range of conductivities across the island. He measured high values of 4.1×10^{-5} m/sec from the fore-island dune province to lower values of 2.4×10^{-6} m/sec from the wind tidal province. The University of Texas Hydrogeology Field Camp (2003) found hydraulic conductivities based on grain-size analysis to be between 6.4×10^{-5} m/sec to 1.0×10^{-4} m/sec. A summary of hydraulic conductivity data are summarized in Table 1.

Hydraulic gradients for the wind-tidal flat are low and range between 6.6 X 10^{-4} and 10^{-5} (Amdurer, 1978). Flow direction is based on topography, the fore-island and back-island dunes provinces being groundwater divides.

Porosity of the eolian and marine sands is between 40 to 45 percent (UTHFC, 2001 and 2003; Berkebile and Hay, 1995; and Berkebile et al., 2001).

The depth to the water table is typically between 0.3 to 1.3 meters (Boylan, 1986). Water quality ranges from saline conditions in the beach along the Gulf of Mexico, to fresh water conditions in the fore-island dunes to brackish water in the barrier island flats to brine conditions in the wind-tidal flats (Boylan, 1985; Berkebile et al., 2001; and Amdurer 1978). The only source of fresh water is precipitation (Wiese and White, 1980).

1.3.3 Climate

Historical climate data for Padre Island are compiled by Wiese and White (1980). The island has a semiarid to subtropical climate with an average air temperature between 22.2 and 23.3 degrees Celsius. The average humidity is 80 to 90 percent in the morning, but drops to 50 to 60 percent in the afternoon. The combination of temperature and humidity create a potential evapotranspiration of approximately 152.4 cm per year—about 81.28 cm greater than the annual average precipitation. Berkebile and Hay (1995) and Berkebile et al. (2001) completed a groundwater resource investigation of Padre Island National Seashore in 2001 that included a numerical model to develop estimates for the recharge of the freshwater lens. They determined that only half the average precipitation was required to maintain the freshwater lens. Berkebile and Hay proposed that the other half of precipitation was lost to evapotranspiration and runoff.

Prevailing winds are from the southeast, however, intermittent northeasterly winds during the winter months can generate a fetch in Laguna Madre that elevates water

levels along the east shore of Padre Island which occasionally inundates the wind-tidal flats.

The salinity of Laguna Madre can be up to three times Gulf of Mexico salinity levels because circulation of Laguna Madre is highly restricted due to the lack of passes to the Gulf Coast (Weise and White, 1980). However, during heavy rains, salinity levels can drop dramatically.

The average depth of Laguna Madre near the test sites is one meter and the width can vary by over a kilometer due to wind-generated tides which flood the broad tidal flats (Fisk, 1959). Astronomical tides are minimal in Laguna Madre, as the mean annual tidal range is only 10 cm. Wind tides, however, can be up to one meter—an elevation which floods the test sites (Fisk, 1959). Long and Gudramovics (1983) examined evaporite minerals in the wind-tidal flats and determined that the subsurface brines are a solution of marine (Laguna Madre source) and evaporated marine and meteoric water. They indicate that marine brine is recharged from the flooding of lagoon water through infiltration. The brine then evolves chemically during evaporitic concentration by the precipitation of calcium carbonate and sulfate minerals.

Because of the importance of climatic conditions that lead to inverted density gradients, climate data for the duration of this study was collected from various weather stations operated by Padre Island National Seashore (PINS), the National Weather Service (NOAA) and the Texas Coastal Ocean Observation Network (TCOON) operated by Texas A&M University.

1.3.4 Padre Island as a Research Type for Density-Driven Free Convection

Based on the geology, aquifer characteristics, and climate, the wind-tidal flats of Padre Island appear to meet the hypothesized conditions necessary for the development

of inverse density-gradients and free convection. Amdurer and Land (1982) described the Laguna Madre wind-tidal flats as a coastal sabkha. Uniform, fine-grained quartz sands up to 12 meters deep observed by Fisk (1959), Shafer and Baker (1973) and Boylan (1986) at Padre Island National Seashore provide a suitable matrix for unimpeded fluid flow. The hydraulic gradient mimics the topography of the broad wind-tidal flats with a low slope in the direction of Laguna Madre (Amdurer, 1978; Boylan, 1986; and The UTHFC, 1997, 2001 and 2003). Additionally, a 0.81 m/yr evapotranspiration excess and periodic flooding of Laguna Madre may lead to inverse fluid density stratification.

Inverted salinity [density] stratification of groundwater has been noted by Amdurer (1978) and Amdurer and Land (1982) from a series of shallow and deep piezometers in the wind-tidal flats. The salinity inversion has been described as coming from one or both of the following sources: evaporation of shallow groundwater concentrating minerals and periodic, wind-generated flooding from the adjacent Laguna Madre. They hypothesized that the concentrated ponded flood waters recharge the sabkha through seepage reflux (see Figure 8). Their conceptual model of seepage reflux could also be density-driven free convection.

In 1997 and again in 2001, The University of Texas Hydrogeology Field Camp conducted resistivity transect surveys in the wind-tidal flats at Bird Island Basin. Data from the surveys exhibited a distinct gradient of less resistive (more saline) conditions near the surface with more resistive (less saline) at depth. The 2001 class report described the phenomena as concentrated brine from evaporation. Graduate student Tom Fenstemaker returned to the site over the course of the summer of 2001 to conduct additional resistivity transect surveys. The following resistivity transect surveys depicted the less resistive (more saline) layer developing descending lobes into the more resistive (less saline) media (Fenstemaker, et al., 2001)(see Figure 9). Fenstemaker et al. (2001)

cited this as possible evidence of density-driven free convection. Following a precipitation event, the final resistivity survey shows a major change in subsurface resistivity interpreted as infiltrating fresh rainwater flushing the media of salt water. However, without physical evidence of groundwater salinity values, it is difficult to conclude whether density-driven free convection occurred. This thesis was spurred by Fenstemaker's preliminary investigation and 2003 University of Texas Hydrogeology Field Camp field project at Padre Island. The study site at Bird Island Basin was selected based on Fenstemaker's results to explore the potential of density-driven free convection.

Chapter 2 Field Methods

2.1 OVERVIEW

The purpose of the field research is to investigate if free convection occurs at the wind-tidal flats of Padre Island. Thus, the field site must be characterized so that environmental influences can be understood and accounted for when interpreting the data. Characterization of the wind-tidal flats at Padre Island require that the following conditions be understood: the geology of the site as it pertains to lithology and homogeneity of the sediment; the hydrogeology of the site as it pertains to hydraulic gradients, flow rates and salinity gradients; and the climate of the site as it pertains to precipitation, recharge, and evaporation.

Once the site is characterized, interpretation of the field data, particularly salinity variations, can be applied to theories of density-driven free convection and its application to field scale problems. Site characterization and monitoring density-driven free convection were done jointly through field investigations involving traditional field hydrogeology methods, surface geophysical methods and climate data acquisition.

The field study began in March 2005 and ended in October 2005. Each study site consisted of 22 monitoring wells, piezometers, and multilevel sampling wells and a 3-D resistivity grid with 84 electrodes.

2.2 SITE SELECTION

To increase the chances of a detecting density-driven free convection, two study sites were chosen on the wind-tidal flats of Padre Island National Seashore. Sites were selected based on accessibility, topography, and surface conditions. Sites needed to be

somewhat accessible by vehicle, have a flat topography and be sparsely vegetated. The most limiting factor was accessibility to the west side of Padre Island and the wind-tidal flats. Near Park Headquarters, Bird Island Basin Road provided an improved route to several small flats. One site was chosen on the wind-tidal flat north of the road approximately 200 meters from Laguna Madre (see Figure 4). This was also the site of the Fenstemaker study. The next access road to Laguna Madre and the wind-tidal flats is Yarborough Pass which is 30 km south of Bird Island Basin. However, access to the wind-tidal flats at Yarborough Pass is limited to four-wheel drive vehicles because no paved roads exist south of Malaquite Beach. Therefore, 24 km of beach driving and crossing the fore island dunes was required to get to the unimproved road at Yarborough Pass. The second site was chosen approximately 1 km east of the Yarborough Pass boat ramp in the large wind-tidal flats located south of Yarborough Pass road (see Figure 4). This site is at the margin between the wind-tidal flats province and the barrier flat province (see Figure 3).

2.3 SEDIMENT SAMPLING

Sediment cores were collected at each site using vibracore techniques to determine material content and hydrogeologic properties including porosity, hydraulic conductivity, and homogeneity and isotropy of the matrix. Vibracore is a technique similar to roto-sonic drill rigs that is used to collect continuous core samples in saturated and unconsolidated sediment, often in river, lake, wetland and coastal areas. Vibracore equipment is light enough to be easily transported to areas unfeasible with larger, heavier drilling equipment. It was a low-impact, no-vehicle-necessary method for the easily disturbed and damaged wind-tidal flats. The shallow water table ensured the sediment would be saturated and liquefied during the advancement of the core barrel. It would also

provide a continuous core sample to log any important changes of material such as clay lenses.

A basic vibracore system consists of a vibration source, a power source, core pipe and extraction tools. The vibration source used for this project consisted of a high-cycle 120 volt Mikasa Multiquip concrete vibrator with a 6 meter whip hose and a 5.08 cm diameter vibrator head (see Figure 10). The concrete vibrator was powered by a 3000 watt gasoline generator. Thin-walled aluminum irrigation pipe with a diameter of 7.62 cm was cut into 6.1 m sections. The inside barrel of the bottom end was outfitted with a basket retainer style core-catcher made from brass shims and attached by rivets to prevent core loss.

Because vibracore uses the principles of liquefaction and gravity to drive the core pipe, the hole was first prepped by digging to the water table. Core handles were then secured to the pipe so that weight and torque could be applied. Once the core pipe hit refusal, a 4-m tripod and come-along puller were initially used to withdraw the core pipe. However, after the second vibracore withdrawal, the tripod failed and thereafter a highlift jack was successfully used to extract the core pipe. To take into account compaction, sediment loss, and plugging; penetration depth and inside pipe depth were recorded before and after extraction. The core pipe was cut open length wise onsite using an angle grinder and then logged for type of material (sand, clay, etc), grain size, grain shape and color. Sediment samples were also collected for laboratory grain-size analysis.

Two cores were collected at Padre Island National Seashore, one at the Bird Island Basin site on May 31, 2005 to a depth of 4.22 m and at Yarborough Pass site on June 1, 2005 to a depth of 2.29 m.

2.4 GROUNDWATER INVESTIGATION

Monitoring wells, piezometers, and multilevel sampling wells were installed at the study locations to measure vertical and horizontal hydraulic and salinity gradients. The groundwater data were used to evaluate if it is possible for free convection to occur. If hydraulic gradients are high, forced convection (advection and dispersion) dominates fluid transport. If inverted density gradients do not exist, then free convection will not occur.

2.4.1 Well Design and Installation

A monitoring well was installed at the center of each site and housed data loggers. The wells were constructed using nominal 5 cm (2-inch) schedule 40, flush-threaded polyvinylchloride (PVC) well casing. The well screen was 30 cm long with 0.0254 cm (0.01-inch) factory slot PVC and a drive point installed on the base. The monitoring wells were installed in the vibracore boreholes. However, due to flowing sand, vibracore techniques were additionally applied to advance the monitoring wells to approximately 2 meter depths (see Table 2).

At Bird Island Basin, three sets of nested piezometers and multilevel wells were installed approximately 10 meters apart in a triangular pattern with the 5 cm monitoring well in the center (see Figures 11 and 12). At Yarborough Pass, three sets of piezometers were installed approximately 10 meters apart in a triangular pattern with the 5 cm monitoring well in the center. Additionally, three sets of nested piezometers and multilevel wells were installed approximately 20 meters apart in a triangular pattern with

the 5 cm monitoring well in the center (see Figure 13 and 14). The added distance at Yarborough Pass was to ensure more accurate hydraulic gradient measurements.

Each nest consisted of two 2.54 cm (1-inch) schedule 40, flush threaded PVC well casing. The screened portion was 15 cm long with 0.015 cm (0.006-inch) factory slots and a drive point installed on the base. Installation depths for each set of piezometers were approximately 1-meter (shallow) and 2.5-meters (deep). The shallow piezometer was installed using a post driver. The deep piezometer also acted as a support for the multilevel sampling wells. Sampling ports were placed at 0.5 meter intervals above the piezometer screen using 0.65 cm (1/4-inch) ID, 0.79 cm (5/16 inch) OD polyethylene tubing wrapped to the piezometer using electrical tape. Strips of nylon stocking zip-tied to the tube ends served as filters. To install the combination piezometer and multilevel sampling well, a 5 cm (2 inch) steel conduit fitted with a sacrificial or loose drive point was used as a casing. Vibracore techniques were used to advance the steel conduit to approximately 2.5 meter depths. When the depth acquired using vibracore was insufficient, post-drivers and sledges were used to drive the steel conduit to the desired depth. Then the assembled piezometer/multilevel sampling well was inserted into the steel conduit casing. The conduit was extracted, leaving the sacrificial drive point and piezometer/multilevel sampling well. Filling the annulus was not necessary due to flowing sand conditions. The piezometer/multilevel well stickup was covered with capped section of 7.62 cm (3-inch) PVC and installed a few inches into the ground to protect the sampling tubes. The wells were developed to remove fines, particularly the 2-inch monitoring wells installed by direct vibracore methods. Locations of the monitoring wells were determined in UTM coordinates (meters) using a Magellan handheld GPS unit. Well elevations were surveyed in feet and recorded to the nearest hundredth of a foot. The top of casing of one well at each site (BIB09 and YP05) was chosen as a

temporary benchmark and assigned an arbitrary datum of 100.00 feet. Other well elevations were referenced relative to the temporary benchmark and converted to meters. Well information is summarized in Table 2.

2.4.2 Groundwater Data Collection Methods

Three instruments were used to collect groundwater data at the sites: a Solinst water level meter, a Myron Ultrameter multiparameter handheld meter, and two InSitu Troll 9000 multiparameter down-hole meters. During each sampling event, the wells at each site where purged as necessary and monitored for several field parameters including: water level, water temperature, specific conductance, total dissolved solids (TDS), pH, and oxygen reduction potential (ORP). The water level meter measured hydraulic head values in the monitoring wells and piezometers. Water pumped from the wells using a peristaltic pump was measured by the Ultrameter, which was calibrated before each visit, to directly determine specific conductance, total dissolved solids, water temperature, pH, and oxidation reduction potential (ORP). The nested piezometers and multi-level sampling ports allowed discrete sampling of the groundwater with depth. At each site, an InSitu Troll 9000 multiparameter data logging device was placed in the center 5 cm (2-inch) well to hourly log pressure, specific conductivity, temperature at the screened interval (Yarborough Pass additionally had pH and ORP sensors). Representative water samples were also collected and taken to the laboratory for water density analysis to correct hydraulic heads.

2.5 GEOPHYSICAL METHODS

Electrical resistivity, a surface geophysical method, was used at each site to measure changes in subsurface conductivity. Resistivity measures the bulk resistivity of the medium, which is influenced by mineral conductivity, porosity, moisture content, dissolved electrolytes, and temperature. Core samples, logs, and water samples from wells can account for each of these physical properties that affect subsurface conductivity and be used to calibrate the resistivity surveys. However, sediment core and monitoring well data are limited to point locations. The three-dimensional resistivity surveys provide a big picture of salinity variations between wells and therefore provide much more information on the development of density inversions and free convection. In addition, the only parameter expected to vary significantly is dissolved electrolytes, thus repeated resistivity surveys will examine changes in subsurface salinity over time.

2.5.1 Resistivity Design and Layout

Traditional resistivity meters inject current into the ground through a pair of electrodes or transmitters and subsequently measure voltage between another pair of electrodes or receivers. The resistivity can then be calculated through Ohm's Law from the known current and voltage. Modern resistivity meters, such as the Advanced Geosciences Inc (AGI) SuperSting R8, follow the same principle but can rapidly compute resistivity with multiple electrodes. The electrical resistivity setup used for this project consisted of an AGI SuperSting R8 eight channel resistivity meter, switch box, six cables containing 14 takeouts each, eighty-four electrodes and a deep-cycle 12-volt battery. Because the purpose was to collect time-lapse measurements, the surveys needed to be

the same every time, which included the position of the electrodes. Due to the highly corrosive environment, steel stakes could not be left in position during the study period. Instead, 1.27 cm (0.5-inch) by 45.72 cm (18-inch) long carbon rods were used as electrodes and installed at each site for the duration of the project. Each site contained eighty-four carbon electrodes placed 2 meters apart in a 10 meter by 26 meter grid with the center of the grid being the 5.08 cm (2-inch) monitoring well. At Bird Island Basin, the long side of the grid was oriented east to west to maximize the measurable area of groundwater flow towards Laguna Madre (see Figures 11 and 12). At Yarborough Pass, the grid was oriented north to south along an un-vegetated area of sand between a pond and a slough (see Figure 13 and 14). The resistivity surveys were acquired using a dipole-dipole array.

Spatial resolution is one half the electrode spacing, therefore with a two meter electrode spacing, objects smaller than one meter are difficult to resolve. Exploration is estimated to be 15 to 20 percent of the largest electrode spread length (Stewart and Bretnall, 1986), therefore with a corner to corner spread length of 27.85 m, the quality of data declines beyond 5.6 meters.

Some initial 2-D surveys, which provided larger scale images of the subsurface, were conducted to gather preliminary data for locating favorable research sites. Additionally, 2-D surveys were conducted at each site midway through the study period to again look at the subsurface in a larger scale. Those surveys used the same AGI electrical equipment with 56 electrodes at a 3-meter spacing. Locations of the mid-project 2-D surveys are presented on Figures 15 and 16. The maximum exploration for these 165-m transect surveys is approximately 33 m.

Resistivity data were inverted using Advanced Geosciences EarthImager 2-D and EarthImager 3-D to produce pseudo sections.

2.6 CLIMATE DATA

A key for the development of density-driven free convection is a climate that encourages high evaporation rates with little precipitation. This would be the driving force in the development of salinity inversions as water near the surface became more concentrated. Climatic influences, including temperature and precipitation, and tidal fluctuations were compiled from the weather stations at the Padre Island National Seashore ranger station (PINS), Corpus Christi Airport (CRP) and Texas A&M's Texas Coastal Ocean Observation Network (TCOON)(see Figure 17). Barometric pressure was also used to correct pressure head data in the InSitu Troll 9000 data loggers. Pressure values were converted to pressure head by first correcting for atmospheric pressure from the nearest station logging hourly atmospheric pressure. Texas Coastal Oceanic Observation Network (TCOON) stations at Bob Hall Pier (TCOON Station 014), which is approximately 16 km north-northeast of the Bird Island Basin site, and Baffin Bay (TCOON Station 068) which is approximately 10 km northwest from the Yarborough Pass site, were for atmospheric pressure corrections (see Figure 17). Corrected pressure values where then used to calculate pressure head or height of the water column using measured densities from each well and an assumed gravitational constant of 9.8 m/s^2.

Chapter 3 Results and Interpretation

3.1 CLIMATE

Climate, in particular temperature and precipitation, may have significant role in the development of density inversions on Padre Island. The PINS weather station (Figure 17) provided basic climate data including daily temperature, precipitation, wind speed, wind direction, and barometric pressure. The National Weather Service provided the same information as the PINS station but included hourly and historical data. TCOON stations provided data on water temperature, water levels and salinity for the Gulf of Mexico, Laguna Madre and several bays in addition to limited atmospheric weather data.

The closest weather station to the study sites is operated by PINS and is located at the park headquarters. However, historical weather data were not readily available for PINS station. Historical data were required to examine annual trends in temperature and precipitation. The closest station with historical data is the Corpus Christi International Airport (CRP) which is approximately 40 km to the northwest of the PINS station. Temperature data from the PINS and CRP station were compared to each other for 2005 to determine whether the CRP station would be a suitable proxy for temperatures and precipitation for the study sites. As presented in Figure 18, daily maximum and minimum temperatures trends correlate reasonably well. Also noted is the temperature buffer seen at PINS due its location adjacent to the Gulf of Mexico which dampens temperature extremes.

Examination of historical temperature and precipitation data with those during the 2005 study period reveal a hotter and dryer than normal spring and summer (see Figures 19 and 20). Daily precipitation totals from the PINS station are presented in Figure 21 and show very little rainfall occurring during the summer, particularly beginning mid-

July and ending in the beginning of September. This same period experienced temperatures that exceeded the monthly average by almost five degrees Celsius. These climatic conditions created a high potential for evaporation on the Island. This is confirmed by visual observations and measurements of diminishing surface water ponds, lowering of the water table, and increased salinity in surface water and groundwater which is discussed in the following sections. Following the hot and dry spell a heavy storm between September 9th and 13th dropped 14.7 cm of rain at the PINS station and flooded the study areas. During the September 14th visit, the Bird Island Basin site was under 25 to 30 cm of water and the Yarborough Pass site was partly covered with water 5 to 10 cm deep.

3.2 FIELD HYDROGEOLOGY RESULTS

Each field site was characterized for hydrogeology parameters through sediment cores and monitoring wells. The sediment cores provided data on lithology, grain-size distribution, porosity, and hydraulic conductivity. Site wells included monitoring wells, piezometers, and multi-port sampling wells. These wells provided data on hydraulic gradients, water chemistry, and housed data loggers that recorded pressure and water chemistry parameters.

3.2.1 Sediment Log and Grain Size Analysis

The sediment cores were collected and analyzed with the aid of the 2005 University of Texas Hydrogeology Field Camp students (UTFHC, 2005). The core collected at Bird Island Basin using vibracore methods reached a depth of 4.22 m and 2.65 m of sediment core was recovered. The same depth to sediment inside the core

before and after extraction with no sediment gaps indicates that no sediment was lost during retrieval. It is assumed that the remaining1.57 m loss or 37% reduction is from sediment compaction/consolidation and minor plugging of the core barrel as it advanced downhole, pushing aside sediment. The core collected from Yarborough Pass reached depths of 2.29 m with 1.65 m of sediment recovered. The same depth to sediment inside the core before and after extraction with no sediment gaps indicates the no sediment was lost during retrieval. It is assumed the 0.64 m loss or 28% reduction is due to sediment compaction/consolidation and minor plugging of the core barrel as it advanced downhole, pushing aside sediment. To get extrapolated sediment intervals, compaction was assumed to be uniform throughout the core and the core lengths were divided by the compaction ratio. A summary of the core logs is presented in Tables 3 and 4.

Sediment from Bird Island Basin, based on field observations, alternates between fine-grained quartz sand and clay horizons of 0.21 to 0.99 m thick. The much of the tidal flat at Bird Island Basin is covered with a dried and cracked algal mat. Layer thickness and lithology from the surface to refusal or 4.22 m is as follows: 0.21 m of fine-grained sand, 0.36 m of clay, 0.41 m of fine-grained to clayey sand, 0.99 m of clay, 1.82 m of fine-grained sand, and 0.43 m of sandy clay (see Table 3). In addition, during the electrical resistivity electrode installation, a 6 m wide by 0.3 m thick oyster bed was found 0.15 m below the surface that transected the western edge of the survey grid from north to south.

Sediment from Yarborough Pass indicates fairly uniform and homogeneous fine-grained quartz sand to refusal or 2.29 m (see Table 4).

Selected sediment samples from the Bird Island Basin core were collected by the 2005 University of Texas Hydrogeology Field Camp (UTHFC, 2005) to conduct grain size analysis and get estimations of porosity and hydraulic conductivity. Nine sediment

samples were collected and underwent a sieve analysis to determine grain size distribution. Grain size is fairly uniform with the expected increased content of fines from the clay rich zones (see Figure 22). The dominant grain size falls within the 125 - 75 μm size (fine-grain) range. Representative samples from the core were also saturated, weighed, dried and weighed again and revealed an average porosity of 35%. Based on these values, hydraulic conductivities were estimated using the Panda and Lake (1994) modification of the Kozeny-Carmen equation which is useful for fine-grained, unconsolidated sands. Estimated hydraulic conductivity ranged between 2.93 X 10^{-8} m/s in the clay horizons to 3.18 X 10^{-5} m/s in the sand horizons. These values of porosity and hydraulic conductivity compare reasonably well with previous values from other studies conducted at Padre Island (see Table 1).

3.2.2 Hydraulic Gradients

Because the wells contained groundwater of varying density, direct comparison based on water levels could be invalid due to pressure head's dependence on fluid density. Following Lusczynski's (1961) explanation of head in water of variable density, water levels were converted to fresh water head and environmental water head values. To do so, water densities were needed to determine pressure head. Water samples were collected from three wells for density measurements. In the lab, the waters from the three wells YP01, YP17 and BIB01 had specific conductance values of 65,000 μS, 102,000 μS and 129,000 μS respectively. Corresponding density measurements for YP01, YP17 and BIB01 resulted in 1.021 g/ml, 1.055 g/ml, and 1.101 g/ml respectively. The specific conductance and density results were plotted and presented on Figure 23. From this relationship, densities for all waters were derived. Fresh water head and environmental water head were calculated using the specific conductance and density relationship from

Figure 23 and are illustrated in Figure 24 with the equations shown below. The results are presented on Table 5.

$$h_f = z + h_p\left(\frac{\rho_i}{\rho_f}\right) \quad (2)$$

$$h_e = z + h_p\left(\frac{\rho_i}{\rho_a}\right) \quad (3)$$

where

h_f = Fresh water head

h_e = Environmental water head

z = Elevation head

h_p = Pressure head

ρ_i = Water density at a point

ρ_f = Fresh water density

ρ_a = Average water density within the piezometer nest

Fresh water head values were inputted into Surfer 7.0 to produce groundwater contour maps. Horizontal groundwater gradients and direction were calculated in a series of groundwater gradient spreadsheets created by Delvin (2003) and are included in Appendix C. Horizontal hydraulic gradient contour maps with gradient magnitudes for each site are presented in Figures 25 through 38 and discussed below.

Horizontal hydraulic gradients from Bird Island Basin were calculated using data from the three shallow piezometers BIB02, BIB08 and BIB16 which were placed approximately one meter below the surface. During the study period, horizontal groundwater gradients at Bird Island Basin ranged from 4.8 X 10^{-4} to 7.1 X 10^{-3} and flow

generally trended northwest towards Laguna Madre (see Figures 25-29). The water table at Bird Island Basin is shallow and did not drop below 0.69 m from the surface (see Figure 30). The water table shows a decrease in horizontal hydraulic gradient with a decrease in water elevation. Following a large precipitation event in September (see Figure 21), the site became inundated with approximately 0.25 to 0.30 m of rainwater. This increased water levels in the piezometers to approximately 0.20 m above the ground surface.

The nested piezometers containing a shallow and a deep piezometer allowed comparison of vertical hydraulic gradients. Comparison of shallow and deep piezometers of varying density required calculating environmental water head after Lusczynski (1961). As presented in Table 6, Bird Island Basin had three sets of nested piezometers where the shallow and deep piezometers were separated by 1.74 to 1.84 m. Comparison of the environmental water head values between the shallow and deep piezometers revealed a transition from an upward component of groundwater flow to a downward component occurring in July (see Table 6). This reversal may be a result of the increasing density of groundwater in the shallow zone.

Horizontal hydraulic gradients at Yarborough Pass were calculated initially using YP02, YP03, and YP04 until the outer triangle of nested piezometers were constructed, after which, YP05, YP11 and YP17 were used. All of these wells were placed at approximately 1 meter depths. Horizontal hydraulic gradients at Yarborough Pass were similar to those seen at Bird Island Basin. During the study period, horizontal groundwater gradients at Yarborough Pass ranged from 9.3×10^{-4} to 6.7×10^{-3} and flow generally trended southwest towards Laguna Madre (see Figures 31-37). The water table at Yarborough Pass is shallow and did not drop below 0.59 m from the surface (see Figure 38). The water table shows a decrease in horizontal hydraulic gradient with a

decrease in water elevation. Unlike data from Bird Island Basin, water levels increased at the July 27, 2005 sampling event. This is likely due to a rainfall event that occurred at Yarborough Pass but not at Bird Island Basin. Following a large precipitation event in September (see Figure 21), the site had approximately 0.05 to 0.10 m of water flowing slowly toward ponds to the north. This increased water levels in the piezometers to approximately the same level of surface water. Horizontal hydraulic gradients and flow direction following this precipitation event were very similar to what was seen at Bird Island Basin; the hydraulic gradient was still relatively low and was flowing to the southeast towards the center of the island.

Vertical hydraulic gradients at Yarborough Pass were calculated using environmental water head values between the nested shallow and deep piezometers. As presented in Table 6, Yarborough Pass had three sets of nested piezometers where the shallow and deep piezometers were separated from 1.42 to 1.68 m. Comparison of the environmental water head values between the shallow and deep piezometers show a transition from an upward component of groundwater flow to a downward component occurring between the July 27th and August 16th field visits (see Table 6). This reversal may be a result of the increasing density of groundwater in the shallow zone.

3.2.3 Bird Island Basin Data Logger

The pressure head or height of the water column in well BIB01 compared with hydraulic head values measured from BIB02, BIB03 and BIB04 shows good correlation with a decrease in water levels from June through August and a sharp increase following the large storm event in September (see Figures 30 and 39). Figure 39 demonstrates that the water level shows a good response to precipitation. Following precipitation events, the water level quickly returns close to previous water levels and rate of water level

decline. Water column height was compared to Laguna Madre water levels measured at South Bird Island (TCOON Station 013, see Figure 17) to determine if the daily oscillations seen in the pressure head were caused by tidal fluctuations. As presented in Figure 40, larger scale high and low stages of Laguna Madre do not appear to affect groundwater in BIB01. The daily oscillations of 0.02 to 0.05 m seen in BIB01 and Laguna Madre are likely from atmospheric pressure influences.

Specific conductivity measurements recorded by the data logger in BIB01 vary little (167,000 – 171,700 μS/cm) during the study period and are presented with pressure head in Figure 41. Plumes associated with free convection would likely be reflected in the data logger as a breakthrough curve of a high conductivity pulse. Stable conductivity values seen in BIB01 reveal that free convection processes did not impact the immediate area around the data logger. However, the stability throughout the study may be a result of the screened interval lying in a clay unit. The extrapolated vibracore log for this well indicates a clay unit from 0.98 to 1.97 m depth and the total depth of the installed well is 2.17 m (see Tables 2 and 3). In addition to possibly isolating the data logger, the clay layer would also likely slow and dissipate downward migrating, high-density plumes.

Water temperature rises from June through August and then begins to decline in September (see Figure 42).

3.2.4 Bird Island Basin Point Sampling

Water samples from the three nested piezometers and multilevel sampling ports provided vertical data on conductivity, temperature, pH and ORP and are presented in Appendix D. Conductivity plots of each nest are presented on Figures 43-45.

In the BIB02-08 nest (approximately 5.7 m east of BIB01), specific conductance values ranged from 128,000 to 169,000 or three to four times the salinity of seawater.

There is little variation of conductivity with depth (see Figure 43). Over time, conductivity values fluctuate back and forth between field visits. Conductivity values go from high on June 20th to lower on July 5th to higher on July 27th to lower on August 16th and then stabilize on September 14th. The large precipitation event in early September had no influence on conductivity with depth during the September 14th field visit (see Figure 43). Ponded surface water had a specific conductance of 1,400 µS/cm, which is within the range of typical surface water values. Conversely, the previously dry sampling port BIB03 at a depth of 0.18 m had a conductivity of 150,000 µS/cm on September 14th. This is over two orders of magnitude difference within 0.18 m. Sampling port BIB07 remained clogged during the study period.

In the BIB09-15 nest (approximately 5.7 m southwest of BIB01), specific conductance values ranged from 123,000 to 167,000 µS/cm (excluding the 180,000 µS/cm outlier) or three to four times the salinity of seawater. Vertically, there is little variation of conductivity with depth (see Figure 44). The profile does consistently show an arc in conductivity values from lower values at the top to higher values in the middle and back to lower values at the bottom. The interval of higher conductivity lies at about a one to two meter depth which corresponds to the clay unit seen in the sediment log which may be impacting conductivity values at this well. Over time, conductivity values follow the same pattern seen in the BIB01-08 nest. Conductivity values go from high on June 20th to lower on July 5th to higher on July 27th to lower on August 16th and then stabilize on September 14th. On September 14th the previously dry sampling port BIB10 at a depth of 0.08 m, had a conductivity value of 71,000 µS/cm. This is about halfway between the surface water value and the rest of the sampling points and helps further define the mixing zone between the surface water and groundwater.

In the BIB16-22 nest (approximately 5.4 m northwest of BIB01), specific conductance values ranged from 115,000 to 157,000 μS/cm or two to four times the salinity of seawater. Vertically, there is little variation of conductivity with depth (see Figure 45). Over time, conductivity values follow the same pattern seen in the BIB01-08 and BIB09-15 nests. Conductivity values go from high on June 20th to lower on July 5th to higher on July 27th to lower on August 16th and then stabilize on September 14th. The previously dry sampling port BIB17 at a depth of 0.10 m, contained a conductivity value of 95,000 μS/cm which further delineates the mixing zone between the surface water and groundwater.

Between the nests there is little variation in conductivity values and they show the same fluctuation pattern over the study period. Overall, the July 5th sampling event had the lowest conductivity values and the July 27th sampling event contained the highest conductivity values.

Temperature, pH, and ORP did not vary much during the study period (See Appendix D). Temperature typically decreased with depth and increased over time. pH values typically ranged between 6.5 and 7.5. ORP measurements demonstrated increasing anaerobic conditions with depth.

3.2.5 Yarborough Pass Data Logger

Pressure head or water column levels show good correlation with water level measurements collected from the piezometers YP02, YP03, YP04, YP05, YP11 and YP17 (see Figures 38 and 46). Beginning with installation of the data logger on June 20th the height of the water column reflects the high value on June 20th, the lower value on July 5th, the higher value on July 27th, the lower value on August 16th, and the higher value on September 14th. Compared to precipitation data from the PINS station at the

park headquarters, water column data shows increases in water levels following precipitation events (see Figure 46). Water level increases on July 6th, July 22nd and August 17th do not have a precipitation event directly associated with them as recorded by the PINS station. These increases may be from isolated thunderstorms that may not have occurred at the PINS station. Following rain events there is a steady decline in water column height of approximately 0.017 meters a day. Daily oscillations of 0.02 to 0.09 meters are on the same scale as the water level oscillations in Laguna Madre as recorded from the Baffin Bay (TCOON 068, see Figure 17) station (see Figure 47). The water levels in Laguna Madre are similar to the water level in YP01. However, some of the large scale fluctuations in water levels in Laguna Madre, such as the peak on June 29th and the gradual increase beginning on August 15th, do not correspond well with the water level log in YP01 (see Figure 47). Close examination of daily water level oscillations reveals that Laguna Madre is diurnal whereas the water level in YP01 is semi-diurnal (see Figure 48). Therefore, the site at Yarborough Pass may be buffered from the influence of Laguna Madre.

Specific conductance measurements from the data logger show conductivity values that begin near 90,000 µS/cm on June 20th, decline rapidly to approximately 75,000 µS/cm on July 25th, level out with some minor oscillations until August 22nd where they increase rapidly to over 95,000 µS/cm mid-September and fall back late September (see Figure 49). Plotted with water column height, conductivity does not appear to have a strong correlation. Both begin and end high with possible daily oscillation, but precipitation events such as on July 22nd which caused water levels to rise did not have an impact on conductivity.

Water temperature steadily rose with air temperature during the study period (see Figure 50). The pH sensor, showed a constant pH of 6.7 to 6.8 (see Figure 51) before

fouling on July 19th. Oxygen reduction potential (ORP) measured anoxic conditions (see Figure 51).

3.2.6 Yarborough Pass Point Sampling

Water samples from the three nested piezometers and multilevel sampling ports provided data on vertical changes in conductivity, temperature, pH and ORP and are presented in Appendix D. Conductivity plots of each nest are presented on Figures 52-54.

In the YP05-10 nest (approximately 11.7 m northeast of YP01), specific conductance values ranged from 57,300 to 102,000 µS/cm or just above seawater to twice the salinity of seawater (see Figure 52). Vertically, there is significant variation in conductivity, especially between YP07, YP08 and YP09 at 1.0, 1.5 and 2.0 m depths respectively. The top one meter contains the highest conductivity values with much lower values (29,500 µS/cm average difference) at 1.5 m and 2.0 m. Between June 20th and July 27th, the boundary between more conductive water and less conductive water was between 1.0 and 1.5 m. At the August 16th field event, the boundary shifted down between 1.5 m and 2.0 m. The deep piezometer, YP10, remained relatively constant between 85,000 and 90,000 µS/cm during the study period. The large storm event in early September and associated ponded water had no impact on the groundwater conductivity values.

In the YP11-16 nest (approximately 11.7 m south of YP01), specific conductance values ranged from 57,200 to 147,000 µS/cm or just above seawater to three times the salinity of seawater (see Figure 53). Conductivity widely varied vertically and between field visits. During the study period, conductivity in the top 1.26 to 1.76 meters increased greatly (YP14 saw an increase in 79,000 µS/cm from June 20th to September 14th) in

conductivity values whereas the bottom piezometer YP16 at 2.26 meters remained relatively constant except for an increase seen in the Sept 14th field visit. The difference between the upper, more conductive water and the lower, less conductive water increased from 6,600 to 73,000 µS/cm during the study period. These increases in conductivity values demonstrate the development of density inversions through evaporative concentration. The previously clogged port YP15 at 1.76 m shows a transitional value between 1.26 and 2.26 meters. Conductivity in the previously dry port YP12 at 0.26 m was not affected by the storm event and associated ponded water in early September.

In the YP17-22 nest (approximately 11.2 m northwest of YP01), specific conductance values ranged from 64,000 to 141,000 µS/cm or typical Laguna Madre water to three times the salinity of seawater (see Figure 54). Vertically, conductivity generally follows an arc of increasing conductivity to 1.78 meters and then decreasing conductivity to 2.28 meters. On July 27th, a specific conductance difference of approximately 25,000 µS/cm developed between 1.28 m (YP20) and 1.78 m (YP21) suggesting a density inversion. By the next field visit on August 16th, the density inversion dropped half a meter to 1.78 m (YP21) and 2.28 m (YP22). On September 14th the density inversion dissipated to a difference of 5,000 µS/cm. The storm event and associated ponded water in early September did not impact groundwater conductivity values.

Between the nests, there is a general increase in conductivity from YP05-10 to YP11-16 to YP17-22 or east to west. Temperature, pH and ORP did not vary much during the study period (See Appendix D). Temperature typically was warmer near the surface and increased through the summer. pH values typically ranged between 6.5 and 7.5. ORP measurements demonstrated increasing anaerobic conditions with depth.

The Yarborough Pass site has several ponds to the north and south of the study area. Surface water from these ponds in addition to Laguna Madre and Gulf of Mexico

water nearest Yarborough Pass were measured for conductivity, temperature, pH and ORP parameters (see Appendix D). Conductivity data were plotted and are presented on Figure 55. Gulf water stayed within the typical seawater range except for an outlier on June 20th, possibly due to measurement error. Laguna Madre water also stayed within typical conductivity values except for the outlier on June 20th. The ponds to the north of the study area are large and elongated to the east and west. The largest pond (northwest pond) being approximately 200 m by 50 m. Conductivity values in the north ponds were similar and ranged from seawater values on June 20th to twice the conductivity of seawater on August 16th and then back down to seawater conditions on September 14th following heavy rain. Surface area of the ponds also greatly diminished with the rise in conductivity associated with the hot and dry conditions during mid summer. Between June 20th and August 16th, the north ponds were reduced to approximately one quarter their early-summer size. The two south ponds are much smaller (20 m by 30 m) and are part of a slough that feeds the north ponds during heavy rain. Conductivity of these ponds is at or near typical surface water conductivity values. Because of their size and dependence on rain, the south ponds were dry during the July 27th and August 16th field visits. During the September 14th field visit, the heavy rain had renewed the two south ponds and the north ponds had become interconnected. The study site contained ponded water that had a conductivity value of 23,000 µS/cm. This was an intermediate value between the south ponds which had values of 6,000 and 12,000 µS/cm and the north ponds which had a value of 42,000 µS/cm (see Figure 55). This supports the field observation of surface water flowing towards the north.

3.3 RESISTIVITY RESULTS

Resistivity surveys where conducted at the Bird Island Basin and Yarborough Pass sites during the May 2nd (Yarborough Pass only), June 20th, July 5th, July 27th and August 16th field visits. Due to ponded water conditions during the September 14th field visit, resistivity surveys were not conducted. In addition, 2-D resistivity surveys were conducted at each site during the July 27th field visit. The 3-D resistivity surveys contained 84 electrodes in 10 m by 26 m grid centered on the center monitoring well. The size of reliable data from the 3-D resistivity surveys is 10 m wide by 26 m long by 6 m deep with a 1 m resolution. Compared to the monitoring wells which have a maximum depth of 2.7 m, the 3-D resistivity surveys more than double the investigation depth. However, beyond 2.7 m the resistivity data cannot be cannot be verified by groundwater data. The 2-D resistivity surveys are transects of 165 m which have reliable data to a depth of 14 m. The surveys report bulk apparent resistivity in ohm-m. The inverse of apparent resistivity is apparent conductivity which has units of mho/m or Siemen/m. For comparison and consistency, resistivity units of ohm-m will also be reported in conductivity units of μS/cm. When resistivity pseudo sections or plots are presented in figures, it is important to remember the resistivity and conductivity values are apparent bulk values. Apparent bulk resistivity or conductivity is the average resistivity or conductivity of the entire media including the geologic framework and pore fluid between respective electrodes.

3.3.1 Bird Island Basin Resistivity

The resistivity surveys conducted at Bird Island Basin are plotted and presented in Figures 56-60. In the individual 3-D plots, a top view and bottom view display all six sides of the plot. Locations of the wells are also indicated. The average resistivity and conductivity for the survey are also noted. On Figure 60, the four plots are displayed for easier comparison. Beginning on June 20th, the resistivity plot shows several zones of greater conductivity typically at depth of 2 to 4 meters as well as near the surface (see Figure 56). The area near the nested wells BIB16-22 appears less conductive which is consistent with groundwater data. The July 5th survey shows an increase in the conductivity of the site (see Figure 57). The July 27th survey resulted in greater conductance overall and individual zones of higher conductance at 2 to 4 m merging into a layer of greater conductance overlying a layer of lesser conductance (see Figure 58). The August 16th survey resulted in greater definition of the layering between the upper, more conductive zone with the lower, less conductive zone with possible plumes developing on the northeast corner (see Figure 59). Figure 60 shows that the site at Bird Island Basin experiences an increase in conductivity over the study period with the development of a layer of greater conductance overlying a less conductive zone. The 2-D resistivity survey conducted on July 27th, shows larger scale conductivity variation beneath the wind-tidal flats (see Figure 61). The upper 3.5 m is very conductive transitioning to less conductive material with depth. This suggests that larger-scale density inversions are occurring beneath the Bird Island Basin site.

3.3.2 Yarborough Pass Resistivity

The resistivity surveys conducted at Yarborough Pass are plotted and presented in Figures 62-67. In the individual 3-D plots, a top view and bottom view display all six sides of the plot. Locations of the well are also indicated. On Figure 67, the five plots are displayed for easier comparison. Beginning on May 2nd, there is a trend of less conductive media in the southeast corner to more conductive media in the northwest corner (see Figure 62). The transition or interface is angled upward towards the northwest corner, with less conductive media on the hanging wall and more conductive media on the footwall similar to the edge of a freshwater lens. The June 20th survey revealed the development of more conductive zones in the northwest corner concentrated between 2 and 4 meters (see Figure 63). The southeast corner shows the beginning of a reversal of density stratification. The July 5th survey shows an increase in conductivity values with more conductive zones consolidating (see Figure 64). The surface also shows an increase in conductivity in areas that are not vegetated. The inverted interface in the southeast corner also becomes more defined. The July 27th and August 16th surveys continue in the same pattern of progressively increasing conductivity and possible downward plume development in the north end (see Figures 65 and 66). The 2-D resistivity transect on July 27th reveals that the study site at Yarborough Pass is at the margin of a wedge of less conductive material to the east (see Figure 68). This is likely the edge of the freshwater lens which could explain the less conductive zone in the southeast edge of the 3-D surveys. Below and to the west of the less conductive lens, the conductivity increases rapidly. A second less conductive layer and isolated zones of lower conductivity between 3 and 6 meters may be a change in lithology or isolated zones of fresher water from small dunes to the south.

3.3.3 Resistivity Correlations to Groundwater

The apparent bulk resistivity values from the resistivity surveys can be correlated to groundwater conductivity through Archie's Law which states that the formation factor accounts for the ratio between bulk resistivity and pore-water resistivity. The formation factor equals the coefficient of saturation times the porosity to the negative power of the cementation factor.

$$F = \rho_o / \rho_\omega = a\phi^{-m} \qquad (4)$$

therefore $$\rho_\omega = \frac{\rho_o}{a\phi^{-m}} \qquad (5)$$

where

F = formation factor
ρ_o = bulk resistivity
ρ_ω = pore-water resistivity
a = coefficient of saturation (0.6 to 1.0), 1.0 being saturated
ϕ = porosity
m = cementation factor, 1.4 (uncemented) to 2.2 (cemented)

Calculations using Archie's Law apply apparent bulk resistivity values from the surveys to estimate pore-water resistivity which are then converted to conductivity for comparison to the nearest measured groundwater conductivity values. Assumptions include a coefficient of saturation of 1.0 and a cemented factor of 1.4. For porosity, two values are used; the first is a porosity of 35 percent measured from samples collected from the vibracore log (UTHFC, 2005) and the second is the average porosity estimated from Archie's Law by applying the measured groundwater conductivity as the pore-water resistivity. For Bird Island Basin, the average estimated porosity is 45 percent with a range of 34 to 57 percent (see Table 7). For Yarborough Pass, the average estimated porosity is 40 percent with a range of 26 to 62 percent (see Table 8). These average

values are within the range of previous studies at Padre Island that found porosity of the eolian and marine sands to be between 40 and 45 percent (UTHFC, 2001 and 2003 and Berkebile and Hay, 1995 and 2001). Resistivity surveys measure apparent or average resistivity between two electrodes and actual groundwater conductivities measure the conductivity at a point and thus reflect greater heterogeneity of conductivity. Therefore, an exact match between apparent pore-water conductivity and actual conductivity is not expected, but values should be similar. Tables 7 and 8 show there is a wide variation between apparent pore-water conductivity and measured groundwater conductivity, but on average they are close. At Bird Island Basin, applying 35 percent porosity generally gave apparent pore-water conductivity values that were greater (apparent has an average percent difference of 41 percent greater than measured) than measured groundwater conductivity vales. When the estimated porosity of 45 percent was applied, apparent pore-water conductivity values were much closer (apparent has an average percent difference of 3 percent less than measured) to measured groundwater conductivity values (see Table 7). At Yarborough Pass, applying 35 percent porosity also generally gave much higher (apparent has an average percent difference of 20 percent greater than measured) apparent pore-water conductivity values than the measured groundwater conductivity values. When the estimated porosity of 40 percent was applied, apparent pore-water conductivity values became much closer (apparent has an average percent difference of 11 percent less than measured) to measured groundwater conductivity values. This shows relatively good correlation of resistivity survey data with groundwater data.

3.4 RAYLEIGH NUMBER CALCULATIONS

The Rayleigh Number defines the critical point in an unstable system where buoyancy and gravitational forces overcome viscous resistance and dispersive dissipation. For the simplest system, this unitless number has the critical value of $4\pi^2$ or approximately 40 (Lapwood, 1948). Using collected hydrogeologic field data including specific conductivity, hydraulic conductivity (average from Table 1), horizontal hydraulic gradients, and porosity (from Table 7 and 8), unique Rayleigh Numbers could be calculated for each site and field visit date. As described in Chapter 1, the mixed convection Rayleigh Number equation used takes into consideration mechanical dispersion of ambient velocity from hydraulic gradients and assumes homogeneous and isotropic media. For the purpose of these calculations, the sites are assumed homogenous and isotropic despite the presence of clay layers at Bird Island Basin. The site at Yarborough Pass appears to have the ideal media based on sediment cores. Presented in Table 9, Rayleigh Numbers are calculated for each well nest and date. Measured and assumed parameters are also listed. Values can be compared to critical thermal Rayleigh Numbers calculated by Nield (1968) for an infinite, homogeneous, and horizontal layer under varying boundary conditions (see Table 10). Only two instances exist at the field sites where the Rayleigh Number is greater than the conservative critical Rayleigh Number of $4\pi^2$ ($\approx$ 40), between YP14 and YP16 on July 5th and August 16th with Rayleigh Numbers of 89 and 54 respectively. Several other locations have Rayleigh Numbers that are near the critical value and due to the sensitive nature of the equation, Rayleigh Numbers with values greater than 5 are noted on Figures 69-74 as potential sites for free convection.

Chapter 4 Discussion

4.1 Evidence for Density-Driven Flow

There are multiple lines of evidence for the development of density-driven free convection at Padre Island, particularly at Yarborough Pass. Inverse density gradients are evident in the groundwater wells and resistivity data. The data logger in YP01 records a conductivity spike. Calculations using the Rayleigh Number indicate unstable conditions. Downward movement of high conductivity fronts are measured in two nests at Yarborough Pass. Vertical hydraulic gradients at both sites indicate a transition from upward to downward flow. These demonstrate the potential for and movement of density-driven flow and are discussed below.

4.1.1 Density Inversions

The key to density-driven flow are mechanisms that promote unstable situations. Climate has a significant impact on density inversions and density-driven flow. Hot and dry conditions promote evaporation, concentrating groundwater and lowering the water table and the horizontal hydraulic gradient. Instability was the greatest when horizontal hydraulic gradients were the lowest (see Table 9). Density inversions were evident in every nest during the study period (See Figures 69-74). Density inversions likely caused the reverse in vertical hydraulic gradients from upward to downward between July and August (see Table 6). Resistivity surveys also show density inversions at both sites (see Figures 56-68).

4.1.2 Rayleigh Numbers

At both field sites, density inversions based on specific conductance were measured in the wells and were seen in the resistivity data. Whether or not these density inversions are unstable depends on many factors including the ambient groundwater velocity and concentration difference between two points. If the system is unstable, buoyancy forces will dominate and the fluid of greater density will invade the underlying fluid. The Rayleigh Number of $4\pi^2$ (≈ 40) is often referred to as the critical Rayleigh Number (Lapwood, 1948 and Nield, 1968) when perturbations begin to form into wavelets that begin the free convection process. This is only valid for no-flow boundaries with constant densities, and therefore, is conservative. Two Rayleigh Numbers of 89 and 54 were calculated between YP14 and YP16 on July 5th and August 16th respectively. The strictness of instability adhering to an exact value may be inadequate due to the varying boundary conditions shown in Table 10. Additionally, Wooding et al. (1997a,b) conducted Hele-Shaw and numerical experiments of a model evaporating "dry" salt lake which is analogous to conditions at the Padre Island field sites. Their experiments found instabilities at Rayleigh Numbers as low as 8.9. Application of lower critical Rayleigh Numbers validates field observations of density-driven free convection. For example, the downward conductivity shifts in YP05-10 and YP17-22 between July 27th and August 16th are possible evidence of density-driven free convection, but may also be thickening of the conductive layer. Rayleigh Numbers calculations between the conductivity contrasting wells found values lower than $4\pi^2$ ($\approx$ 40) during the respective field visits (see Figures 72 and 74). This example also illustrates that higher Rayleigh Numbers and instabilities may be more prevalent. Field data is limited to point or instantaneous sampling conducted in approximately three to

four week intervals. Therefore, at any time between field sampling events, the Rayleigh Number may have been different and possibly higher.

4.1.3 Conductivity Fluxes

In laboratory experiments, the invading fluid often takes the form of intricate fingers and plumes that may coalesce or bifurcate (Simmons et al., 1999; Cooper et al., 2001)(see Figure 1). The scale of the fingers in these experiments are millimeters to centimeters in size, but scaled up to field size they can become meters in size (Wooding et al., 1997a,b). This can be illustrated by field observations of isolated conductivity changes in some wells and not others at Yarborough Pass. The density inversion shift between YP07 and YP09 and between YP20 and YP22 from July 27th to August 16th is consistent with plumes or fingering from density-induced flow (see Figures 72 and 74). The lack of conductivity changes in nest YP11-16 and YP01 during this same time period support isolated free convection fingers or plumes (see Figure 73). If a site-wide solute concentration change caused by a fluctuating water table or a high conductivity pulse occurred, it would be expected to be seen site-wide not just in two nests. However, nest YP11-16 had a key sampling port (YP15 at 1.76 m) clogged in the same depth interval (1.0 to 2.28 m) as the density flux. Nevertheless, YP01, which is in the middle of the nests with a conductivity data logger sensor within that depth interval, did not record a conductivity change during this time period (see Figure 49). This suggests that the plume development was isolated to the area around nests YP05-10 and YP17-22 during this time period.

A significant conductivity change that may represent a breakthrough curve of density-dependent flow was observed in YP01 beginning September 2nd, peaking on September 17th and decreasing thereafter (see Figure 49). A plume of higher

conductivity may have passed in the vicinity of YP01 causing the increase and then decrease of conductivity. Water column height is not behaving in manner that would cause this phenomenon, so water table fluctuations can eliminated as an explanation (see Figure 49).

4.1.4 Resistivity

Evidence for density-driven flow using resistivity is difficult to establish because of the resolution of data and that apparent resistivity is an average between the electrodes. Resistivity monitoring does indicate zones of higher conductivity, which may show where density-driven flow is occurring. Examples of possible plumes are observed at both sites during the study period. At Bird Island Basin on August 16th, there is a downward plume in the northeast corner (see Figure 59). At Yarborough Pass, on July 27th and August 16th, a large plume appears to be descending in the southwest corner of the plot (Figures 65 and 66). Density inversions in the resistivity data also coincide with density inversions in the nested well data at Yarborough Pass. If the resistivity plots are extrapolated out to Nest YP05-10, then the inverted wedge could easily conform to well data. Additionally, the greater conductivity observed in the northern part of the plot of Yarborough Pass appears to encroach towards the south, bringing with it density inversions and density-driven free convection. Evidence of this is also observed in the groundwater data. A downward density flux occurred between July 27th and August 16th in YP05-10 and YP17-22 (see Figures 52-54 or 72-74) and then beginning September 2nd, a conductivity spike was recorded at YP01 (see Figure 49).

The resistivity plots at both sites also indicate wide-spread and possibly greater density inversions with depth. Between 4 and 6 meters, resistivity differences become

larger with more defined separation. However, without groundwater specific conductivity or similar data, these cannot be confirmed.

4.2 RATES OF DENSITY-DRIVEN FLOW

Examination of the density inversions in nests YP05-10 and YP17-22 between the July 27th and August 16th field sampling events may indicate rates of density-driven flow. The nests show a conductivity inversion (28,500 µS/cm difference at YP05-10 and 28,000 µS/cm difference at YP17-22) beginning at 1 and 1.28 m depths respectively and ending at 1.5 and 1.78 m respectively on July 27th (see Figures 52-54 or 72-74). Twenty days later on August 16th, the density inversion (36,000 µS/cm difference at YP05-10 and 25,000 µS/cm difference at YP17-22) shifted down 0.5 m to the next set of sampling ports (see Figures 52-54 or 72-74). Conservatively, this would give a rate of 0.025 m/day for downward movement. This is conservative because data are limited to the time between sampling intervals and separation between sampling ports.

The conductivity measurements recorded by the data logger in YP01 may show a breakthrough curve of density-induced flow that may also help define density flux rates. Beginning September 2nd, conductivity began to rise until it peaked on September 17th and then began to decline (see Figure 49). In approximately 15 days, conductivity increased 17,700 µS/cm (1,180 µS/cm-day). This compares relatively close to the conductivity increases seen in nests YP05-10 and YP17-22 during the downward density inversion shift between July 27th and August 16th. Sampling port YP08 saw an increase of 27,500 µS/cm in 20 days (1,375 µS/cm-day). Sampling port YP21 saw an increase of 26,000 µS/cm in 20 days (1,300 µS/cm-day). Therefore, if the conductivity spike seen in YP01 is a breakthrough curve of density induced flow, then the downward flux rate of 0.025 m/day from YP05-10 and YP17-22 may be pretty close to the actual.

Comparison to experimental rates of density flux from Hele-Shaw cells, sand tanks, and numerical models, reveal that the rates seen in YP05-10 and YP17-22 may be on the low end (Wooding et al., 1997a,b; Wood et al., 2004; Simmons et al., 1999; Narayan and Simmons, 1998; Cooper et al., 2001; Prasad and Simmons, 2003; Simmons et al., 2001; Schincariol and Schwartz, 1990). However, these rates vary widely due to media properties and concentration differences. For example, in a sand column experiment examining breakthrough of density-driven flow (Wood et al., 2004), density flux rates were between approximately 2.8 m/day and 9.7 m/day. Wooding et al. (1997a,b) and Simmons et al. (1999) conducted Hele-Shaw and numerical experiments representing density-driven flow below an evaporating salt lake, which is similar in concept to the wind-tidal flats. From their results, density flux rates appear to be around 0.36 m/day. In another model of a saline lake bed, Narayan and Simmons (1998) observed density fluxes between approximately 9.8×10^{-3} and 4.9×10^{-2} m/day. Therefore, the downward flux rate of 0.025 m/day observed at Yarborough Pass is in the low but reasonable range.

4.3 SITE VARIATION

Yarborough Pass exhibited greater propensity for density-driven free convection than Bird Island Basin possibly due to differing site characteristics.

Core logs show that Yarborough Pass is nearly uniform sand to the known depth whereas Bird Island Basin cores contain alternating clays and sand (see Tables 3-4). The lack of low hydraulic conductivity layers at Yarborough Pass may have aided downward migration of dense fluids.

The location of the sites with respect to island provinces may have also contributed to site results (see Figure 3). The Yarborough Pass site is located at the

margin between the barrier flat province and wind-tidal flat province. This is evident in the resistivity transect presented in Figure 68 showing the fresh water lens under the barrier flat province. The high evaporation rates and wide range of groundwater densities in this zone may contribute to density inversions. The fresh water lens continuously supplies fresh, less dense water and intense evaporation continuously concentrates near surface water. The lower the saturation and density of water the greater the rate of evaporation and therefore, the faster the rate of density inversion development. Thus, the transition zone at the barrier flat and wind-tidal flat margin may contribute to a greater tendency for free convection development. In contrast, the Bird Island Basin site is located at the western end of small wind-tidal flat. In the resistivity transect presented on Figure 61, there is little to no variation laterally at the Bird Island Basin site. In the upper 4 m of the 3-D and groundwater investigation, the high-density groundwater appears to be relatively stable without much fresher water input. The lack of strong inverse density gradients is possibly due to the already dense groundwater. The greater the saturation and density of water the slower the rate of evaporation and therefore the slower the rate of density inversion development. However, on a larger scale, a large density inversion is evident.

Despite variations in geology, the two sites did have some commonalities. Hydraulic gradients at both sites had similar ranges and, during field visits, had comparable values. Climate was essentially the same, except for a few isolated thunderstorms at Yarborough Pass. However, based on the differences mentioned above, it appears that the lack of strong density inversions at the Bird Island Basin site may be due to one or a combination of the following: a lack of more vertically homogenous geology, lack of groundwater density variability, and possible reduced evaporation rates

due to the higher groundwater concentration. However, the resistivity transect at Bird Island Basin suggests that there is a strong density inversion at depth (see Figure 61).

4.4 HYPOTHESES EVALUATION

Initial hypotheses of field requirements of a hot and dry climate and a low hydraulic gradient for density inversions and density-induced flow are consistent with the results. The results show that a hot and dry climate induced high evaporation rates which increased conductivity, decreased the water table, and developed density inversions. During periods of lower hydraulic gradients, the instability increases.

Climate shows strong correlation which likely caused greater density near one meter which resulted in an inverted gradient at Yarborough Pass and to a lesser extent at Bird Island Basin. Evidence for the importance of evaporation is observed in the comparison of groundwater conductivity to Gulf of Mexico and Laguna Madre water conductivity (see Figures 43-45 and 52-54 or 69-74). The only mechanism to induce conductivity to nearly three times that of seawater is evaporation.

The magnitude and direction of the hydraulic gradient is significant to density-driven flow. Rayleigh Number calculations show that when the hydraulic gradient is low, instability is more likely even when the concentration gradient may not be large. For example, the greatest concentration difference was seen between YP14 and YP16 with a difference of 75,000 μS/cm on July 27th (see Figure 73). The horizontal hydraulic gradient at this time was 6.7 X 10^{-3} and the vertical hydraulic gradient was 4.1 X 10^{-2} upward (see Appendix C and Table 6). On July 5th, the concentration difference was 35,000 μS/cm with a hydraulic gradient of 9.3 X 10^{-4} and vertical hydraulic gradient of 3.0 X 10^{-2} upward (see Appendix C and Table 6). The Rayleigh Number for July 27th was 20 and the Rayleigh Number for July 5th was 89 (see Table 9).

The hydrogeologic media also may play a role as noted at Bird Island Basin. The clay layers may have inhibited the development of density inversions and downward migration, whereas the geology at Yarborough Pass was more uniform. However, this may not be entirely due to Bird Island Basin's heterogeneous geology but also the lack of groundwater density variability and possible reduced evaporation rates due to the higher groundwater concentration.

Based on these results, climate, the hydraulic gradient, and geology are the key factors for density-driven free convection development in the field. With affirmation of field requirements for the development of density-driven free convection and supporting evidence of conductivity fluxes, the hypothesis that free convection occurs in the natural environment is valid.

Chapter 5 Conclusions

5.1 Study Findings

This report demonstrates that density-driven flow is occurring in the shallow groundwater of the wind-tidal flats at Padre Island National Seashore. Field-scale density-driven flow, which hitherto has not been conclusively detected or measured in the field, has been monitored through hydrogeology and geophysical field methods. Nested piezometers with multi-level sampling ports and data loggers captured the development of density inversions, descending density fronts, density spikes, and the reversal of vertical hydraulic gradients from upward to downward. Geophysical surveys using 3-D electrical resistivity techniques captured the development of density inversions and plumes of high-density water. Estimated calculations of the Rayleigh Number using field data confirm that inverted density gradients, particularly those that are descending, can be unstable. The development of inverted density gradients in the shallow groundwater of the wind-tidal is likely evaporative-driven and enhanced by low horizontal hydraulic gradients which reduce advection and dispersion. These findings show that the wind-tidal flats along Padre Island National Seashore are conducive to density-driven flow and that said flow can be monitored and measured in the field.

5.2 Study Implications

The results of this study suggest that the development and flow of variable-density fluids in groundwater can be detected and monitored through field techniques. It demonstrates that the development of density inversions may overcome the dissipating forces of dispersion and diffusion to create a sufficiently large unstable gradient to induce free convection.

This study implies that field research of variable density fluid flow may occur in locations with a shallow water table, high evapotranspiration, low hydraulic gradients, and porous media. An established and well documented field site would allow further study of density-driven flow, particularly with respect to field scale issues. For example, the results of this project suggest that density-driven flow rates are slower than comparative laboratory experiments. Additional research is required to test these findings.

5.3 IMPORTANCE OF RESULTS

Findings of this project are important to the field of variable-density fluid flow from research to practical applications. They support density-driven free convection as a valid groundwater transport mechanism. This process may be used to explain the interesting and heavily researched area of dolomitization. Laboratory models, which are faster and easier to control and replicate than field conditions, need to be calibrated to represent real-world conditions or benchmarks. Because models predict how fluids behave under varying conditions, incorporation of field data could test accuracy and robustness. The slow density-driven flow rates, for example, would have a significant impact on variable-density transport models. This study demonstrated that monitoring wells combined with resistivity surveys complement each other. Similar field methods can be used in areas of variable-density fluids to evaluate seawater intrusion in coastal aquifers to leachate plume monitoring.

5.4 FUTURE WORK

This project also demonstrates the need for future research. Ideas for continued research are based on the questions and limitations that developed during the course of this study and are discussed below.

Because measurements were limited by "snapshots" of field conditions, the Rayleigh Numbers calculations were also discrete representations of what was occurring at that instant in time. Therefore, at any one time between field sampling events, the Rayleigh Number may have been different. A statistical analysis of the range of specific conductivity or density values and hydraulic gradients from field data could provide the likelihood for density inversions and a possible range of Rayleigh Numbers throughout the study period. This statistical analysis would likely strengthen the argument for probability of free convection to occur at the field sites.

An important question is how a numerical model based on the field parameters of Padre Island would compare. Would the model predict the development of density inversions and density-driven flow?

A more intense field study monitoring site conditions would also be valuable and would help define several questions, such as: On what kind of time scale does free convection operate on? How significant is the climate in developing near surface density inversions. The 2-D resistivity survey at Bird Island Basin shows a larger scale density inversion and appears to be a likely candidate for free convection study (see Figure 61). This would require more rigorous field work including resistivity surveys and groundwater wells. An evaluation of the field methods used during this project demonstrates that certain methods were more effective than others in monitoring variable-density development and flow. The multilevel wells proved useful in

determining gradients and shifts in density. The data loggers were also very helpful in observing changes in conductivity over time. A suggested tool or method for variable-density monitoring would combine multilevel wells with logging conductivity and temperature meters. This would enable real-time evolution and flow of variable-density fluids. The geophysical technique of three-dimensional resistivity lost small details but was helpful to for site visualization, particularly between wells. A larger grid with smaller electrode spacing would improve its resolution but would significantly increase measurement time.

Appendix A Tables

Table 1 Hydraulic Conductivity Values Measured at Padre Island National Seashore

Hydraulic Conductivity (m/s)	Location	Method	Source
9.8×10^{-5}	Fore-Island Dunes at Novillo Line Camp (Bird Island Basin)	Pump Test	Berkebile et al., 2001
6.4×10^{-5}	Barrier Island Flats at Novillo Line Camp (Bird Island Basin)	Pump Test	Berkebile et al., 2001
7.2×10^{-5}	Wind-Tidal Flats at Dunn Ranch	Pump Test	Berkebile et al, 2001
4.1×10^{-5}	Fore-Island Dunes at Novillo Line Camp (Bird Island Basin)	Slug Test	Boylan, 1986
2.4×10^{-6}	Wind-tidal flats at Bird Island Basin	Slug Test	Boylan, 1986
1×10^{-4}	Fore-Island Dunes at Novillo Line Camp (Bird Island Basin)	Grain Size Analysis	The University of Texas Hydrogeology Field Camp, 2003
6.4×10^{-5}	Wind-tidal flats at Bird Island Basin	Grain Size Analysis	The University of Texas Hydrogeology Field Camp, 2003
2.93×10^{-7} to 3.18×10^{-4}	Wind-tidal flats at Bird Island Basin	Grain Size Analysis	The University of Texas Hydrogeology Field Camp, 2005
6.3×10^{-5} [5.4 m/day]	**Average**		

Table 2 Well Information

Well ID	Well Type	Date Installed	Installation Depth (m)	Relative Ground Elevation (m)	Relative TOC Elevation (m)	Installation Method
BIB01	2" MW	5/31/05	2.17	29.864	30.514	Vibracore/Hammer
BIB02	1" Piez	5/31/05	0.99	29.947	30.477	Post Driver
BIB03	Multi Port	5/31/05	0.18	29.947	NA	Vibracore/Hammer
BIB04	Multi Port	5/31/05	0.68	29.947	NA	Vibracore/Hammer
BIB05	Multi Port	5/31/05	1.18	29.947	NA	Vibracore/Hammer
BIB06	Multi Port	5/31/05	1.68	29.947	NA	Vibracore/Hammer
BIB07	Multi Port	5/31/05	2.18	29.947	NA	Vibracore/Hammer
BIB08	1" Piez	5/31/05	2.83	29.930	30.510	Vibracore/Hammer
BIB09	1" Piez	5/31/05	0.99	29.960	30.480	Post Driver
BIB10	Multi Port	5/31/05	0.08	29.960	NA	Vibracore/Hammer
BIB11	Multi Port	5/31/05	0.58	29.960	NA	Vibracore/Hammer
BIB12	Multi Port	5/31/05	1.08	29.960	NA	Vibracore/Hammer
BIB13	Multi Port	5/31/05	1.58	29.960	NA	Vibracore/Hammer
BIB14	Multi Port	5/31/05	2.08	29.960	NA	Vibracore/Hammer
BIB15	1" Piez	5/31/05	2.73	29.951	30.501	Vibracore/Hammer
BIB16	1" Piez	5/31/05	0.99	29.947	30.477	Post Driver
BIB17	Multi Port	5/31/05	0.10	29.947	NA	Vibracore/Hammer
BIB18	Multi Port	5/31/05	0.60	29.947	NA	Vibracore/Hammer
BIB19	Multi Port	5/31/05	1.10	29.947	NA	Vibracore/Hammer
BIB20	Multi Port	5/31/05	1.60	29.947	NA	Vibracore/Hammer
BIB21	Multi Port	5/31/05	2.10	29.947	NA	Vibracore/Hammer
BIB22	1" Piez	5/31/05	2.75	29.933	30.453	Vibracore/Hammer
YP01	2" MW	4/10/05	2.16	29.940	30.684	Vibracore/Hammer
YP02	1" Piez	4/10/05	0.99	29.968	30.498	Hammer
YP03	1" Piez	4/10/05	0.98	29.955	30.495	Hammer
YP04	1" Piez	4/10/05	1.18	29.957	30.477	Hammer
YP05	1" Piez	6/2/05	0.98	29.930	30.480	Post Driver
YP06	Multi Port	6/2/05	0.50	29.930	NA	Vibracore/Hammer
YP07	Multi Port	6/2/05	1.00	29.930	NA	Vibracore/Hammer
YP08	Multi Port	6/2/05	1.50	29.930	NA	Vibracore/Hammer
YP09	Multi Port	6/2/05	2.00	29.930	NA	Vibracore/Hammer
YP10	1" Piez	6/2/05	2.83	29.917	30.517	Vibracore/Hammer
YP11	1" Piez	6/2/05	0.99	29.945	30.477	Post Driver
YP12	Multi Port	6/2/05	0.26	29.945	NA	Vibracore/Hammer
YP13	Multi Port	6/2/05	0.76	29.945	NA	Vibracore/Hammer
YP14	Multi Port	6/2/05	1.26	29.945	NA	Vibracore/Hammer
YP15	Multi Port	6/2/05	1.76	29.945	NA	Vibracore/Hammer
YP16	1" Piez	6/2/05	2.59	29.941	30.541	Vibracore/Hammer
YP17	1" Piez	6/2/05	1.00	29.942	30.462	Post Driver
YP18	Multi Port	6/2/05	0.28	29.942	NA	Vibracore/Hammer
YP19	Multi Port	6/2/05	0.78	29.942	NA	Vibracore/Hammer
YP20	Multi Port	6/2/05	1.28	29.942	NA	Vibracore/Hammer
YP21	Multi Port	6/2/05	1.78	29.942	NA	Vibracore/Hammer
YP22	1" Piez	6/2/05	2.61	29.943	30.498	Vibracore/Hammer

TOC = Top of casing, MW= Monitoring well, Piez = piezometer, Multi Port = Multilevel port sampling well, NA = Not Applicable. The TOC of BIB09 and YP05 served as temporary benchmarks for each site and were assigned an arbitrary datum of 100.00 feet.

Table 3 Bird Island Basin Vibracore Log

Core Segment (m)	Extrapolated Depth (m)	Description
Surface	Surface	Dried, flakey algal mat that covers 30 – 50 % percent of the surface
0.00 – 0.13	0.00 – 0.21	SAND, fine to medium grained, quartz, subrounded, light brown
0.13 – 0.36	0.21 – 0.57	CLAY, grey marine, 15% mollusk fragments
0.36 – 0.57	0.57 – 0.91	SAND, fine to medium grained, quartz, subrounded, light brown
0.57 – 0.62	0.91 – 0.98	Clayey SAND, fine-grained, subrounded, grey
0.62 – 1.24	0.98 – 1.97	CLAY, grey marine, 5% mollusk fragments
1.24 – 2.28	1.97 – 3.62	SAND, fine to medium grained, quartz, subrounded, light grey, 10% organic matter
2.28 – 2.39	3.62 – 3.79	SAND, fine-grained, subrounded, quartz, grey, 50% shell fragments
2.39 – 2.65	3.79 – 4.22	Sandy CLAY, dark grey, 15% shell fragments

For Bird Island Basin, vibracore methods reached a depth of 4.22 m and 2.65 m of sediment was recovered with no apparent sediment loss. It is assumed that the resultant 1.57 m loss or 37% reduction is from sediment compaction/consolidation and minor plugging of the core barrel as it advanced downhole, pushing aside sediment. Extrapolated Depth is estimated by dividing the core segment by the compaction ratio.

Table 4 Yarborough Pass Vibracore Log

Core Segment (m)	Extrapolated Depth (m)	Description
0.00 – 0.99	0.00 – 1.37	SAND, fine grained, well rounded, quartz, 10% organic matter, 5% clay, 5% mollusk fragments
0.99 – 1.65	1.37 – 2.29	SAND, fine-grained, well rounded, quartz, 15% organic matter, 5% clay, 5% mollusk fragments

For Yarborough Pass, vibracore methods reached a depth of 2.29 m and 1.65 m of sediment was recovered with no apparent sediment loss. It is assumed that the resultant 0.64 m loss or 28% reduction is from sediment compaction/consolidation and minor plugging of the core barrel as it advanced downhole, pushing aside sediment. Extrapolated Depth is estimated by dividing the core segment by the compaction ratio.

Table 5 Hydraulic Heads

Date	Well ID	X Grid Location (m)	Y Grid Location (m)	Specific Conduct-ance (uS/cm)	Water Density (kg/m^3) ρ_i	Ave. Piez. Nest Density (kg/m^3) ρ_a	Relative Surface Elevation (m)	Depth to Top of Screen (m)	Depth to Water Below Surface (m)	Elevation Head (m) z	Pressure Head (m) h_p	Hydraulic Head (m) h	Fresh Water Head (m) h_f	Environ-mental Water Head (m) h_e
4/10/2005	YP01	11.0	13.0	NA	1056	NA	29.940	1.853	0.163	28.087	1.691	29.778	29.872	NA
	YP02	15.0	17.0	NA	1070	NA	29.968	0.842	0.233	29.127	0.609	29.735	29.778	NA
	YP03	12.8	7.0	NA	1065	NA	29.955	0.832	0.255	29.124	0.577	29.700	29.738	NA
	YP04	5.5	14.6	NA	1089	NA	29.957	0.852	0.260	29.105	0.592	29.697	29.750	NA
5/2/2005	YP01	11.0	13.0	157,500	1152	NA	29.940	1.853	0.216	28.087	1.637	29.724	29.973	NA
	YP02	15.0	17.0	149,900	1139	NA	29.968	0.842	0.420	29.127	0.422	29.548	29.607	NA
	YP03	12.8	7.0	148,900	1138	NA	29.955	0.832	0.440	29.124	0.392	29.515	29.569	NA
	YP04	5.5	14.6	149,700	1139	NA	29.957	0.852	0.440	29.105	0.412	29.517	29.574	NA
6/20/2005	BIB01	13.0	7.0	150,000	1140	NA	29.864	1.825	0.440	28.038	1.385	29.424	29.617	NA
	BIB02	19.0	7.0	148,000	1137	1138	29.947	0.842	0.485	29.105	0.357	29.462	29.511	29.462
	BIB08	19.0	7.0	169,000	1175		29.930	2.680	0.530	27.250	2.150	29.400	29.777	29.470
	BIB09	10.7	1.3	180,000	1200	1135	29.960	0.842	0.540	29.118	0.302	29.420	29.480	29.437
	BIB15	10.7	1.3	150,000	1140		29.951	2.580	0.522	27.371	2.058	29.429	29.717	29.438
	BIB16	10.4	11.4	150,000	1140	1128	29.947	0.842	0.550	29.105	0.292	29.397	29.438	29.400
	BIB22	10.4	11.4	150,000	1140		29.933	2.600	0.530	27.333	2.070	29.403	29.692	29.425
	YP01	11.0	13.0	100,100	1056	NA	29.940	1.853	0.271	28.087	1.582	29.669	29.758	NA
	YP02	15.0	17.0	111,200	1070	NA	29.968	0.842	0.350	29.127	0.492	29.618	29.653	NA
	YP03	12.8	7.0	107,600	1065	NA	29.955	0.832	0.365	29.124	0.467	29.590	29.621	NA
	YP04	5.5	14.6	122,800	1089	NA	29.957	0.852	0.390	29.105	0.462	29.567	29.608	NA
	YP05	20.5	20.0	93,800	1048	1032	29.930	0.852	0.292	29.078	0.560	29.638	29.665	29.647
	YP10	20.5	20.0	86,700	1039		29.917	2.500	0.220	27.417	2.280	29.697	29.785	29.712
	YP11	12.7	1.3	96,860	1051	1028	29.945	0.839	0.345	29.106	0.494	29.600	29.625	29.611
	YP16	12.7	1.3	61,460	1017		29.941	2.260	0.230	27.681	2.030	29.711	29.745	29.689
	YP17	0.8	18.5	107,500	1067	1066	29.942	0.852	0.385	29.090	0.467	29.557	29.588	29.557
	YP22	0.8	18.5	117,800	1080		29.943	2.280	0.315	27.663	1.965	29.628	29.785	29.654

Table 5 Hydraulic Heads Continued

Date	Well ID	X Grid Location (m)	Y Grid Location (m)	Specific Conduct-ance (uS/cm)	Water Density (kg/m^3) ρ_i	Ave Piez Nest Density (kg/m^3) ρ_a	Relative Surface Elevation (m)	Depth to Top of Screen (m)	Depth to Water Below Surface (m)	Elevation Head (m) z	Pressure Head (m) h_p	Hydraulic Head (m) h	Fresh Water Head (m) h_f	Environ-mental Water Head (m) h_e
7/5/2005	BIB01	13.0	7.0	136,000	1116	NA	29.864	1.825	0.437	28.038	1.388	29.427	29.588	NA
	BIB02	19.0	7.0	128,000	1098	1107	29.947	0.842	0.607	29.105	0.235	29.340	29.363	29.338
	BIB08	19.0	7.0	138,000	1117		29.930	2.680	0.615	27.250	2.065	29.315	29.557	29.334
	BIB09	10.7	1.3	134,000	1110	1101	29.960	0.842	0.617	29.118	0.225	29.343	29.368	29.345
	BIB15	10.7	1.3	128,000	1100		29.951	2.580	0.605	27.371	1.975	29.346	29.544	29.345
	BIB16	10.4	11.4	118,000	1081	1090	29.947	0.842	0.621	29.105	0.221	29.326	29.344	29.324
	BIB22	10.4	11.4	135,000	1110		29.933	2.600	0.608	27.333	1.992	29.325	29.544	29.361
	YP01	11.0	13.0	76,830	1029	NA	29.940	1.853	0.480	28.087	1.373	29.460	29.500	NA
	YP02	15.0	17.0	105,000	1064	NA	29.968	0.842	0.555	29.127	0.287	29.413	29.432	NA
	YP03	12.8	7.0	115,600	1077	NA	29.955	0.832	0.554	29.124	0.278	29.401	29.423	NA
	YP04	5.5	14.6	123,200	1090	NA	29.957	0.852	0.560	29.105	0.292	29.397	29.423	NA
	YP05	20.5	20.0	87,800	1041	1033	29.930	0.852	0.520	29.078	0.332	29.410	29.424	29.413
	YP10	20.5	20.0	87,800	1041		29.917	2.500	0.460	27.417	2.040	29.457	29.540	29.472
	YP11	12.7	1.3	92,300	1046	1030	29.945	0.839	0.554	29.106	0.285	29.391	29.404	29.395
	YP16	12.7	1.3	57,150	1014		29.941	2.260	0.475	27.681	1.785	29.466	29.491	29.438
	YP17	0.8	18.5	106,700	1065	1066	29.942	0.852	0.546	29.090	0.306	29.396	29.416	29.395
	YP22	0.8	18.5	105,700	1064		29.943	2.280	NA	NA	NA	NA	NA	NA
7/27/2005	BIB01	13.0	7.0	153,000	1142	NA	29.864	1.825	0.593	28.038	1.232	29.271	29.446	NA
	BIB02	19.0	7.0	155,000	1145	1148	29.947	0.842	0.661	29.105	0.181	29.286	29.312	29.285
	BIB08	19.0	7.0	158,000	1150		29.930	2.680	0.668	27.250	2.012	29.262	29.564	29.266
	BIB09	10.7	1.3	160,000	1155	1150	29.960	0.842	0.674	29.118	0.168	29.286	29.312	29.287
	BIB15	10.7	1.3	149,000	1138		29.951	2.580	0.661	27.371	1.919	29.290	29.555	29.270
	BIB16	10.4	11.4	149,000	1138	1141	29.947	0.842	0.675	29.105	0.167	29.272	29.295	29.272
	BIB22	10.4	11.4	154,000	1144		29.933	2.600	0.661	27.333	1.939	29.272	29.551	29.277
	YP01	11.0	13.0	77,060	1030	NA	29.940	1.853	0.257	28.087	1.596	29.683	29.731	NA
	YP02	15.0	17.0	113,700	1074	NA	29.968	0.842	0.350	29.127	0.492	29.618	29.655	NA
	YP03	12.8	7.0	120,500	1085	NA	29.955	0.832	0.407	29.124	0.425	29.548	29.584	NA
	YP04	5.5	14.6	126,400	1093	NA	29.957	0.852	0.381	29.105	0.471	29.576	29.620	NA
	YP05	20.5	20.0	93,400	1049	1039	29.930	0.852	0.282	29.078	0.570	29.648	29.676	29.653
	YP10	20.5	20.0	88,400	1040		29.917	2.500	0.220	27.417	2.280	29.697	29.788	29.699
	YP11	12.7	1.3	109,800	1069	1062	29.945	0.839	0.433	29.106	0.406	29.512	29.540	29.515
	YP16	12.7	1.3	60,000	1015		29.941	2.260	0.280	27.681	1.980	29.661	29.691	29.573
	YP17	0.8	18.5	124,000	1091	1079	29.942	0.852	0.362	29.090	0.490	29.580	29.624	29.585
	YP22	0.8	18.5	111,000	1070		29.943	2.280	0.299	27.663	1.981	29.644	29.783	29.628

Table 5 Hydraulic Heads Continued

Date	Well ID	X Grid Location (m)	Y Grid Location (m)	Specific Conduct-ance (uS/cm)	Water Density (kg/m^3) ρ_i	Ave Piez Nest Density (kg/m^3) ρ_a	Relative Surface Elevation (m)	Depth to Top of Screen (m)	Depth to Water Below Surface (m)	Elevation Head (m) z	Pressure Head (m) h_p	Hydraulic Head (m) h	Fresh Water Head (m) h_f	Environ-mental Water Head (m) h_e
8/16/2005	BIB01	13.0	7.0	135,000	1110	NA	29.864	1.825	0.639	28.038	1.186	29.225	29.355	NA
	BIB02	19.0	7.0	135,000	1110	1124	29.947	0.842	0.714	29.105	0.128	29.233	29.247	29.231
	BIB08	19.0	7.0	146,000	1130		29.930	2.680	0.715	27.250	1.965	29.215	29.471	29.226
	BIB09	10.7	1.3	144,000	1129	1124	29.960	0.842	0.723	29.118	0.119	29.237	29.252	29.238
	BIB15	10.7	1.3	137,000	1112		29.951	2.580	0.710	27.371	1.870	29.241	29.451	29.221
	BIB16	10.4	11.4	127,000	1097	1108	29.947	0.842	0.712	29.105	0.130	29.235	29.248	29.234
	BIB22	10.4	11.4	137,000	1112		29.933	2.600	0.713	27.333	1.887	29.220	29.431	29.226
	YP01	11.0	13.0	74,000	1027	NA	29.940	1.853	0.556	28.087	1.297	29.384	29.419	NA
	YP02	15.0	17.0	109,000	1068	NA	29.968	0.842	0.595	29.127	0.247	29.373	29.390	NA
	YP03	12.8	7.0	118,000	1081	NA	29.955	0.832	0.598	29.124	0.234	29.357	29.376	NA
	YP04	5.5	14.6	124,000	1091	NA	29.957	0.852	0.595	29.105	0.257	29.362	29.385	NA
	YP05	20.5	20.0	91,000	1045	1045	29.930	0.852	0.554	29.078	0.298	29.376	29.389	29.376
	YP10	20.5	20.0	88,000	1041		29.917	2.500	0.544	27.417	1.956	29.373	29.453	29.365
	YP11	12.7	1.3	103,000	1060	1059	29.945	0.839	0.604	29.106	0.235	29.341	29.355	29.341
	YP16	12.7	1.3	59,000	1015		29.941	2.260	0.555	27.681	1.705	29.386	29.412	29.315
	YP17	0.8	18.5	120,000	1085	1090	29.942	0.852	0.616	29.090	0.236	29.326	29.346	29.325
	YP22	0.8	18.5	114,000	1075		29.943	2.280	0.609	27.663	1.671	29.334	29.460	29.311
9/14/2005	BIB01	13.0	7.0	127,000	1096	NA	29.864	1.825	-0.148	28.038	1.973	30.011	30.200	NA
	BIB02	19.0	7.0	154,000	1144	1129	29.947	0.842	-0.085	29.105	0.927	30.032	30.165	30.044
	BIB08	19.0	7.0	140,000	1120		29.930	2.680	-0.064	27.250	2.744	29.994	30.324	29.973
	BIB09	10.7	1.3	156,000	1150	1111	29.960	0.842	-0.072	29.118	0.914	30.032	30.169	30.064
	BIB15	10.7	1.3	135,000	1113		29.951	2.580	NA	NA	NA	NA	NA	NA
	BIB16	10.4	11.4	132,000	1108	1100	29.947	0.842	-0.110	29.105	0.952	30.057	30.160	30.064
	BIB22	10.4	11.4	141,000	1121		29.933	2.600	-0.054	27.333	2.654	29.987	30.308	30.037
	YP01	11.0	13.0	98,000	1055	NA	29.940	1.853	-0.035	28.087	1.888	29.975	30.079	NA
	YP02	15.0	17.0	120,000	1084	NA	29.968	0.842	-0.004	29.127	0.846	29.972	30.043	NA
	YP03	12.8	7.0	124,000	1090	NA	29.955	0.832	0.001	29.124	0.831	29.954	30.029	NA
	YP04	5.5	14.6	126,000	1093	NA	29.957	0.852	-0.033	29.105	0.885	29.990	30.072	NA
	YP05	20.5	20.0	101,000	1058	1052	29.930	0.852	-0.021	29.078	0.873	29.951	30.002	29.956
	YP10	20.5	20.0	89,000	1041		29.917	2.500	-0.046	27.417	2.546	29.963	30.067	29.936
	YP11	12.7	1.3	116,000	1077	1086	29.945	0.839	0.008	29.106	0.831	29.937	30.001	29.930
	YP16	12.7	1.3	74,000	1027		29.941	2.260	-0.057	27.681	2.317	29.998	30.061	29.872
	YP17	0.8	18.5	125,000	1091	1092	29.942	0.852	-0.028	29.090	0.880	29.970	30.050	29.969
	YP22	0.8	18.5	129,000	1100		29.943	2.280	0.020	27.663	2.260	29.923	30.149	29.940

Table 6 Vertical Hydraulic Gradient

Well ID's (Shallow minus Deep)	Distance Between Shallow and Deep (m)	Difference in Environmental Water Head from Table 5 (m)					Vertical Hydraulic Gradient (+ down, - up)				
		6/20/2005	7/5/2005	7/27/2005	8/16/2005	9/14/2005	6/20/2005	7/5/2005	7/27/2005	8/16/2005	9/14/2005
BIB02 vs BIB08	1.84	-0.008	0.004	0.019	0.005	0.071	-4.3E-03	2.2E-03	1.0E-02	2.7E-03	3.9E-02
BIB09 vs BIB15	1.74	-0.001	0.000	0.017	0.017	NA	-5.7E-04	0.0E+00	9.8E-03	9.8E-03	NA
BIB16 vs BIB22	1.76	-0.025	-0.037	-0.005	0.008	0.027	-1.4E-02	-2.1E-02	-2.8E-03	4.5E-03	1.5E-02
YP05 vs YP10	1.68	-0.065	-0.059	-0.046	0.011	0.020	-3.9E-02	-3.5E-02	-2.7E-02	6.5E-03	1.2E-02
YP11 vs YP16	1.42	-0.078	-0.043	-0.058	0.026	0.058	-5.5E-02	-3.0E-02	-4.1E-02	1.8E-02	4.1E-02
YP17 vs YP22	1.43	-0.097	NA	-0.043	0.014	0.029	-6.8E-02	NA	-3.0E-02	9.8E-03	2.0E-02

Table 7 Bird Island Basin Apparent Resistivity and Measured Conductivity Correlation

Date	Well ID	Well Grid Location x (m)	Well Grid Location y (m)	Well Grid Location z (m)	Resistivity Measurement Grid Location x (m)	Resistivity Measurement Grid Location y (m)	Resistivity Measurement Grid Location z (m)	Apparent Bulk Resistivity ρ_o (ohm-m)	Apparent Pore Water Resistivity (35% porosity) ρ_{w35} (ohm-m)	Apparent Pore Water Conductivity (35% porosity) (uS/cm)	Apparent Pore Water Resistivity (45% porosity) ρ_{w45} (ohm-m)	Apparent Pore Water Conductivity (45% porosity) (uS/cm)	Measured Well Water Resistivity ρ_{wm} (ohm-m)	Measured Well Water Conductivity (uS/cm)	Estimated Porosity φ_m
6/20/2005	BIB01	13	5	-1.8	13.5	5.5	-1.9	0.217	0.050	200,653	0.071	141,138	0.067	150,000	0.43
	BIB04	19	5	-0.7	19.5	5.5	-0.6	0.239	0.055	181,779	0.078	127,862	NA	NA	NA
	BIB08	19	5	-2.7	19.5	5.5	-3.4	0.266	0.061	163,587	0.087	115,066	0.059	169,000	0.34
	BIB11	11	-0.5	-0.6	10.5	0.5	-0.6	0.277	0.064	156,860	0.091	110,334	0.071	140,000	0.38
	BIB14	11	-0.5	-2.1	10.5	0.5	-1.9	0.224	0.051	194,201	0.073	136,599	0.067	150,000	0.42
	BIB15	11	-0.5	-2.6	10.5	0.5	-3.4	0.252	0.058	172,614	0.082	121,416	0.067	150,000	0.39
	BIB18	11	9.5	-0.6	10.5	9.5	-0.6	0.224	0.051	194,374	0.073	136,721	NA	NA	NA
	BIB21	11	9.5	-2.1	10.5	9.5	-1.9	0.178	0.041	244,141	0.058	171,727	0.072	139,000	0.52
	BIB22	11	9.5	-2.6	10.5	9.5	-3.4	0.206	0.047	211,589	0.067	148,830	0.067	150,000	0.45
7/5/2005	BIB01	13	5	-1.8	13.5	5.5	-1.9	0.194	0.045	223,901	0.063	157,490	0.074	136,000	0.50
	BIB04	19	5	-0.7	19.5	5.5	-0.6	0.211	0.048	206,367	0.069	145,157	0.074	135,000	0.47
	BIB08	19	5	-2.7	19.5	5.5	-3.4	0.259	0.059	168,142	0.085	118,270	0.072	138,000	0.40
	BIB11	11	-0.5	-0.6	10.5	0.5	-0.6	0.266	0.061	163,219	0.087	114,807	0.081	123,000	0.43
	BIB14	11	-0.5	-2.1	10.5	0.5	-1.9	0.215	0.049	202,522	0.070	142,453	0.075	134,000	0.47
	BIB15	11	-0.5	-2.6	10.5	0.5	-3.4	0.248	0.057	175,683	0.081	123,574	0.078	128,000	0.44
	BIB18	11	9.5	-0.6	10.5	9.5	-0.6	0.193	0.044	225,410	0.063	158,551	0.080	125,000	0.53
	BIB21	11	9.5	-2.1	10.5	9.5	-1.9	0.192	0.044	226,113	0.063	159,046	0.087	115,000	0.57
	BIB22	11	9.5	-2.6	10.5	9.5	-3.4	0.231	0.053	188,313	0.075	132,458	0.074	135,000	0.44
7/28/2005	BIB01	13	5	-1.8	13.5	5.5	-1.9	0.204	0.047	213,354	0.067	150,072	0.065	153,000	0.44
	BIB04	19	5	-0.7	19.5	5.5	-0.6	0.248	0.057	175,399	0.081	123,375	0.063	159,000	0.38
	BIB08	19	5	-2.7	19.5	5.5	-3.4	0.224	0.051	194,548	0.073	136,844	0.063	158,000	0.41
	BIB11	11	-0.5	-0.6	10.5	0.5	-0.6	0.217	0.050	200,838	0.071	141,268	0.068	146,000	0.44
	BIB14	11	-0.5	-2.1	10.5	0.5	-1.9	0.181	0.042	240,628	0.059	169,256	0.060	167,000	0.45
	BIB15	11	-0.5	-2.6	10.5	0.5	-3.4	0.211	0.048	206,563	0.069	145,295	0.067	149,000	0.44
	BIB18	11	9.5	-0.6	10.5	9.5	-0.6	0.210	0.048	206,858	0.069	145,502	0.065	153,000	0.43
	BIB21	11	9.5	-2.1	10.5	9.5	-1.9	0.198	0.045	219,826	0.065	154,624	0.066	151,000	0.46
	BIB22	11	9.5	-2.6	10.5	9.5	-3.4	0.222	0.051	195,598	0.073	137,582	0.065	154,000	0.42
8/16/2005	BIB01	13	5	-1.8	13.5	5.5	-1.9	0.197	0.045	220,271	0.065	154,937	0.074	135,000	0.50
	BIB04	19	5	-0.7	19.5	5.5	-0.6	0.222	0.051	196,039	0.073	137,893	0.069	145,000	0.43
	BIB08	19	5	-2.7	19.5	5.5	-3.4	0.241	0.055	180,272	0.079	126,802	0.068	146,000	0.41
	BIB11	11	-0.5	-0.6	10.5	0.5	-0.6	0.248	0.057	175,046	0.081	123,126	0.076	131,000	0.43
	BIB14	11	-0.5	-2.1	10.5	0.5	-1.9	0.204	0.047	212,728	0.067	149,631	0.067	150,000	0.45
	BIB15	11	-0.5	-2.6	10.5	0.5	-3.4	0.230	0.053	189,132	0.075	133,034	0.073	137,000	0.44
	BIB18	11	9.5	-0.6	10.5	9.5	-0.6	0.218	0.050	199,457	0.071	140,296	0.075	134,000	0.47
	BIB21	11	9.5	-2.1	10.5	9.5	-1.9	0.189	0.043	230,305	0.062	161,995	0.078	128,000	0.53
	BIB22	11	9.5	-2.6	10.5	9.5	-3.4	0.210	0.048	207,252	0.069	145,780	0.073	137,000	0.47
							Average	**0.221**	**0.051**	**198,988**	**0.072**	**139,967**	**0.071**	**142,647**	**0.45**

Constants include a Coefficient of Saturation of 1.0 and a Cementation Factor of 1.4

Table 8 Yarborough Pass Apparent Resistivity and Measured Conductivity Correlation

Date	Well ID	Well Grid Location x (m)	y (m)	z (m)	Resistivity Measurement Grid Location x (m)	y (m)	z (m)	Apparent Bulk Resistivity ρ_o (ohm-m)	Apparent Pore Water Resistivity (35% porosity) $\rho_{\omega 35}$ (ohm-m)	Apparent Pore Water Conductivity (35% porosity) (uS/cm)	Apparent Pore Water Resistivity (40% porosity) $\rho_{\omega 45}$ (ohm-m)	Apparent Pore Water Conductivity (40% porosity) (uS/cm)	Measured Well Water Resistivity $\rho_{\omega m}$ (ohm-m)	Measured Well Water Conductivity (uS/cm)	Estimated Porosity φ_m
5/22/2005	YP01	13	5	-1.9	13.5	5.5	-1.9	0.399	0.092	109,113	0.110	90,508	0.063	157,500	0.27
	YP02	9	9	-0.8	9.5	9.5	-0.6	0.445	0.102	97,711	0.123	81,051	0.067	149,900	0.26
	YP03	19	6.5	-0.8	19.5	6.5	-0.6	0.400	0.092	108,677	0.111	90,146	0.067	148,900	0.28
	YP04	12	-0.5	-0.9	11.5	0.5	-0.6	0.395	0.091	110,080	0.110	91,310	0.067	149,700	0.28
6/20/2005	YP01	13	5	-1.9	13.5	5.5	-1.9	0.377	0.087	115,274	0.105	95,619	0.100	100,100	0.39
	YP02	9	9	-0.8	9.5	9.5	-0.6	0.390	0.090	111,577	0.108	92,552	0.090	111,200	0.35
	YP03	19	6.5	-0.8	19.5	6.5	-0.6	0.399	0.092	109,058	0.111	90,463	0.093	107,600	0.35
	YP04	12	-0.5	-0.9	11.5	0.5	-0.6	0.356	0.082	122,276	0.099	101,427	0.081	122,800	0.35
	YP11	25	6.5	-0.8	24.5	6.5	-0.6	0.399	0.092	109,004	0.111	90,417	0.103	96,860	0.38
	YP16	25	6.5	-2.3	24.5	6.5	-1.9	0.431	0.099	101,002	0.119	83,780	0.163	61,460	0.50
7/5/2005	YP01	13	5	-1.9	13.5	5.5	-1.9	0.336	0.077	129,448	0.093	107,376	0.130	76,830	0.51
	YP02	9	9	-0.8	9.5	9.5	-0.6	0.403	0.093	108,029	0.112	89,609	0.095	105,000	0.36
	YP03	19	6.5	-0.8	19.5	6.5	-0.6	0.363	0.084	119,718	0.101	99,305	0.087	115,600	0.36
	YP04	12	-0.5	-0.9	11.5	0.5	-0.6	0.384	0.088	113,351	0.106	94,024	0.081	123,200	0.33
	YP11	25	6.5	-0.8	24.5	6.5	-0.6	0.337	0.078	128,987	0.093	106,993	0.108	92,300	0.44
	YP16	25	6.5	-2.3	24.5	6.5	-1.9	0.366	0.084	118,802	0.101	98,545	0.175	57,150	0.59
7/27/2005	YP01	13	5	-1.9	13.5	5.5	-1.9	0.324	0.074	134,327	0.090	111,423	0.130	77,060	0.52
	YP02	9	9	-0.8	9.5	9.5	-0.6	0.365	0.084	119,225	0.101	98,896	0.088	113,700	0.36
	YP03	19	6.5	-0.8	19.5	6.5	-0.6	0.367	0.084	118,446	0.102	98,250	0.083	120,500	0.35
	YP04	12	-0.5	-0.9	11.5	0.5	-0.6	0.386	0.089	112,617	0.107	93,415	0.079	126,400	0.32
	YP11	25	6.5	-0.8	24.5	6.5	-0.6	0.396	0.091	109,830	0.110	91,103	0.091	109,800	0.35
	YP16	25	6.5	-2.3	24.5	6.5	-1.9	0.473	0.109	91,966	0.131	76,285	0.167	60,000	0.47
8/16/2005	YP01	13	5	-1.9	13.5	5.5	-1.9	0.333	0.077	130,458	0.092	108,213	0.135	74,000	0.52
	YP02	9	9	-0.8	9.5	9.5	-0.6	0.378	0.087	115,183	0.105	95,543	0.092	109,000	0.36
	YP03	19	6.5	-0.8	19.5	6.5	-0.6	0.363	0.083	119,817	0.101	99,387	0.085	118,000	0.35
	YP04	12	-0.5	-0.9	11.5	0.5	-0.6	0.281	0.065	154,794	0.078	128,400	0.081	124,000	0.41
	YP11	25	6.5	-0.8	24.5	6.5	-0.6	0.328	0.075	132,485	0.091	109,895	0.097	103,000	0.42
	YP16	25	6.5	-2.3	24.5	6.5	-1.9	0.334	0.077	130,340	0.092	108,116	0.169	59,000	0.62
							Average	**0.375**	**0.086**	**117,200**	**0.104**	**97,216**	**0.102**	**106,091**	**0.40**

Constants include a Coefficient of Saturation of 1.0 and a Cementation Factor of 1.4

Table 9 Rayleigh Numbers for Mixed Convection

Well Nest	Date	Well ID	Depth to Screen (m)	Specific Conductivity (uS/cm)	Bottom Fluid Concentration C_1 (uS/cm)	Top Fluid Concentration C_2 (uS/cm)	Concentration Difference [mass fraction] ΔC (unitless)	Depth of Porous Layer H (m)	Porosity (ε)	Hydraulic Gradient I (unitless)	Ambient velocity V_{amb} (m/s)	Rayleigh Number Ra (unitless)
BIB02-08	6/20/2005	BIB03	0.18									
		BIB04	0.68									
		BIB02	0.84	148,000								
		BIB05	1.18	145,000	145,000	148,000	0.010	0.34	0.45	7.10E-03	4.47E-07	0.15
		BIB06	1.68	145,000	145,000	145,000	0.000	0.50	0.45	7.10E-03	4.47E-07	0.00
		BIB07	2.18									
		BIB08	2.68	169,000	169,000	145,000	-0.076	1.00	0.45	7.10E-03	4.47E-07	-3.35
	7/5/2005	BIB03	0.18									
		BIB04	0.68	135,000								
		BIB02	0.84	128,000	128,000	135,000	0.027	0.34	0.45	3.60E-03	2.27E-07	0.78
		BIB05	1.18	130,000	130,000	128,000	-0.008	0.50	0.45	3.60E-03	2.27E-07	-0.33
		BIB06	1.68									
		BIB07	2.18									
		BIB08	2.68	138,000	138,000	130,000	-0.030	1.5	0.45	3.60E-03	2.27E-07	-3.87
	7/27/2005	BIB03	0.18									
		BIB04	0.68	159,000								
		BIB02	0.84	155,000	155,000	159,000	0.013	0.34	0.45	2.10E-03	1.32E-07	0.64
		BIB05	1.18	158,000	158,000	155,000	-0.010	0.50	0.45	2.10E-03	1.32E-07	-0.71
		BIB06	1.68									
		BIB07	2.18									
		BIB08	2.68	158,000	158,000	158,000	0.000	1.5	0.45	2.10E-03	1.32E-07	0.00
	8/16/2005	BIB03	0.18									
		BIB04	0.68	145,000								
		BIB02	0.84	135,000	135,000	145,000	0.036	0.34	0.45	4.80E-04	3.02E-08	7.82
		BIB05	1.18	147,000	147,000	135,000	-0.043	0.50	0.45	4.80E-04	3.02E-08	-13.70
		BIB06	1.68									
		BIB07	2.18									
		BIB08	2.68	146,000	146,000	147,000	0.003	1.5	0.45	4.80E-04	3.02E-08	3.30
	9/14/2005	BIB03	0.18	150,000								
		BIB04	0.68	146,000	146,000	150,000	0.014	0.5	0.45	1.20E-03	7.56E-08	1.75
		BIB02	0.84	154,000	154,000	146,000	-0.027	0.34	0.45	1.20E-03	7.56E-08	-2.34
		BIB05	1.18	145,000	145,000	154,000	0.030	0.50	0.45	1.20E-03	7.56E-08	3.89
		BIB06	1.68									
		BIB07	2.18									
		BIB08	2.68	140,000	140,000	145,000	0.018	1.5	0.45	1.20E-03	7.56E-08	6.80

Table 9 Rayleigh Numbers for Mixed Convection Continued

Well Nest	Date	Well ID	Depth to Screen (m)	Specific Conductivity (uS/cm)	Bottom Fluid Concentration C_1 (uS/cm)	Top Fluid Concentration C_2 (uS/cm)	Concentration Difference [mass fraction] ΔC (unitless)	Depth of Porous Layer H (m)	Porosity (ε)	Hydraulic Gradient I (unitless)	Ambient velocity V_{amb} (m/s)	Rayleigh Number Ra (unitless)
BIB09-15	6/20/2005	BIB10	0.08									
		BIB11	0.58	140,000								
		BIB09	0.84	180,000	180,000	140,000	-0.125	0.26	0.45	7.10E-03	4.47E-07	-1.42
		BIB12	1.08	135,000	135,000	180,000	0.143	0.24	0.45	7.10E-03	4.47E-07	1.50
		BIB13	1.58	140,000	140,000	135,000	-0.018	0.5	0.45	7.10E-03	4.47E-07	-0.40
		BIB14	2.08	150,000	150,000	140,000	-0.034	0.5	0.45	7.10E-03	4.47E-07	-0.76
		BIB15	2.58	150,000	150,000	150,000	0.000	0.5	0.45	7.10E-03	4.47E-07	0.00
	7/5/2005	BIB10	0.08									
		BIB11	0.58	123,000								
		BIB09	0.84									
		BIB12	1.08	127,000	127,000	123,000	-0.016	0.5	0.45	3.60E-03	2.27E-07	-0.69
		BIB13	1.58	135,000	135,000	127,000	-0.031	0.5	0.45	3.60E-03	2.27E-07	-1.32
		BIB14	2.08	134,000	134,000	135,000	0.004	0.5	0.45	3.60E-03	2.27E-07	0.16
		BIB15	2.58	128,000	128,000	134,000	0.023	0.5	0.45	3.60E-03	2.27E-07	0.99
	7/28/2005	BIB10	0.08									
		BIB11	0.58	146,000								
		BIB09	0.84	160,000	160,000	146,000	-0.046	0.26	0.45	2.10E-03	1.32E-07	-1.76
		BIB12	1.08	161,000	161,000	160,000	-0.003	0.24	0.45	2.10E-03	1.32E-07	-0.11
		BIB13	1.58	165,000	165,000	161,000	-0.012	0.5	0.45	2.10E-03	1.32E-07	-0.91
		BIB14	2.08	167,000	167,000	165,000	-0.006	0.5	0.45	2.10E-03	1.32E-07	-0.45
		BIB15	2.58	149,000	149,000	167,000	0.057	0.5	0.45	2.10E-03	1.32E-07	4.21
	8/16/2005	BIB10	0.08									
		BIB11	0.58	131,000								
		BIB09	0.84	144,000	144,000	131,000	-0.047	0.26	0.45	4.80E-04	3.02E-08	-7.91
		BIB12	1.08	148,000	148,000	144,000	-0.014	0.24	0.45	4.80E-04	3.02E-08	-2.12
		BIB13	1.58	150,000	150,000	148,000	-0.007	0.5	0.45	4.80E-04	3.02E-08	-2.16
		BIB14	2.08	150,000	150,000	150,000	0.000	0.5	0.45	4.80E-04	3.02E-08	0.00
		BIB15	2.58	137,000	137,000	150,000	0.045	0.5	0.45	4.80E-04	3.02E-08	14.58
	9/14/2005	BIB10	0.08	71,000								
		BIB11	0.58	134,000	134,000	71,000	-0.307	0.5	0.45	1.20E-03	7.56E-08	-39.73
		BIB09	0.84	156,000	156,000	134,000	-0.076	0.26	0.45	1.20E-03	7.56E-08	-5.10
		BIB12	1.08	147,000	147,000	156,000	0.030	0.24	0.45	1.20E-03	7.56E-08	1.84
		BIB13	1.58	147,000	147,000	147,000	0.000	0.5	0.45	1.20E-03	7.56E-08	0.00
		BIB14	2.08	146,000	146,000	147,000	0.003	0.5	0.45	1.20E-03	7.56E-08	0.44
		BIB15	2.58	135,000	135,000	146,000	0.039	0.5	0.45	1.20E-03	7.56E-08	5.06

Table 9 Rayleigh Numbers for Mixed Convection Continued

Well Nest	Date	Well ID	Depth to Screen (m)	Specific Conductivity (uS/cm)	Bottom Fluid Concentration C_1 (uS/cm)	Top Fluid Concentration C_2 (uS/cm)	Concentration Difference [mass fraction] ΔC (unitless)	Depth of Porous Layer H (m)	Porosity (ε)	Hydraulic Gradient I (unitless)	Ambient velocity V_{amb} (m/s)	Rayleigh Number Ra (unitless)
BIB16-22	6/20/2005	BIB17	0.1									
		BIB18	0.6									
		BIB16	0.84	150,000								
		BIB19	1.1	139,000	139,000	150,000	0.038	0.26	0.45	7.10E-03	4.47E-07	0.43
		BIB20	1.6	149,000	149,000	139,000	-0.035	0.5	0.45	7.10E-03	4.47E-07	-0.76
		BIB21	2.1	139,000	139,000	149,000	0.035	0.5	0.45	7.10E-03	4.47E-07	0.76
		BIB22	2.6	150,000	150,000	139,000	-0.038	0.5	0.45	7.10E-03	4.47E-07	-0.83
	7/5/2005	BIB17	0.1									
		BIB18	0.6	125,000								
		BIB16	0.84	118,000	118,000	125,000	0.029	0.24	0.45	3.60E-03	2.27E-07	0.60
		BIB19	1.1	123,000	123,000	118,000	-0.021	0.26	0.45	3.60E-03	2.27E-07	-0.47
		BIB20	1.6	121,000	121,000	123,000	0.008	0.5	0.45	3.60E-03	2.27E-07	0.35
		BIB21	2.1	115,000	115,000	121,000	0.025	0.5	0.45	3.60E-03	2.27E-07	1.10
		BIB22	2.6	135,000	135,000	115,000	-0.080	0.5	0.45	3.60E-03	2.27E-07	-3.45
	7/28/2005	BIB17	0.1									
		BIB18	0.6	153,000								
		BIB16	0.84	149,000	149,000	153,000	0.013	0.24	0.45	2.10E-03	1.32E-07	0.47
		BIB19	1.1	156,000	156,000	149,000	-0.023	0.26	0.45	2.10E-03	1.32E-07	-0.88
		BIB20	1.6	157,000	157,000	156,000	-0.003	0.5	0.45	2.10E-03	1.32E-07	-0.24
		BIB21	2.1	151,000	151,000	157,000	0.019	0.5	0.45	2.10E-03	1.32E-07	1.44
		BIB22	2.6	154,000	154,000	151,000	-0.010	0.5	0.45	2.10E-03	1.32E-07	-0.73
	8/16/2005	BIB17	0.1									
		BIB18	0.6	134,000								
		BIB16	0.84	127,000	127,000	134,000	0.027	0.24	0.45	4.80E-04	3.02E-08	4.14
		BIB19	1.1	140,000	140,000	127,000	-0.049	0.26	0.45	4.80E-04	3.02E-08	-8.15
		BIB20	1.6	135,000	135,000	140,000	0.018	0.5	0.45	4.80E-04	3.02E-08	5.85
		BIB21	2.1	128,000	128,000	135,000	0.027	0.5	0.45	4.80E-04	3.02E-08	8.57
		BIB22	2.6	137,000	137,000	128,000	-0.034	0.5	0.45	4.80E-04	3.02E-08	-10.93
	9/14/2005	BIB17	0.1	95,000								
		BIB18	0.6	138,000	138,000	95,000	-0.185	0.5	0.45	1.20E-03	7.56E-08	-23.86
		BIB16	0.84	132,000	132,000	138,000	0.022	0.24	0.45	1.20E-03	7.56E-08	1.38
		BIB19	1.1	133,000	133,000	132,000	-0.004	0.26	0.45	1.20E-03	7.56E-08	-0.25
		BIB20	1.6	132,000	132,000	133,000	0.004	0.5	0.45	1.20E-03	7.56E-08	0.49
		BIB21	2.1	130,000	130,000	132,000	0.008	0.5	0.45	1.20E-03	7.56E-08	0.99
		BIB22	2.6	141,000	141,000	130,000	-0.041	0.5	0.45	1.20E-03	7.56E-08	-5.25

Table 9 Rayleigh Numbers for Mixed Convection Continued

Well Nest	Date	Well ID	Depth to Screen (m)	Specific Conductivity (uS/cm)	Bottom Fluid Concentration C_1 (uS/cm)	Top Fluid Concentration C_2 (uS/cm)	Concentration Difference [mass fraction] ΔC (unitless)	Depth of Porous Layer H (m)	Porosity (ε)	Hydraulic Gradient I (unitless)	Ambient velocity V_{amb} (m/s)	Rayleigh Number Ra (unitless)
YP05-10	6/20/2005	YP06	0.5	82,600								
		YP05	0.82	93,800	93,800	82,600	-0.063	0.32	0.40	3.90E-03	2.46E-07	-1.82
		YP07	1	89,200	89,200	93,800	0.025	0.18	0.40	3.90E-03	2.46E-07	0.41
		YP08	1.5	57,300	57,300	89,200	0.218	0.5	0.40	3.90E-03	2.46E-07	9.76
		YP09	2	60,800	60,800	57,300	-0.030	0.5	0.40	3.90E-03	2.46E-07	-1.33
		YP10	2.5	86,700	86,700	60,800	-0.176	0.5	0.40	3.90E-03	2.46E-07	-7.87
	7/5/2005	YP06	0.5	87,600								
		YP05	0.82	87,800	87,800	87,600	-0.001	0.32	0.40	9.30E-04	5.86E-08	-0.14
		YP07	1	84,200	84,200	87,800	0.021	0.18	0.40	9.30E-04	5.86E-08	1.41
		YP08	1.5	65,100	65,100	84,200	0.128	0.5	0.40	9.30E-04	5.86E-08	23.99
		YP09	2	63,500	63,500	65,100	0.012	0.5	0.40	9.30E-04	5.86E-08	2.33
		YP10	2.5	87,800	87,800	63,500	-0.161	0.5	0.40	9.30E-04	5.86E-08	-30.12
	7/27/2005	YP06	0.5	90,700								
		YP05	0.82	93,400	93,400	90,700	-0.015	0.32	0.40	6.70E-03	4.22E-07	-0.25
		YP07	1	99,000	99,000	93,400	-0.029	0.18	0.40	6.70E-03	4.22E-07	-0.27
		YP08	1.5	70,500	70,500	99,000	0.168	0.5	0.40	6.70E-03	4.22E-07	4.39
		YP09	2	70,600	70,600	70,500	-0.001	0.5	0.40	6.70E-03	4.22E-07	-0.02
		YP10	2.5	88,400	88,400	70,600	-0.112	0.5	0.40	6.70E-03	4.22E-07	-2.92
	8/16/2005	YP06	0.5	102,000								
		YP05	0.82	91,000	91,000	102,000	0.057	0.32	0.40	2.30E-03	1.45E-07	2.77
		YP07	1	98,000	98,000	91,000	-0.037	0.18	0.40	2.30E-03	1.45E-07	-1.01
		YP08	1.5	98,000	98,000	98,000	0.000	0.5	0.40	2.30E-03	1.45E-07	0.00
		YP09	2	62,000	62,000	98,000	0.225	0.5	0.40	2.30E-03	1.45E-07	17.10
		YP10	2.5	88,000	88,000	62,000	-0.173	0.5	0.40	2.30E-03	1.45E-07	-13.17
	9/14/2005	YP06	0.5	101,000								
		YP05	0.82	101,000	101,000	101,000	0.000	0.32	0.40	2.70E-03	1.70E-07	0.00
		YP07	1	106,000	106,000	101,000	-0.024	0.18	0.40	2.70E-03	1.70E-07	-0.56
		YP08	1.5	105,000	105,000	106,000	0.005	0.5	0.40	2.70E-03	1.70E-07	0.31
		YP09	2	75,000	75,000	105,000	0.167	0.5	0.40	2.70E-03	1.70E-07	10.79
		YP10	2.5	89,000	89,000	75,000	-0.085	0.5	0.40	2.70E-03	1.70E-07	-5.53

Table 9 Rayleigh Numbers for Mixed Convection Continued

Well Nest	Date	Well ID	Depth to Screen (m)	Specific Conductivity (uS/cm)	Bottom Fluid Concentration C_1 (uS/cm)	Top Fluid Concentration C_2 (uS/cm)	Concentration Difference [mass fraction] ΔC (unitless)	Depth of Porous Layer H (m)	Porosity (ε)	Hydraulic Gradient I (unitless)	Ambient velocity V_{amb} (m/s)	Rayleigh Number Ra (unitless)
YP11-16	6/20/2005	YP12	0.26									
		YP13	0.76	66,500								
		YP11	0.84	96,860	96,860	66,500	-0.186	0.08	0.40	3.90E-03	2.46E-07	-1.33
		YP14	1.26	68,120	68,120	96,860	0.174	0.42	0.40	3.90E-03	2.46E-07	6.56
		YP15	1.76									
		YP16	2.26	61,460	61,460	68,120	0.051	1.00	0.40	3.90E-03	2.46E-07	4.61
	7/5/2005	YP12	0.26									
		YP13	0.76	59,900								
		YP11	0.84	92,300	92,300	59,900	-0.213	0.08	0.40	9.30E-04	5.86E-08	-6.39
		YP14	1.26	92,470	92,470	92,300	-0.001	0.42	0.40	9.30E-04	5.86E-08	-0.14
		YP15	1.76									
		YP16	2.26	57,150	57,150	92,470	0.236	1.00	0.40	9.30E-04	5.86E-08	88.54
	7/27/2005	YP12	0.26									
		YP13	0.76	98,300								
		YP11	0.84	109,800	109,800	98,300	-0.055	0.08	0.40	6.70E-03	4.22E-07	-0.23
		YP14	1.26	135,000	135,000	109,800	-0.103	0.42	0.40	6.70E-03	4.22E-07	-2.26
		YP15	1.76									
		YP16	2.26	60,000	60,000	135,000	0.385	1.00	0.40	6.70E-03	4.22E-07	20.08
	8/16/2006	YP12	0.26									
		YP13	0.76	119,000								
		YP11	0.84	103,000	103,000	119,000	0.072	0.08	0.40	2.30E-03	1.45E-07	0.88
		YP14	1.26	124,000	124,000	103,000	-0.093	0.42	0.40	2.30E-03	1.45E-07	-5.90
		YP15	1.76									
		YP16	2.26	59,000	59,000	124,000	0.355	1.00	0.40	2.30E-03	1.45E-07	53.98
	9/16/2005	YP12	0.26	114,000								
		YP13	0.76	128,000	128,000	114,000	-0.058	0.5	0.40	2.70E-03	1.70E-07	-3.75
		YP11	0.84	116,000	116,000	128,000	0.049	0.08	0.40	2.70E-03	1.70E-07	0.51
		YP14	1.26	147,000	147,000	116,000	-0.118	0.42	0.40	2.70E-03	1.70E-07	-6.41
		YP15	1.76	132,000	132,000	147,000	0.054	0.5	0.40	2.70E-03	1.70E-07	3.48
		YP16	2.26	74,000	74,000	132,000	0.282	0.5	0.40	2.70E-03	1.70E-07	18.23

Table 9 Rayleigh Numbers for Mixed Convection Continued

Well Nest	Date	Well ID	Depth to Screen (m)	Specific Conductivity (uS/cm)	Bottom Fluid Concentration C_1 (uS/cm)	Top Fluid Concentration C_2 (uS/cm)	Concentration Difference [mass fraction] ΔC (unitless)	Depth of Porous Layer H (m)	Porosity (ε)	Hydraulic Gradient I (unitless)	Ambient velocity V_{amb} (m/s)	Rayleigh Number Ra (unitless)
YP17-22	6/20/2005	YP18	0.28	64,050								
		YP19	0.78	116,000	116,000	64,050	-0.289	0.5	0.40	3.90E-03	2.46E-07	-12.94
		YP17	0.85	107,500	107,500	116,000	0.038	0.07	0.40	3.90E-03	2.46E-07	0.24
		YP20	1.28	116,000	116,000	107,500	-0.038	0.43	0.40	3.90E-03	2.46E-07	-1.47
		YP21	1.78	110,000	110,000	116,000	0.027	0.5	0.40	3.90E-03	2.46E-07	1.19
		YP22	2.28	117,800	117,800	110,000	-0.034	0.5	0.40	3.90E-03	2.46E-07	-1.54
	7/5/2005	YP18	0.28	75,800								
		YP19	0.78	115,000	115,000	75,800	-0.205	0.5	0.40	9.30E-04	5.86E-08	-38.53
		YP17	0.85	106,700	106,700	115,000	0.037	0.07	0.40	9.30E-04	5.86E-08	0.98
		YP20	1.28	116,400	116,400	106,700	-0.043	0.43	0.40	9.30E-04	5.86E-08	-7.01
		YP21	1.78	118,500	118,500	116,400	-0.009	0.5	0.40	9.30E-04	5.86E-08	-1.68
		YP22	2.28	105,700	105,700	118,500	0.057	0.5	0.40	9.30E-04	5.86E-08	10.71
	7/27/2005	YP18	0.28	83,300								
		YP19	0.78	121,500	121,500	83,300	-0.187	0.5	0.40	6.70E-03	4.22E-07	-4.87
		YP17	0.85	124,000	124,000	121,500	-0.010	0.07	0.40	6.70E-03	4.22E-07	-0.04
		YP20	1.28	141,000	141,000	124,000	-0.064	0.43	0.40	6.70E-03	4.22E-07	-1.44
		YP21	1.78	113,000	113,000	141,000	0.110	0.5	0.40	6.70E-03	4.22E-07	2.88
		YP22	2.28	111,000	111,000	113,000	0.009	0.5	0.40	6.70E-03	4.22E-07	0.23
	8/16/2005	YP18	0.28	96,000								
		YP19	0.78	125,000	125,000	96,000	-0.131	0.5	0.40	2.30E-03	1.45E-07	-9.97
		YP17	0.85	120,000	120,000	125,000	0.020	0.07	0.40	2.30E-03	1.45E-07	0.22
		YP20	1.28	139,000	139,000	120,000	-0.073	0.43	0.40	2.30E-03	1.45E-07	-4.79
		YP21	1.78	139,000	139,000	139,000	0.000	0.5	0.40	2.30E-03	1.45E-07	0.00
		YP22	2.28	114,000	114,000	139,000	0.099	0.5	0.40	2.30E-03	1.45E-07	7.51
	9/14/2005	YP18	0.28	105,000								
		YP19	0.78	120,000	120,000	105,000	-0.067	0.5	0.40	2.70E-03	1.70E-07	-4.32
		YP17	0.85	125,000	125,000	120,000	-0.020	0.07	0.40	2.70E-03	1.70E-07	-0.18
		YP20	1.28	135,000	135,000	125,000	-0.038	0.43	0.40	2.70E-03	1.70E-07	-2.14
		YP21	1.78	134,000	134,000	135,000	0.004	0.5	0.40	2.70E-03	1.70E-07	0.24
		YP22	2.28	129,000	129,000	134,000	0.019	0.5	0.40	2.70E-03	1.70E-07	1.23

Table 9 Rayleigh Numbers for Mixed Convection Continued

Rayleigh Number Mixed Convection Constants	Value	Source
Gravity (*g*)	9.81 m/s^2	Assumed sea level
Hydraulic Conductivity (*K*)	6.30 X 10^{-5} m/s	Average from Table 1
Dynamic Viscosity (μ)	0.001 kg/m-s	Assumed for freshwater
Density (ρ)	1000 kg/m^2	Assumed for freshwater
Coefficient of Fluid Density Change ($\delta\rho/\delta C$)	700 kg/m^3	Assumed for seawater (Simmons and Narayan, 1997)
Linear Expansion Coefficient (β)	0.7	Calculated from ρ and $\delta\rho/\delta C$
Kinematic Viscosity (*v*)	1 X 10^{-6} kg/m-s	Calculated from ρ and μ
Molecular Diffusivity (*D*)	1 X 10^{-9} m^2/s	Sharp, et al., 2001
Transverse Dispersivity (α)	5 m	Simmons and Narayan, 1997

Table 10 Nield Critical Rayleigh Numbers

Lower Boundary Pressure	Upper Boundary Pressure	Lower Boundary Temperature	Upper Boundary Temperature	Critical Rayleigh Number
No Flow	No Flow	Const. Temp	Const. Temp	$4\pi^2 \approx 40$
No Flow	No Flow	Const. Temp	Const. Flux	27.1
No Flow	No Flow	Const. Flux	Const. Flux	12
No Flow	Constant	Const. Temp	Const. Temp	27.1
No Flow	Constant	Const. Flux	Const. Temp	17.65
No Flow	Constant	Const. Temp	Const. Flux	9.87
No Flow	Constant	Const. Flux	Const. Flux	3
Constant	Constant	Any	Any	0

(After Nield, 1968)

Appendix B Figures

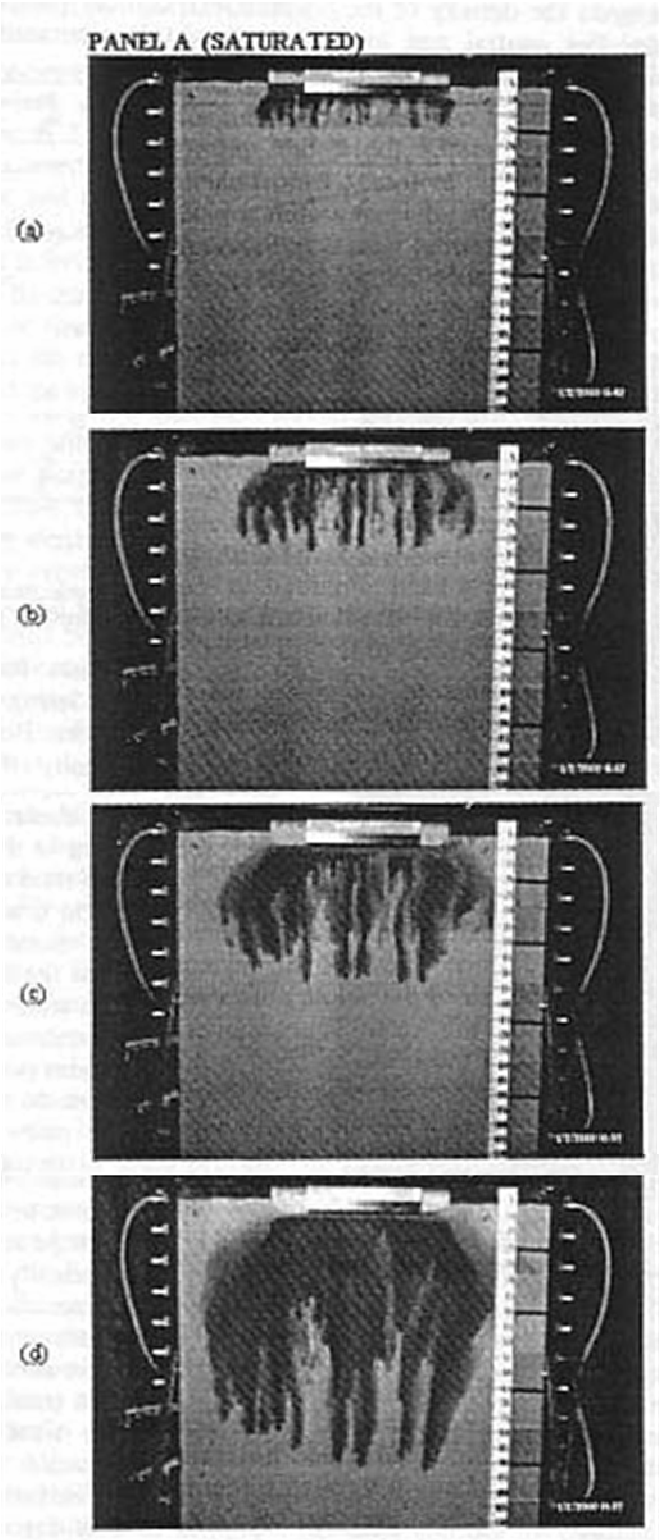

Simmons et al., 2001

Figure 1 Sand Tank Experiment of Density-Driven Free Convection

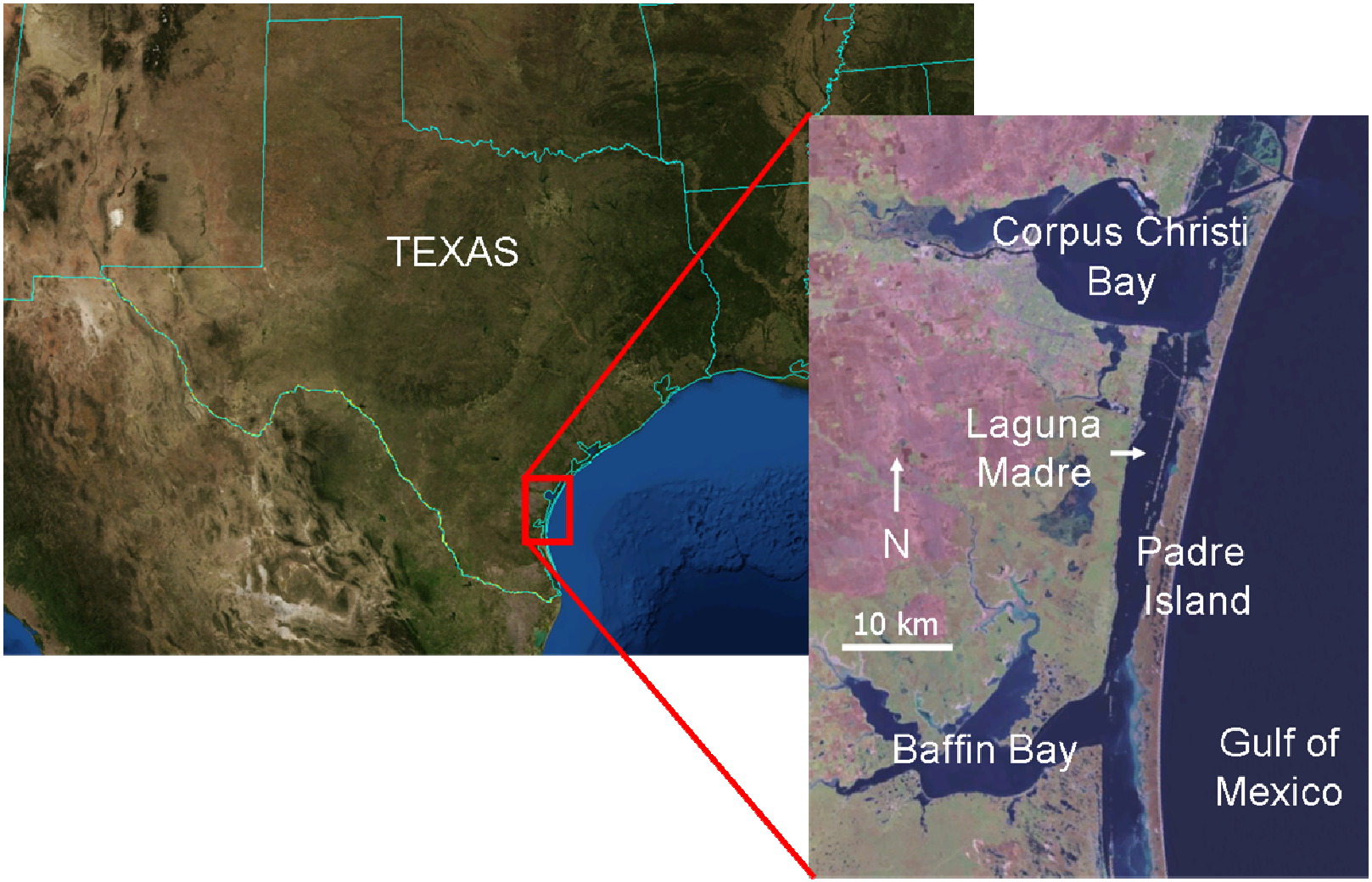

Figure 2 Location of Padre Island, Texas

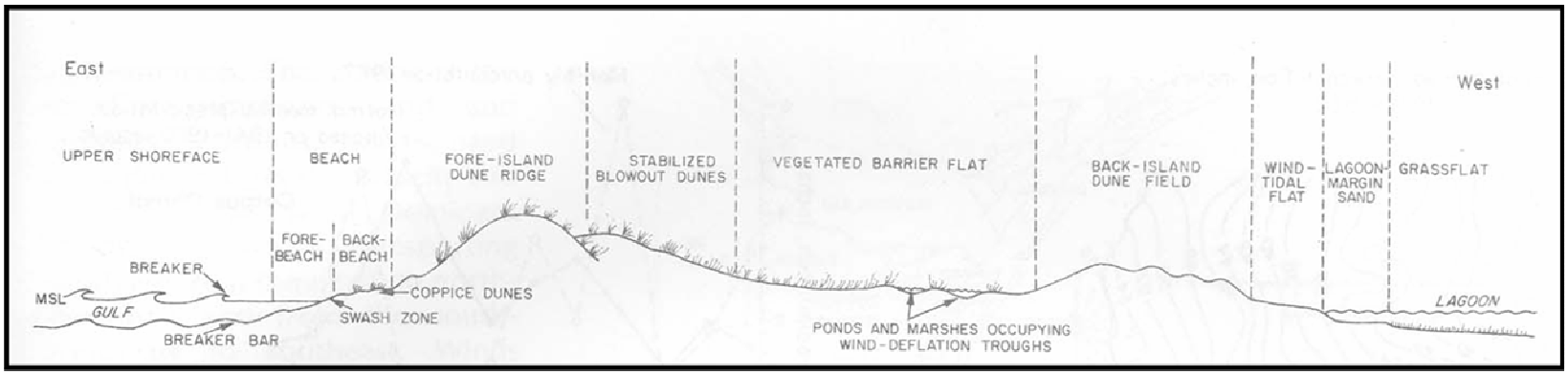

Figure 3 Padre Island Topography Cross-Section

At both the Bird Island Basin and Yarborough Pass sites the back-island dune field is not present. The Bird Island Basin site is in the Wind-Tidal Flat province and the Yarborough Pass site is at the margin between the Vegetated Barrier Flat and the Wind-Tidal Flat province. Illustration by McGowen, 1977 modifed by Wiese and White, 1980.

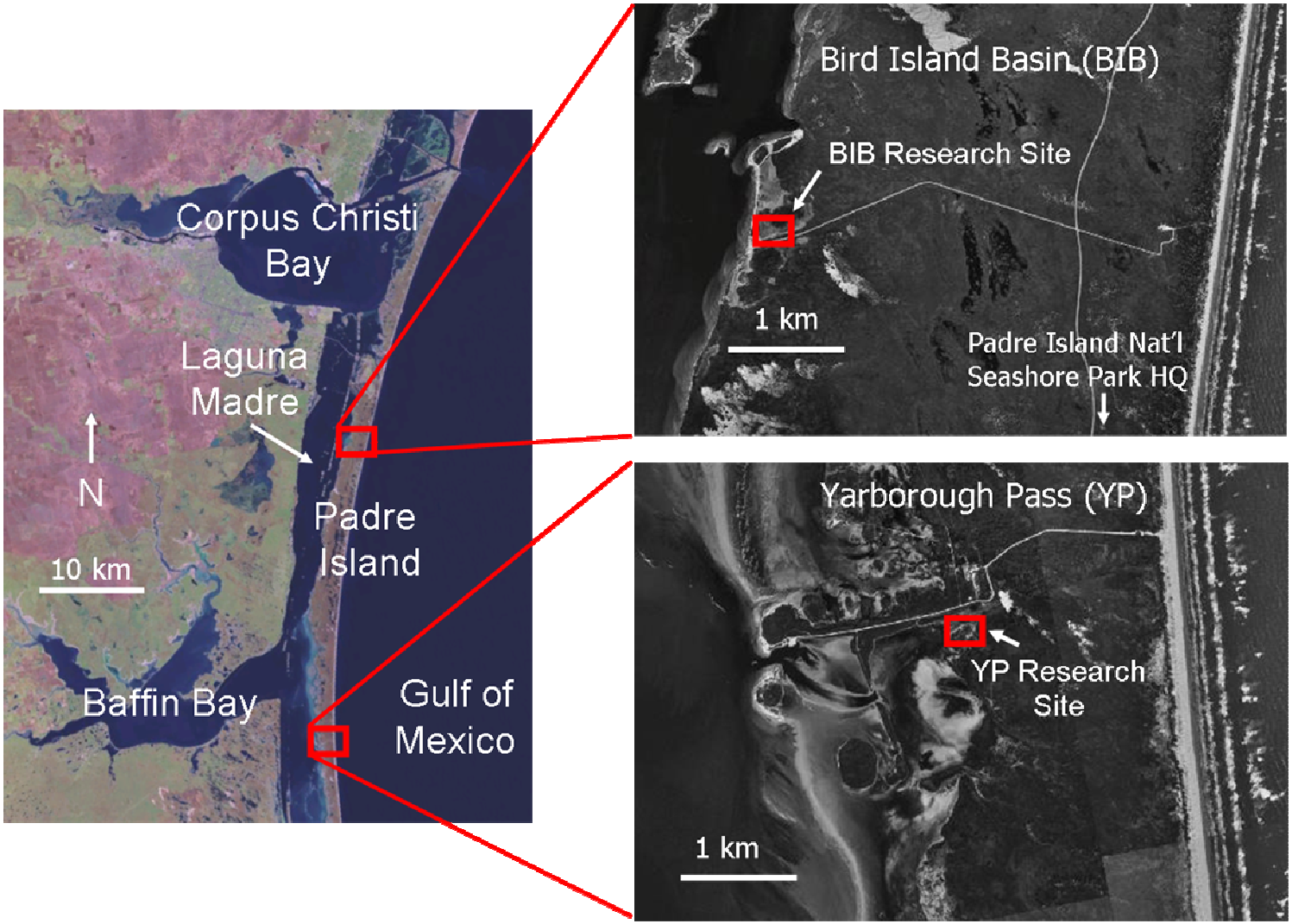

Figure 4 Locations of Research Sites

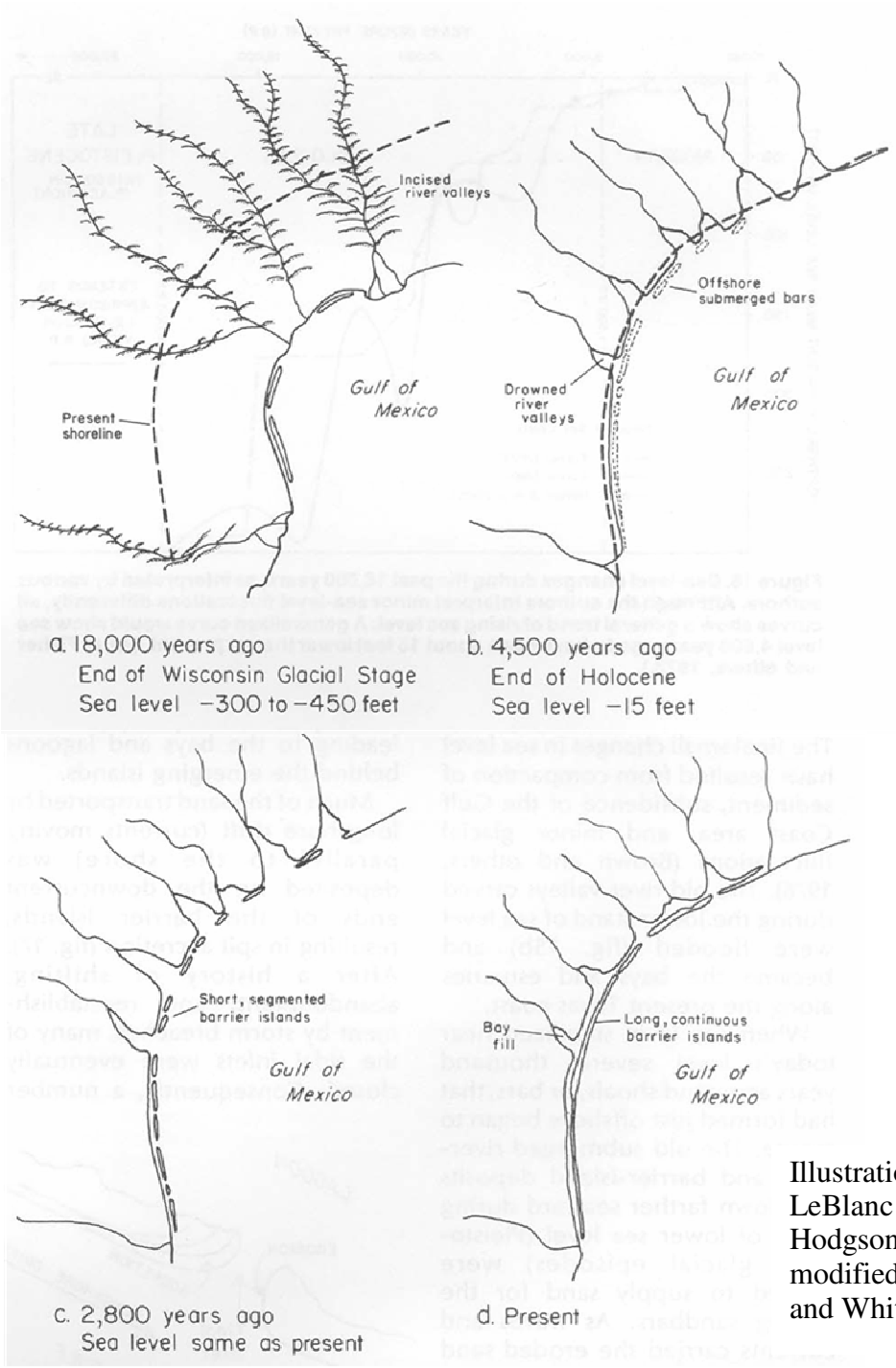

Illustration by LeBlanc and Hodgson, 1959 modified by Wiese and White, 1980.

Figure 5 Historic Coastline of the Texas Gulf Coast

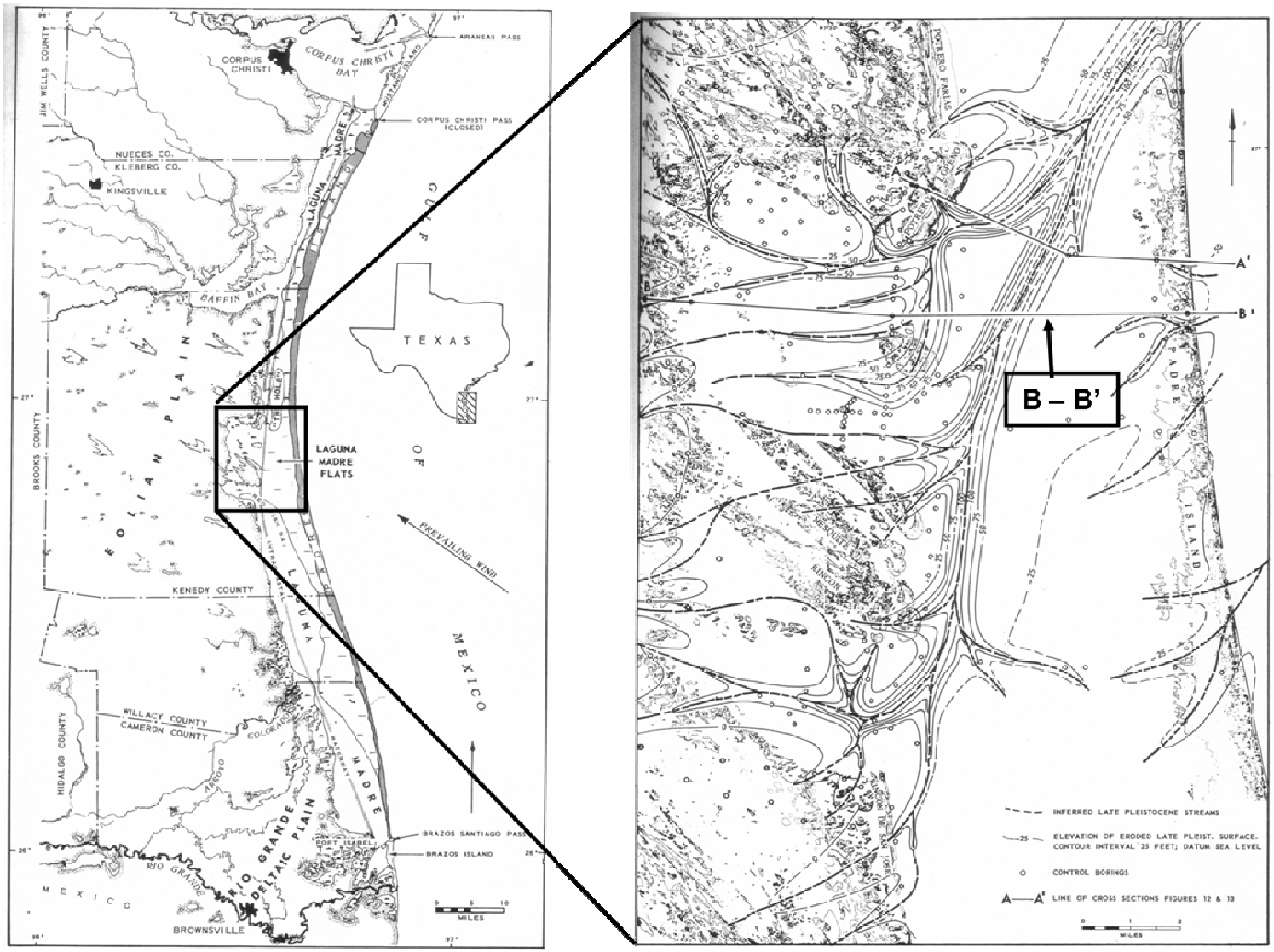

Figure 6 Location of Fisk (1959) Stratigraphic Cross-Section

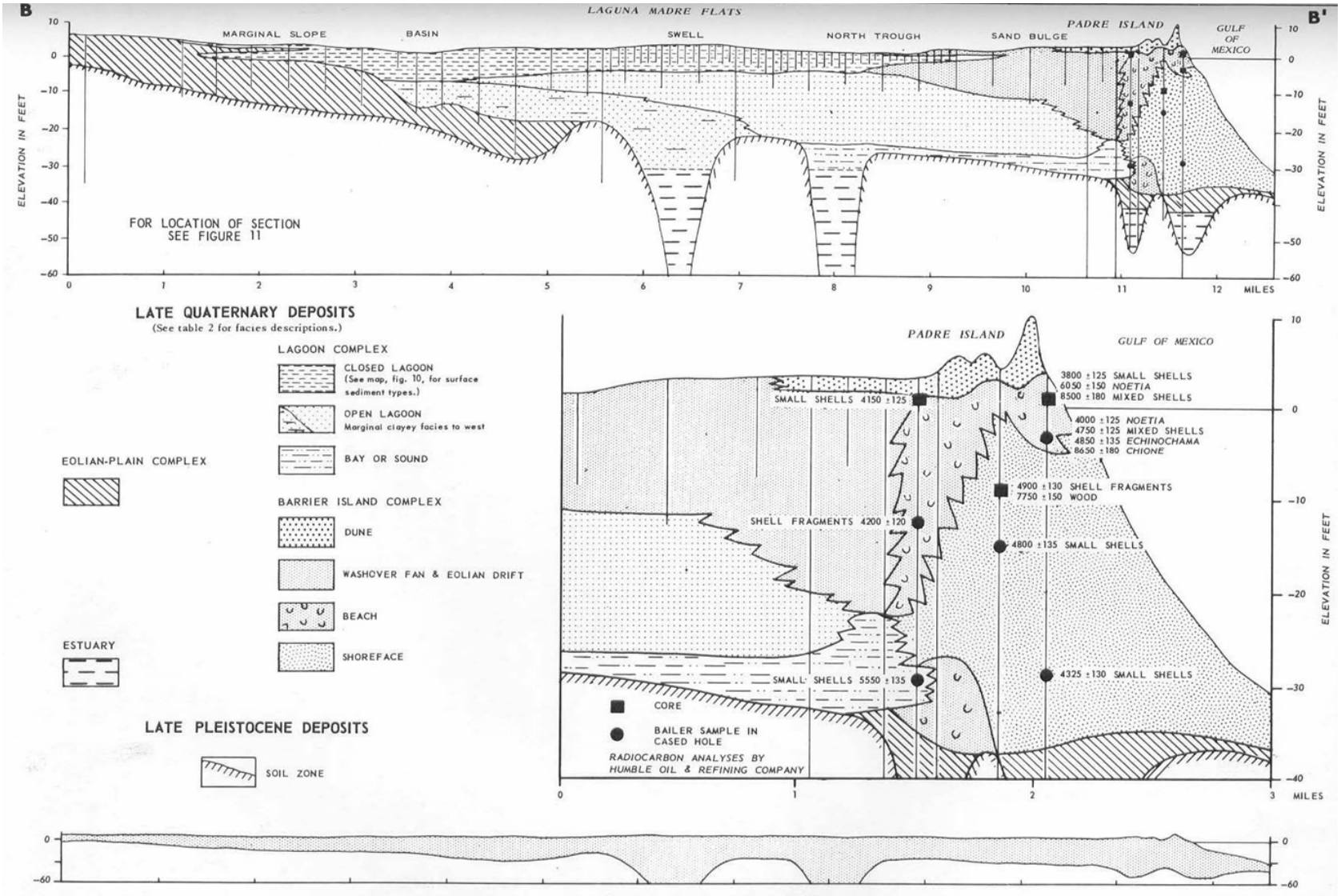

Figure 7 Fisk (1959) Stratigraphic Cross-Section

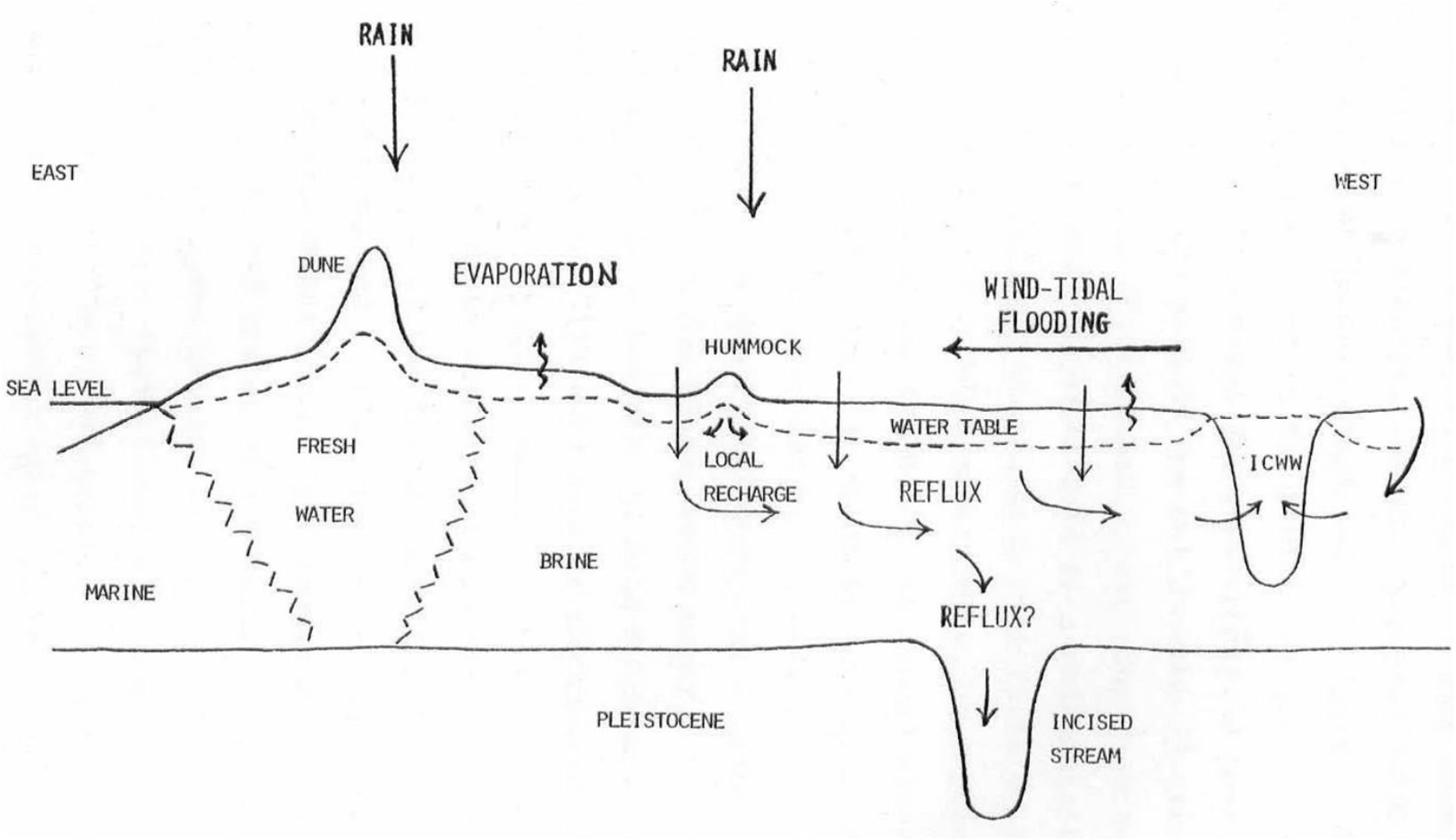

Figure 8 Amdurer (1978) Conceptual Model of Groundwater Flow in the Wind-Tidal Flats of Padre Island
In his illustration, Amdurer hypothesizes that wind-tidal flooding and evaporation of the shallow water table induce seepage reflux of the denser fluid into the deeper sediments of the Laguna Madre Flats. The denser, more saline water then exits the system at the Intra Coastal Water Way (ICWW) or decends deeper to incised streams of the pleistocene which pass under the island to the Gulf.

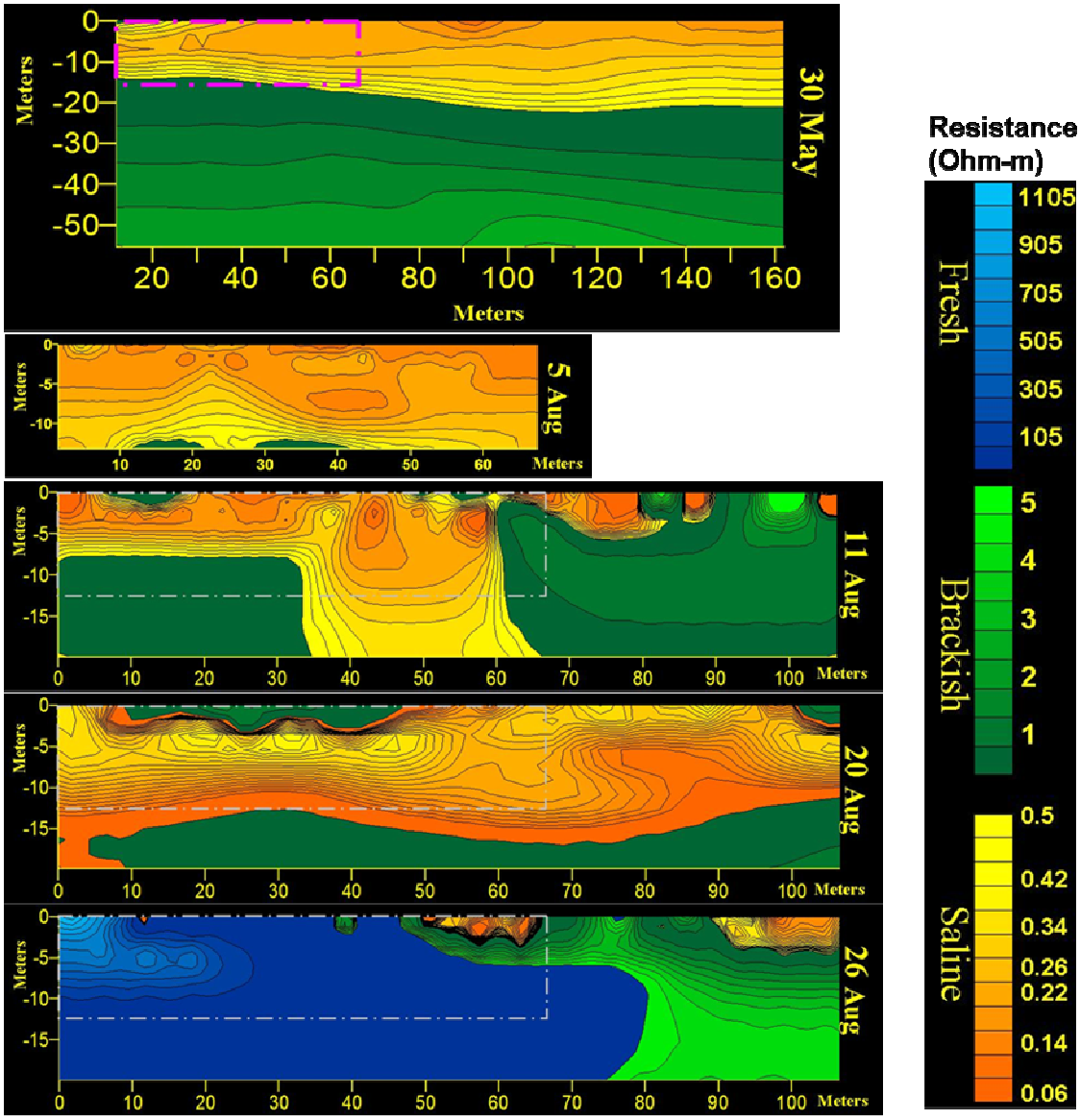

Figure 9 Fenstemaker et al. (2001) Resistivity Profiles at Bird Island Basin
2-D earth resisitivity images taken over a wind-tidal flat at Bird Island Basin during 2001. The May image displays a contrast of saline (dense) water overlying brackish (less dense) water. An apparent breakthrough is shown on Aug 11th. On Aug 26th, the system appears to have been displaced by fresh water.

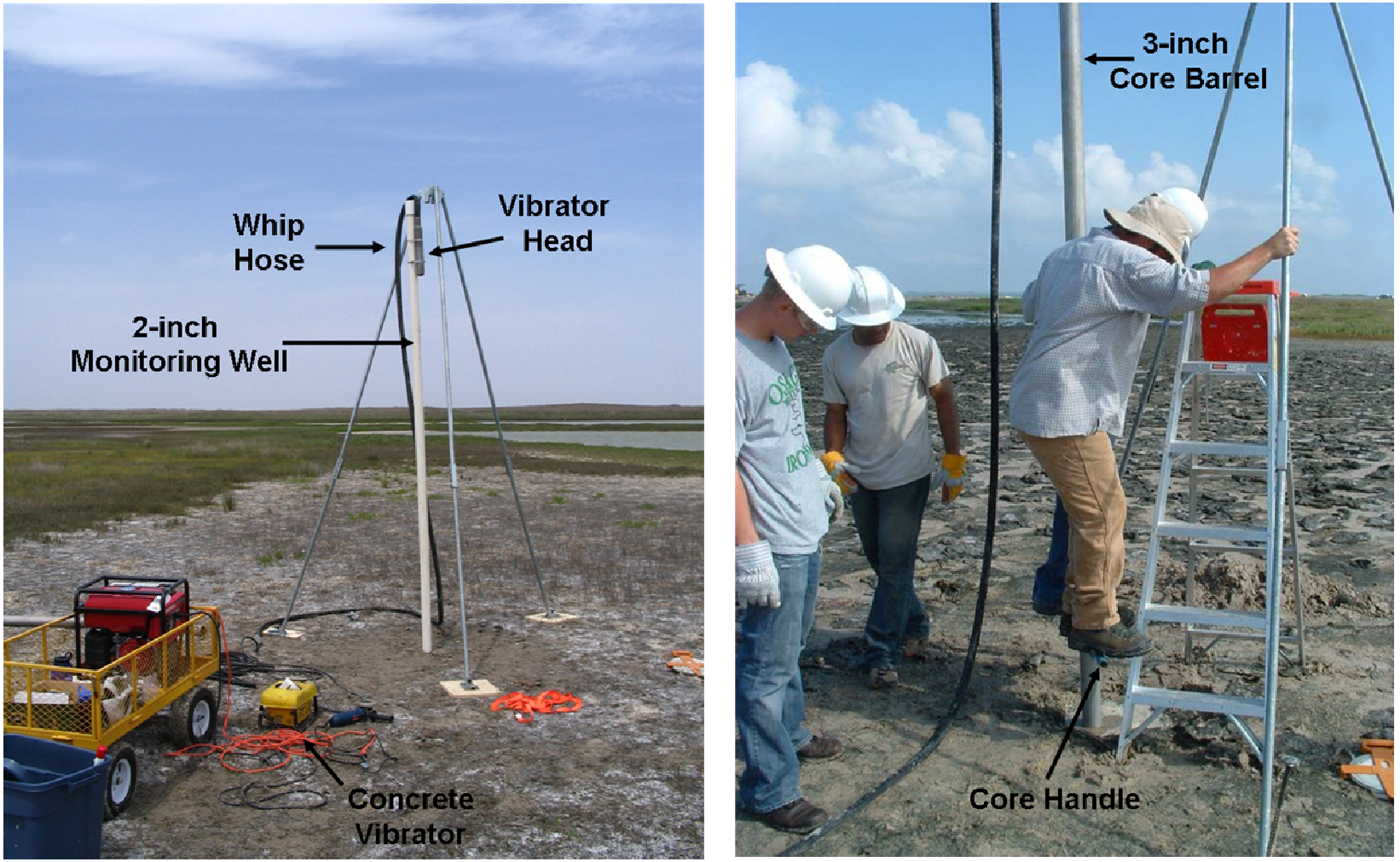

Figure 10 Vibracore Sediment Sampling and Monitoring Well Installation
Vibracore techniques where used to collect sediment cores (right photo) and install Monitoring Wells (left photo).

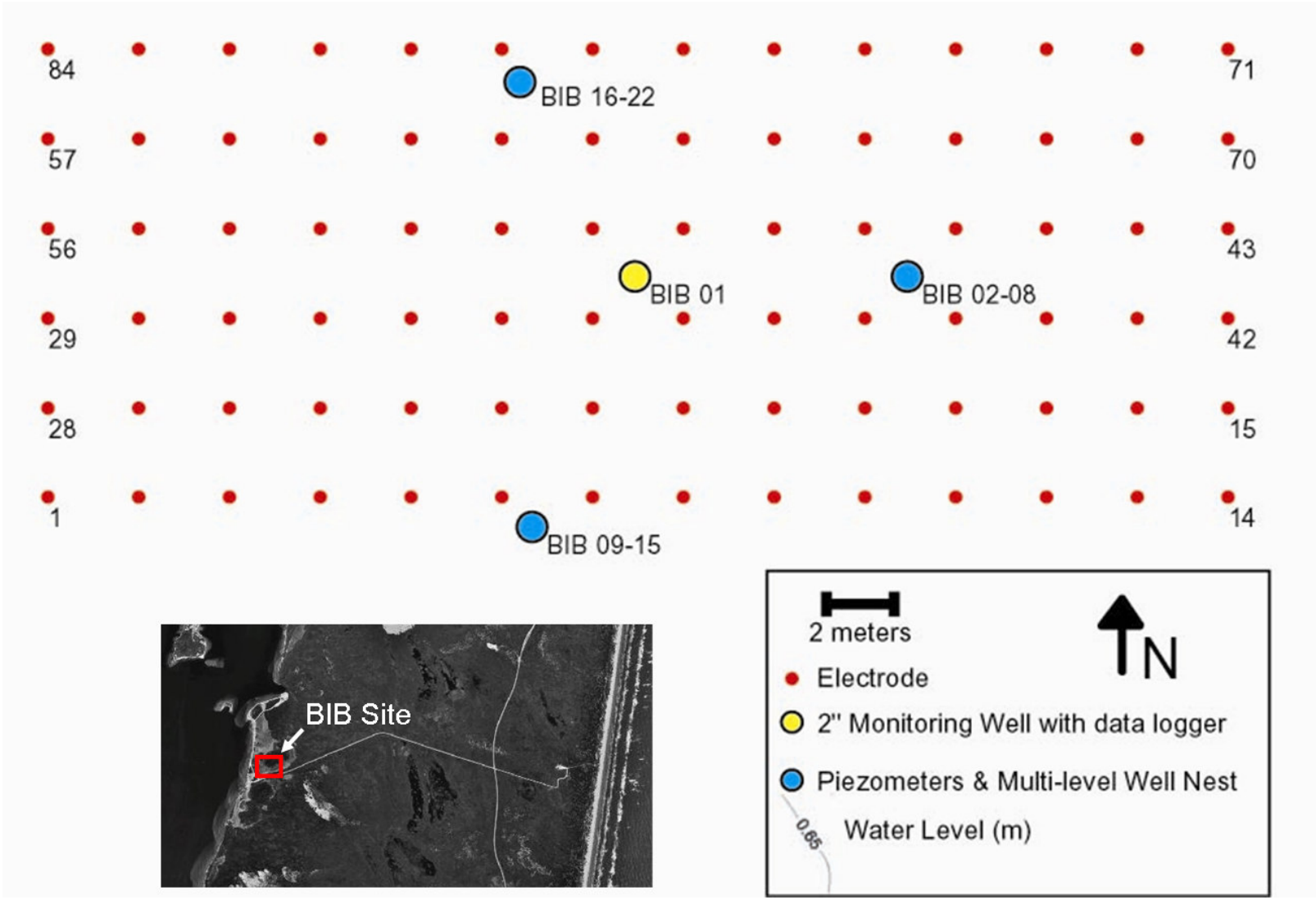

Figure 11 Bird Island Basin Site Setup

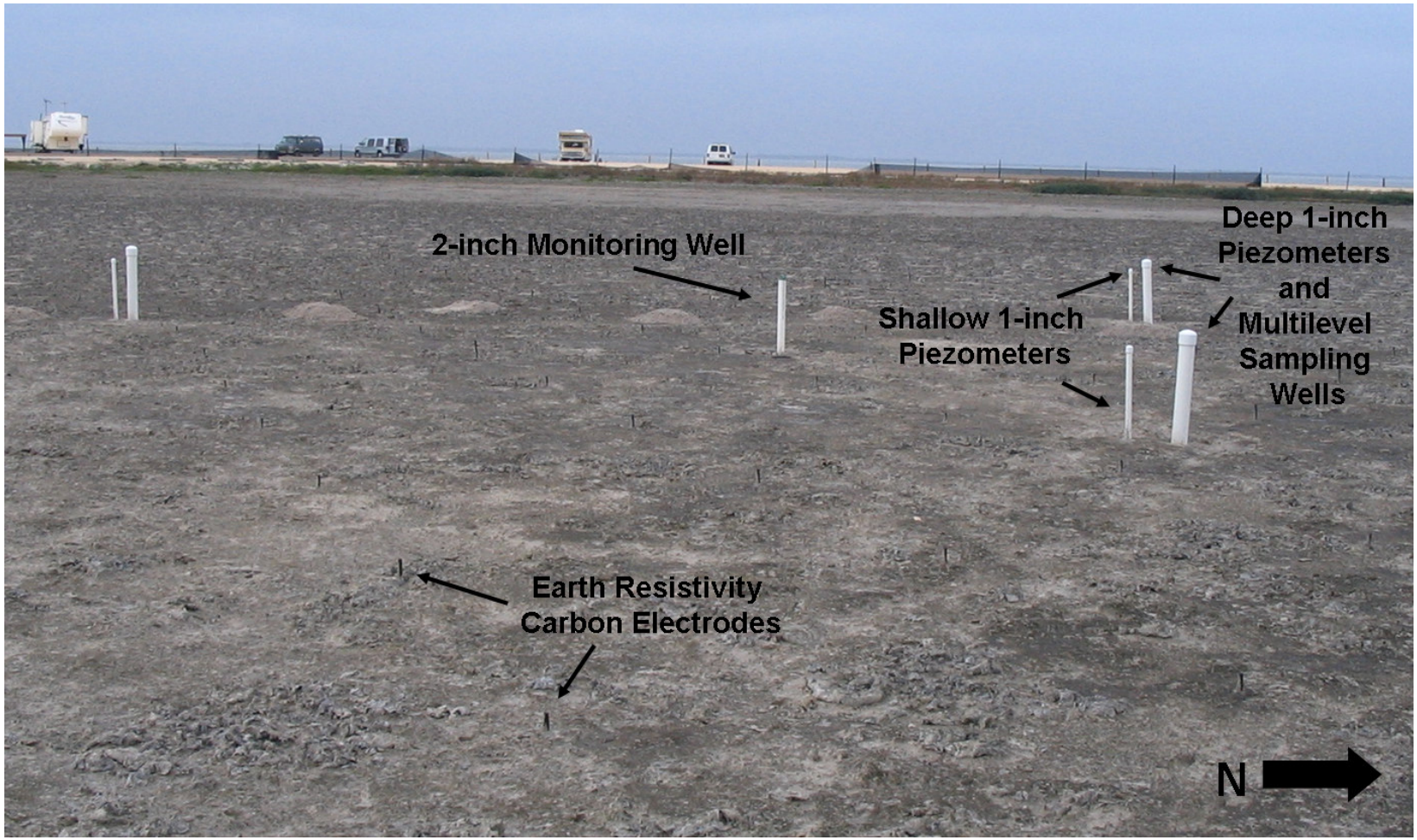

Figure 12 Photo of Bird Island Site

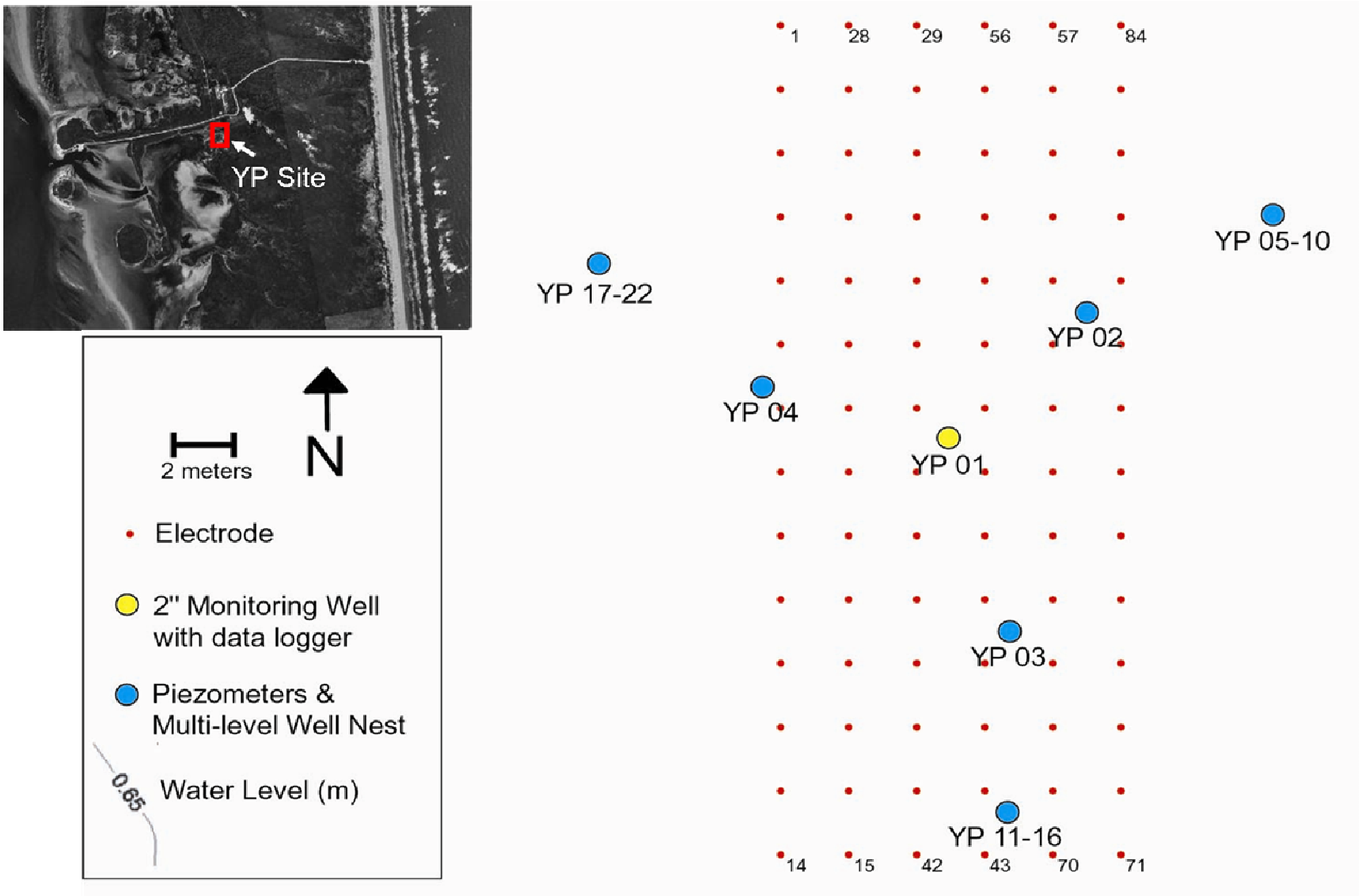

Figure 13 Yarborough Pass Site Setup

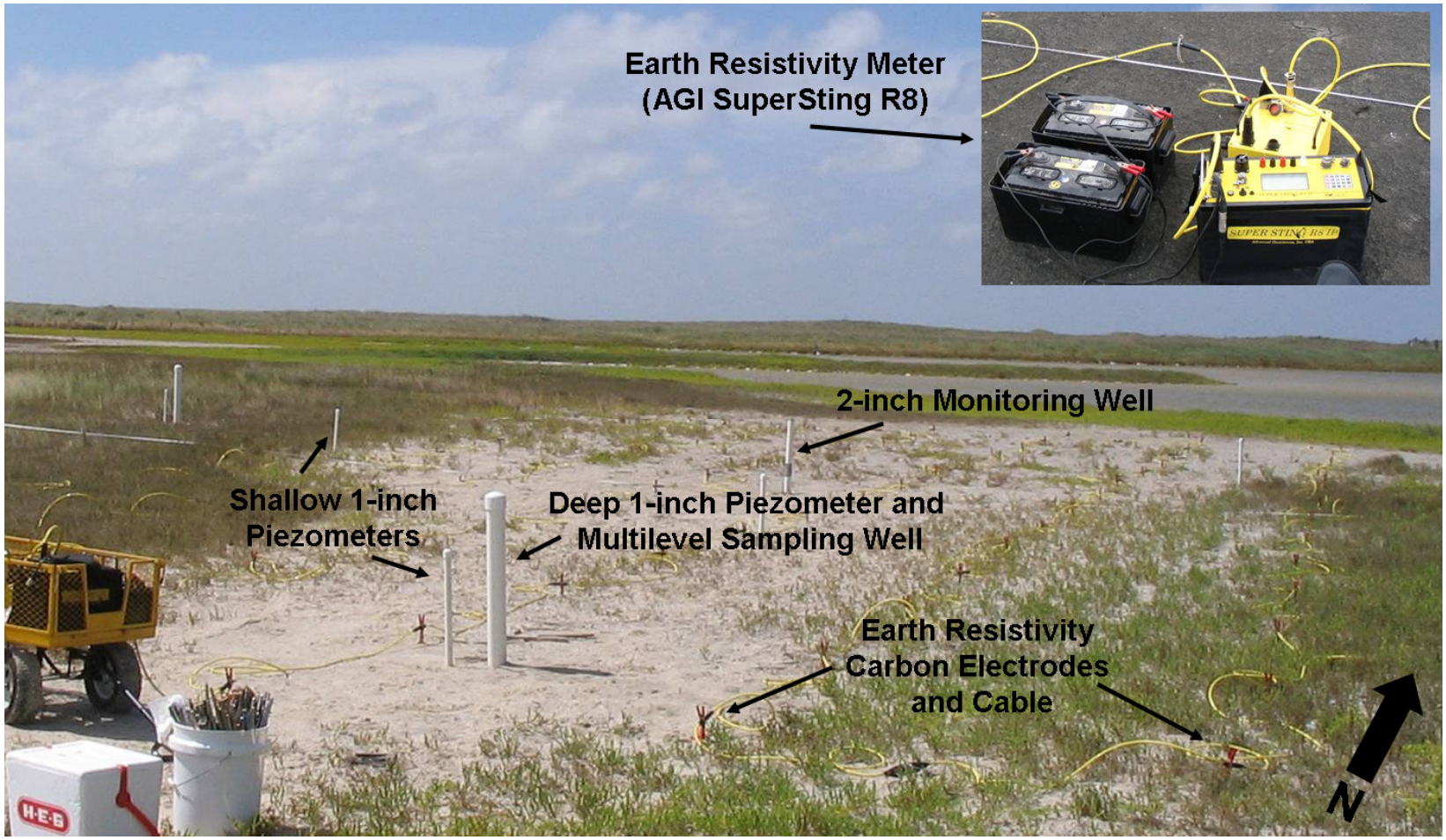

Figure 14 Photo of Yarborough Pass Site

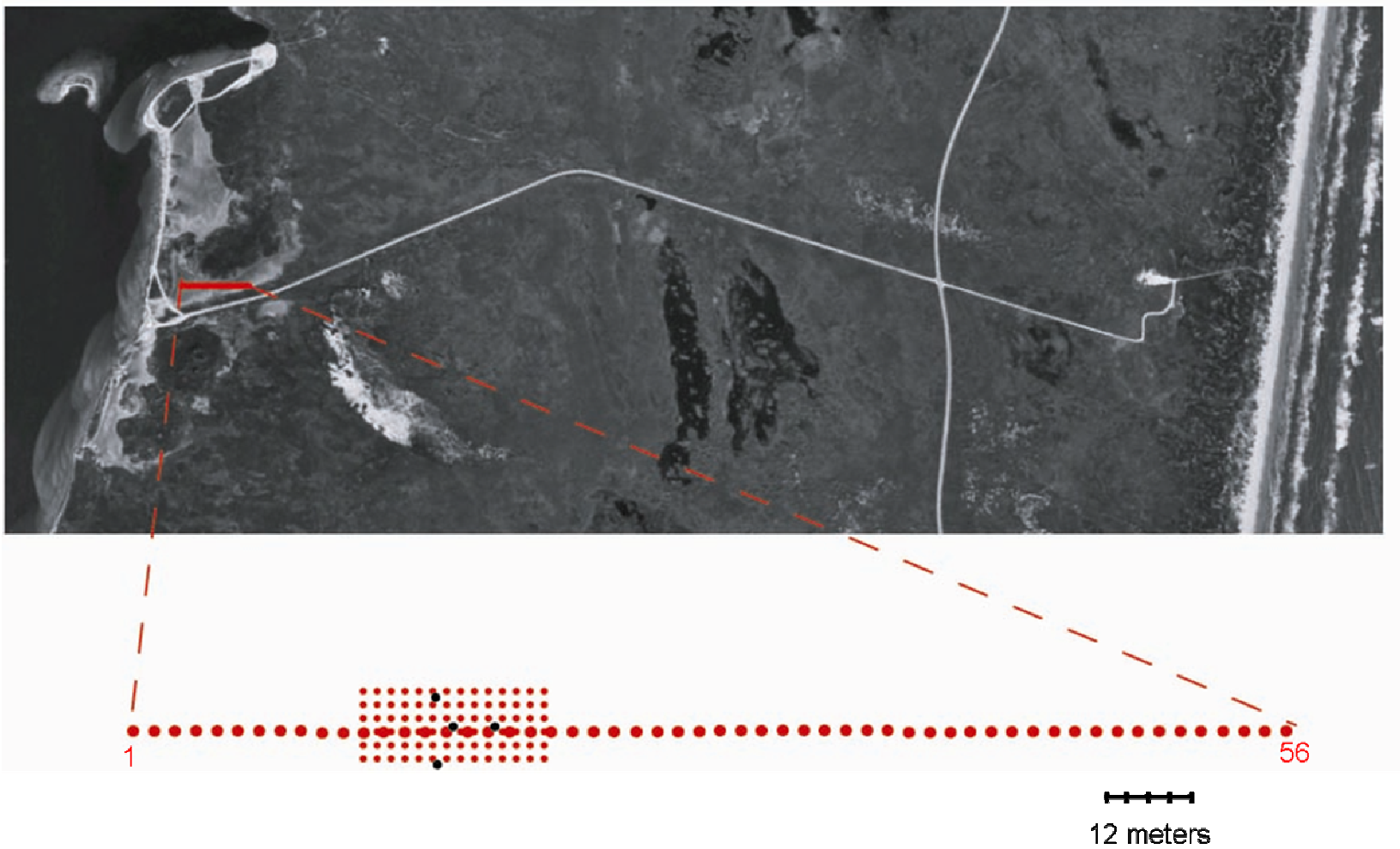

Figure 15 2-D Resistivity Transect at Bird Island Basin
Location and layout of the 2-D resistivity transect conducted at Bird Island Basin July 27, 2005. Survey used 56 electrodes with a 3-meter spacing crossing the 3-D grid and monitoring wells in the insert.

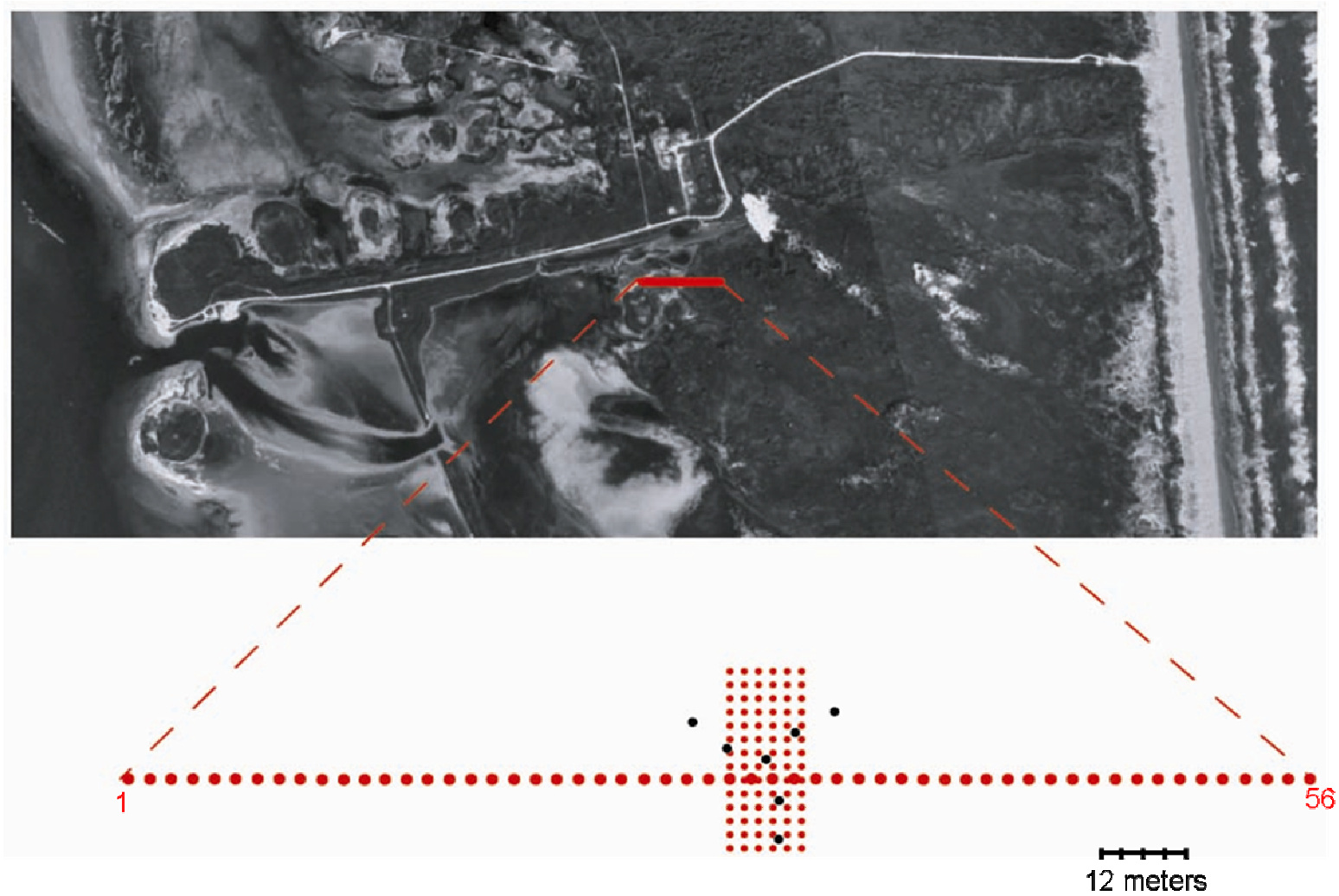

Figure 16 2-D Resistivity Transect at Yarborough Pass
Location and layout of the 2-D resistivity transect conducted at Bird Island Basin July 27, 2005. Survey used 56 electrodes with a 3-meter spacing crossing the 3-D grid and monitoring wells in the insert.

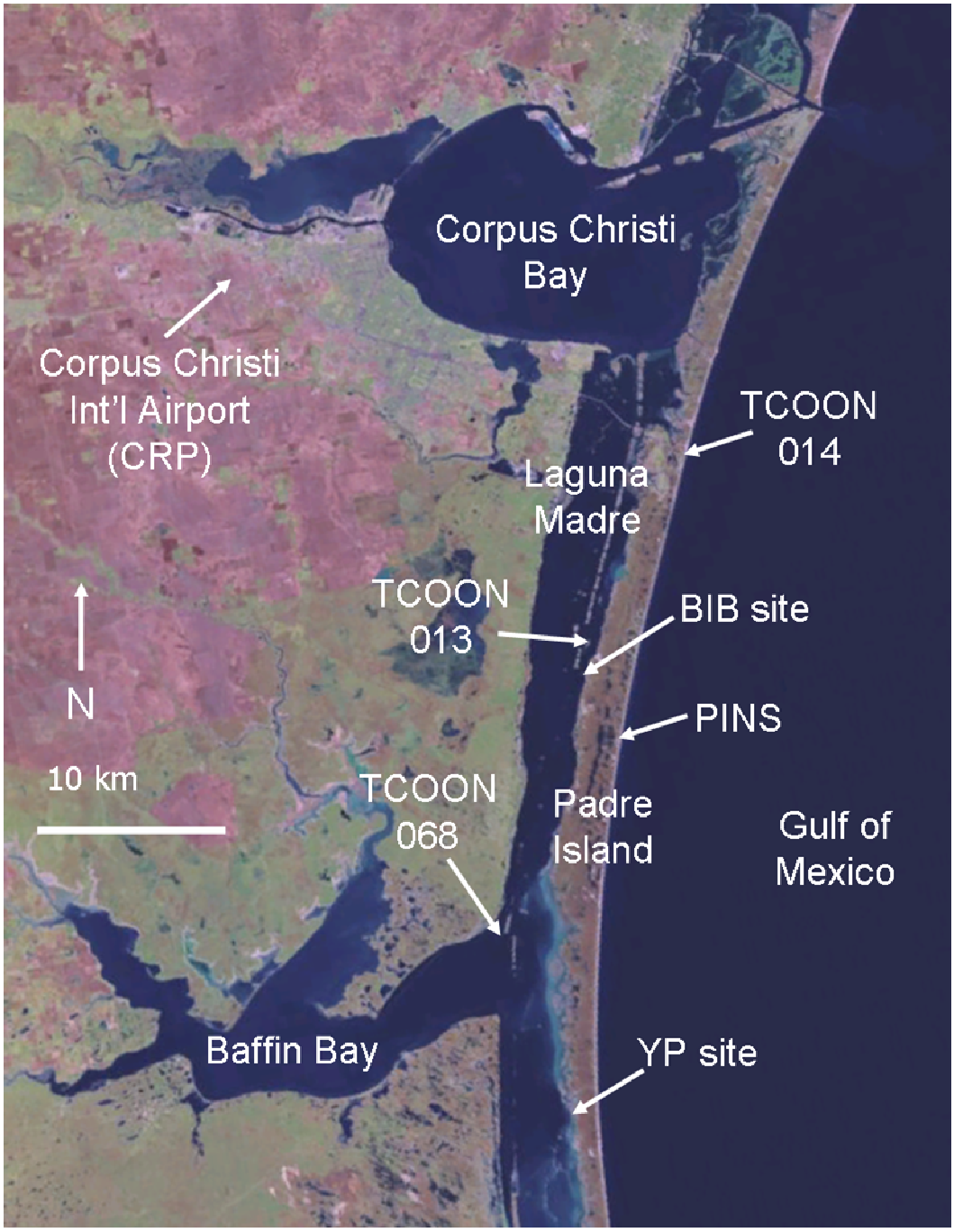

Figure 17 Locations of Weather Stations
Weather stations including the National Weather Service station at Corpus Christi Int'l Airport (CRP), Padre Island National Seashore (PINS), and Texas A&M's Texas Coastal Ocean Observation Network (TCOON) provided climate and tide information for use in this study.

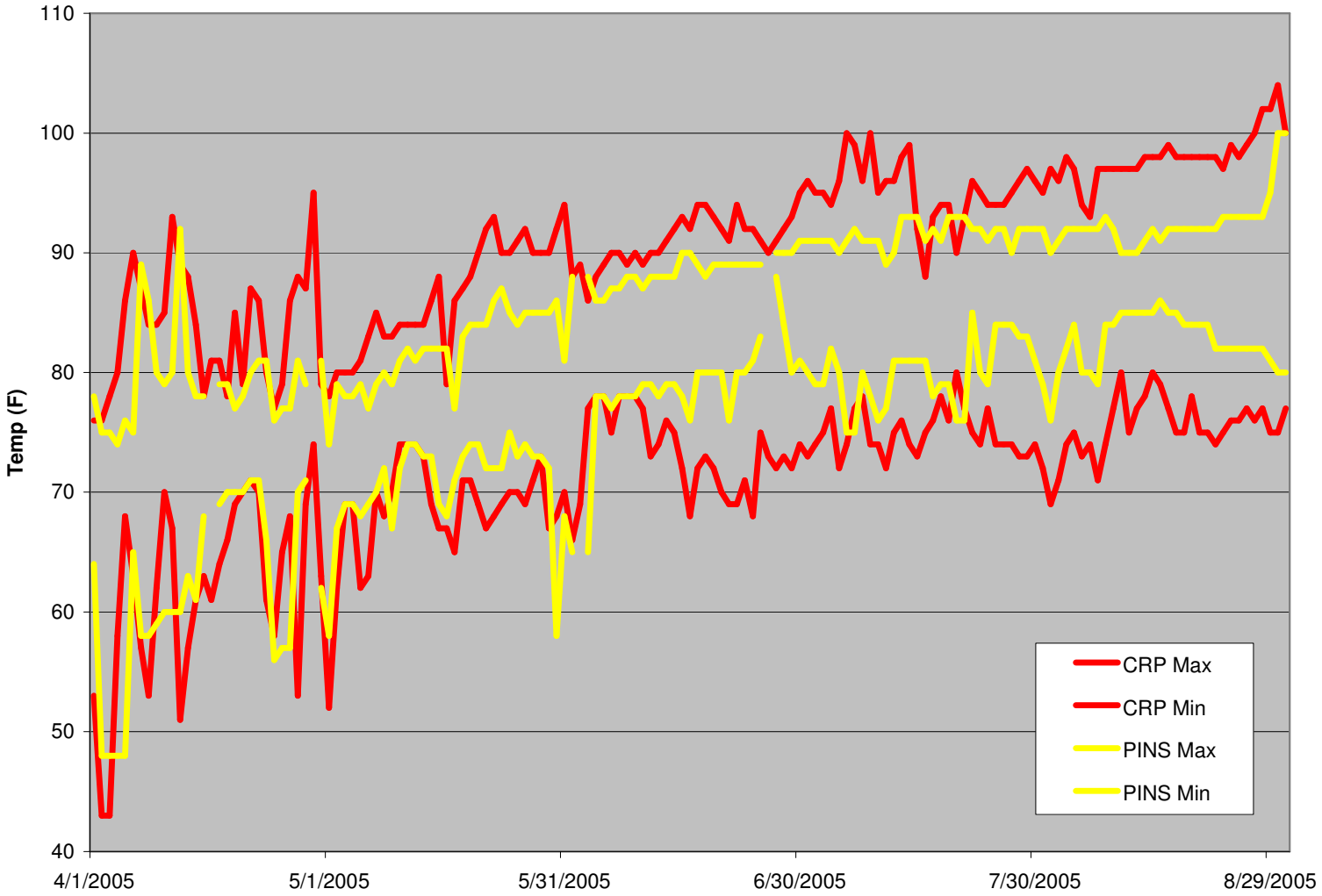

Figure 18 Air Temperature Comparison of Corpus Christi Airport (CRP) and Padre Island National Seashore (PINS)

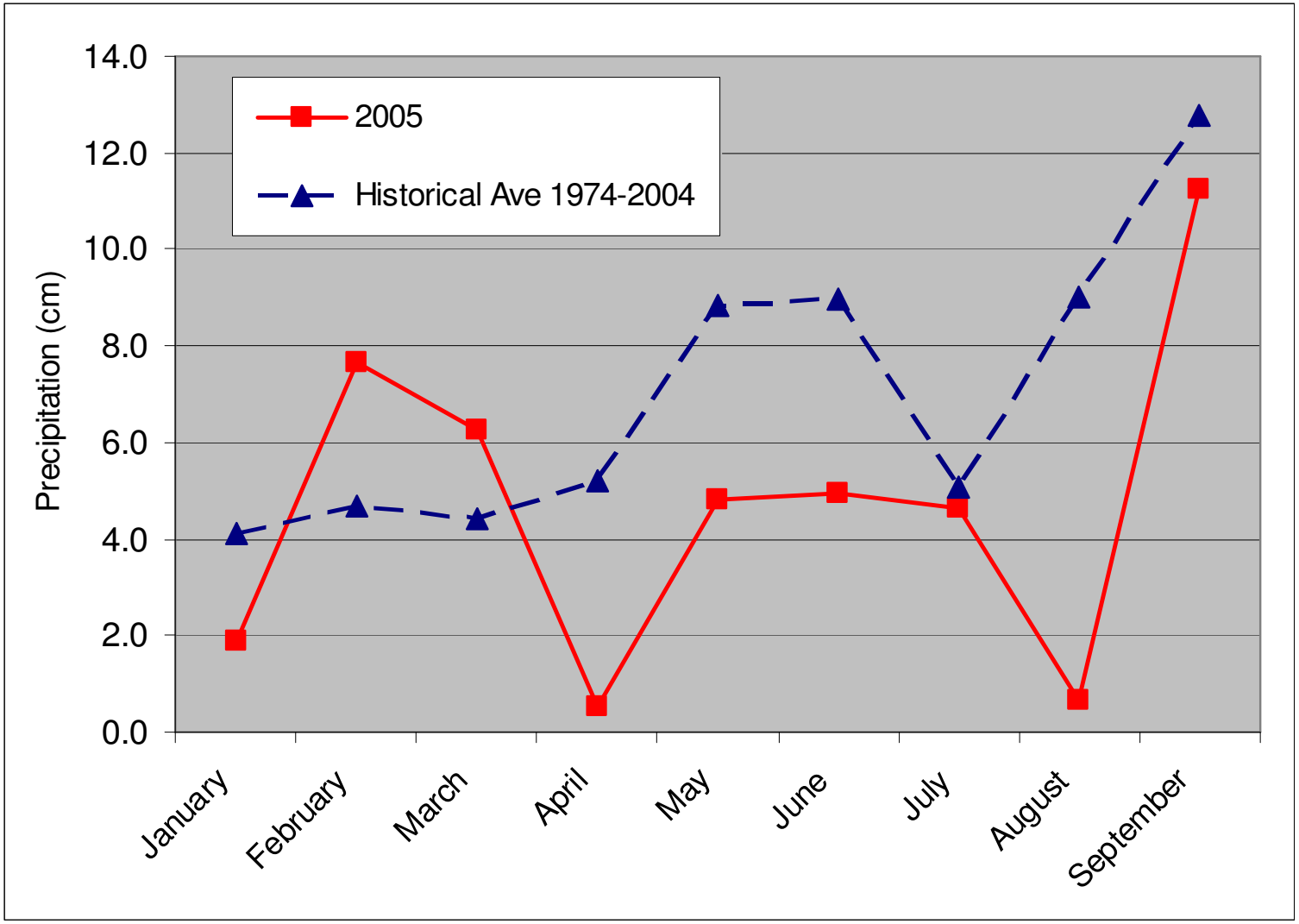

Figure 19 2005 and Historical Average Monthly Precipitation at Corpus Christi Airport

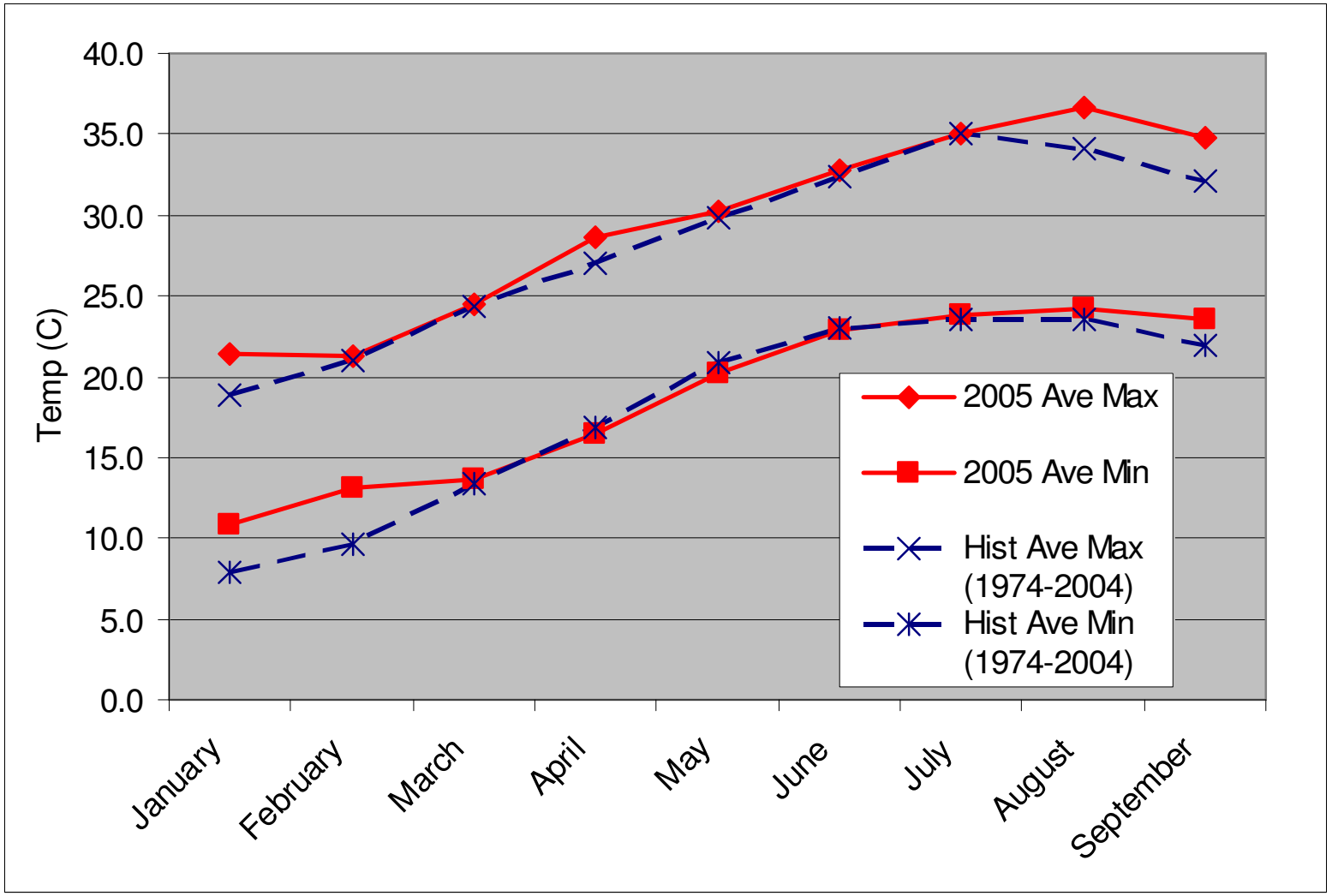

Figure 20 2005 and Historical Average Monthly Temperatures at Corpus Christi Airport

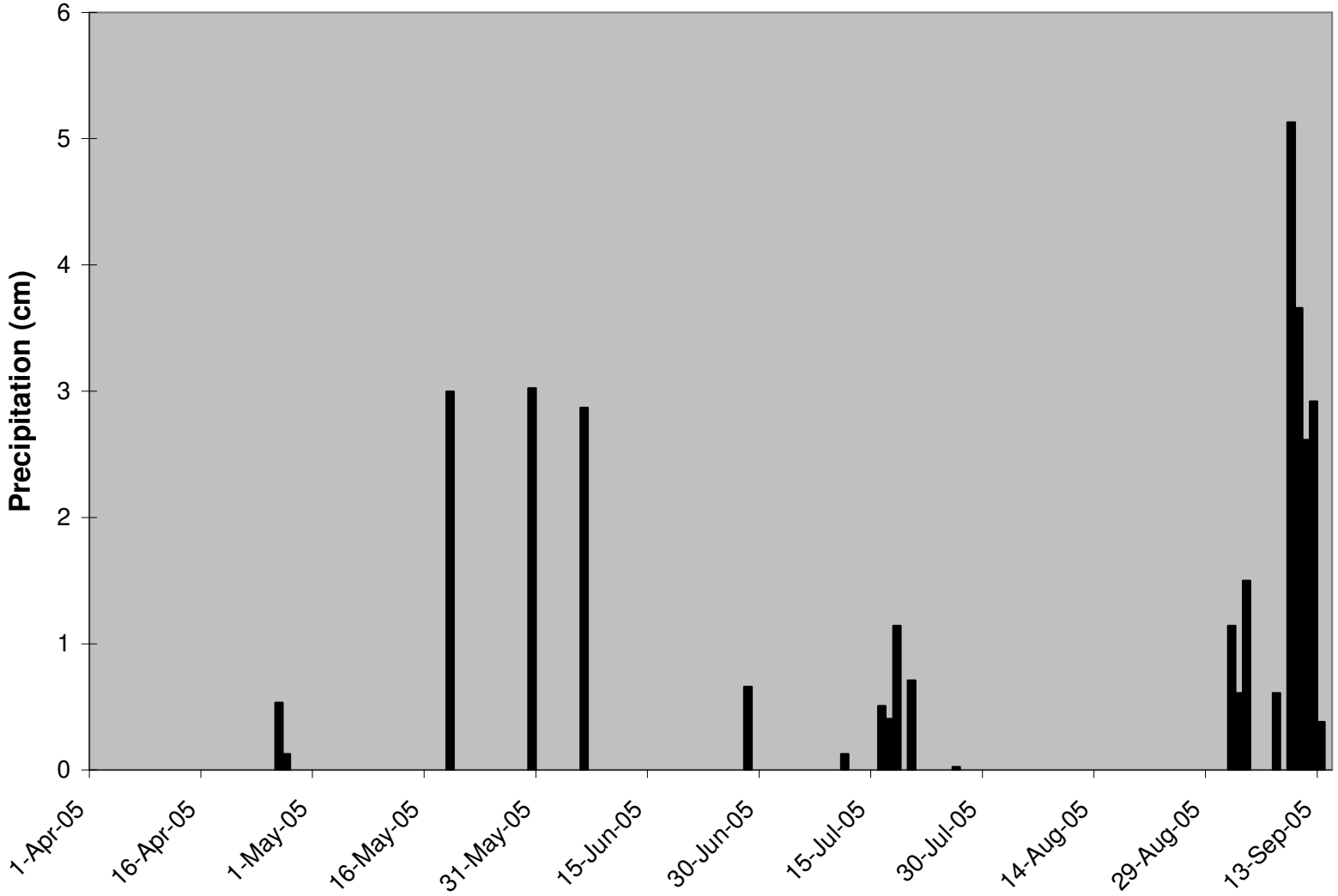

Figure 21 Daily Precipitation Totals at Padre Island National Seashore Park Headquarters

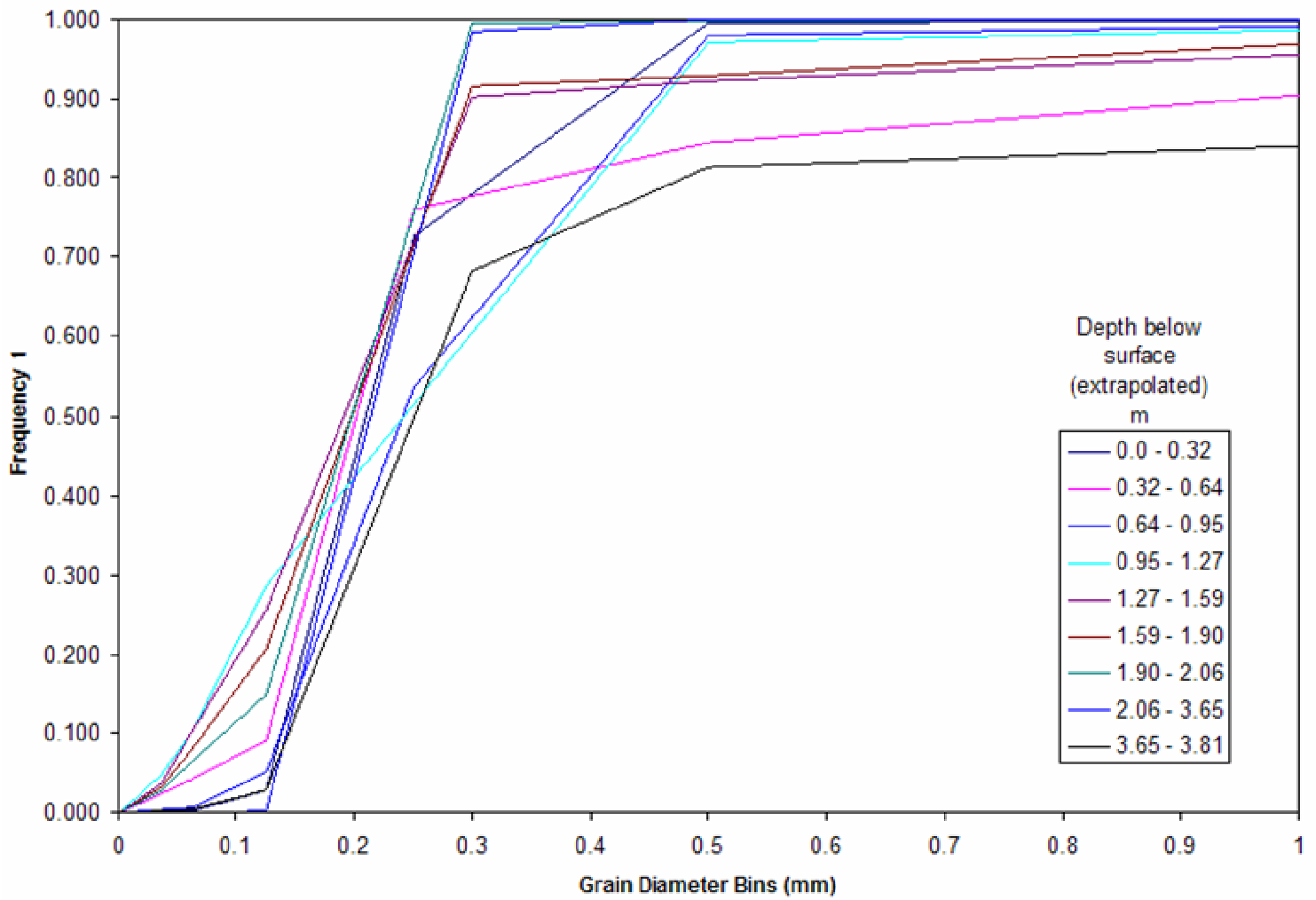

Figure 22 Bird Island Basin Sediment Core Grain-Size Distribution
Compare to Table 3. Modified after UTHFC, 2005.

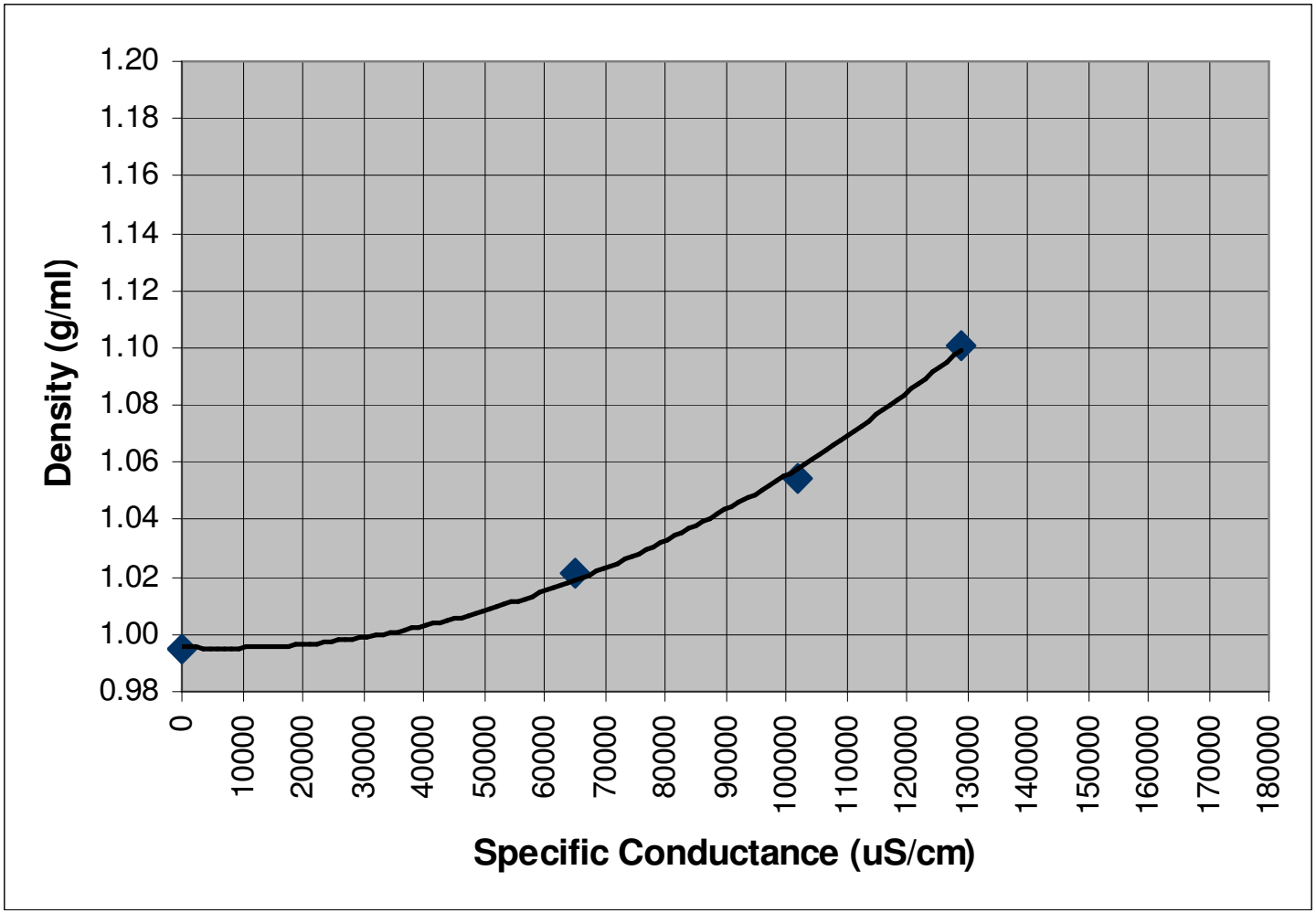

Figure 23 Measured Groundwater Density vs Specific Conductance
Water density measurements conducted on August 16, 2005 for use in correcting for hydraulic head values

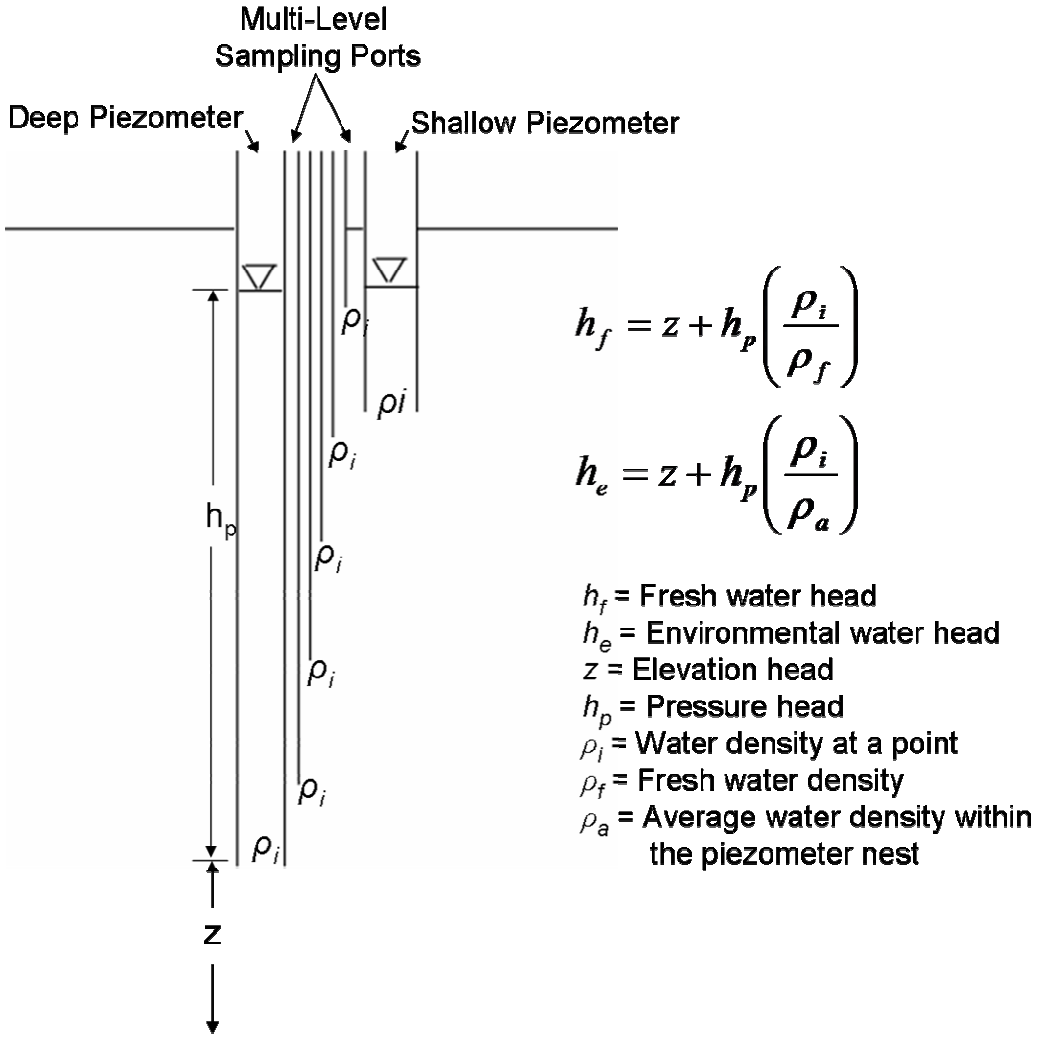

Figure 24 Illustration of a Nested Monitoring Well and the Fresh Water and Environmental Water Head Equations

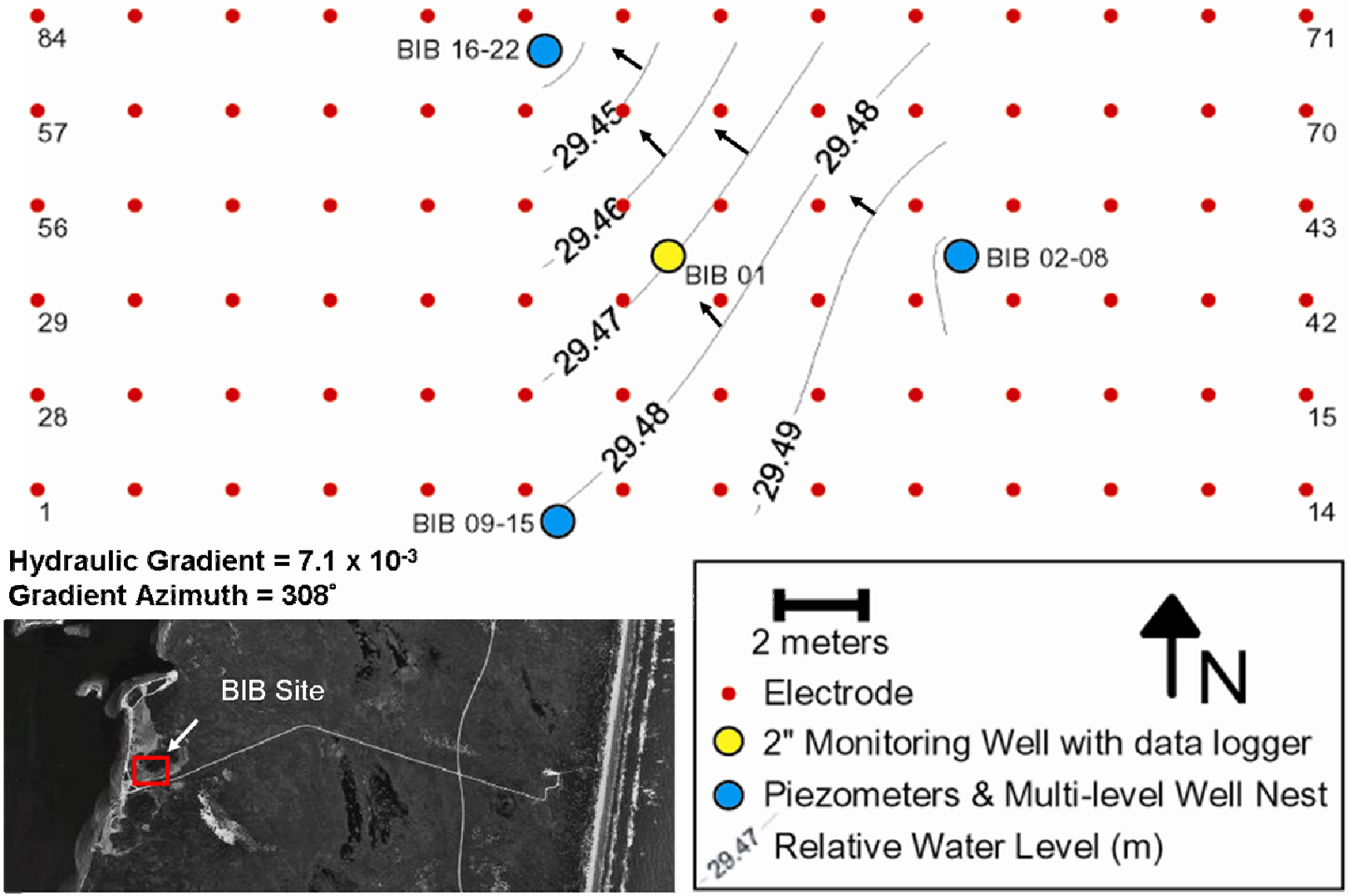

Figure 25 June 20, 2005 Bird Island Basin Relative Freshwater Levels

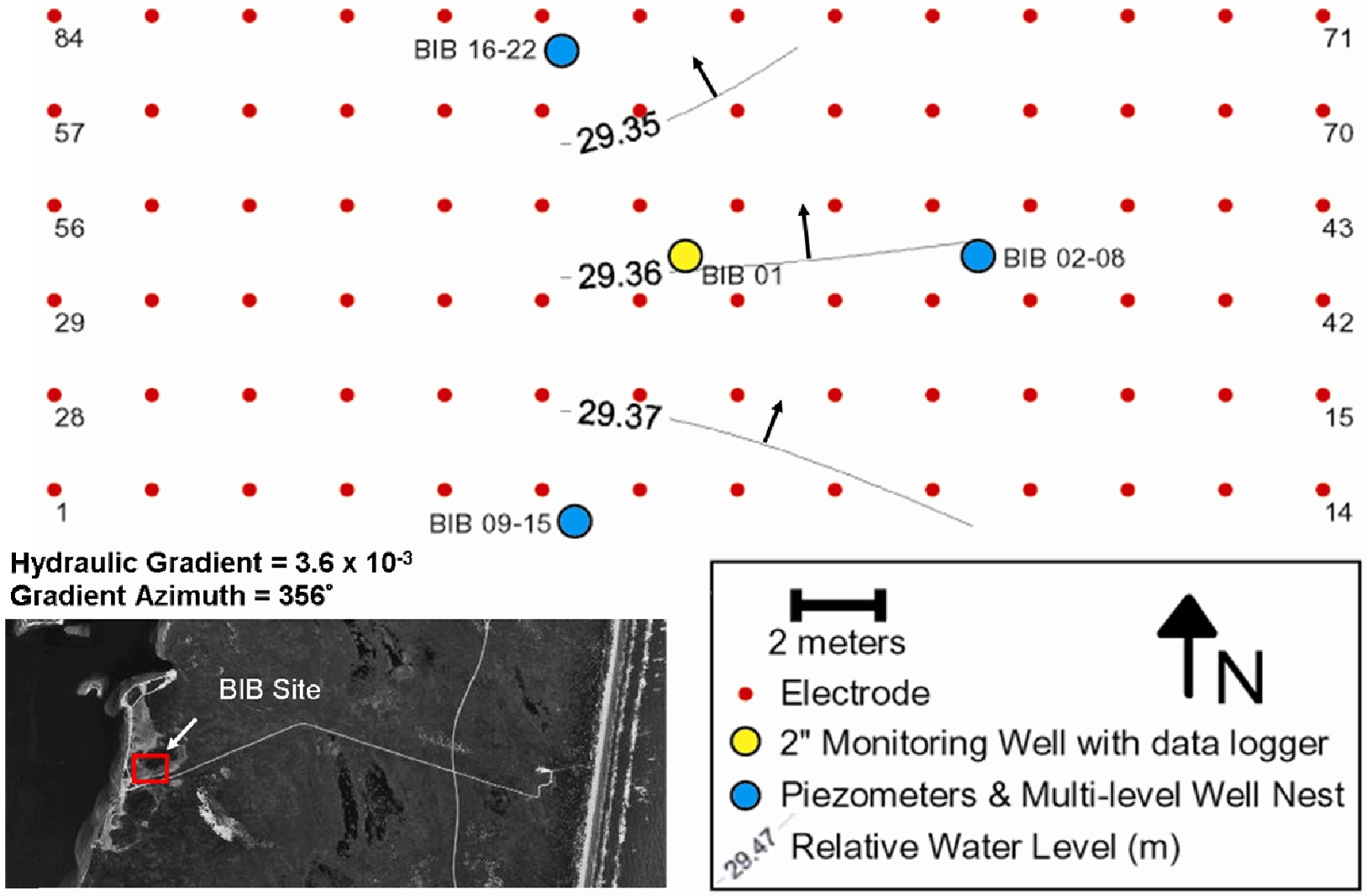

Figure 26 July 5, 2005 Bird Island Basin Relative Freshwater Levels

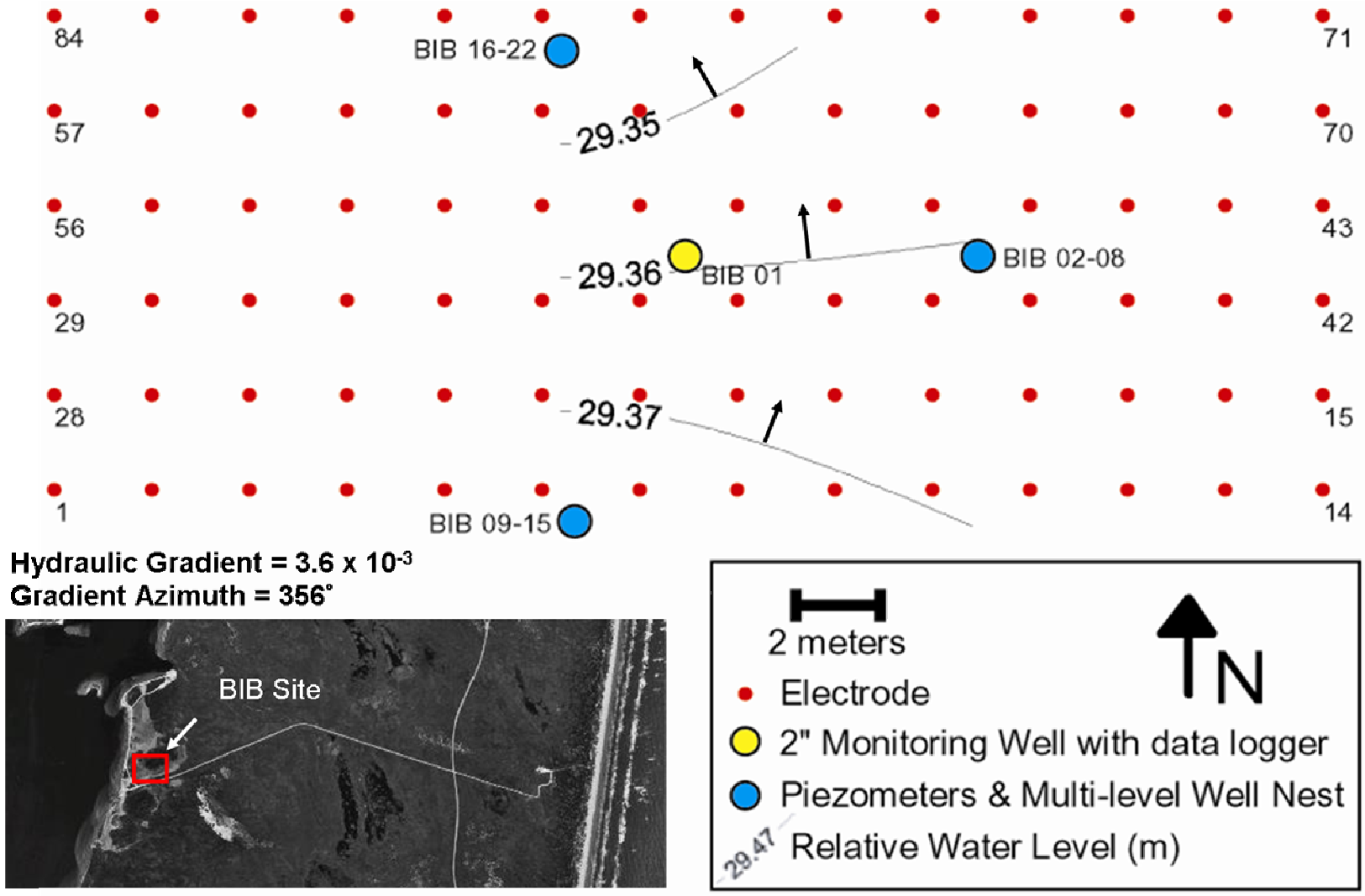

Figure 27 July 27, 2005 Bird Island Basin Relative Freshwater Levels

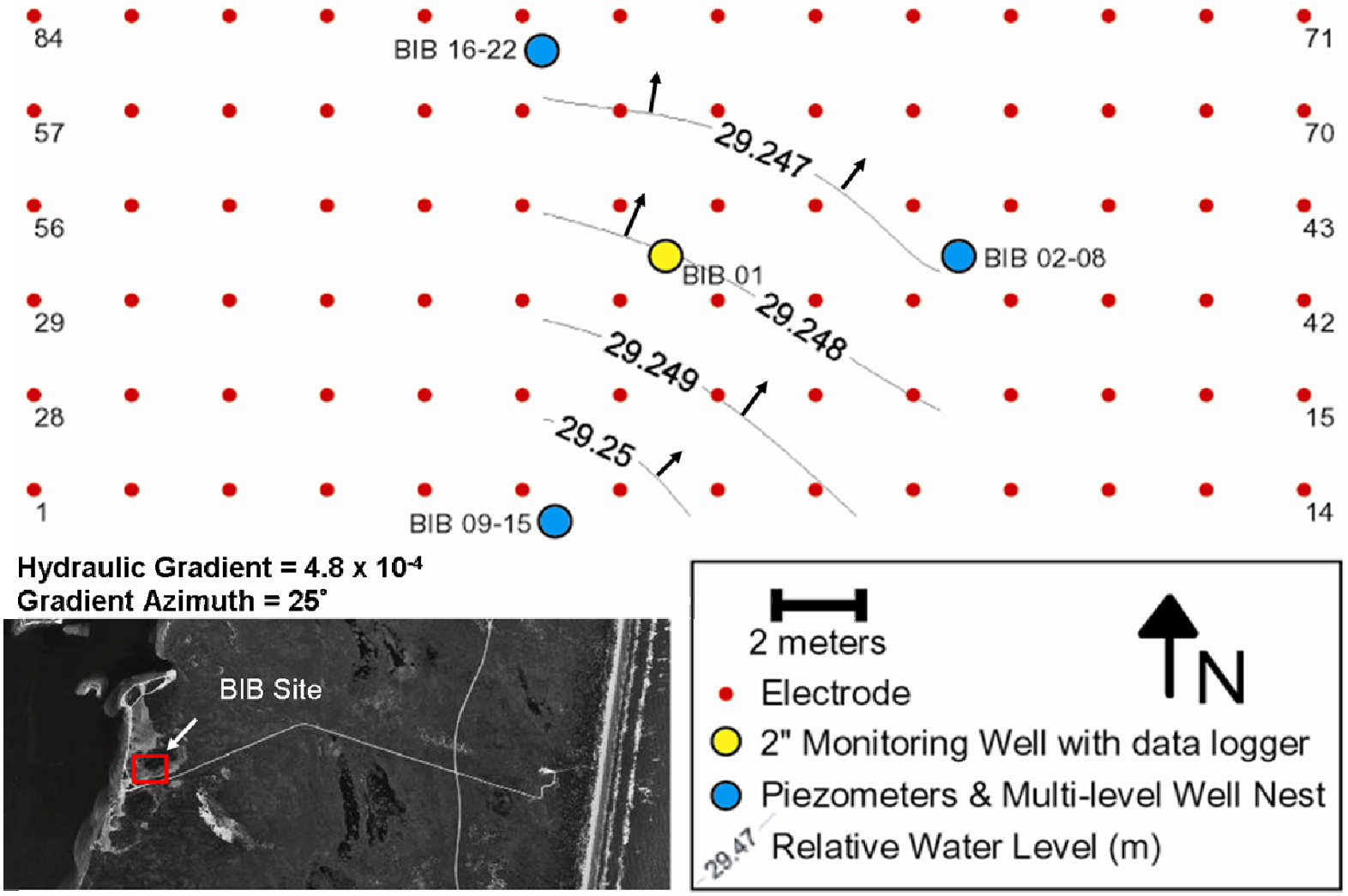

Figure 28 August 16, 2005 Bird Island Basin Relative Freshwater Levels
Note contour interval change from 0.01 meters to 0.001 meters to show detail

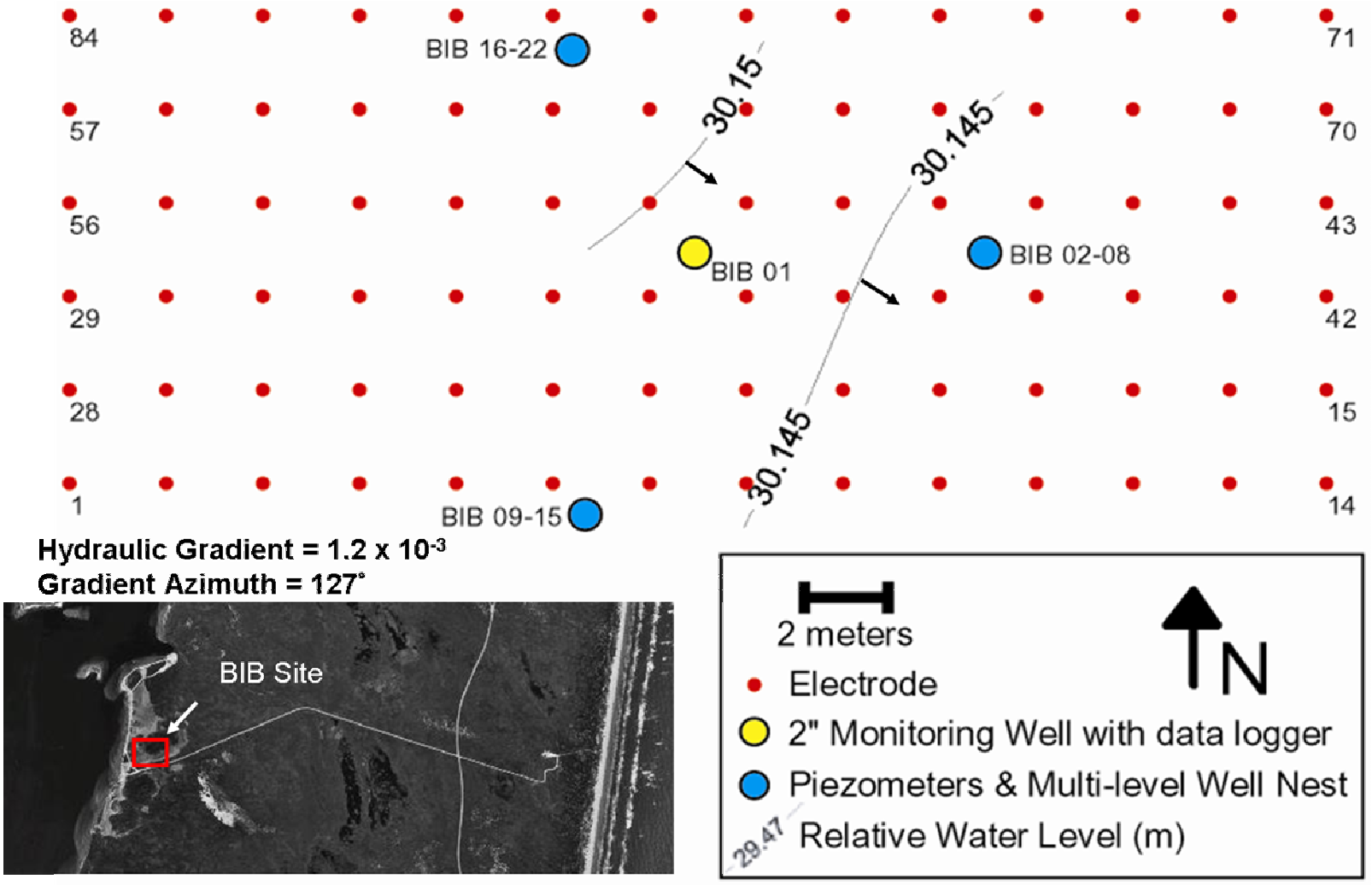

Figure 29 September 14, 2005 Bird Island Basin Relative Freshwater Levels
Note contour interval change from 0.01 meters to 0.005 meters to show detail.

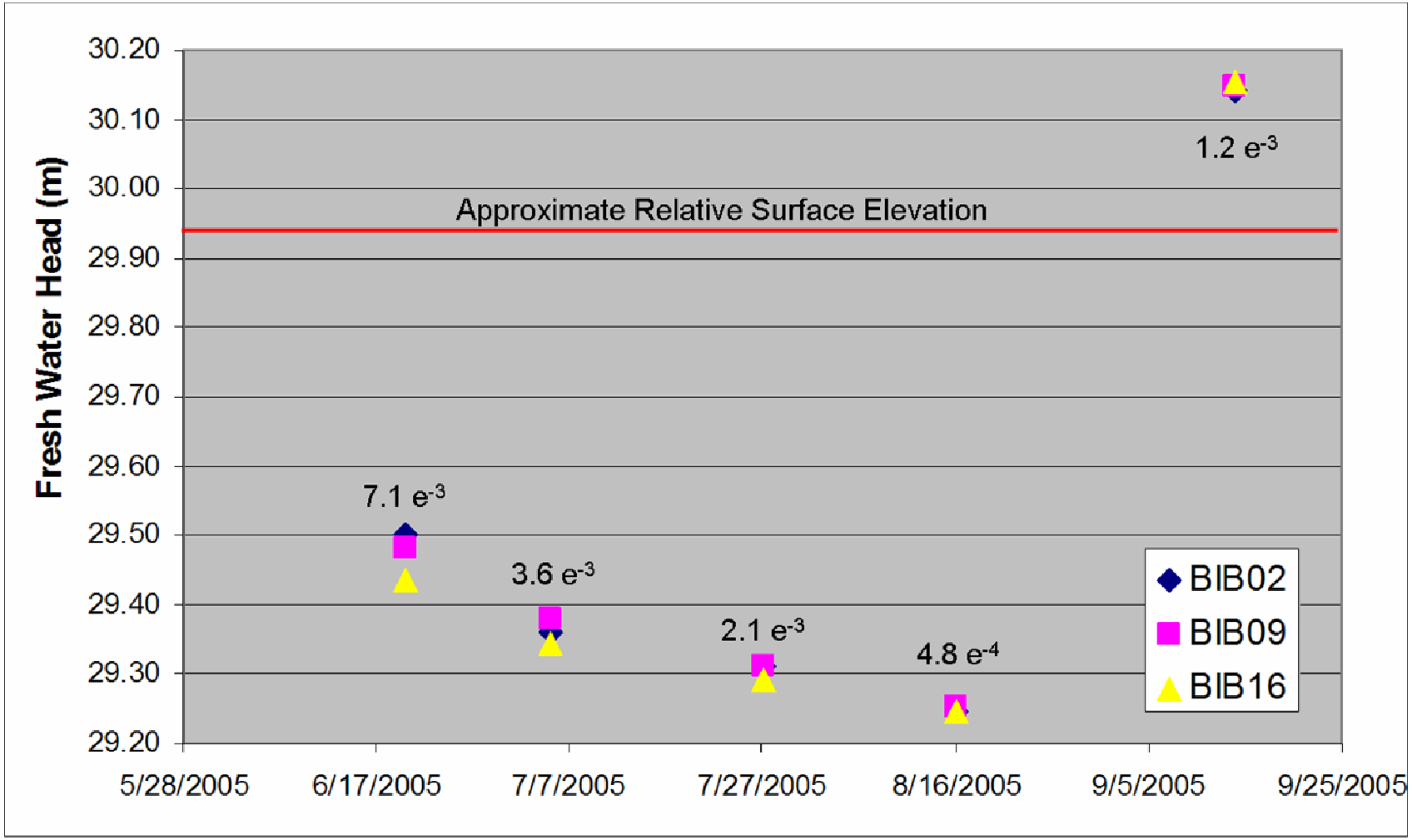

Figure 30 Profile of Bird Island Basin Freshwater Head
Horizontal hydraulic gradients between the wells and the approximate surface elevation are also noted.

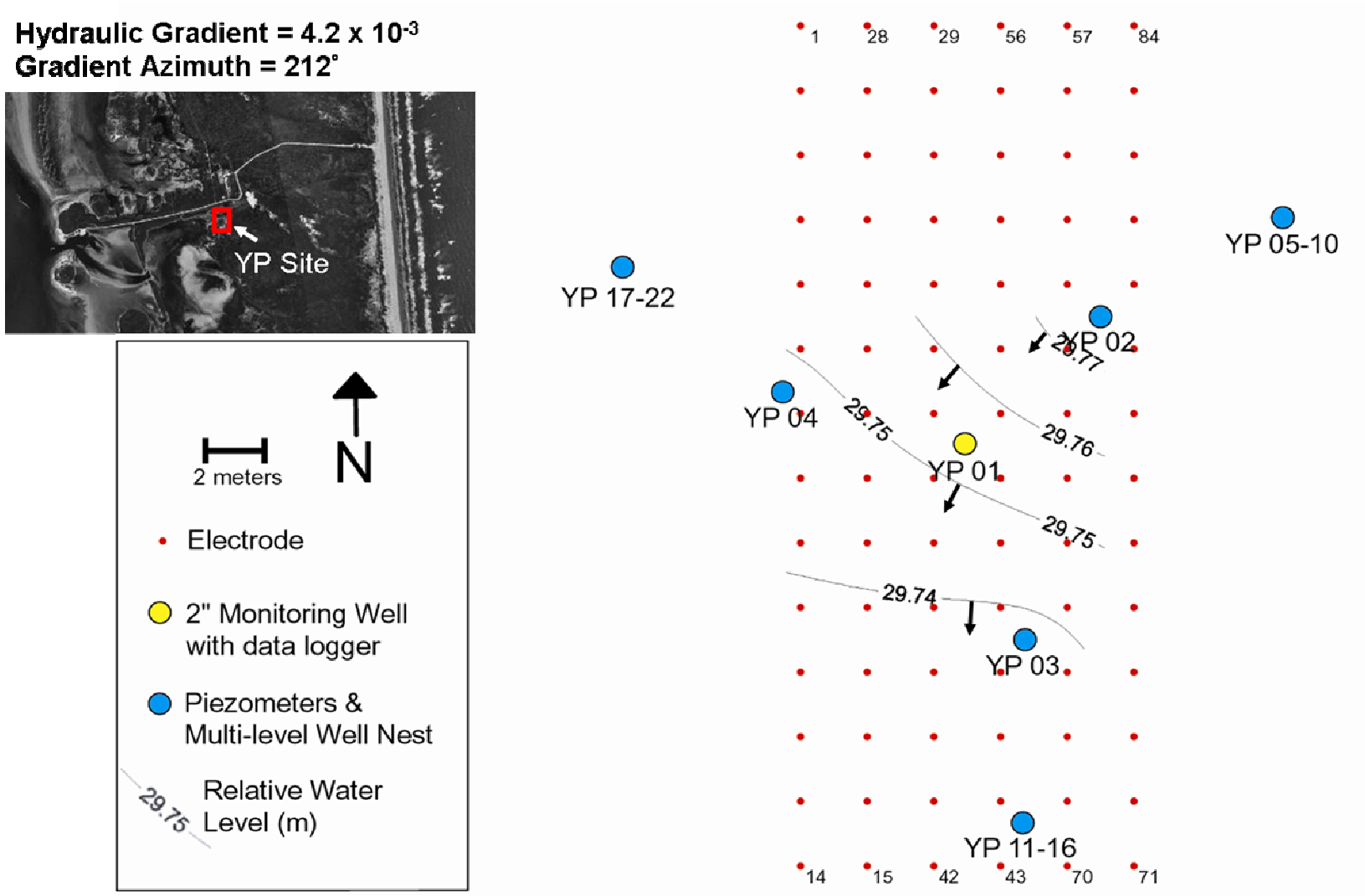

Figure 31 April 10, 2005 Yarborough Pass Relative Freshwater Levels

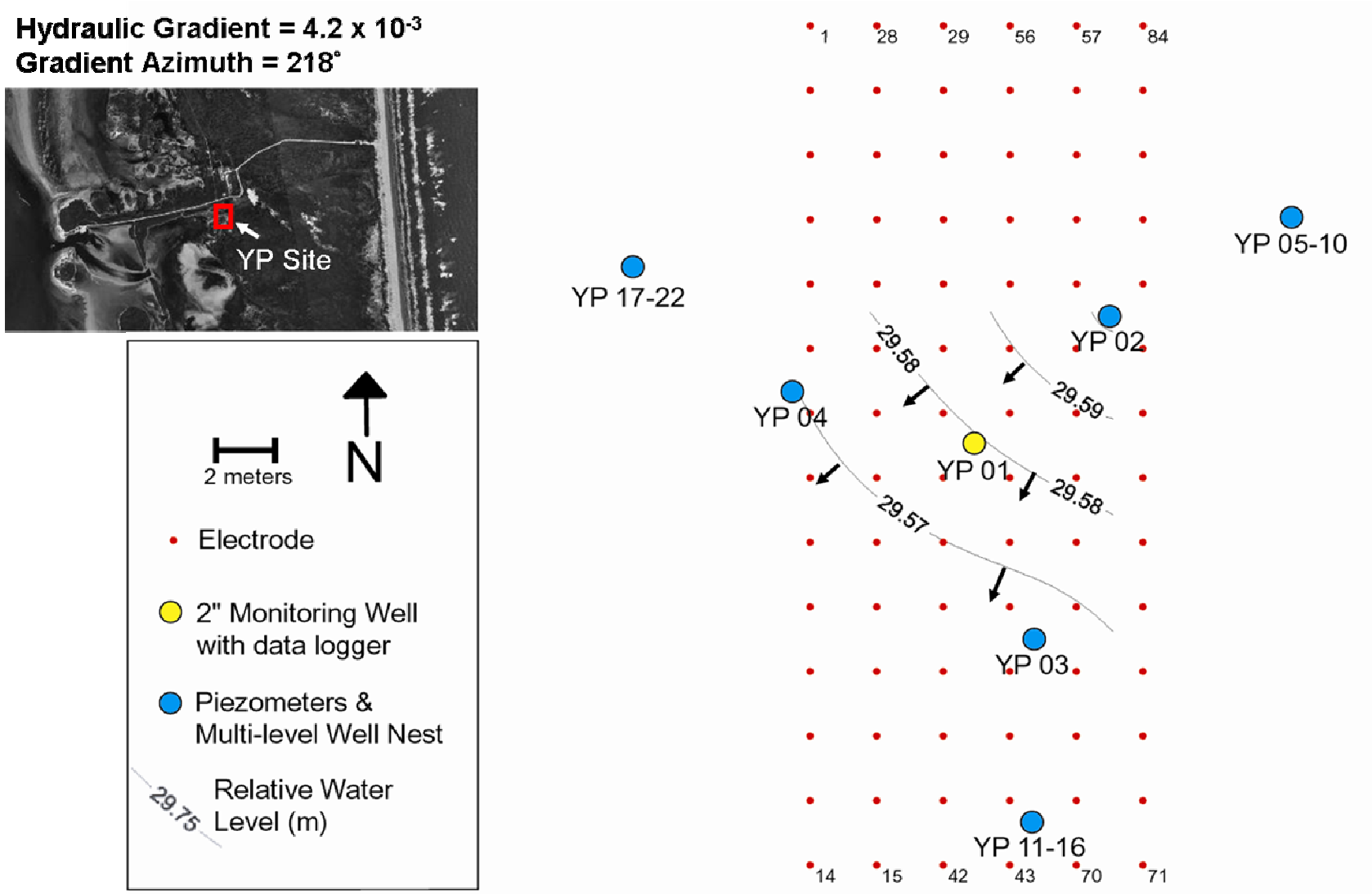

Figure 32 May 2, 2005 Yarborough Pass Relative Freshwater Levels

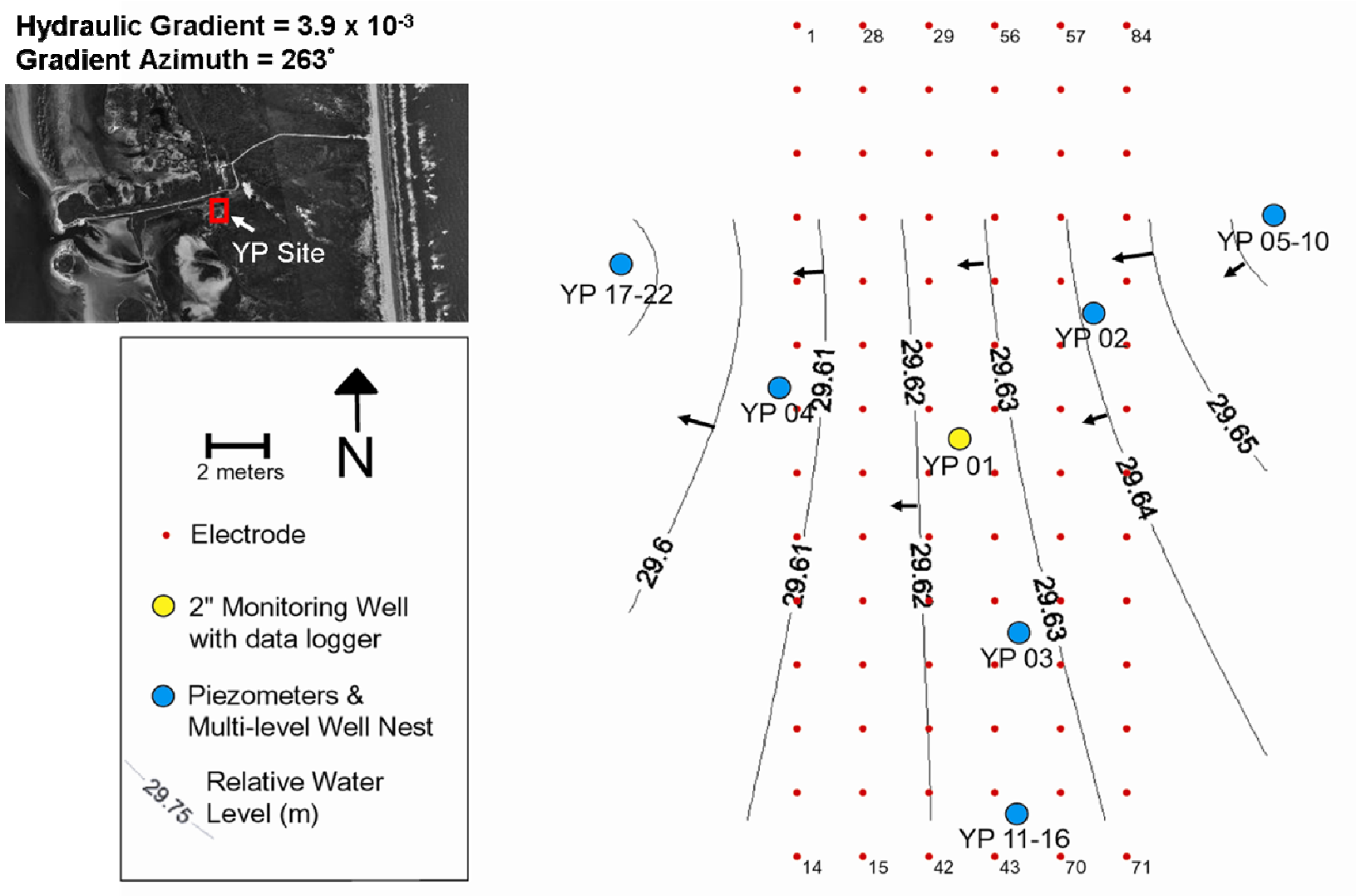

Figure 33 June 20, 2005 Yarborough Pass Relative Freshwater Levels

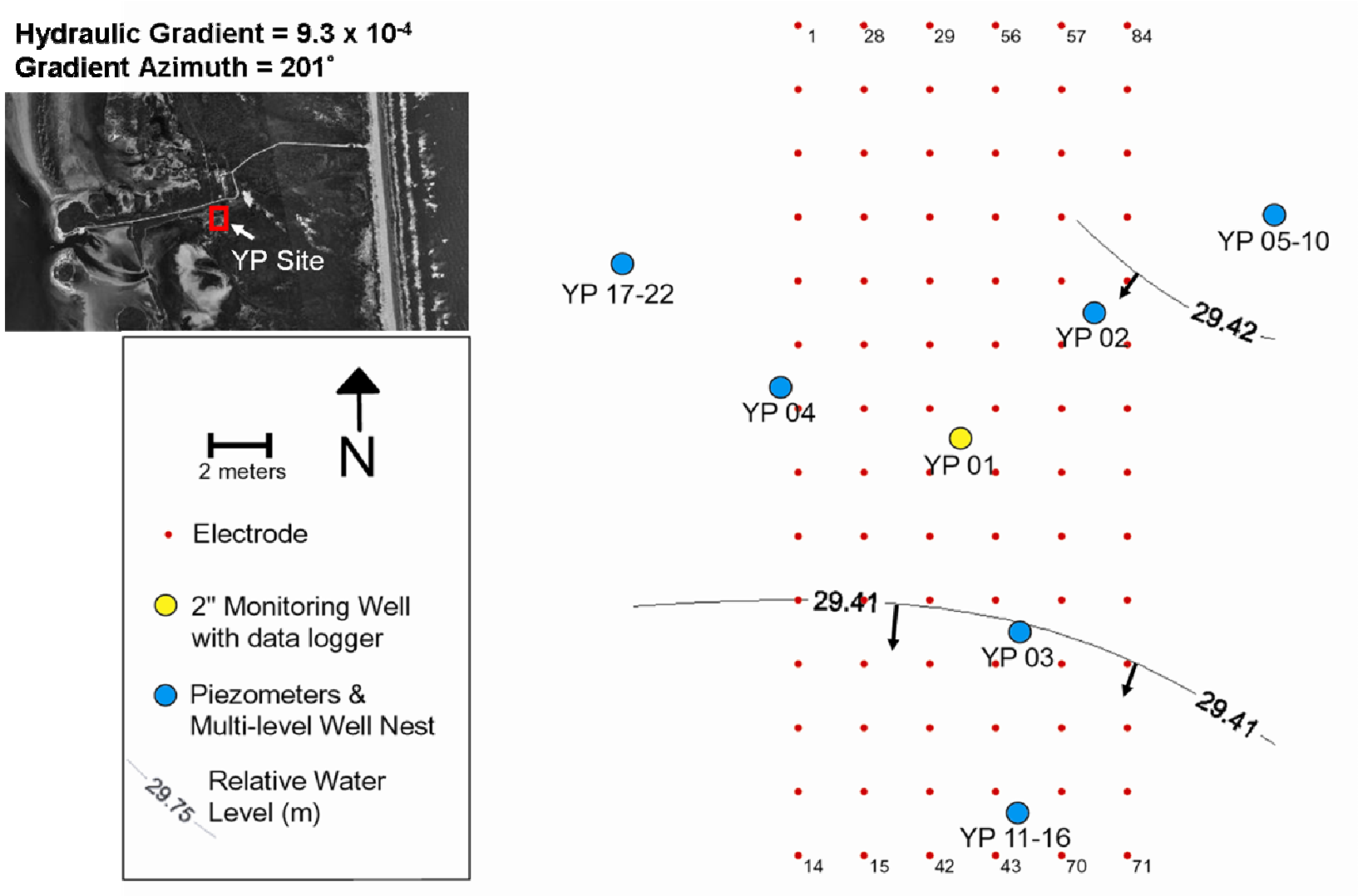

Figure 34 July 5, 2005 Yarborough Pass Relative Freshwater Levels

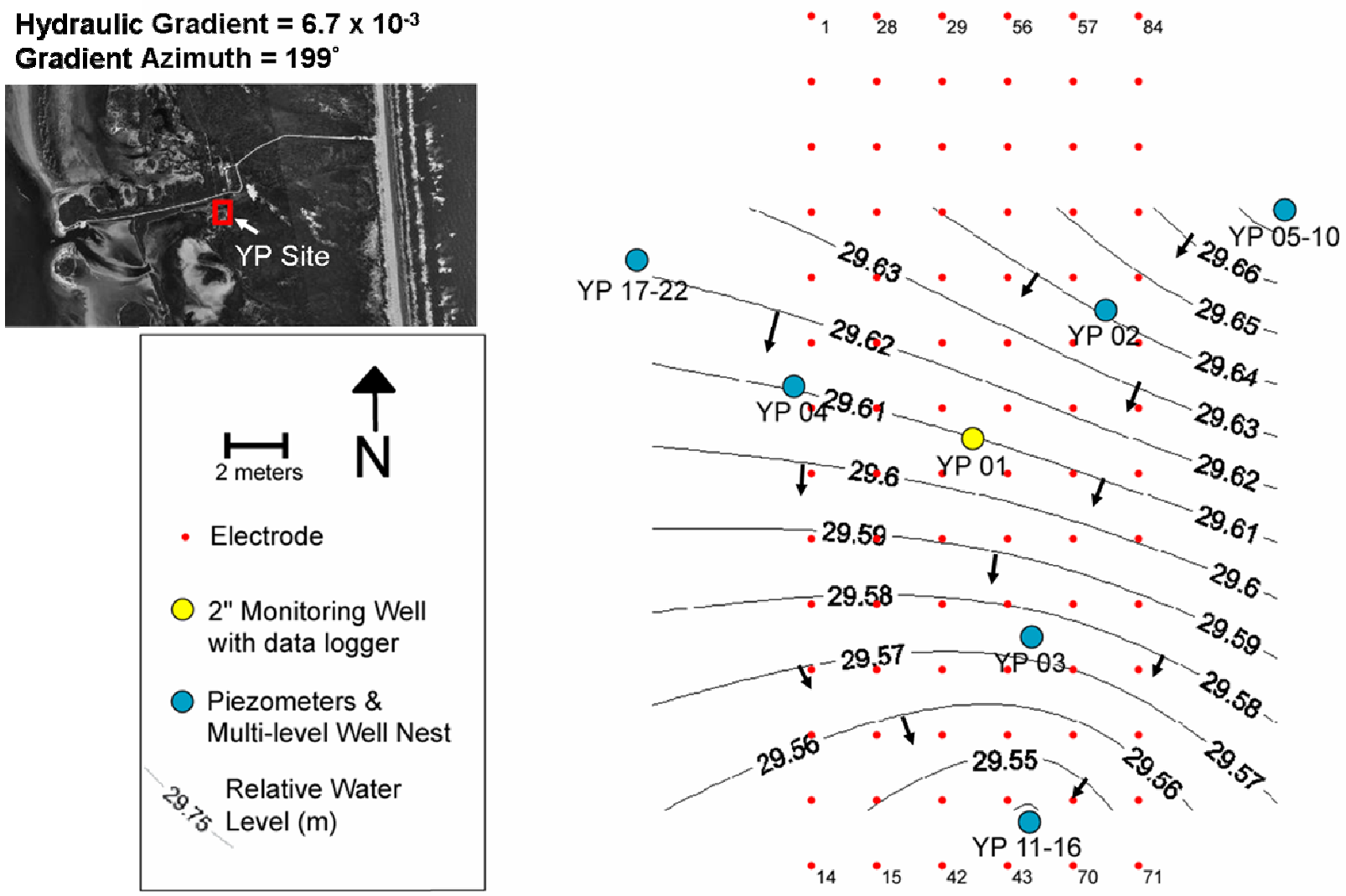

Figure 35 July 27, 2005 Yarborough Pass Relative Freshwater Levels

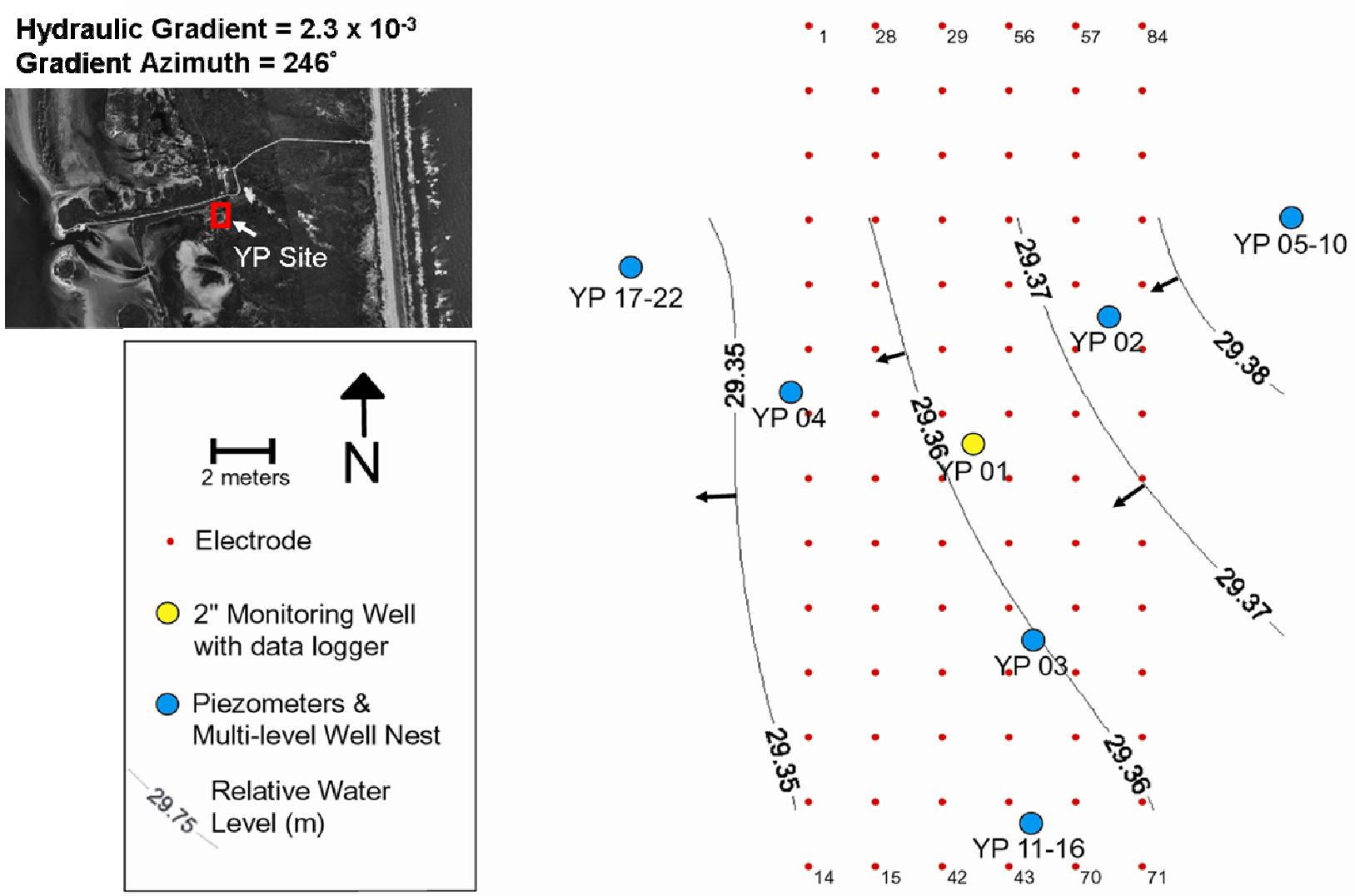

Figure 36 August 16, 2005 Yarborough Pass Relative Freshwater Levels

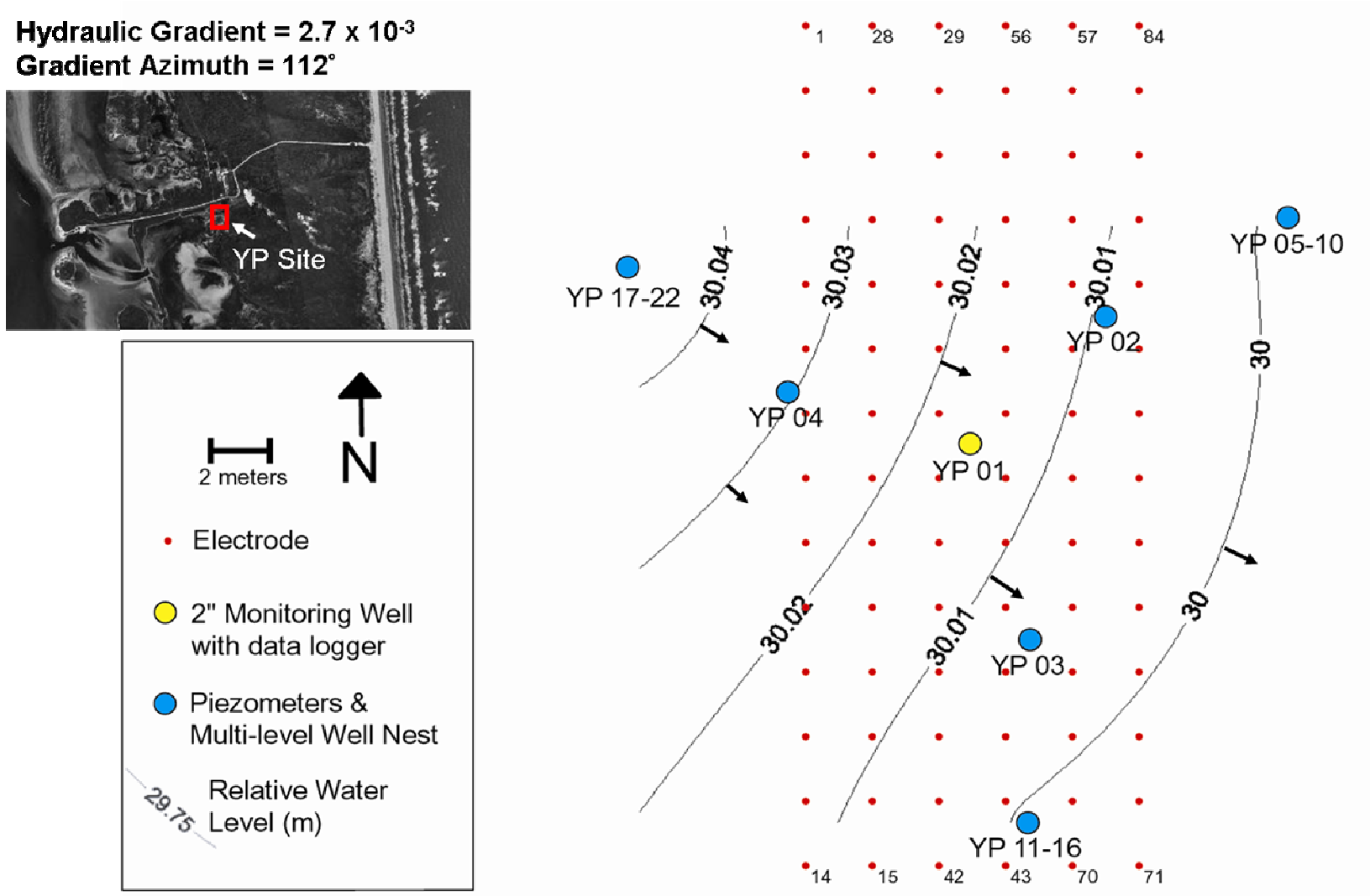

Figure 37 September 14, 2005 Yarborough Pass Relative Freshwater Levels

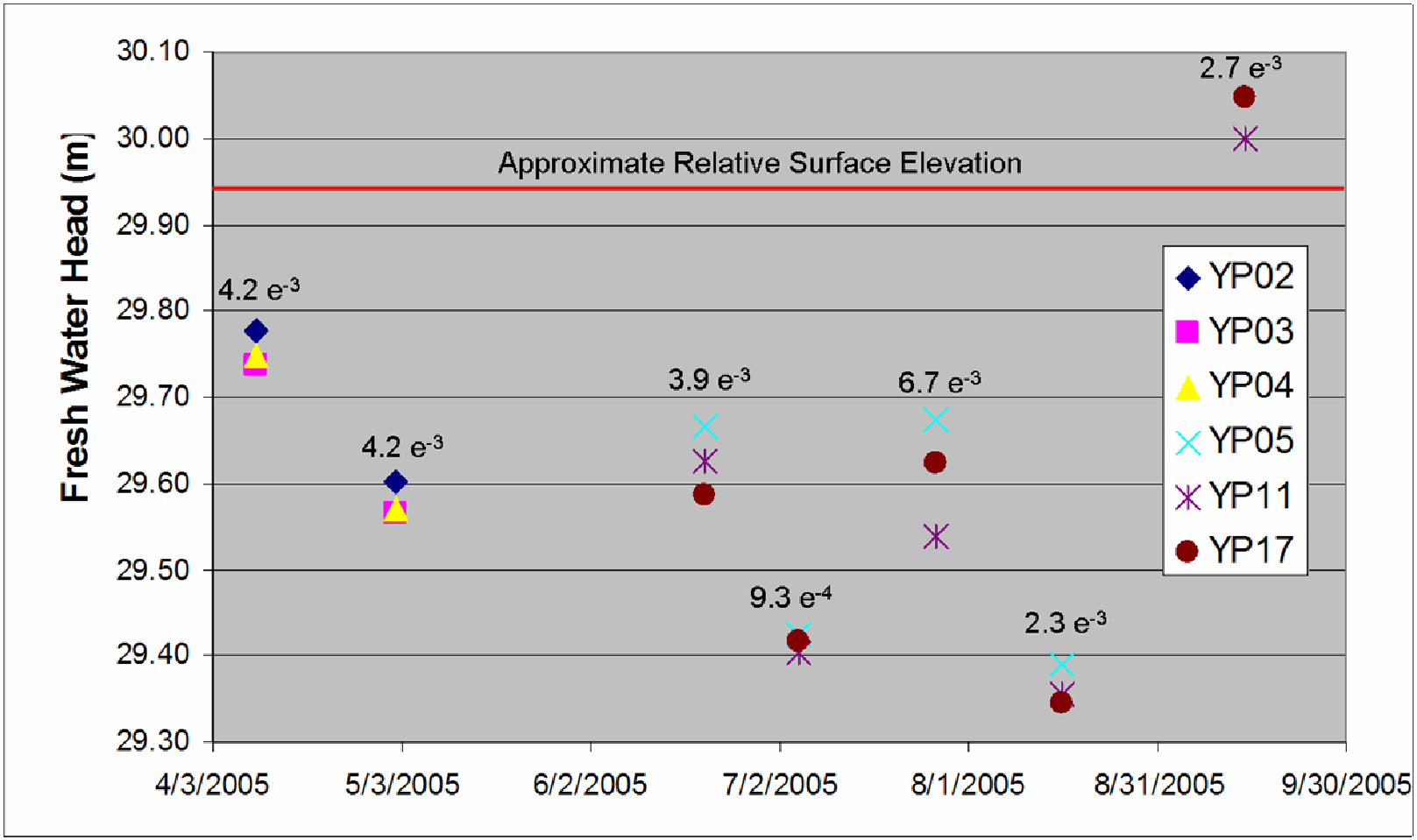

Figure 38 Profile of Yarborough Pass Relative Freshwater Head
Horizontal hydraulic gradients between the wells and the approximate surface elevation are also noted. During the September 14th visit, the site was flooded and was reflected in the fresh water head data.

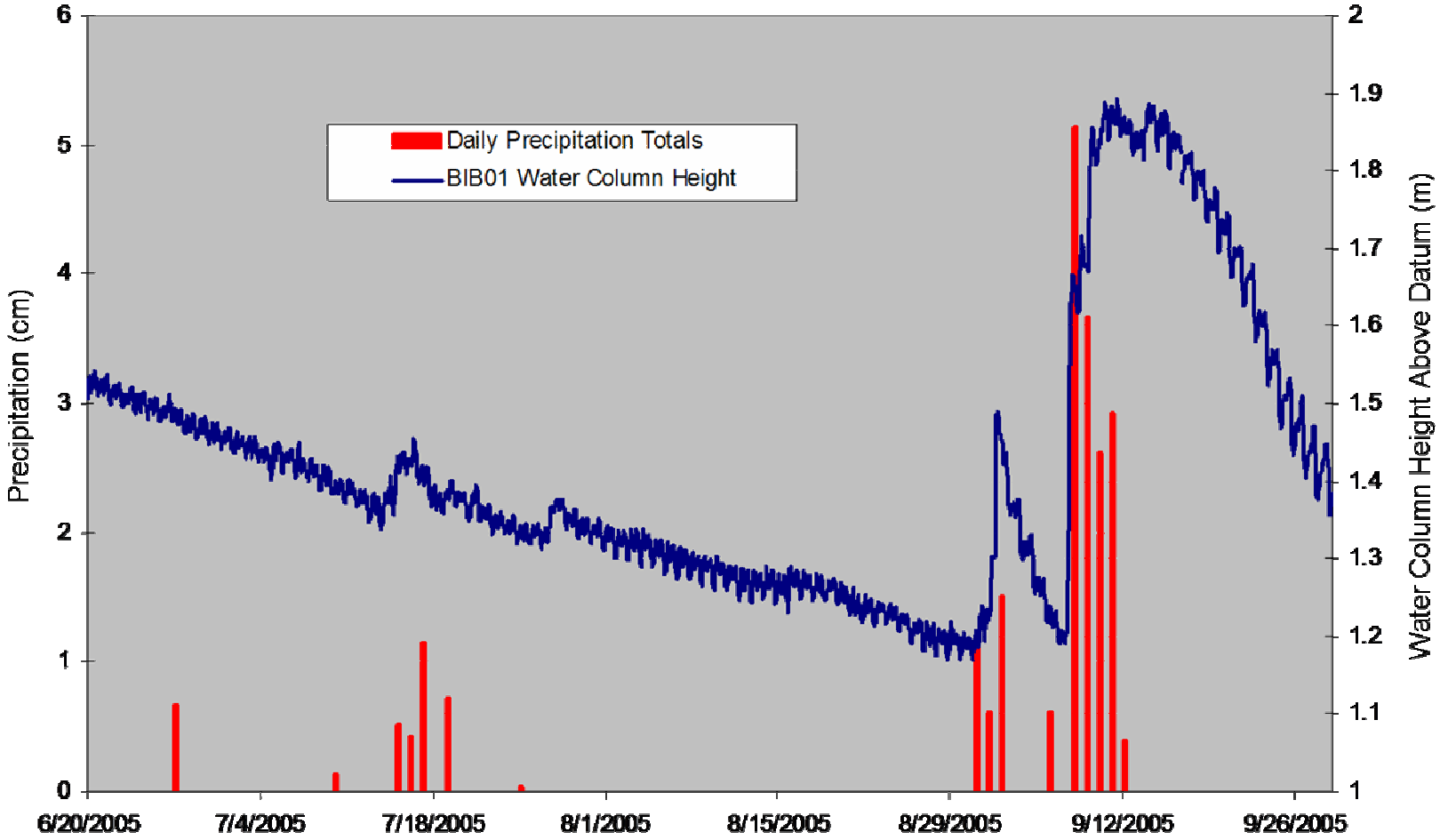

Figure 39 Bird Island Basin Water Column Height and Precipitation
Precipitation data from Padre Island National Seashore weather station and water column height from data logger installed in well BIB01.

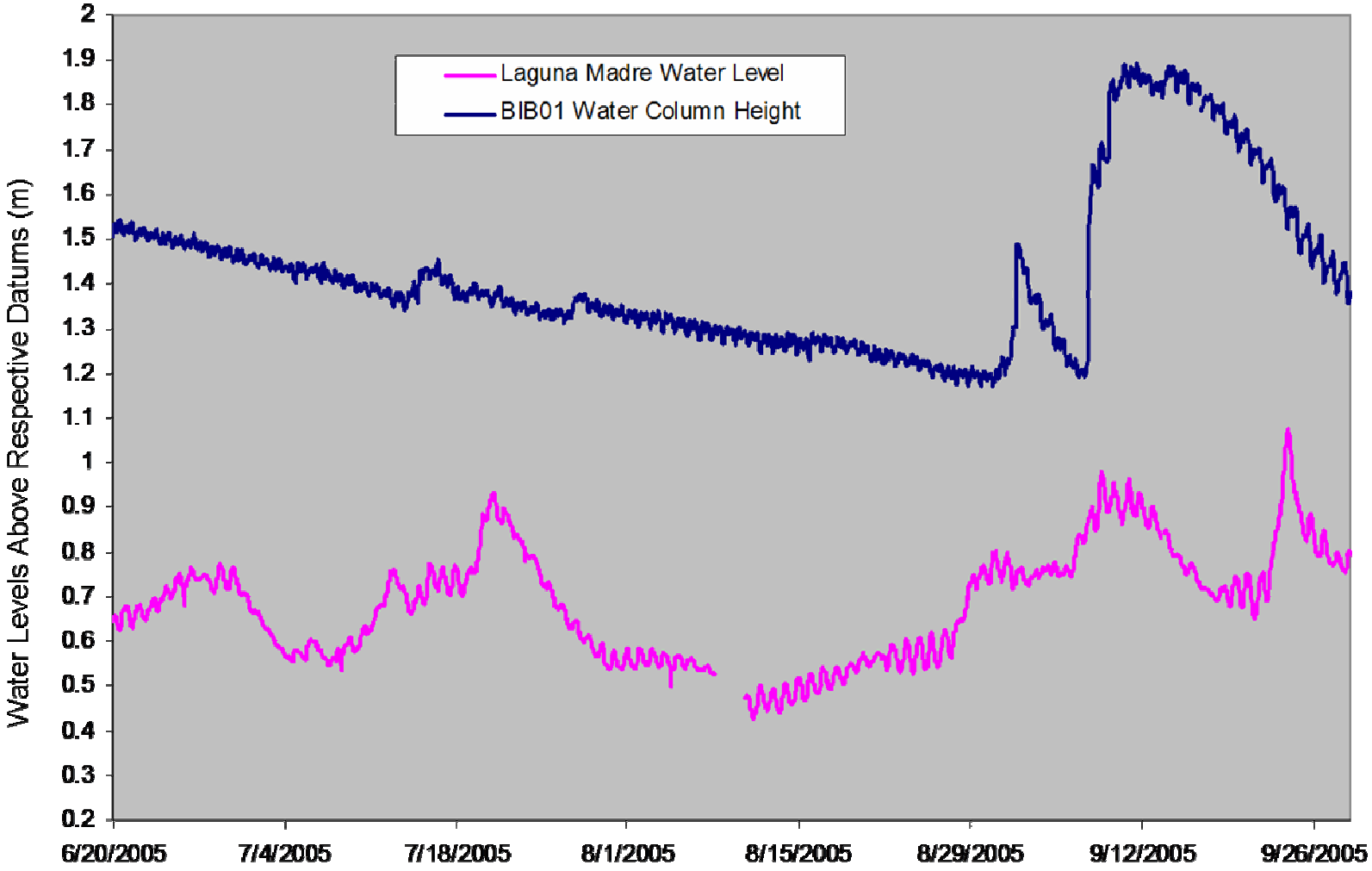

Figure 40 Bird Island Basin Water Column Height and Laguna Madre Level
Laguna Madre water level data from TCOON station 013 at South Bird Island.

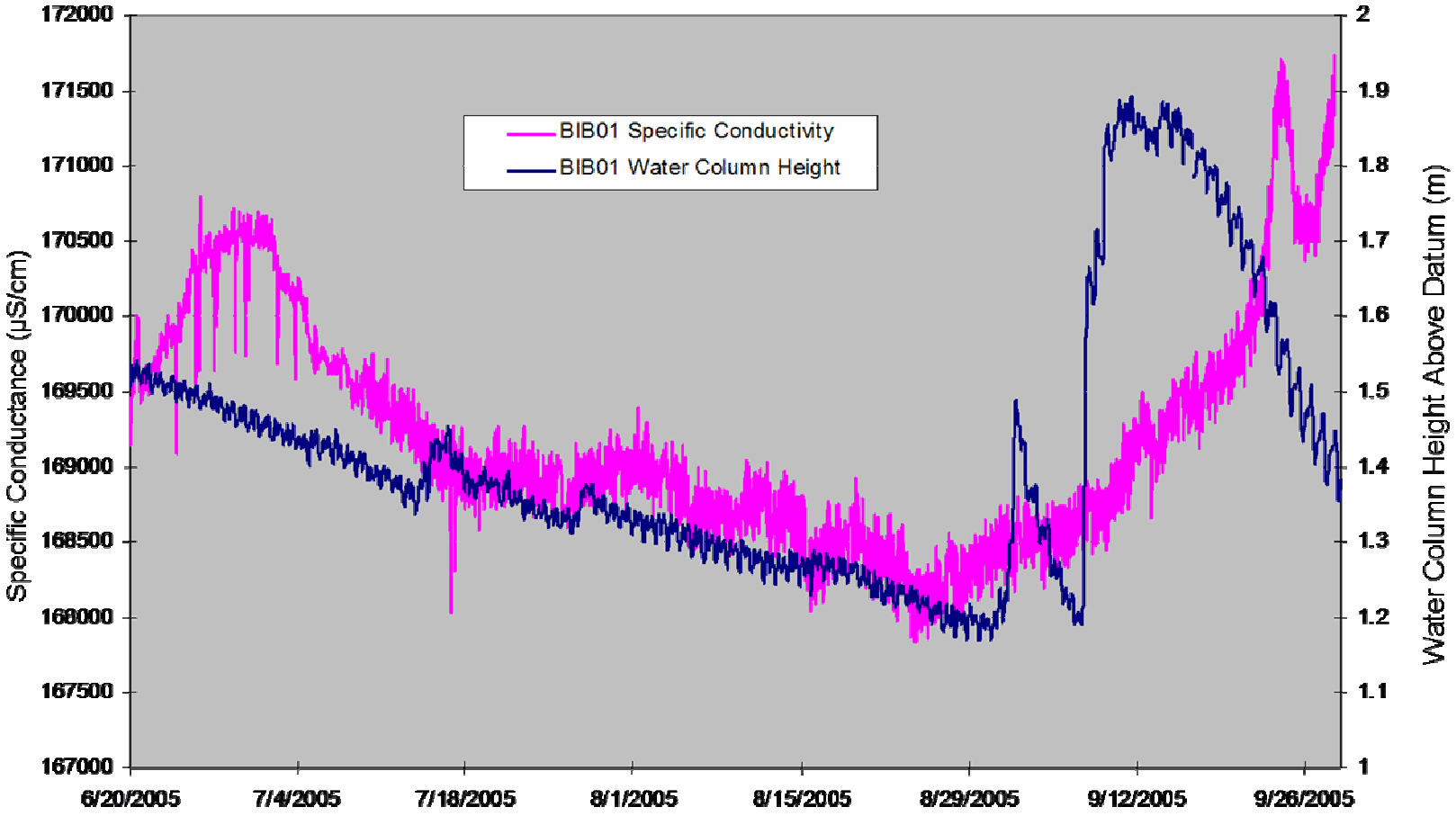

Figure 41 Bird Island Basin Water Column Height and Specific Conductance
Water column height and specific conductance from data logger installed in well BIB01.

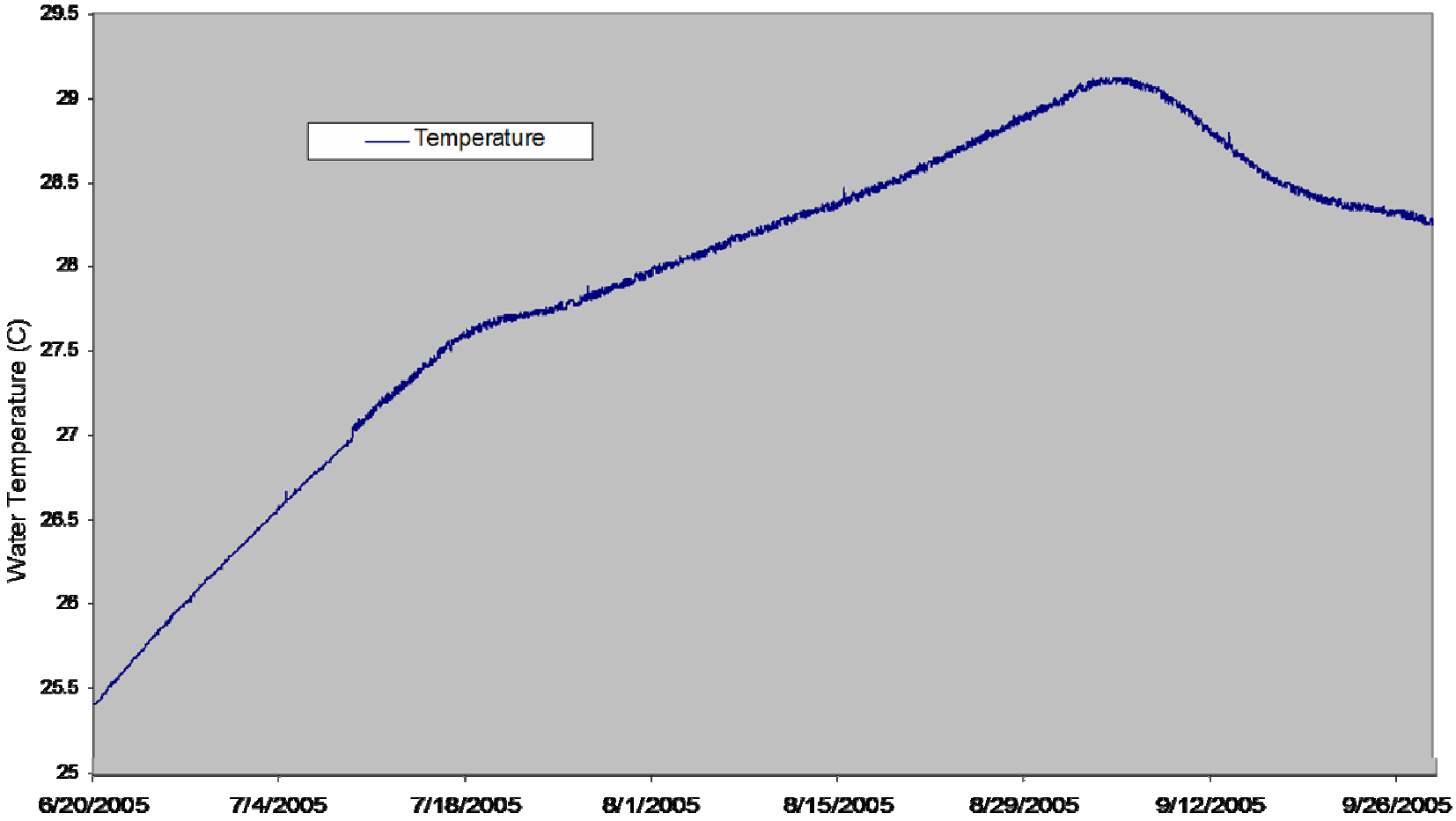

Figure 42 Bird Island Basin Groundwater Temperature
Water temperature from data logger installed in well BIB01.

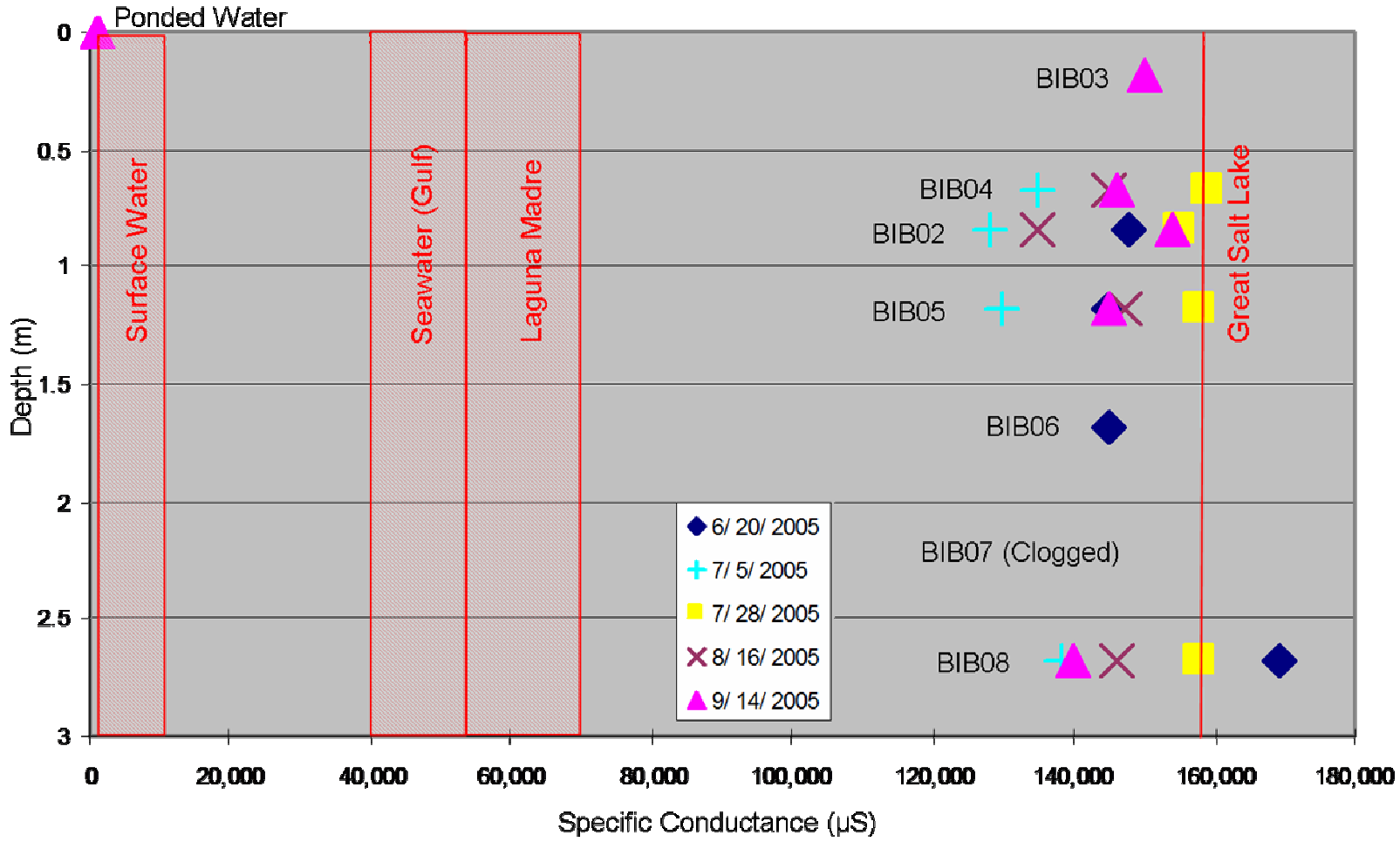

Figure 43 BIB02-08 (East Nest) Specific Conductance Profile

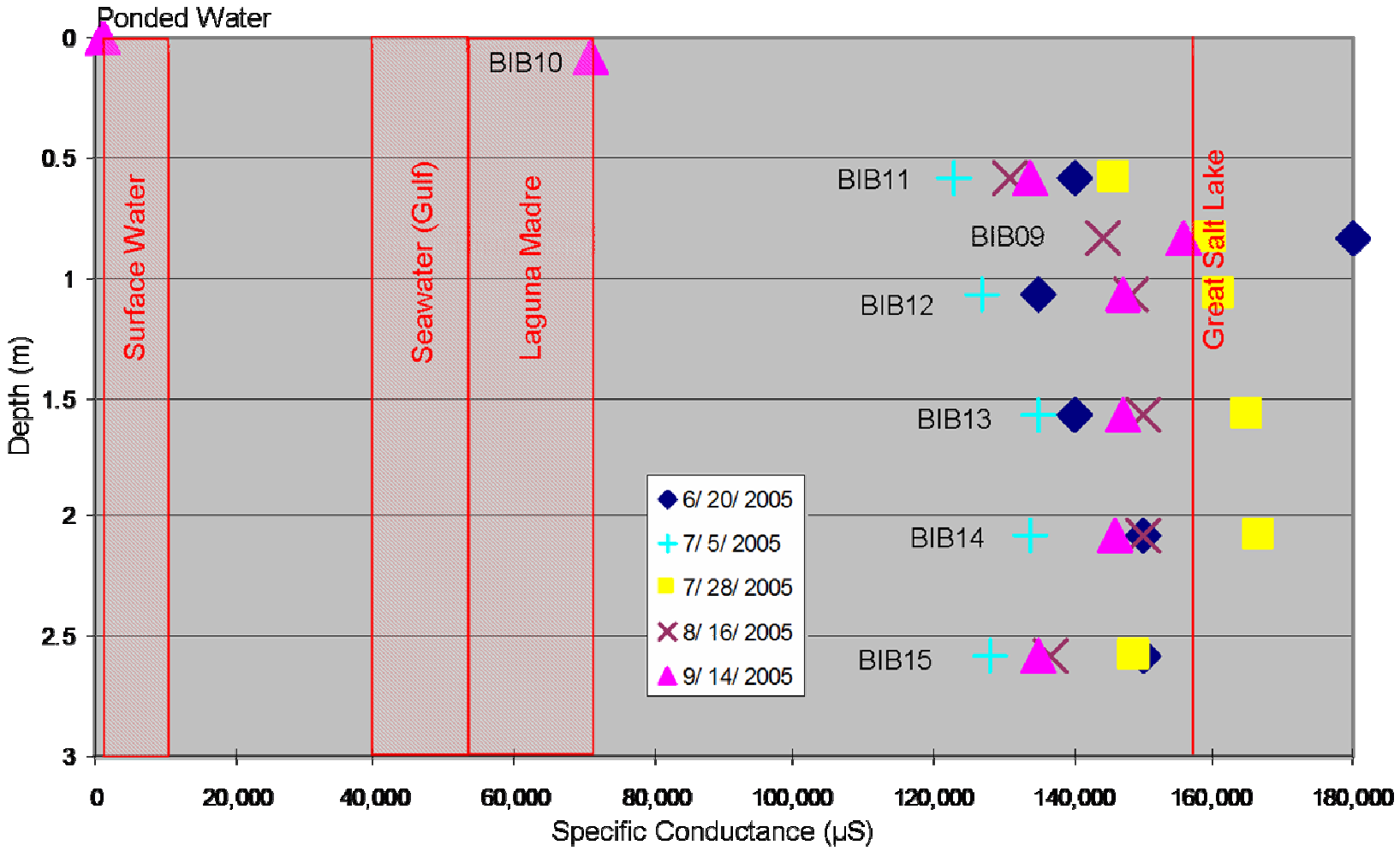

Figure 44 BIB09-15 (Southwest Nest) Specific Conductance Profile

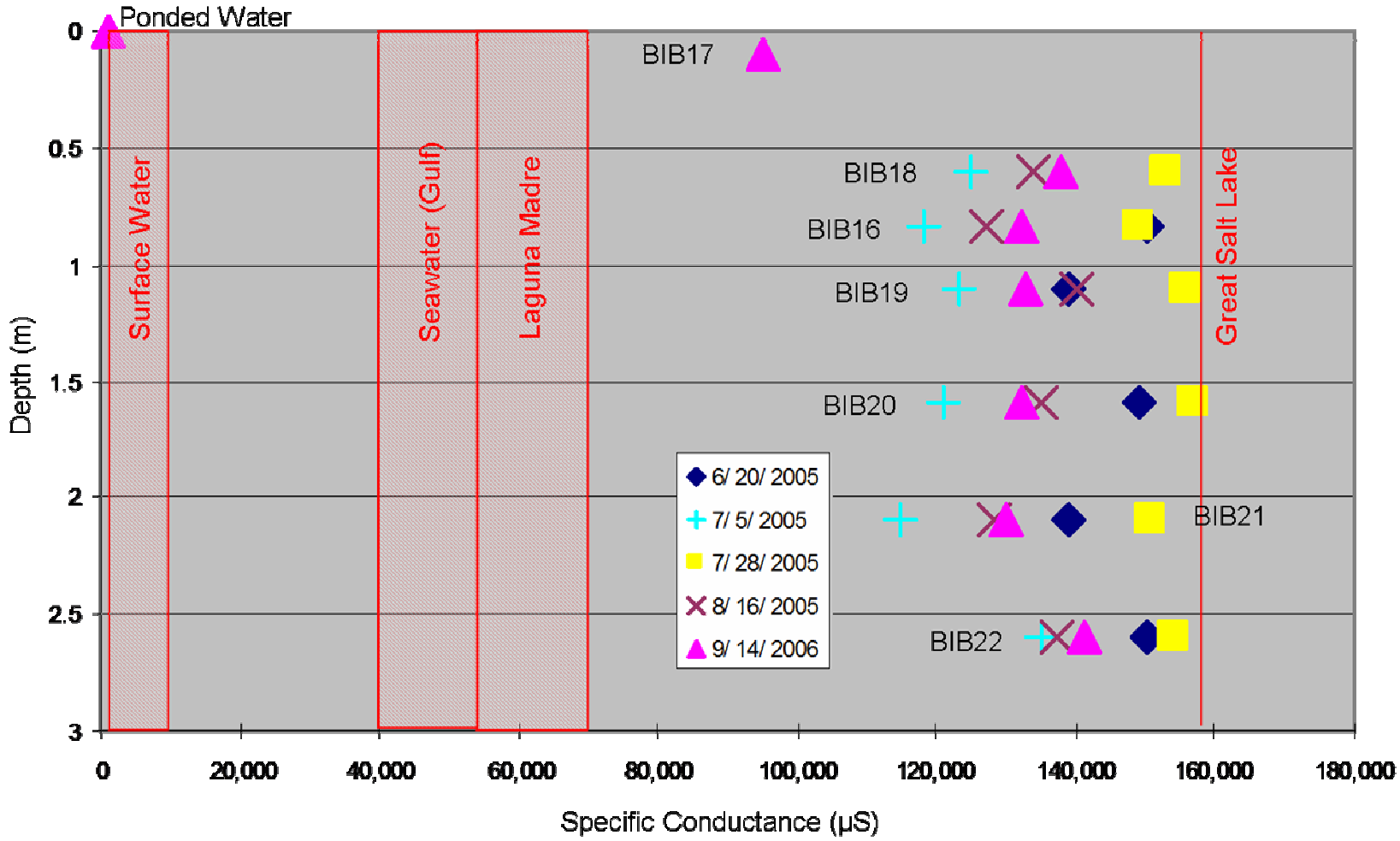

Figure 45 BIB16-22 (Northwest Nest) Specific Conductance Profile

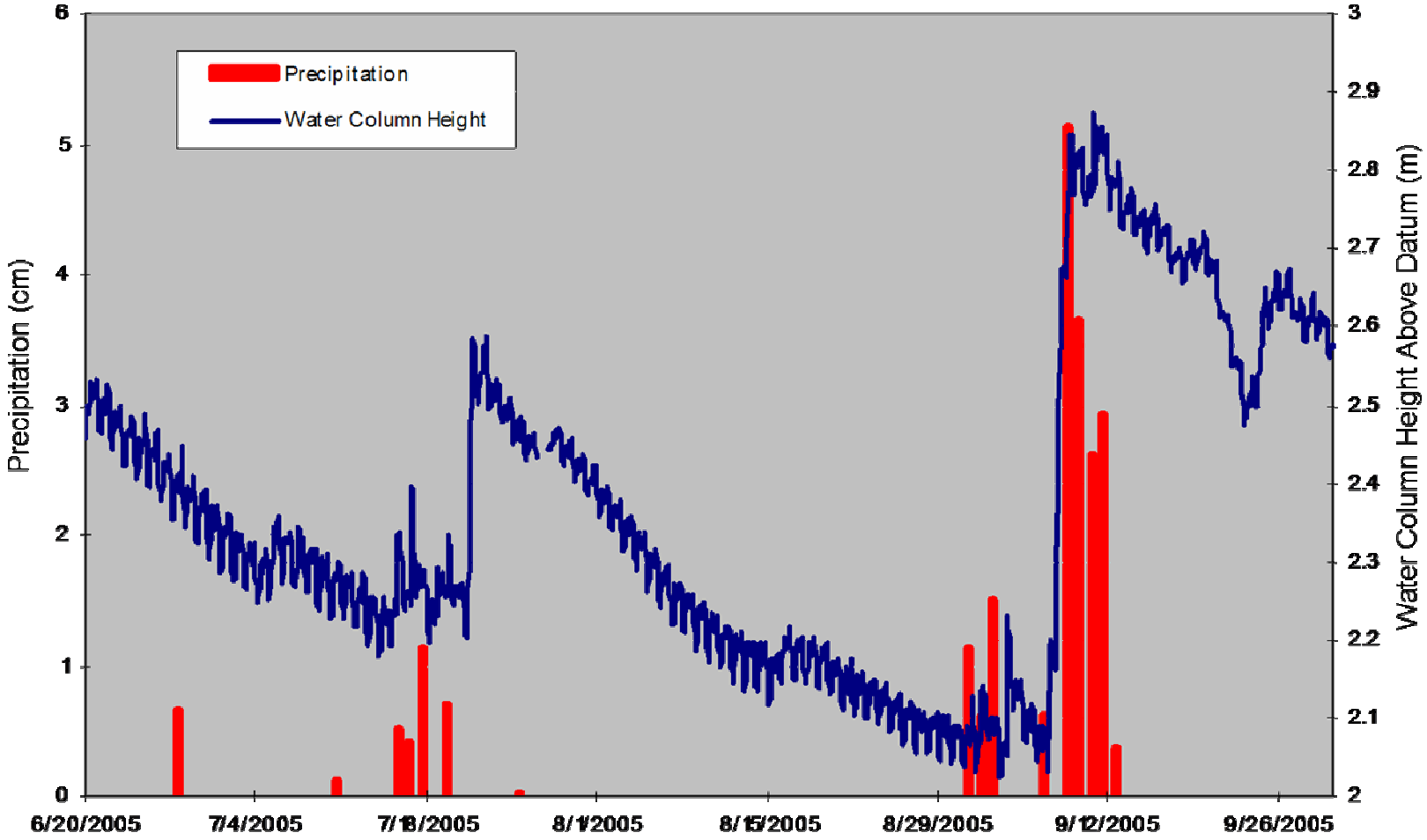

Figure 46 Yarborough Pass Water Column Height and Precipitation
Precipitation data from Padre Island National Seashore Headquarters and water column height from data logger installed in YP01.

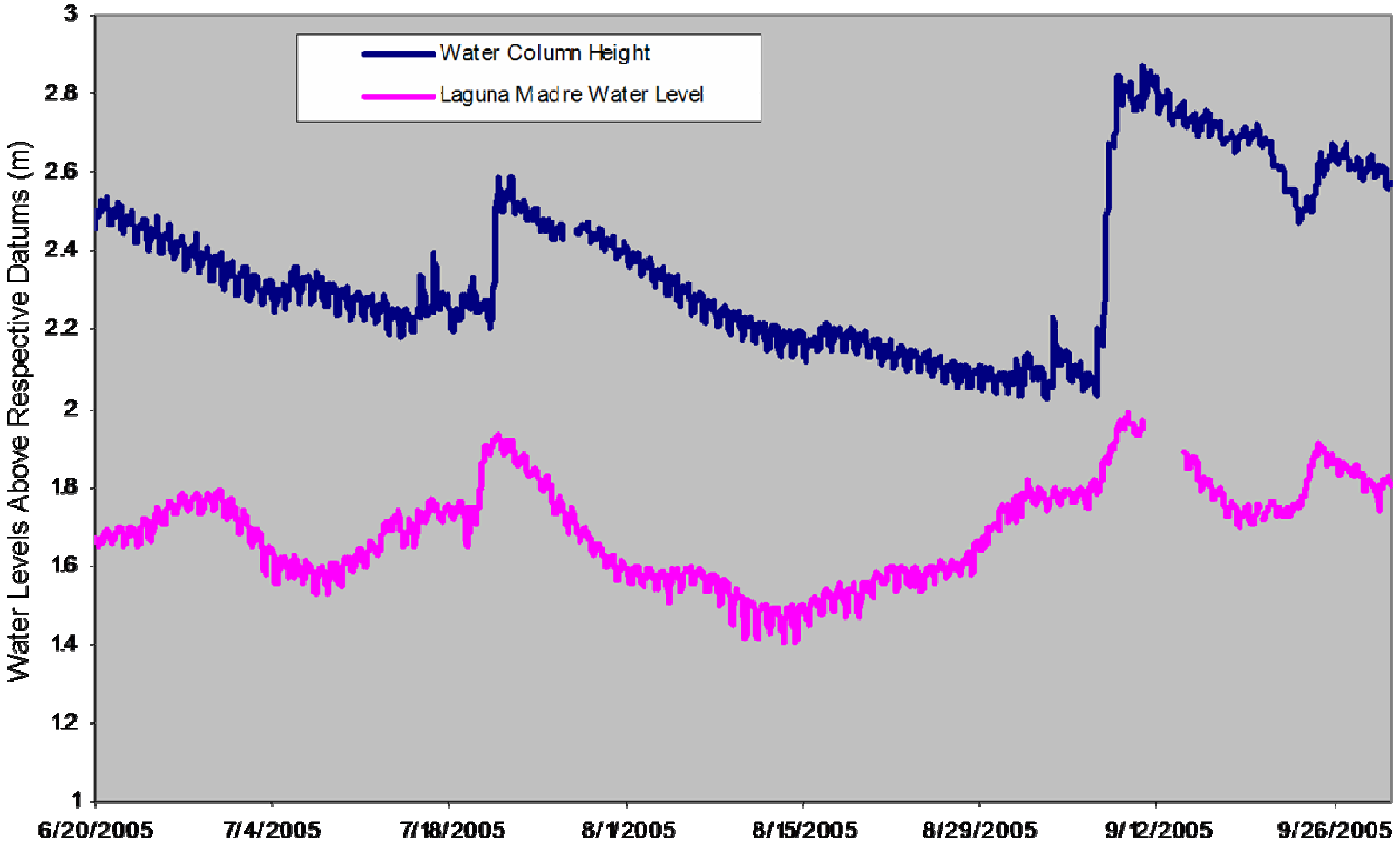

Figure 47 Yarborough Pass Water Column Height and Laguna Madre Level
Laguna Madre level from TCOON station 068 at Baffin Bay and water column height from data logger installed in well YP01.

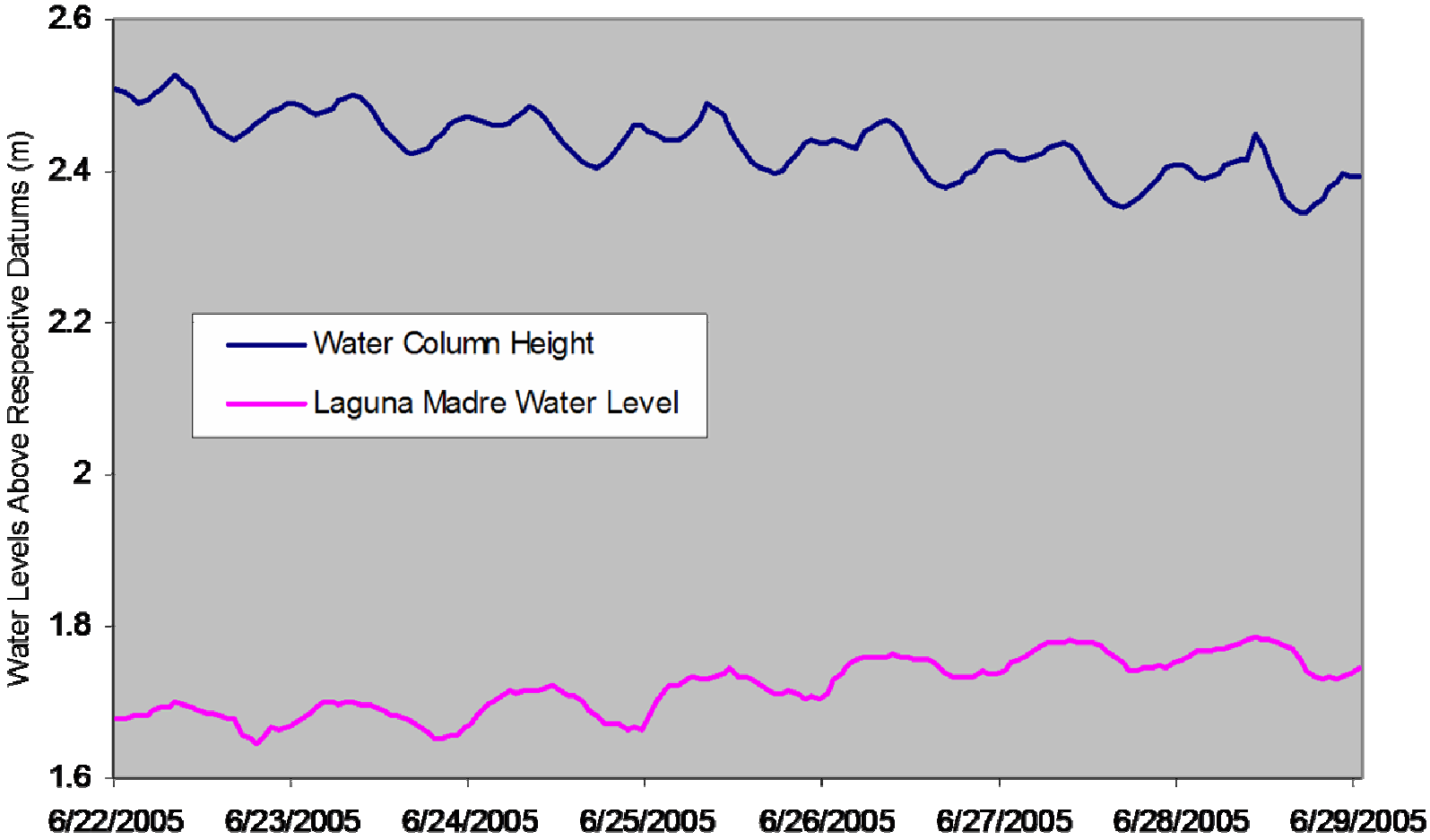

Figure 48 Close Up View of Yarborough Pass Water Column Height and Laguna Madre Level
Examination of fluctuations at Yarborough Pass and Laguna Madre show the diurnal cycle of tides in Laguna Madre and the semi-diurnal cycle of water levels at the Yarborough Pass site.

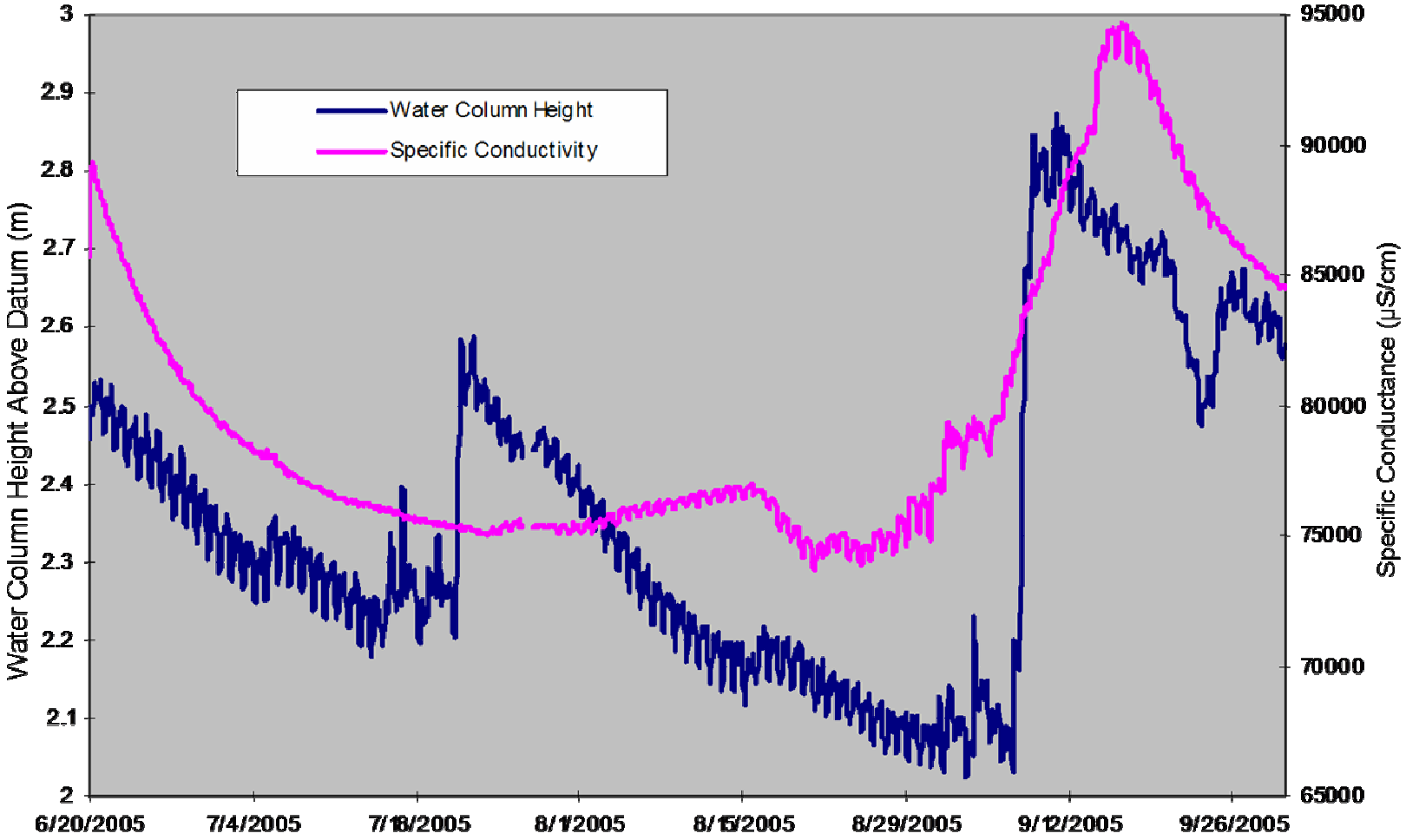

Figure 49 Yarborough Pass Water Column Height and Specific Conductance
Water column height and specific conductance from data logger installed in YP01.

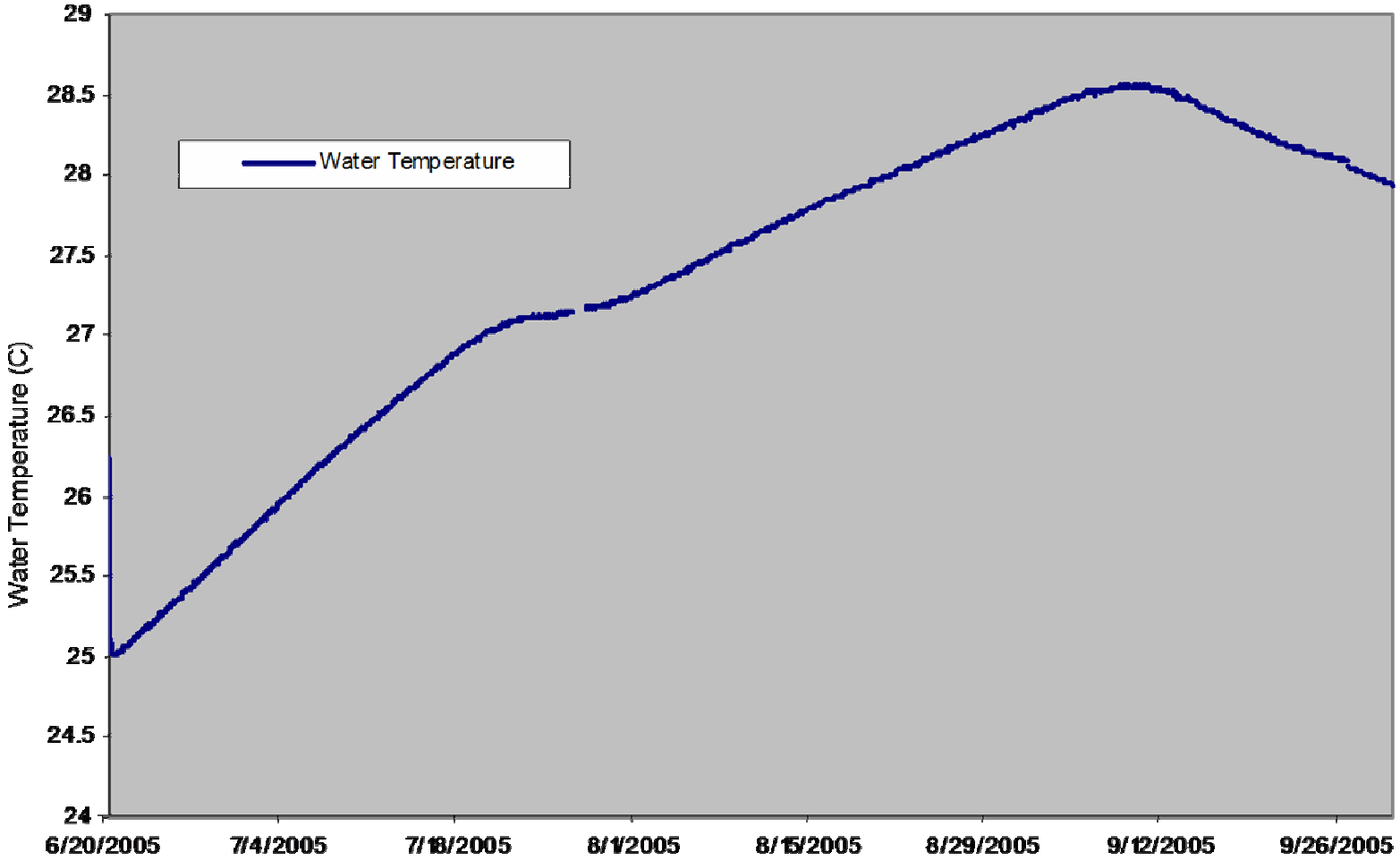

Figure 50 Yarborough Pass Groundwater Temperature
Groundwater temperature from data logger installed in well YP01.

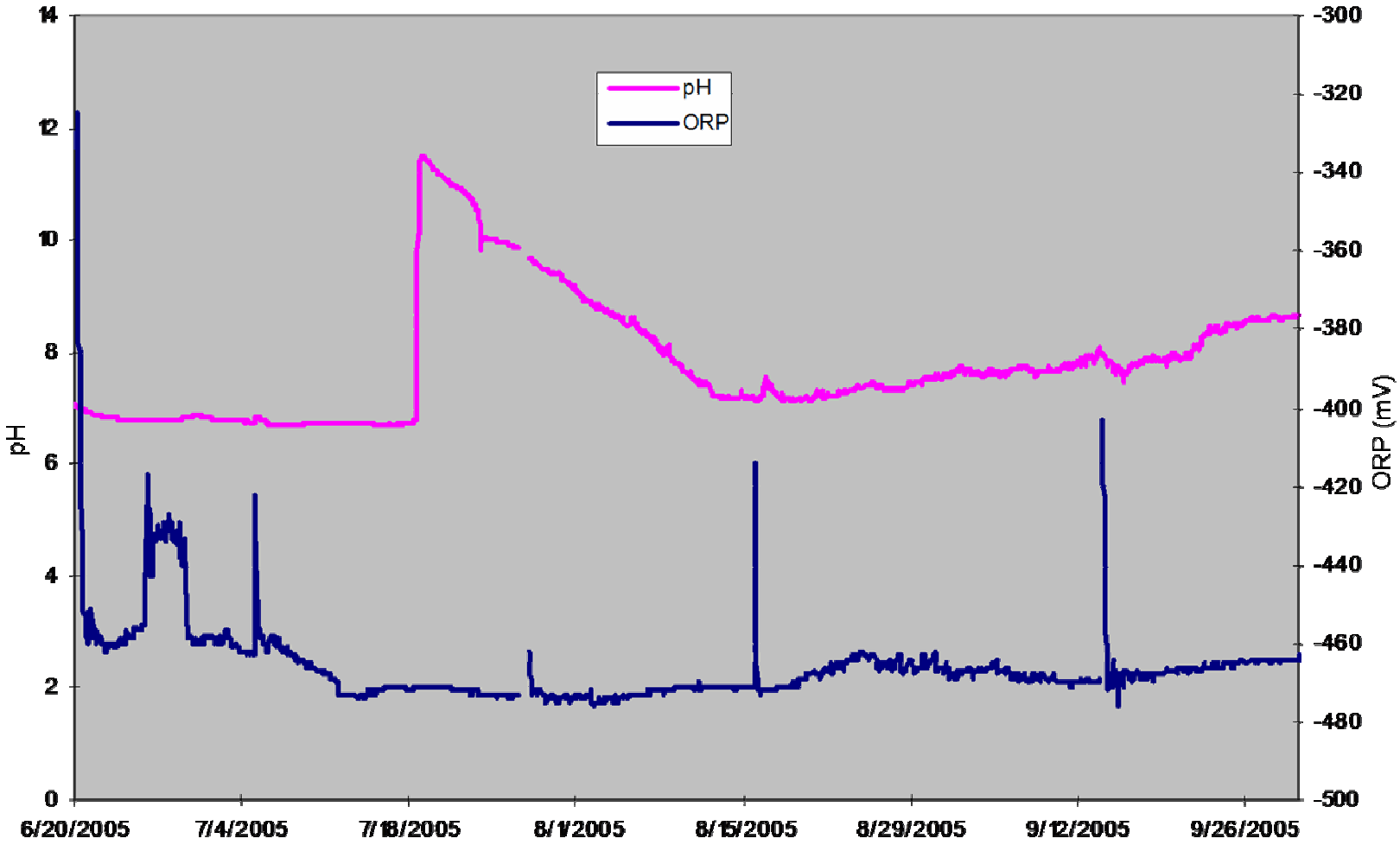

Figure 51 Yarborough Pass pH and Oxygen Reduction Potential (ORP)
pH and ORP from data logger installed in well YP01. Note the fouling of the pH sensor on July 20th and the spikes in ORP data when the data logger was pulled from the well for data download.

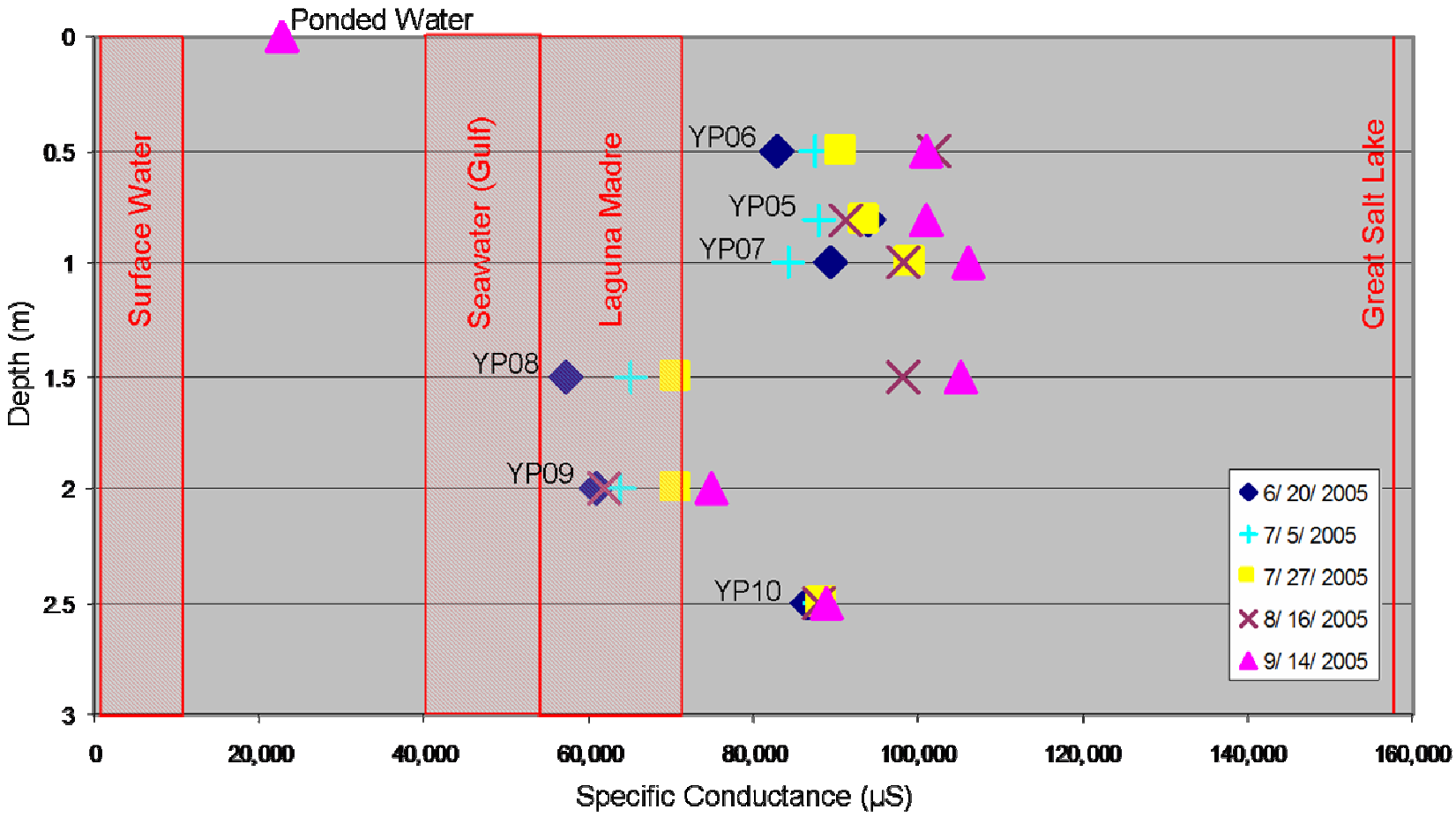

Figure 52 YP05-10 (Northeast Nest) Specific Conductance Profile

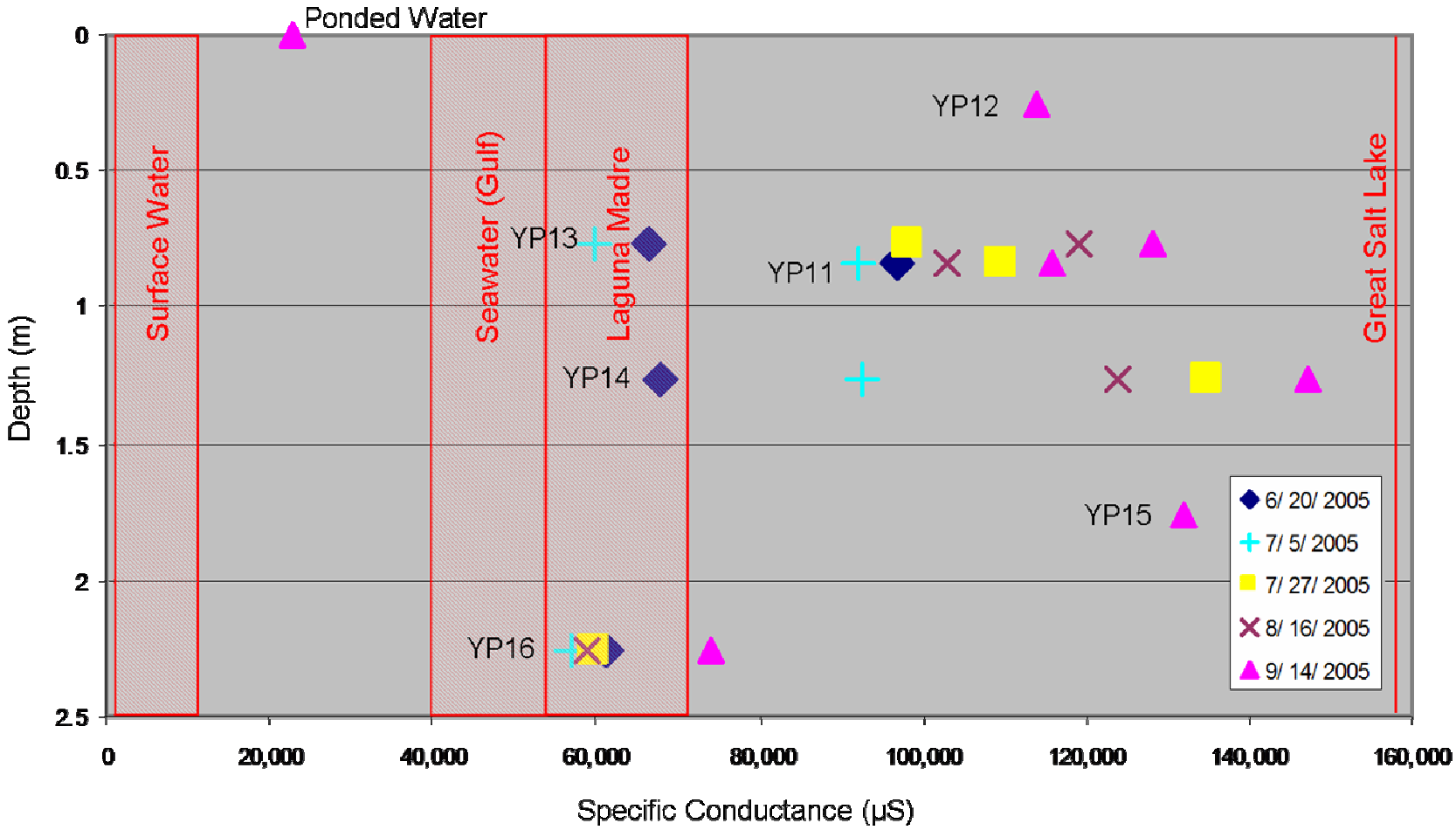

Figure 53 YP11-16 (South Nest) Specific Conductance Profile

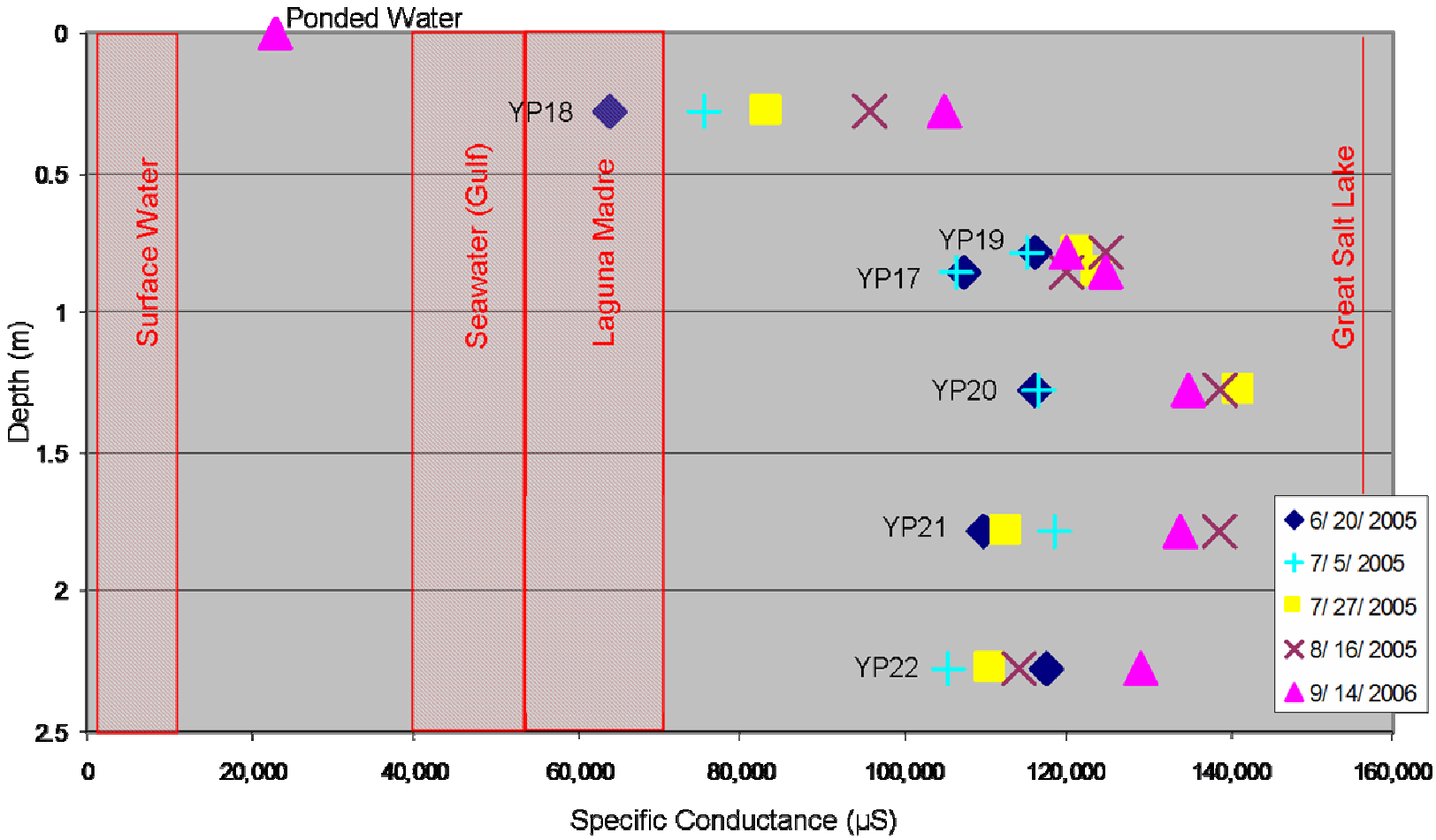

Figure 54 YP17-22 (Northwest Nest) Specific Conductance Profile

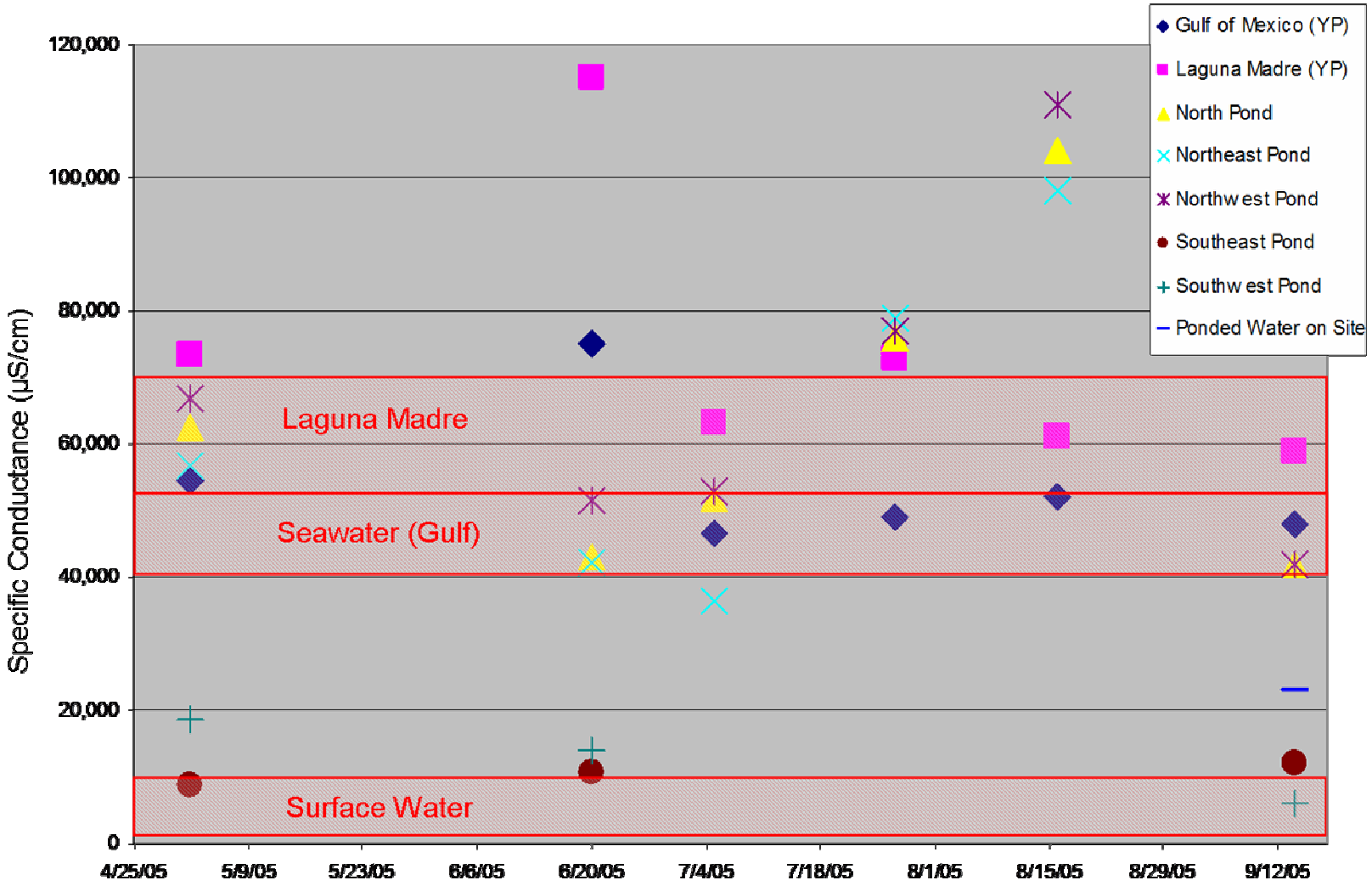

Figure 55 Yarborough Pass Surface Water Specific Condutance

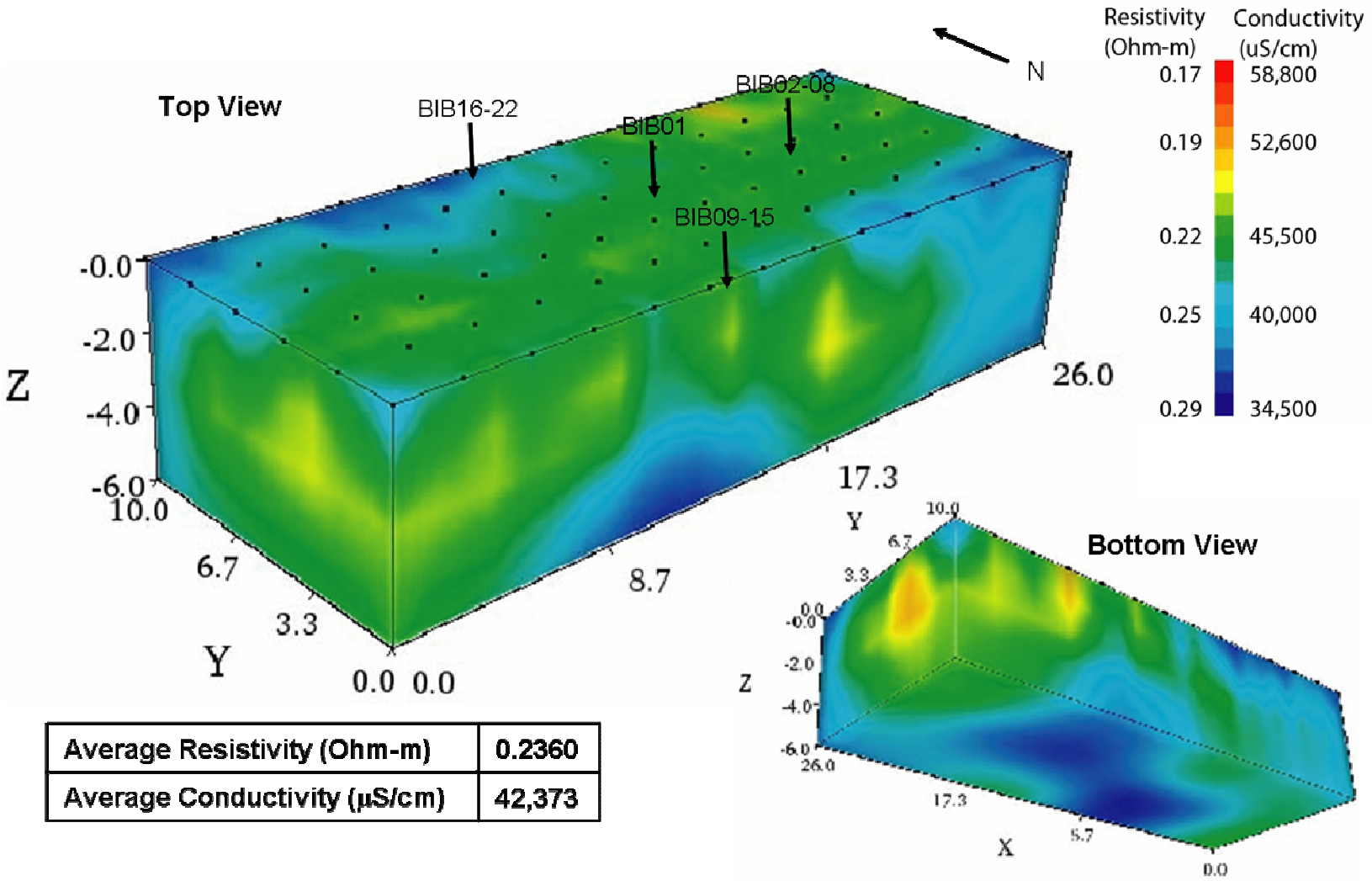

Average Resistivity (Ohm-m)	0.2360
Average Conductivity (µS/cm)	42,373

Figure 56 Bird Island Basin 3-D Resistivity, June 20, 2005
Approximate locations of wells are also noted.

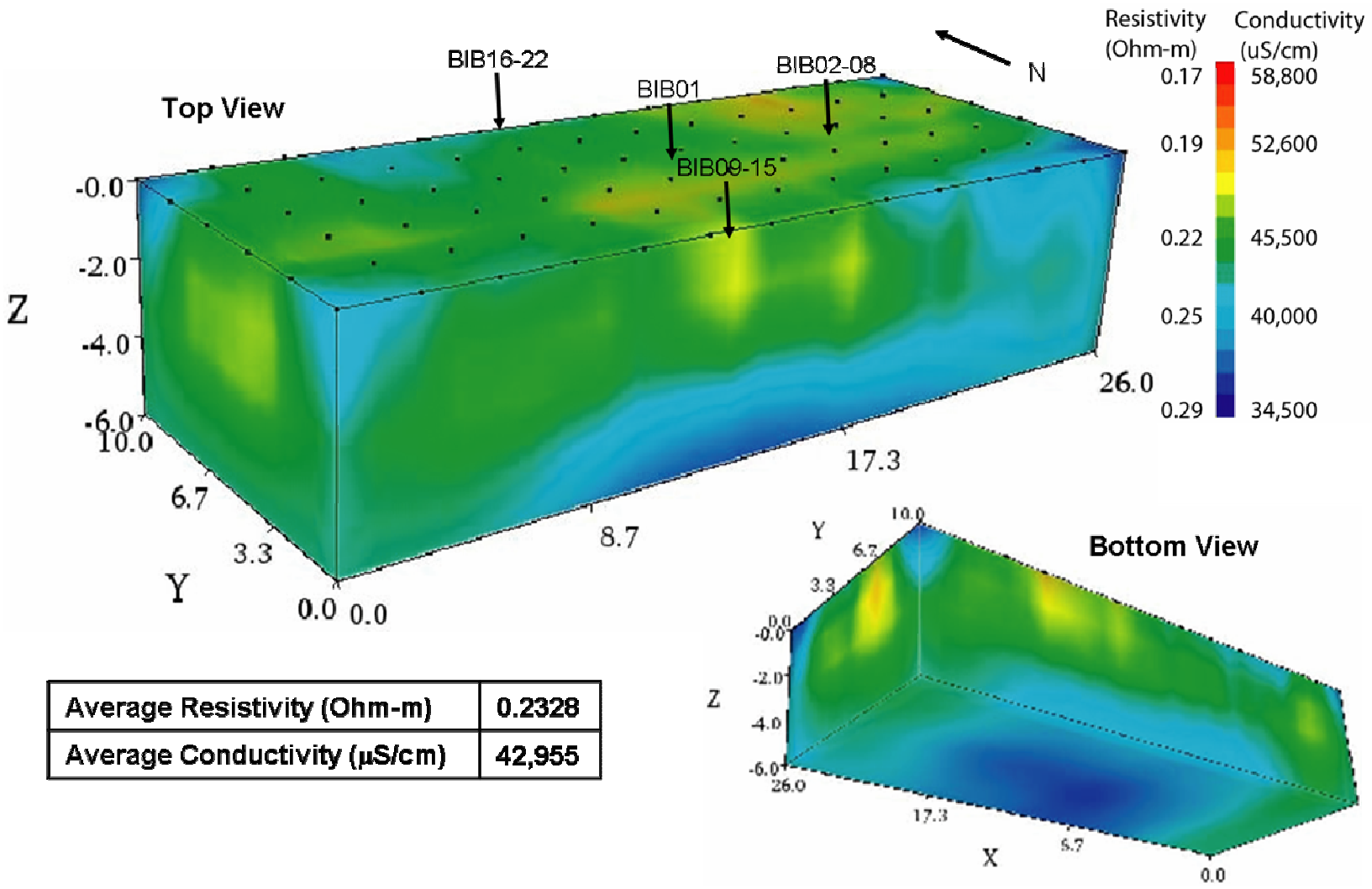

Average Resistivity (Ohm-m)	0.2328
Average Conductivity (µS/cm)	42,955

Figure 57 Bird Island Basin 3-D Resistivity, July 5, 2005

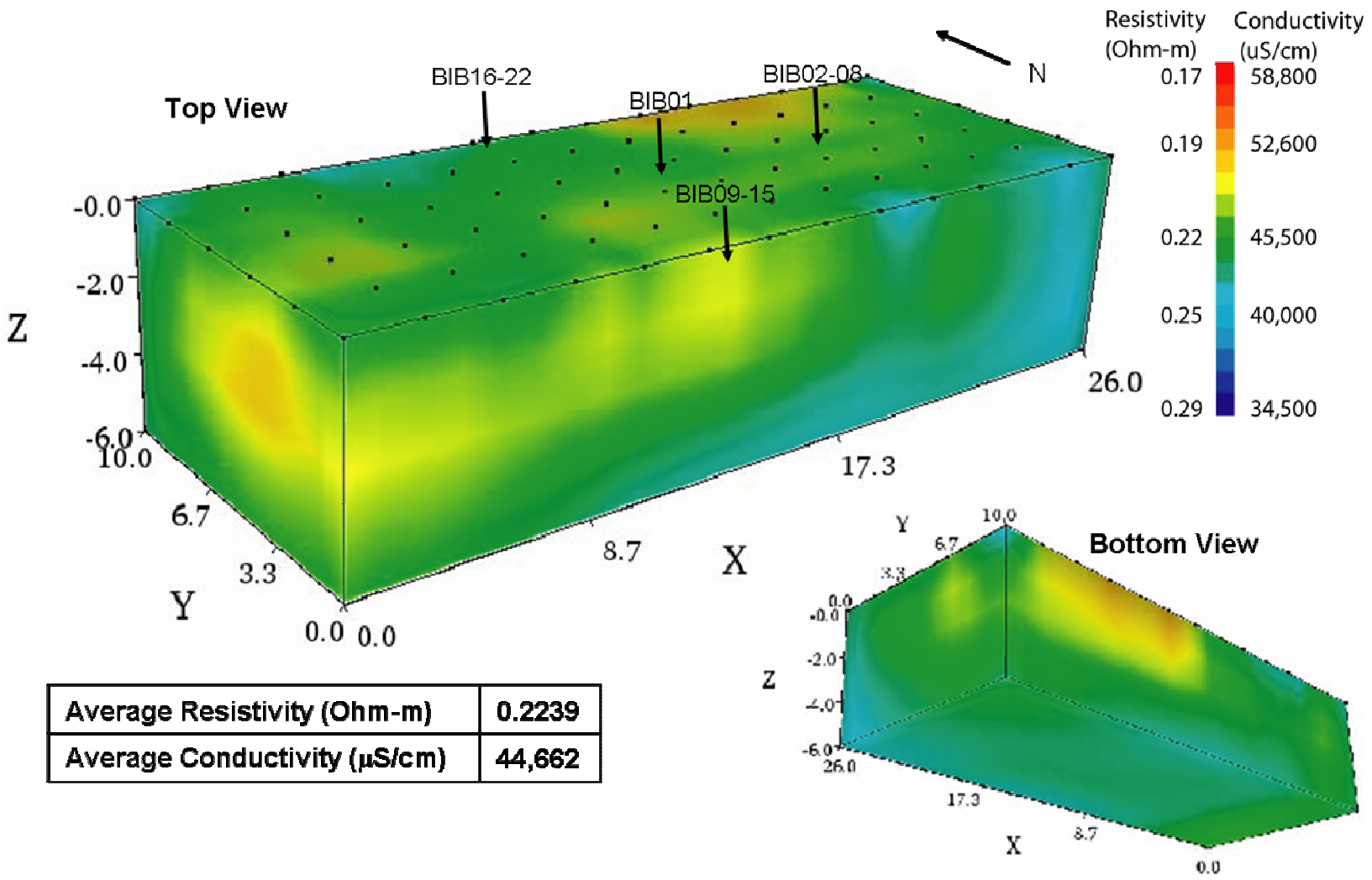

Average Resistivity (Ohm-m)	0.2239
Average Conductivity (µS/cm)	44,662

Figure 58 Bird Island Basin 3-D Resistivity, July 27, 2005

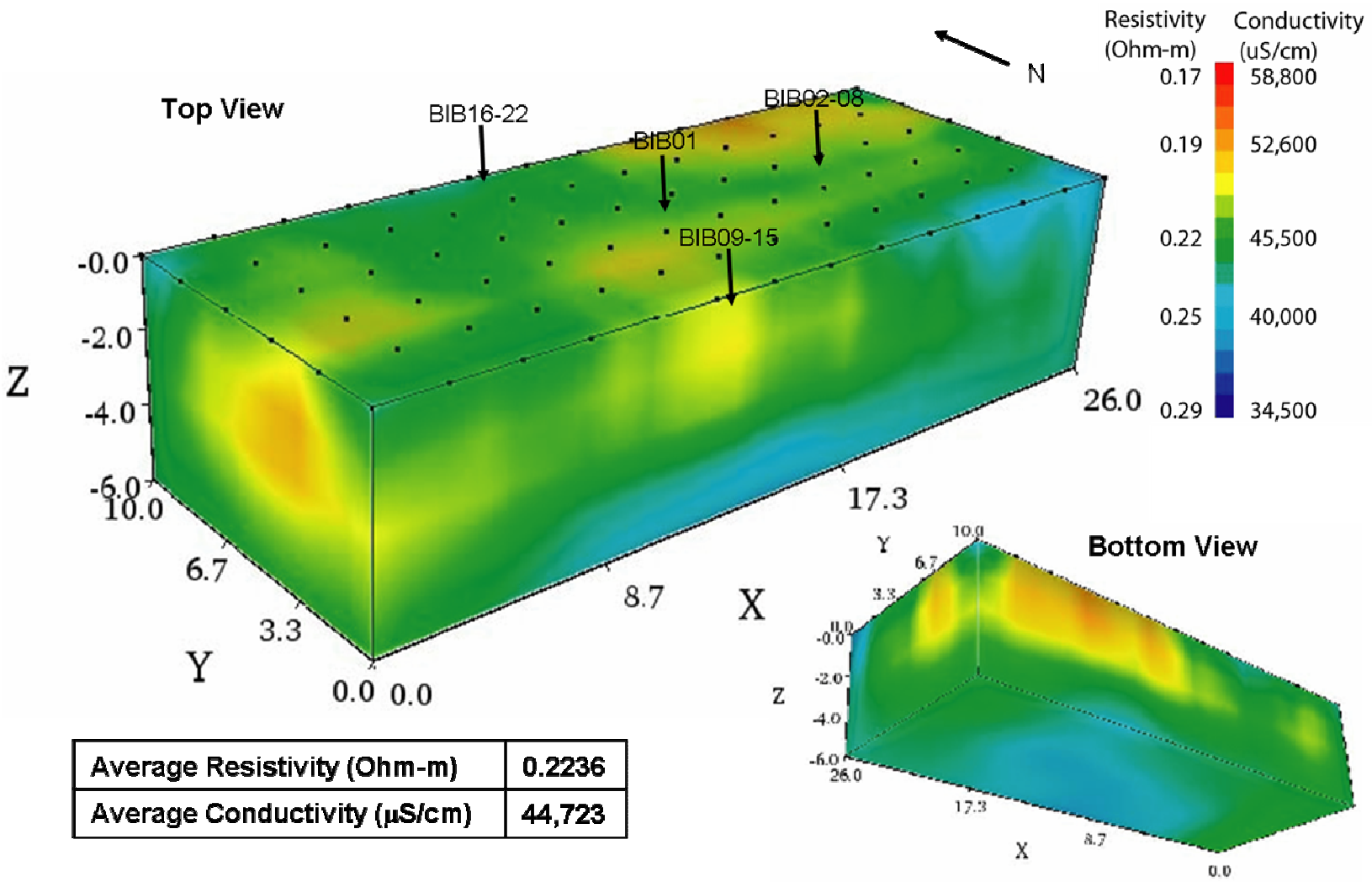

Figure 59 Bird Island Basin 3-D Resistivity, August 16, 2005

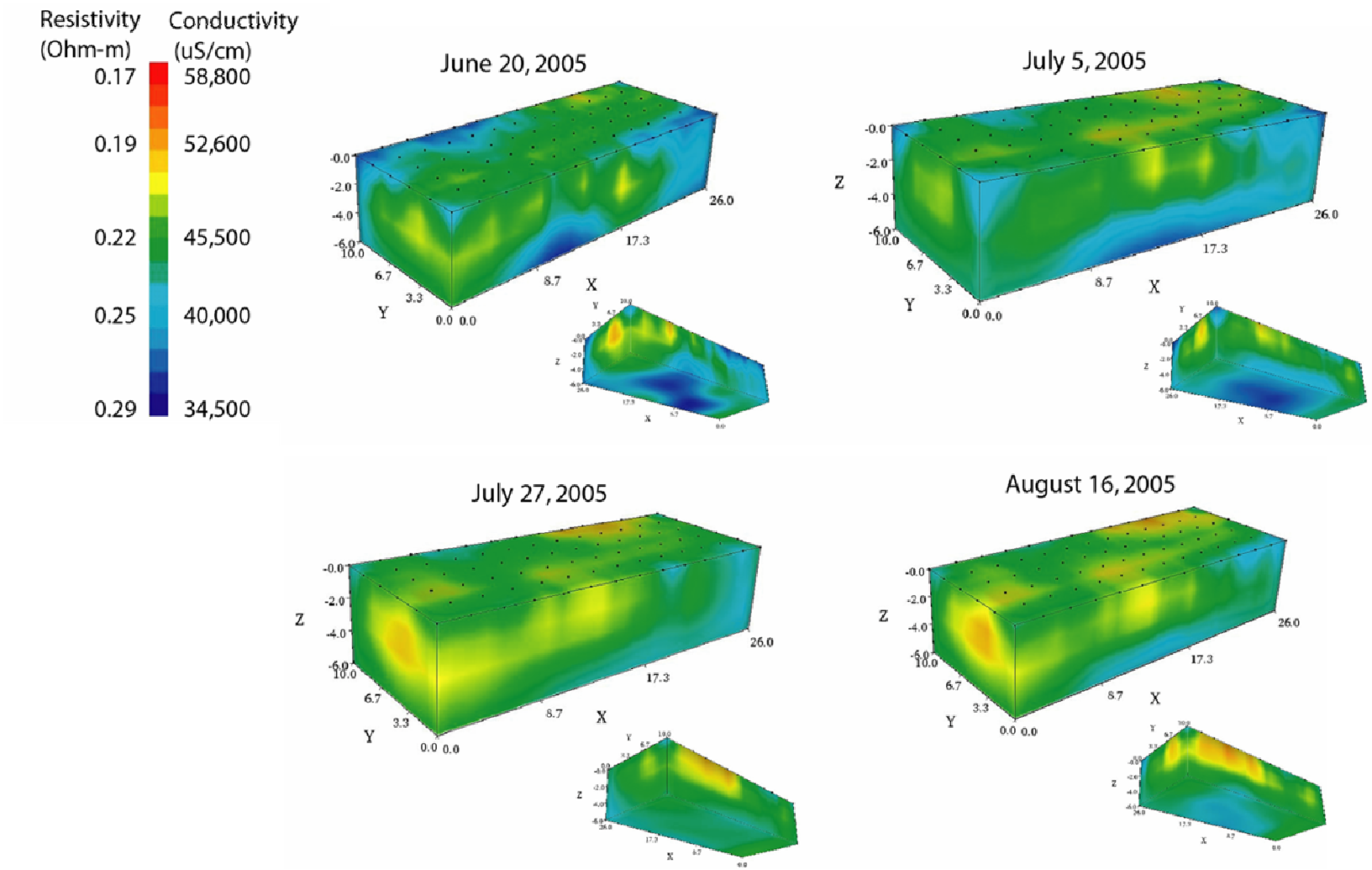

Figure 60 Bird Island Basin 3-D Resistivity Review

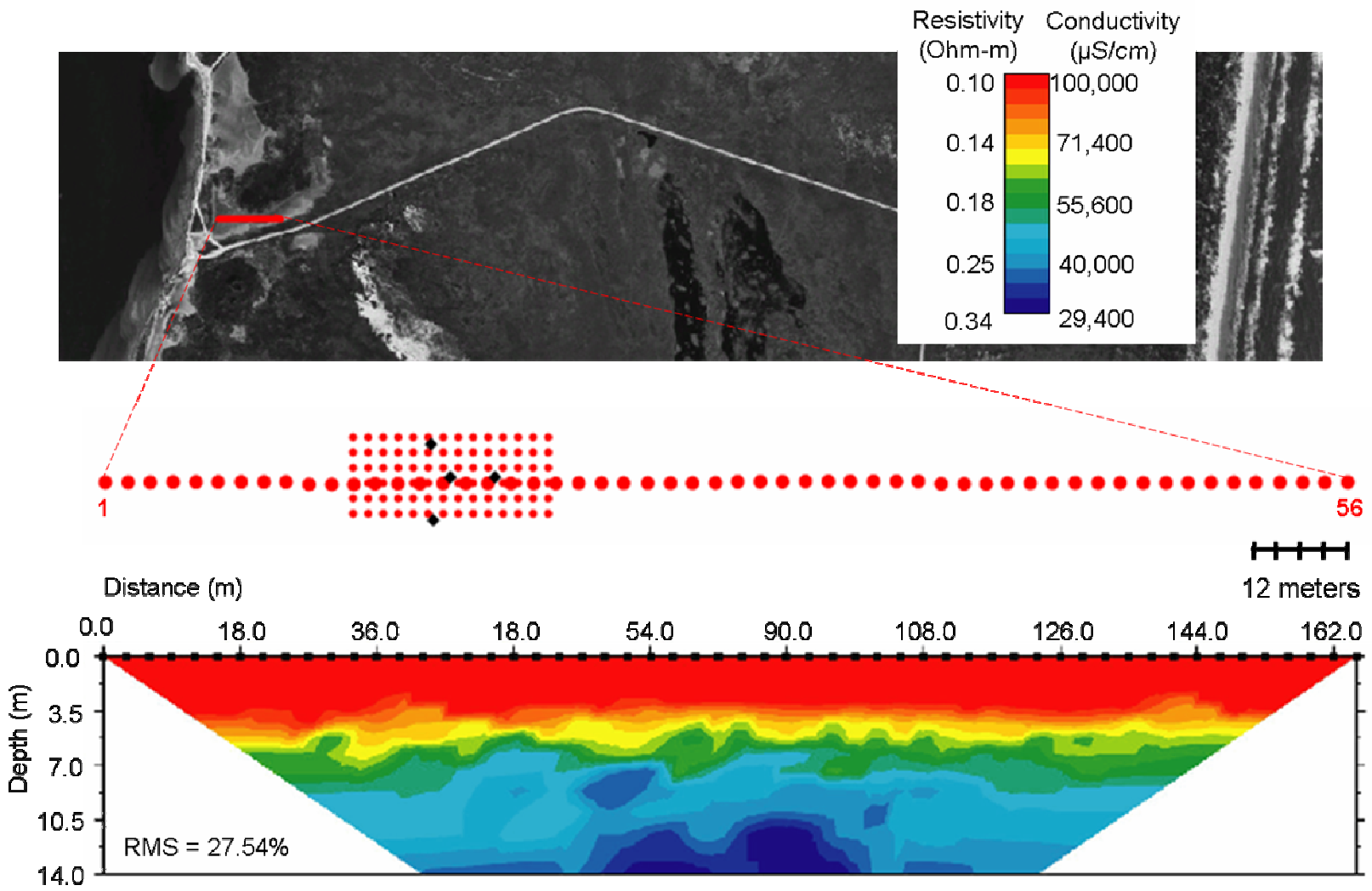

Figure 61 Bird Island Basin 2-D Resistivity, July 27, 2005

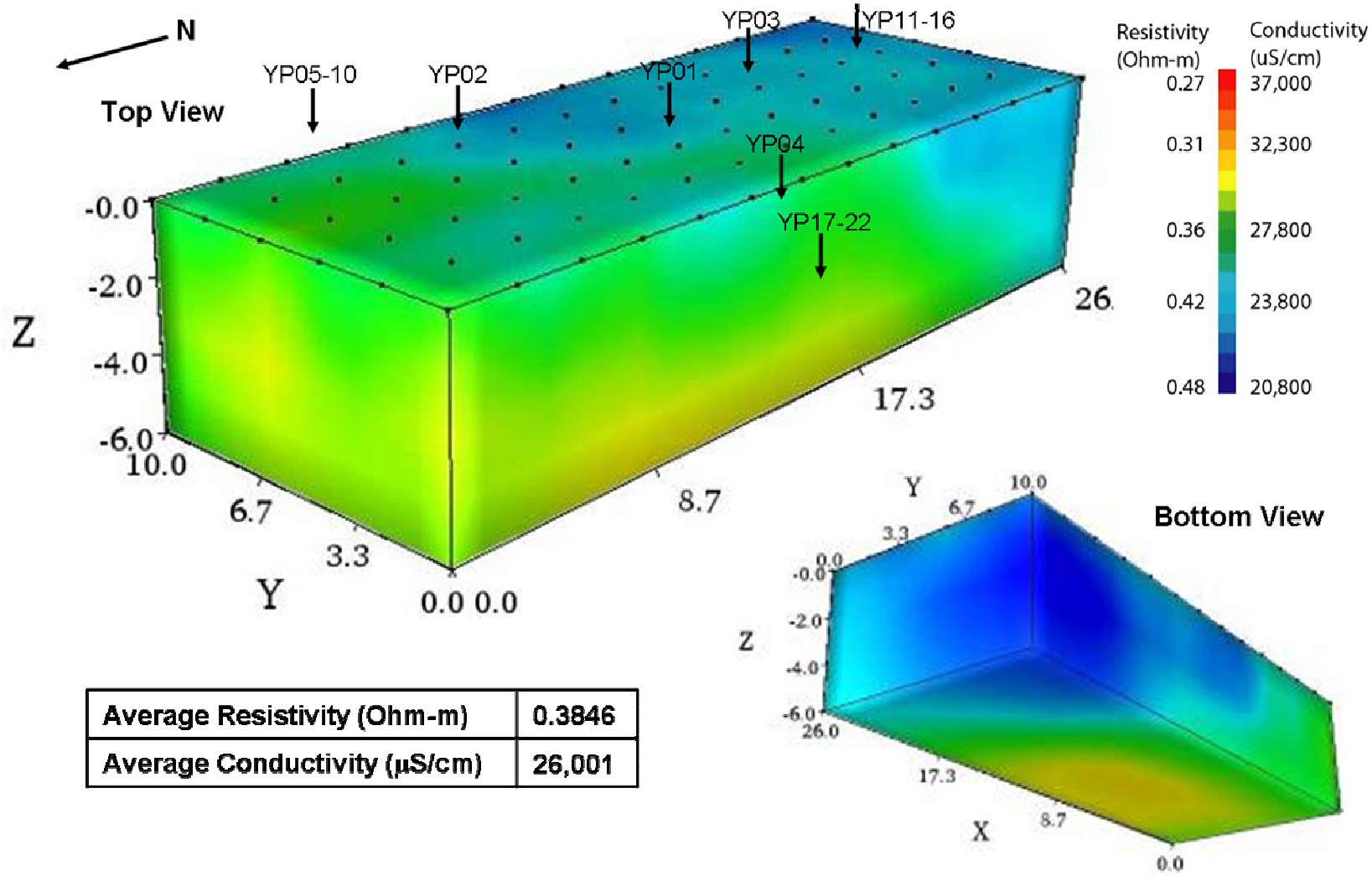

Average Resistivity (Ohm-m)	**0.3846**
Average Conductivity (µS/cm)	**26,001**

Figure 62 Yarborough Pass 3-D Resistivity, May 2, 2005

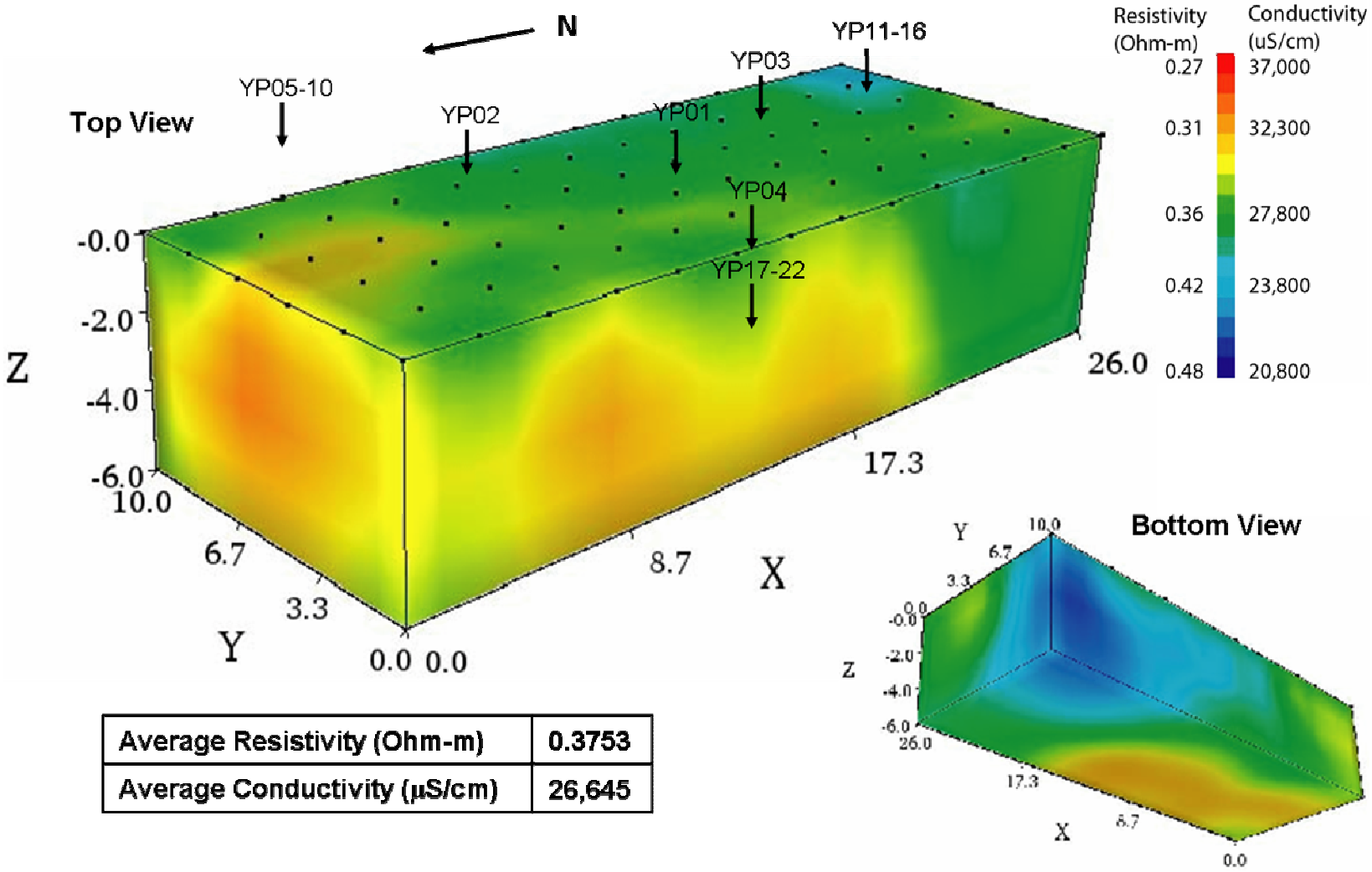

Average Resistivity (Ohm-m)	0.3753
Average Conductivity (µS/cm)	26,645

Figure 63 Yarborough Pass 3-D Resistivity, June 20, 2005

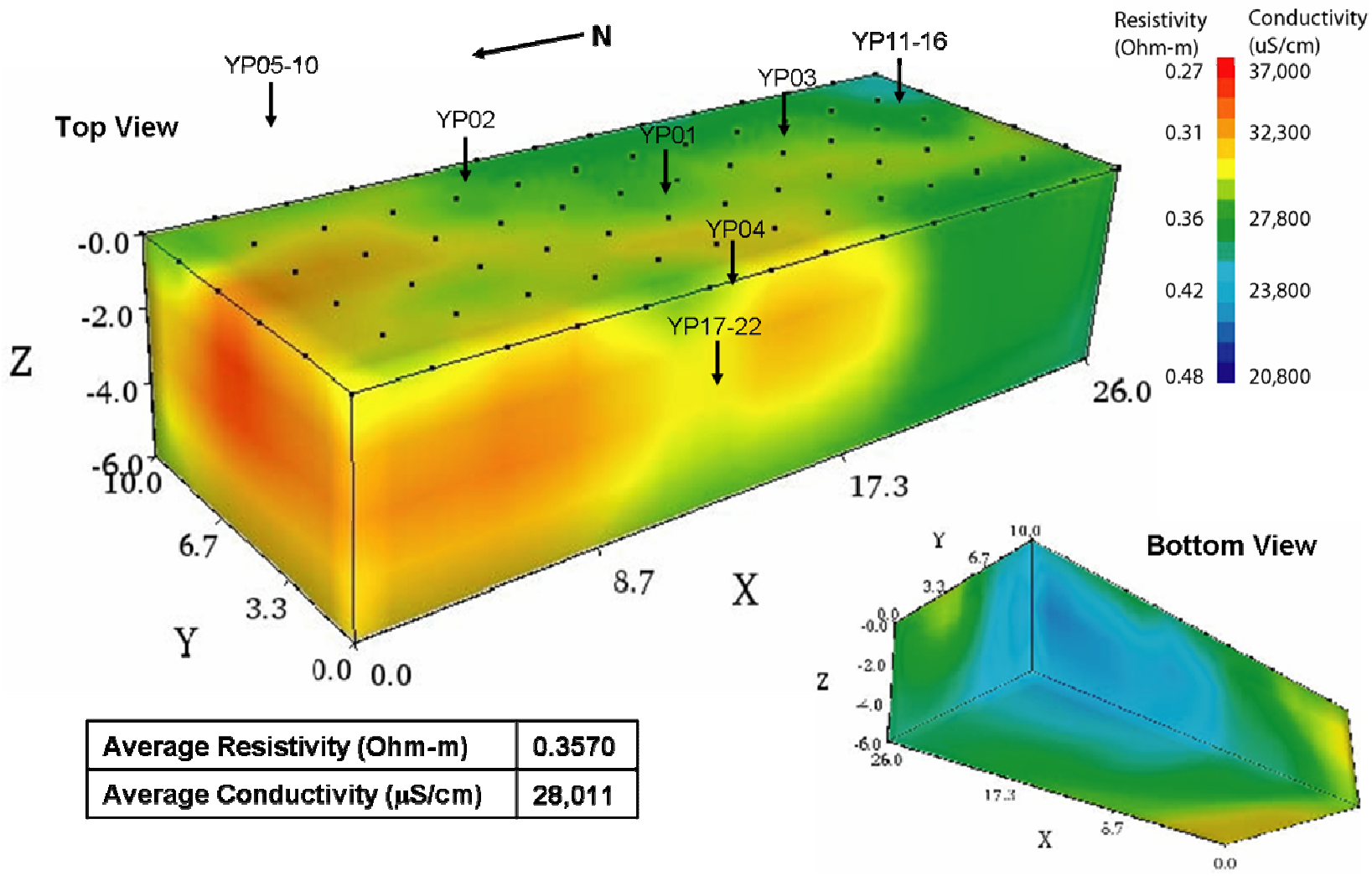

Figure 64 Yarborough Pass 3-D Resistivity, July 5, 2005

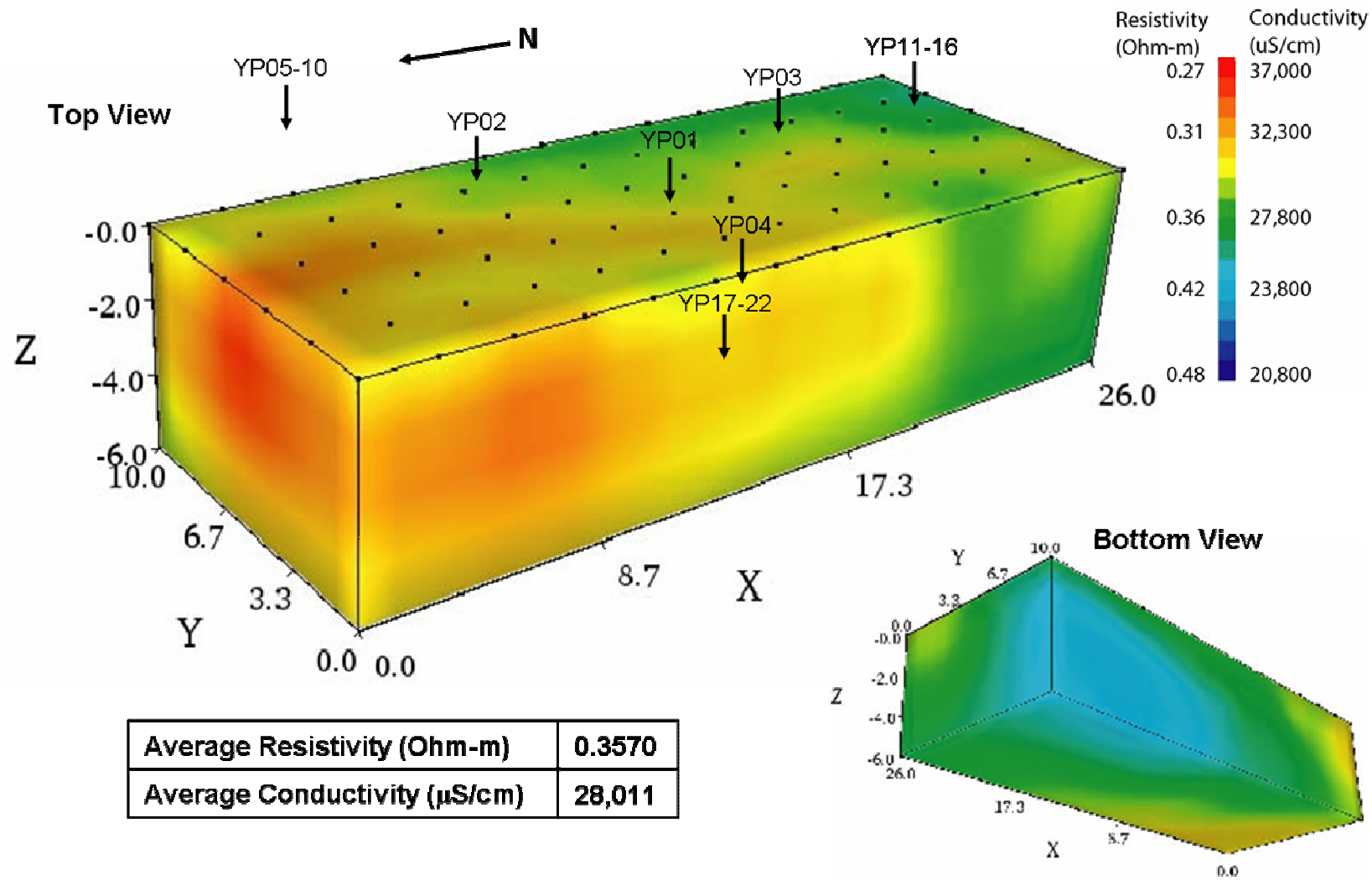

Average Resistivity (Ohm-m)	0.3570
Average Conductivity (µS/cm)	28,011

Figure 65 Yarborough Pass 3-D Resistivity, July 27, 2005

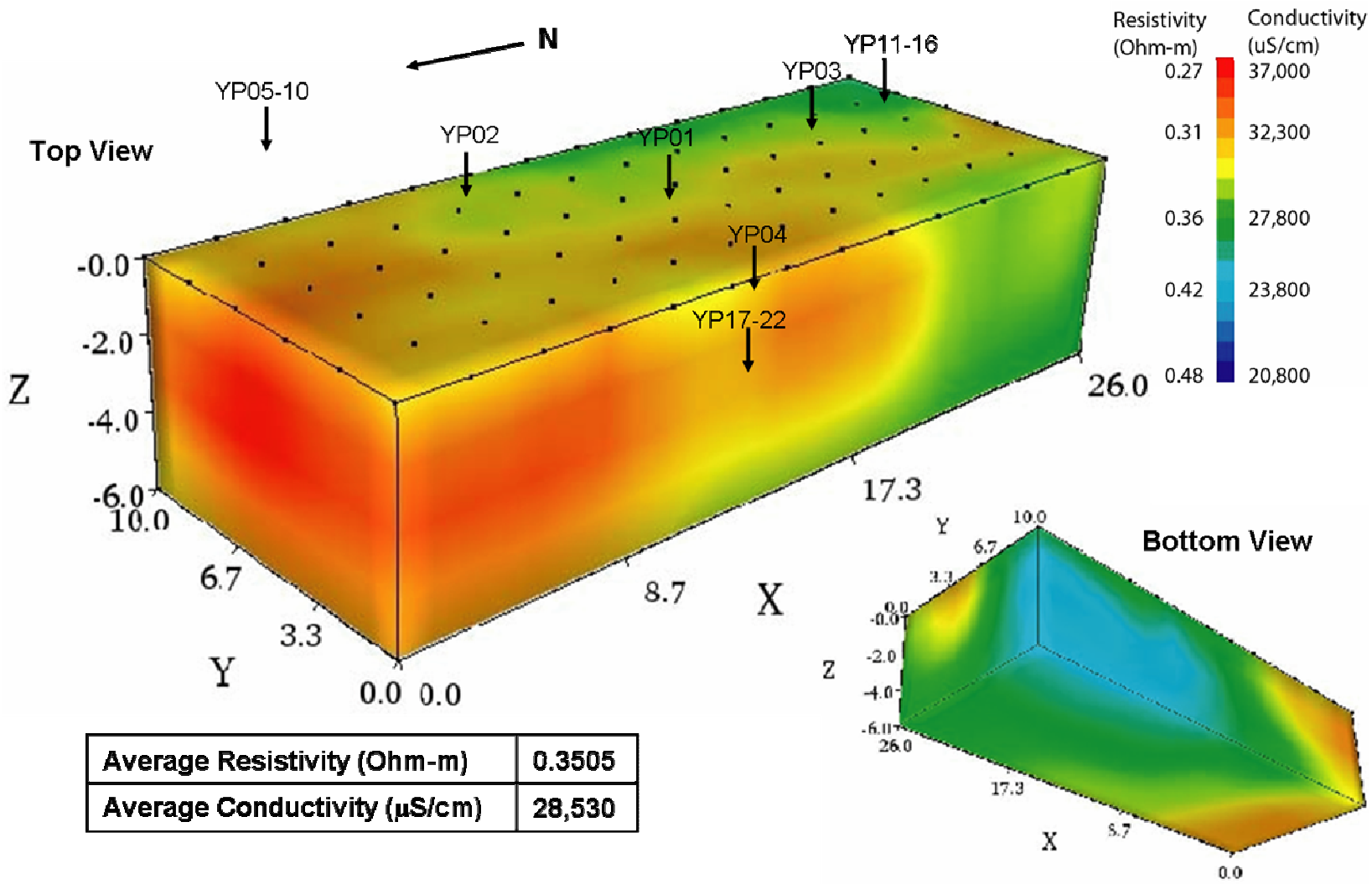

Figure 66 Yarborough Pass 3-D Resistivity, August 16, 2005

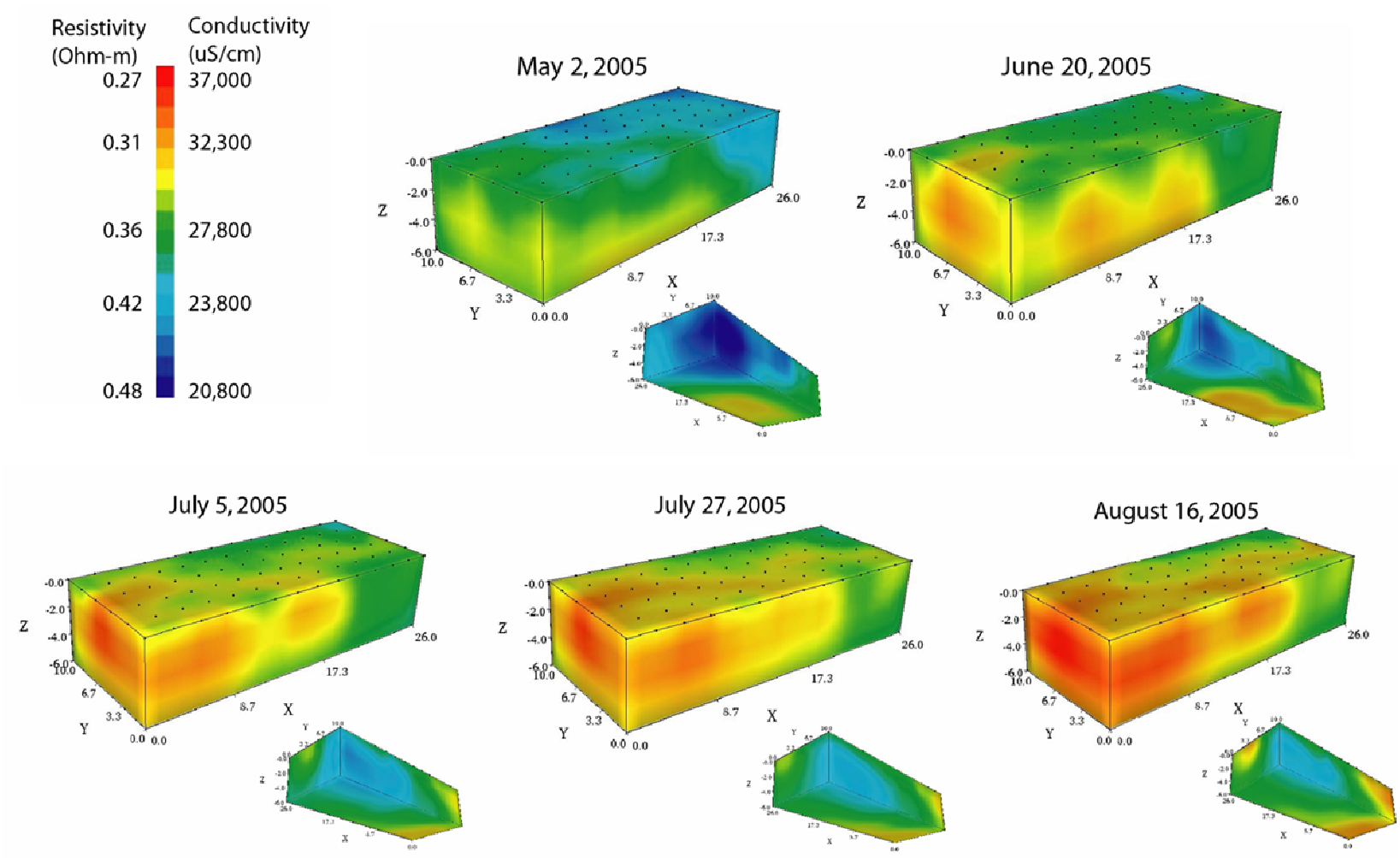

Figure 67 Yarborough Pass 3-D Resistivity Review

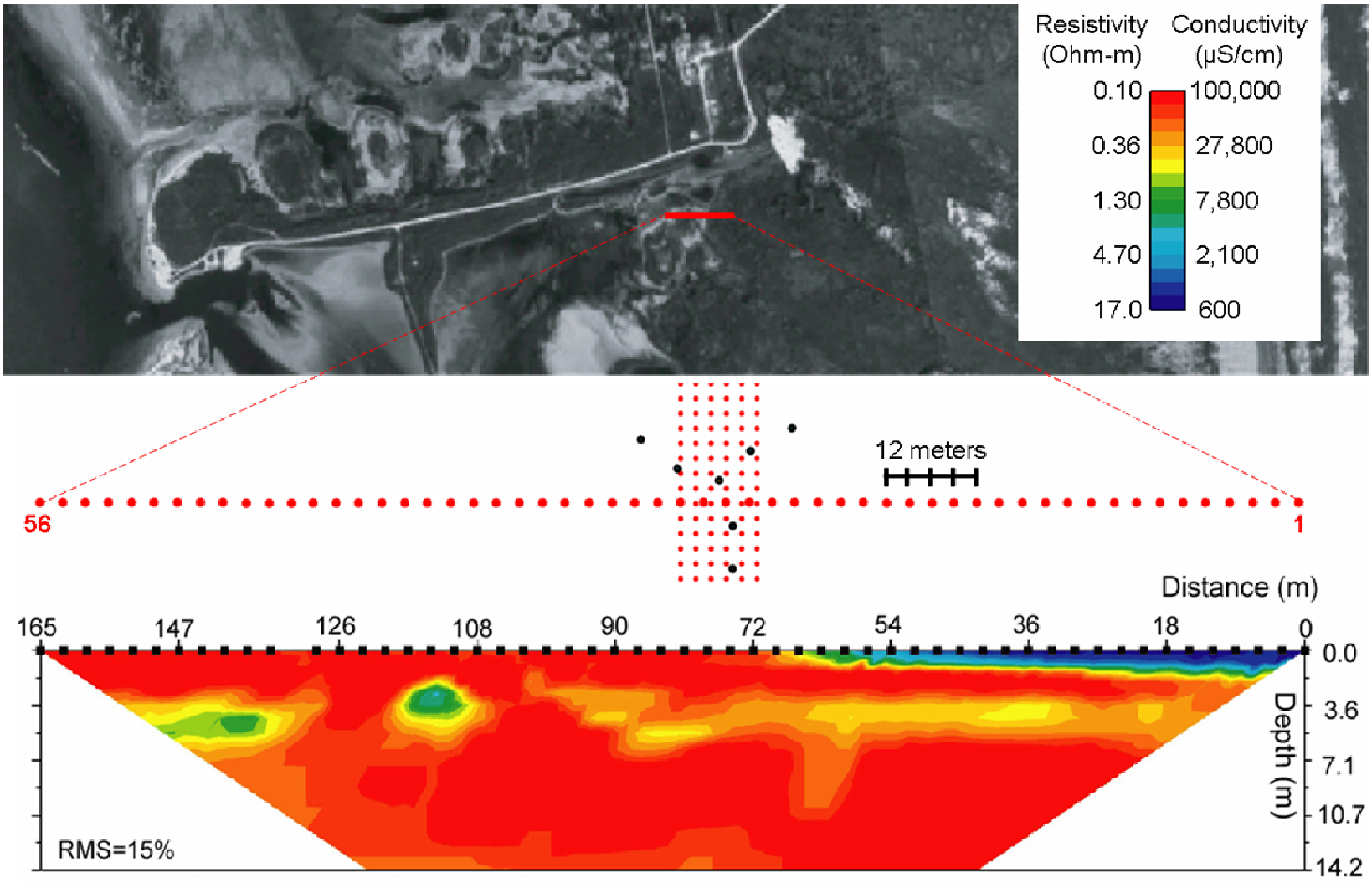

Figure 68 Yarborough Pass 2-D Resistivity Profile, July 27, 2005

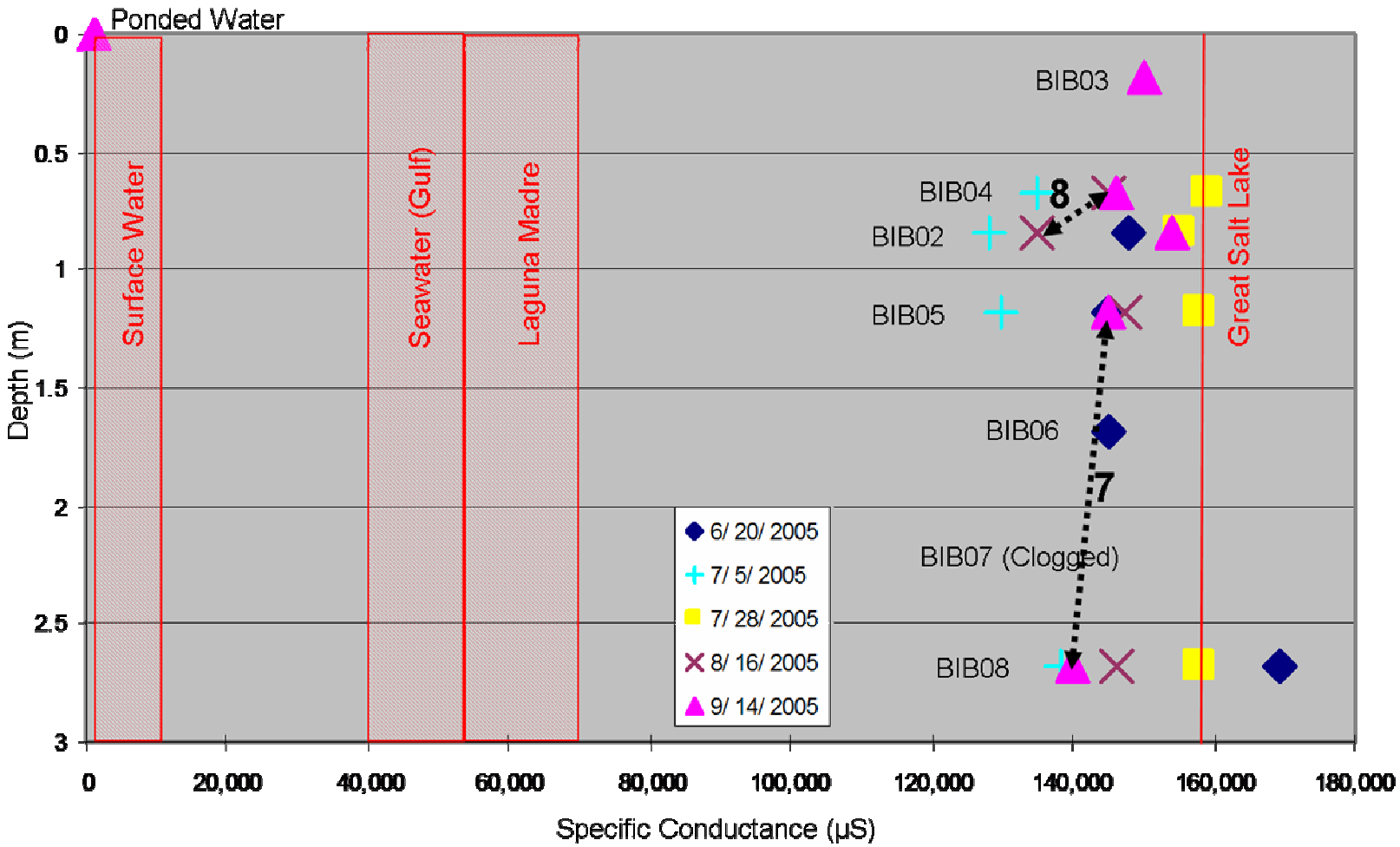

Figure 69 BIB02-08 (East Nest) Specific Conductance Profile with Rayleigh Numbers Greater than 5

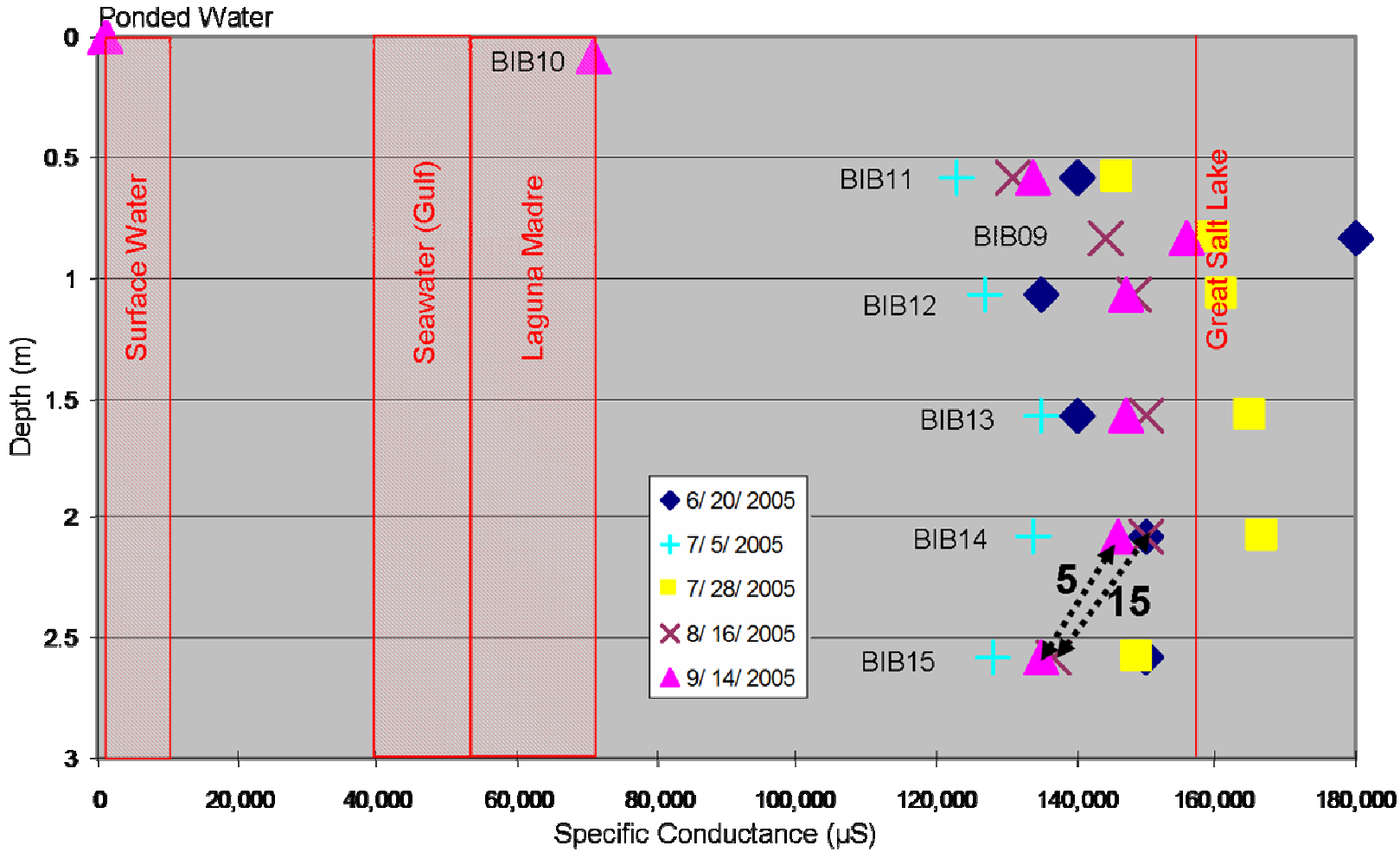

Figure 70 BIB09-15 (Southwest Nest) Specific Conductance Profile with Rayleigh Numbers Greater than 5

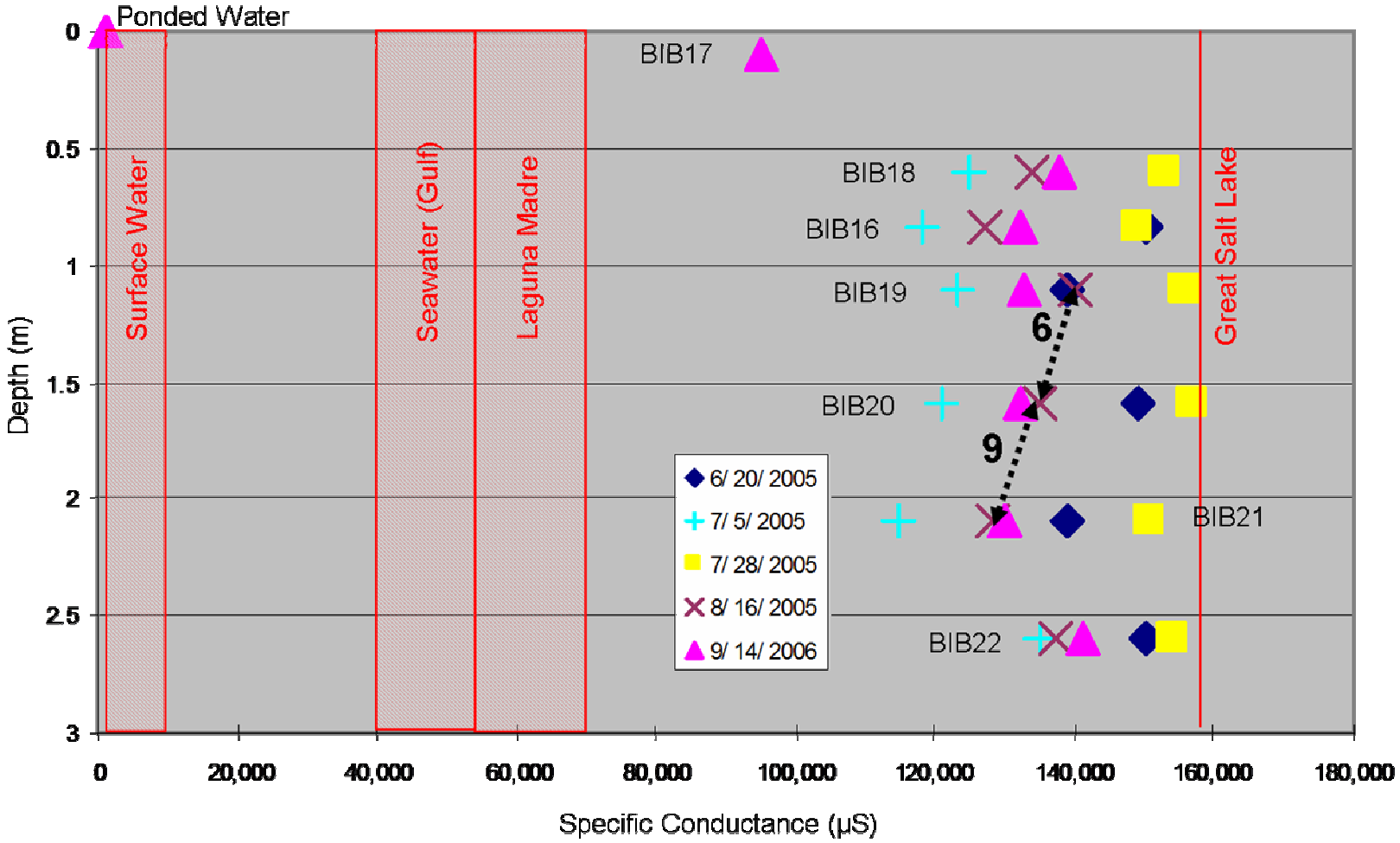

Figure 71 BIB16-22 (Northwest Nest) Specific Conductance Profile with Rayleigh Numbers Greater than 5

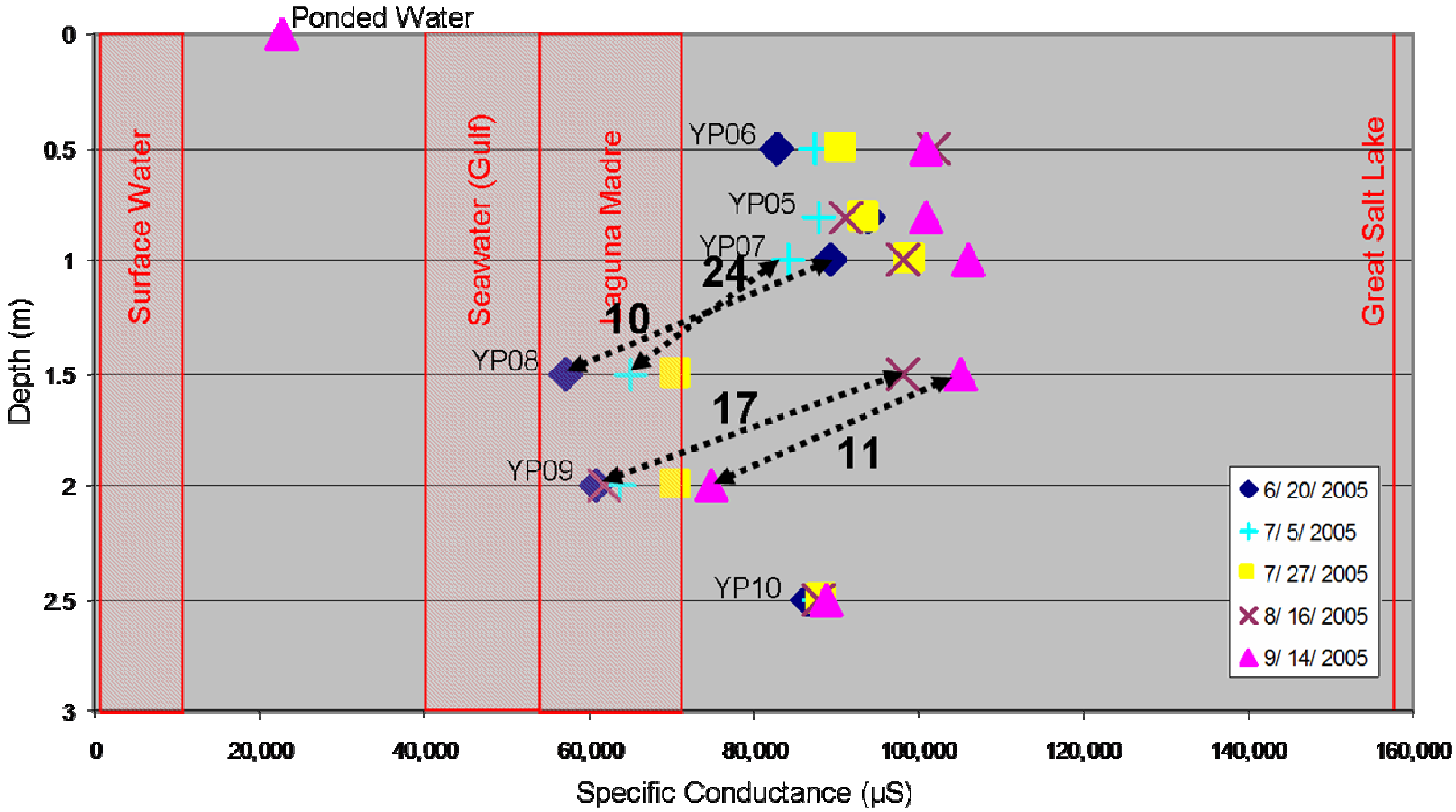

Figure 72 YP05-10 (Northeast Nest) Specific Conductance Profile with Rayleigh Numbers Greater than 5

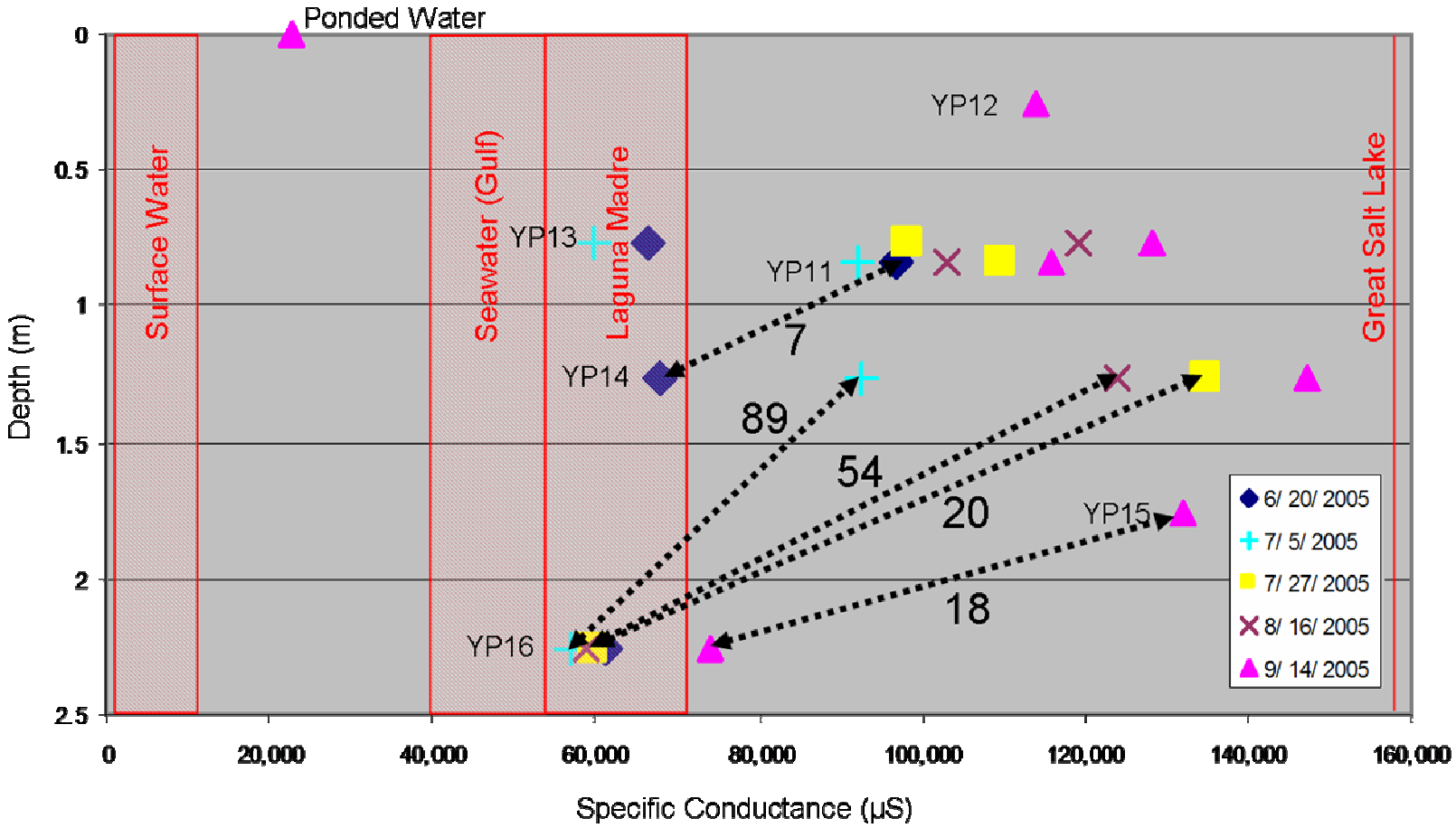

Figure 73 YP11-16 (South Nest) Specific Conductance Profile with Rayleigh Numbers Greater than 5

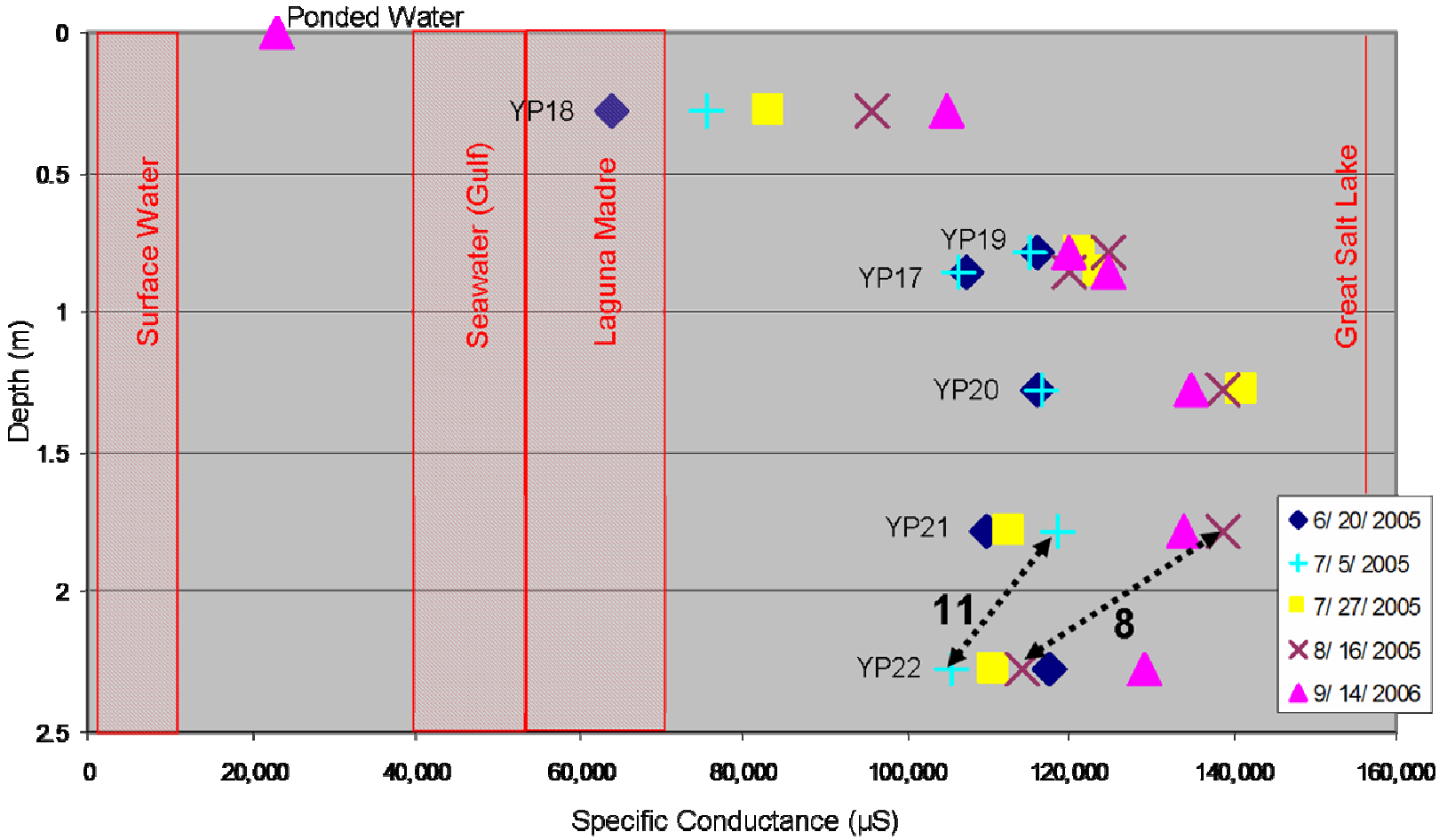

Figure 74 YP17-22 (Northwest Nest) Specific Conductance Profile with Rayleigh Numbers Greater than 5

Appendix C Gradient Spreadsheets

Yarborough Pass
10-Apr-05

	[**X**] matrix			[**D**] matrix
Well ID	x	y	z	D
YP02	15.0	17.0	29.777	1
YP03	12.8	7.0	29.736	1
YP04	5.5	14.6	29.747	1
4	0	0	0	1
5	0	0	0	1
6	0	0	0	1
7	0	0	0	1
8	0	0	0	1
9	0	0	0	1
10	0	0	0	1
11	0	0	0	1
12	0	0	0	1
13	0	0	0	1
14	0	0	0	1
15	0	0	0	1
16	0	0	0	1
17	0	0	0	1
18	0	0	0	1
19	0	0	0	1
20	0	0	0	1

Pt

15	12.8	5.5
17	7	14.6
29.7766728	29.7359892	29.7466464

{[P]t[P]}

419.09	424.9	990.877309
424.9	551.16	1148.656399
990.877309	1148.656399	2655.742269

{[P]t[P]}'

0.020350801	0.00137517	-0.00818782
0.00137517	0.018493745	-0.00851196
-0.00818782	-0.00851196	0.007113058

{[P]t[P]}'[P]t

0.084833813	0.026643459	-0.11155336
0.08156324	-0.10605329	0.024369721
-0.05571752	0.047125949	0.042281928

{[P]t[P]}'[P]t [D] = [**A**] matrix

A	-7.6086E-05
B	-0.00012033
C	0.03369036

gradient	**0.004225643**	
angle off x axis	**57.69335056**	**degrees**

From: Delvin, J.F., 2003, A Spreadsheet Method of Estimating Best-Fit Hydraulic Gradients Using Head Data from Multiple Wells, Ground Water, v. 41, n. 3, pp. 316-320.

Yarborough Pass
2-May-05

Well ID	[**X**] matrix x	y	z	[**D**] matrix D
YP02	15.0	17.0	29.602	1
YP03	12.8	7.0	29.564	1
YP04	5.5	14.6	29.570	1
4	0	0	0	1
5	0	0	0	1
6	0	0	0	1
7	0	0	0	1
8	0	0	0	1
9	0	0	0	1
10	0	0	0	1
11	0	0	0	1
12	0	0	0	1
13	0	0	0	1
14	0	0	0	1
15	0	0	0	1
16	0	0	0	1
17	0	0	0	1
18	0	0	0	1
19	0	0	0	1
20	0	0	0	1

Pt

15	12.8	5.5
17	7	14.6
29.6022528	29.5637984	29.5696368

{[P]t[P]}

419.09	424.9	985.0834139
424.9	551.16	1141.901584
985.0834139	1141.901584	2624.674967

{[P]t[P]}'

0.020356758	0.001375971	-0.008238859
0.001375971	0.018488976	-0.008560312
-0.008238859	-0.008560312	0.007197462

{[P]t[P]}'[P]t

0.084854076	0.026626321	-0.111568735
0.081547629	-0.106040083	0.024381567
-0.056047114	0.047404723	0.042532046

{[P]t[P]}'[P]t [D] = [**A**] matrix

A	-8.83388E-05
B	-0.000110886
C	0.033889655

gradient	**0.004183359**	
angle off x axis	**51.45699146**	**degrees**

Yarborough Pass

20-Jun-05

	[**X**] matrix			[**D**] matrix
Well ID	x	y	z	D
YP05	20.5	20.0	29.664	1
YP11	12.7	1.3	29.625	1
YP17	0.8	18.5	29.587	1
4	0	0	0	1
5	0	0	0	1
6	0	0	0	1
7	0	0	0	1
8	0	0	0	1
9	0	0	0	1
10	0	0	0	1
11	0	0	0	1
12	0	0	0	1
13	0	0	0	1
14	0	0	0	1
15	0	0	0	1
16	0	0	0	1
17	0	0	0	1
18	0	0	0	1
19	0	0	0	1
20	0	0	0	1

Pt

20.5	12.7	0.8
20	1.3	18.5
29.6643012	29.624662	29.5865744

{[P]t[P]}

582.18	441.31	1008.020642
441.31	743.94	1179.149711
1008.020642	1179.149711	2632.956749

{[P]t[P]}'

0.005107589	0.000239552	-0.002062709
0.000239552	0.004643723	-0.002171368
-0.002062709	-0.002171368	0.002141934

{[P]t[P]}'[P]t

0.048307805	0.004070752	-0.052510707
0.033373159	-0.05524689	0.021857177
-0.022173898	0.034434904	0.021552032

{[P]t[P]}'[P]t [D] = [**A**] matrix

A	-0.00013215
B	-1.65537E-05
C	0.033813038

gradient	**0.00393879**	
angle off x axis	**7.139954986**	**degrees**

Yarborough Pass

5-Jul-05

	[**X**] matrix			[**D**] matrix
Well ID	x	y	z	D
YP05	20.5	20.0	29.423	1
YP11	12.7	1.3	29.404	1
YP17	0.8	18.5	29.415	1
4	0	0	0	1
5	0	0	0	1
6	0	0	0	1
7	0	0	0	1
8	0	0	0	1
9	0	0	0	1
10	0	0	0	1
11	0	0	0	1
12	0	0	0	1
13	0	0	0	1
14	0	0	0	1
15	0	0	0	1
16	0	0	0	1
17	0	0	0	1
18	0	0	0	1
19	0	0	0	1
20	0	0	0	1

Pt

20.5	12.7	0.8
20	1.3	18.5
29.423264	29.4043564	29.4152704

{[P]t[P]}

582.18	441.31	1000.144455
441.31	743.94	1170.873446
1000.144455	1170.873446	2595.602772

{[P]t[P]}'

0.005092903	0.000232599	-0.002067336
0.000232599	0.004645395	-0.002185158
-0.002067336	-0.002185158	0.00216758

{[P]t[P]}'[P]t

0.048228719	0.00419357	-0.052433839
0.033381698	-0.05526015	0.021848878
-0.02230625	0.034640441	0.021680672

{[P]t[P]}'[P]t [D] = [**A**] matrix

A	-1.15502E-05
B	-2.95747E-05
C	0.034014862

gradient	**0.00093342**	
angle off x axis	**68.6672235**	**degrees**

Yarborough Pass

27-Jul-05

	[**X**] matrix			[**D**] matrix
Well ID	x	y	z	D
YP05	20.5	20.0	29.675	1
YP11	12.7	1.3	29.539	1
YP17	0.8	18.5	29.622	1
4	0	0	0	1
5	0	0	0	1
6	0	0	0	1
7	0	0	0	1
8	0	0	0	1
9	0	0	0	1
10	0	0	0	1
11	0	0	0	1
12	0	0	0	1
13	0	0	0	1
14	0	0	0	1
15	0	0	0	1
16	0	0	0	1
17	0	0	0	1
18	0	0	0	1
19	0	0	0	1
20	0	0	0	1

Pt

20.5	12.7	0.8
20	1.3	18.5
29.6747712	29.5387612	29.6223072

{[P]t[P]}

582.18	441.31	1007.172923
441.31	743.94	1179.908497
1007.172923	1179.908497	2630.611543

{[P]t[P]}'

0.005100482	0.000247936	-0.00206401
0.000247936	0.004669378	-0.002189283
-0.00206401	-0.002189283	0.002152339

{[P]t[P]}'[P]t

0.048269568	0.004130133	-0.052473543
0.033503773	-0.055449727	0.021730226
-0.02222769	0.03451844	0.021604315

{[P]t[P]}'[P]t [D] = [**A**] matrix

A	-7.38416E-05
B	-0.000215727
C	0.033895065

gradient	**0.00672709**	
angle off x axis	**71.10437786**	**degrees**

Yarborough Pass

16-Aug-05

	[**X**] matrix			[**D**] matrix
Well ID	x	y	z	D
YP05	20.5	20.0	29.389	1
YP11	12.7	1.3	29.355	1
YP17	0.8	18.5	29.346	1
4	0	0	0	1
5	0	0	0	1
6	0	0	0	1
7	0	0	0	1
8	0	0	0	1
9	0	0	0	1
10	0	0	0	1
11	0	0	0	1
12	0	0	0	1
13	0	0	0	1
14	0	0	0	1
15	0	0	0	1
16	0	0	0	1
17	0	0	0	1
18	0	0	0	1
19	0	0	0	1
20	0	0	0	1

Pt

20.5	12.7	0.8
20	1.3	18.5
29.3890944	29.3548288	29.3455024

{[P]t[P]}

582.18	441.31	998.7591629
441.31	743.94	1168.83496
998.7591629	1168.83496	2586.583355

{[P]t[P]}'

0.005100381	0.000236697	-0.002076373
0.000236697	0.00464571	-0.002190717
-0.002076373	-0.002190717	0.002178311

{[P]t[P]}'[P]t

0.048269026	0.004130974	-0.052473016
0.033383306	-0.055262648	0.021847315
-0.022361395	0.034726078	0.021734271

{[P]t[P]}'[P]t [D] = [**A**] matrix

A	-7.30153E-05
B	-3.20268E-05
C	0.034098953

gradient	**0.002338209**	
angle off x axis	**23.68378643**	**degrees**

Yarborough Pass
14-Sep-05

Well ID	[**X**] matrix x	y	z	[**D**] matrix D
YP05	20.5	20.0	29.999	1
YP11	12.7	1.3	29.999	1
YP17	0.8	18.5	30.047	1
4	0	0	0	1
5	0	0	0	1
6	0	0	0	1
7	0	0	0	1
8	0	0	0	1
9	0	0	0	1
10	0	0	0	1
11	0	0	0	1
12	0	0	0	1
13	0	0	0	1
14	0	0	0	1
15	0	0	0	1
16	0	0	0	1
17	0	0	0	1
18	0	0	0	1
19	0	0	0	1
20	0	0	0	1

Pt

20.5	12.7	0.8
20	1.3	18.5
29.998993	29.999292	30.0471168

{[P]t[P]}

582.18	441.31	1020.008058
441.31	743.94	1194.8506
1020.008058	1194.8506	2702.72633

{[P]t[P]}'

0.005081309	0.00022676	-0.002017933
0.00022676	0.004646027	-0.002139546
-0.002017933	-0.002139546	0.002077438

{[P]t[P]}'[P]t

0.048166077	0.00429085	-0.052372953
0.033384924	-0.05526516	0.021845742
-0.021837501	0.033912498	0.021225069

{[P]t[P]}'[P]t [D] = [**A**] matrix

A	8.39729E-05
B	-3.44937E-05
C	0.033300065

gradient	**0.002726163**	
angle off x axis	**-22.3314674**	**degrees**

Bird Island Basin

20-Jun-05

	[**X**] matrix			[**D**] matrix
Well ID	x	y	z	D
BIB02	19.0	7.0	29.501	1
BIB09	10.7	1.3	29.480	1
BIB16	10.4	11.4	29.434	1
4	0	0	0	1
5	0	0	0	1
6	0	0	0	1
7	0	0	0	1
8	0	0	0	1
9	0	0	0	1
10	0	0	0	1
11	0	0	0	1
12	0	0	0	1
13	0	0	0	1
14	0	0	0	1
15	0	0	0	1
16	0	0	0	1
17	0	0	0	1
18	0	0	0	1
19	0	0	0	1
20	0	0	0	1

Pt

19	10.7	10.4
7	1.25	11.4
29.501178	29.48032	29.4342768

{[P]t[P]}

583.65	264.935	1182.078285
264.935	180.5225	578.9094015
1182.078285	578.9094015	2605.785421

{[P]t[P]}'

0.021135893	-0.000944947	-0.009378071
-0.000944947	0.019306289	-0.003860483
-0.009378071	-0.003860483	0.00549565

{[P]t[P]}'[P]t

0.118303188	-0.051495673	-0.066995853
0.00330123	-0.099786354	0.096633714
-0.043078591	0.056842553	0.02021903

{[P]t[P]}'[P]t [D] = [**A**] matrix

A	-0.000188338
B	0.00014859
C	0.033982992

gradient	**0.0070593**	
angle off x axis	**-38.27169877**	**degrees**

Bird Island Basin

5-Jul-05

	[**X**] matrix			[**D**] matrix
Well ID	x	y	z	D
BIB02	19.0	7.0	29.361	1
BIB09	10.7	1.3	29.379	1
BIB16	10.4	11.4	29.343	1
4	0	0	0	1
5	0	0	0	1
6	0	0	0	1
7	0	0	0	1
8	0	0	0	1
9	0	0	0	1
10	0	0	0	1
11	0	0	0	1
12	0	0	0	1
13	0	0	0	1
14	0	0	0	1
15	0	0	0	1
16	0	0	0	1
17	0	0	0	1
18	0	0	0	1
19	0	0	0	1
20	0	0	0	1

Pt

19	10.7	10.4
7	1.25	11.4
29.3605968	29.378936	29.3427176

{[P]t[P]}

583.65	264.935	1177.370217
264.935	180.5225	576.7548282
1177.370217	576.7548282	2586.161601

{[P]t[P]}'

0.021036929	-0.00095781	-0.009363619
-0.00095781	0.019312517	-0.003870945
-0.009363619	-0.003870945	0.005512816

{[P]t[P]}'[P]t

0.118075539	-0.051195288	-0.066889005
0.00333596	-0.09983218	0.096617413
-0.043145818	0.056931259	0.020250583

{[P]t[P]}'[P]t [D] = [**A**] matrix

A	-8.75463E-06
B	0.000121193
C	0.034036024

gradient	**0.003569991**	
angle off x axis	**-85.86827757**	**degrees**

Bird Island Basin

27-Jul-05

	[**X**] matrix			[**D**] matrix
Well ID	x	y	z	D
BIB02	19.0	7.0	29.311	1
BIB09	10.7	1.3	29.311	1
BIB16	10.4	11.4	29.293	1
4	0	0	0	1
5	0	0	0	1
6	0	0	0	1
7	0	0	0	1
8	0	0	0	1
9	0	0	0	1
10	0	0	0	1
11	0	0	0	1
12	0	0	0	1
13	0	0	0	1
14	0	0	0	1
15	0	0	0	1
16	0	0	0	1
17	0	0	0	1
18	0	0	0	1
19	0	0	0	1
20	0	0	0	1

Pt			
	19	10.7	10.4
	7	1.25	11.4
	29.3108748	29.3108048	29.2926104

{[P]t[P]}

583.65	264.935	1175.175381
264.935	180.5225	575.7503882
1175.175381	575.7503882	2576.307684

{[P]t[P]}'

0.021055125	-0.00093719	-0.009394793
-0.00093719	0.019326467	-0.003891561
-0.009394793	-0.003891561	0.005543242

{[P]t[P]}'[P]t

0.118117448	-0.051250587	-0.066908676
0.003413602	-0.09993463	0.096580971
-0.043264718	0.057088148	0.020306389

{[P]t[P]}'[P]t [D] = [**A**] matrix

A	-4.1815E-05
B	5.99436E-05
C	0.03412982

gradient	**0.002141444**	
angle off x axis	**-55.10141432**	**degrees**

Bird Island Basin

16-Aug-05

	[**X**] matrix			[**D**] matrix
Well ID	x	y	z	D
BIB02	19.0	7.0	29.247	1
BIB09	10.7	1.3	29.251	1
BIB16	10.4	11.4	29.247	1
4	0	0	0	1
5	0	0	0	1
6	0	0	0	1
7	0	0	0	1
8	0	0	0	1
9	0	0	0	1
10	0	0	0	1
11	0	0	0	1
12	0	0	0	1
13	0	0	0	1
14	0	0	0	1
15	0	0	0	1
16	0	0	0	1
17	0	0	0	1
18	0	0	0	1
19	0	0	0	1
20	0	0	0	1

Pt

19	10.7	10.4
7	1.25	11.4
29.2468604	29.2509948	29.246616

{[P]t[P]}

583.65	264.935	1172.840798
264.935	180.5225	574.7031887
1172.840798	574.7031887	2566.364087

{[P]t[P]}'

0.021028441	-0.000930343	-0.009401761
-0.000930343	0.019336738	-0.003905035
-0.009401761	-0.003905035	0.005560787

{[P]t[P]}'[P]t

0.11805598	-0.05116948	-0.066879825
0.003470645	-0.100009899	0.096554198
-0.043333135	0.057178425	0.020338501

{[P]t[P]}'[P]t [D] = [**A**] matrix

A	6.67455E-06
B	1.49445E-05
C	0.034183791

gradient	**0.000478801**	
angle off x axis	**65.93333661**	**degrees**

Bird Island Basin
14-Sep-05

Well ID	[**X**] matrix x	y	z	[**D**] matrix D
BIB02	19.0	7.0	30.142	1
BIB09	10.7	1.3	30.146	1
BIB16	10.4	11.4	30.154	1
4	0	0	0	1
5	0	0	0	1
6	0	0	0	1
7	0	0	0	1
8	0	0	0	1
9	0	0	0	1
10	0	0	0	1
11	0	0	0	1
12	0	0	0	1
13	0	0	0	1
14	0	0	0	1
15	0	0	0	1
16	0	0	0	1
17	0	0	0	1
18	0	0	0	1
19	0	0	0	1
20	0	0	0	1

Pt

19	10.7	10.4
7	1.25	11.4
30.1422174	30.1462	30.1540152

{[P]t[P]}

583.65	264.935	1208.868229
264.935	180.5225	592.4340451
1208.868229	592.4340451	2726.611277

{[P]t[P]}'

0.021014004	-0.000922482	-0.009116317
-0.000922482	0.019345771	-0.00379443
-0.009116317	-0.00379443	0.005233007

{[P]t[P]}'[P]t

0.118022702	-0.05112557	-0.066864207
0.003520723	-0.100075977	0.096530694
-0.042036602	0.05546764	0.019729971

{[P]t[P]}'[P]t [D] = [**A**] matrix

A	3.2926E-05
B	-2.45598E-05
C	0.033161008

gradient	**0.001238709**	
angle off x axis	**-36.71958808**	**degrees**

Appendix D Field Parameters

Appendix D April 10, 2005 Field Parameters							
Well ID	Depth to Water from TOC (m)	Specific Conductance (µS/cm)	TDS (PPM)	Temp C	pH	Orp	Comments
YP01	0.907						No Sampling Supplies
YP02	0.763						
YP03	0.795						
YP04	0.780						

Appendix D May 2, 2005 Field Parameters							
Well ID	Depth to Water from TOC (m)	Specific Conductance (µS/cm)	TDS (PPM)	Temp C	pH	Orp	Comments
YP01	0.960	157,500	104,600	24.5	7.28	-277	
YP02	0.950	149,900	102,700	26.0	7.24		
YP03	0.980	148,900	101,600	25.9	7.33		
YP04	0.960	149,700	102,300	27.4	7.3		
N Pond		62,600	57,500	31.2	8.7	-57	
NE Pond		56,700	52,700	28.9	8.52	25	
NW Pond		66,800	59,070	28.0	8.8	6	
SW Pond		18,740	16,700	32.8	8.85	-47	
SE Pond		8,672	6,940	32.8	9.08	-49	
Laguna M.		73,450	63,070	25.3	8.35	40	
Gulf		54,500	50,800	24.3	8.18	49	

Appendix D June 20, 2005 Field Parameters							
Well ID	Depth to Water from TOC (m)	Specific Conductance (µS/cm)	TDS (PPM)	Temp C	pH	Orp	Comments
BIB01	1.090	150,000	100,000	29.5	fouled		
BIB02	1.015	148,000	96,000	30.0	fouled		
BIB03							Dry
BIB04							Dry
BIB05		145,000	95,000	30.0	fouled		
BIB06		145,000	100,000	30.0	fouled		
BIB07					fouled		Clogged
BIB08	1.110	169,000	112,000	24.0	fouled		
BIB09	1.060	180,000	135,000	24.0	fouled		
BIB10							Dry
BIB11		140,000	92,000	28.5	fouled		
BIB12		135,000	85,000	30.0	fouled		
BIB13		140,000	95,000	29.9	fouled		
BIB14		150,000	108,000	30.0	fouled		
BIB15	1.072	150,000	95,000	26.0	fouled		
BIB16	1.080	150,000	104,000	27.0	fouled		
BIB17							Dry
BIB18							Dry
BIB19		139,000	94,100	33.0	fouled		
BIB20		149,000	96,300	30.0	fouled		
BIB21		139,000	91,800	30.9	fouled		
BIB22	1.050	150,000	100,000	24.5	fouled		
YP01	1.015	100,100	66,150	28.5	6.92	-216	
YP02	0.880	111,200	74,350	29.9	6.72	-211	
YP03	0.905	107,600	71,830	29.8	7.06		
YP04	0.910	122,800	83,000	27.8	6.7		
YP05	0.842	93,800	61,800	29.2	6.7	-245	
YP06		82,600	53,900	30.3	6.5	-240	
YP07		89,200	58,500	28.6	6.1	-240	
YP08		57,300	36,500	27.3	6.6	-247	
YP09		60,800	38,800	27.5	6.6	-247	
YP10	0.820	86,700	56,800	26.7	6.6	-241	
YP11	0.877	96,860	63,850	30.7	7.2	-210	
YP12							Dry
YP13		66,500	42,760	30.6	7.06	-239	
YP14		68,120	43,900	29.3	7.19	-229	
YP15							Clogged
YP16	0.830	61,460	39,370	27.3	7.12	-260	
YP17	0.905	107,500	71,600	27.2	6.7	-195	
YP18		64,050	41,100	29.4	6.45	-181	
YP19		116,000	78,100	28.0	6.7	-156	
YP20		116,000	78,020	27.5	6.6	-253	
YP21		110,000	73,400	27.2	6.6	-261	
YP22	0.870	117,800	79,600	25.1	7.4	-269	
N Pond		43,100	26,800	31.9	7.9	-44	
NE Pond		42,200	26,500	32.8	8.42	-8	
NW Pond		51,500	32,300	26.4	7.8	-8	
SW Pond		14,000	8,070	33.6	8.3		
SE Pond		10,800	6,100	36.0	8.07	-28	
Laguna M.		115,000	84,600	11.0	13.6	-725	Ultrameter fouled
Gulf		75,000	49,000	17.4	13.9		Ultrameter fouled

Appendix D July 5, 2005 Field Parameters							
Well ID	Depth to Water from TOC (m)	Specific Conductance (µS/cm)	TDS (PPM)	Temp C	pH	Orp	Comments
BIB01	1.087	136,000	85,500	24.7	6.9	-329	
BIB02	1.137	128,000	84,000	28.5	7.3	-220	
BIB03							Dry
BIB04		135,000	85,000	30.2	7.35	-183	
BIB05		130,000	88,000	30.2	7.67	-302	
BIB06							Clogged
BIB07							Clogged
BIB08	1.195	138,000	92,000	23.2	fouled		
BIB09	1.137						Dry
BIB10							Dry
BIB11		123,000	86,000	27.4	fouled		
BIB12		127,000	85,000	28.8	fouled		
BIB13		135,000	96,000	30.2	fouled		
BIB14		134,000	92,000	31.3	fouled		
BIB15	1.155	128,000	89,000	25.0	fouled		
BIB16	1.151	118,000	79,000	29.8	fouled		
BIB17							Dry
BIB18		125,000	84,000	28.0	fouled		
BIB19		123,000	88,000	28.4	fouled		
BIB20		121,000	86,000	29.8	fouled		
BIB21		115,000	77,900	30.5	fouled		
BIB22	1.128	135,000	90,000	25.9	fouled		
YP01	1.224	76,830	49,990	31.6	7.2	-278	
YP02	1.085	105,000	70,450	31.4	7.47	-243	
YP03	1.094	115,600	77,600	31.4	7.09	-164	
YP04	1.080	123,200	83,060	30.6	7.27	-173	
YP05	1.070	87,800	57,400	30.5	7.02	-280	
YP06		87,600	57,700	31.9	7.19	-290	
YP07		84,200	55,100	31.1	7.05	-289	
YP08		65,100	41,800	29.8	7.08	-293	
YP09		63,500	40,640	28.7	7.02	-291	
YP10	1.060	87,800	57,600	31.1	7.04	-270	
YP11	1.086	92,300	61,200	31.6	7.3	-238	
YP12							Dry
YP13		59,900	38,440	31.9	7.18	-284	
YP14		92,470	61,260	32.1	7.02	-277	
YP15							Clogged
YP16	1.075	57,150	36,500	28.4	7.25	-275	
YP17	1.066	106,700	71,400	29.5	7.29	-229	
YP18		75,800	49,190	30.8	6.95	-155	
YP19		115,000	77,700	30.1	7	-178	
YP20		116,400	78,300	29.9	6.99	-274	
YP21		118,500	79,900	29.5	7	-269	
YP22	NA	105,700	70,700	26.5	7.15	-300	
N Pond		51,700	32,500	34.8	8.15	-103	
NE Pond		36,400	22,300	35.8	9.09	-102	
NW Pond		52,800	34,000	34.7	8.79	-95	
SW Pond							Dry
SE Pond							Dry
Laguna M.		63,200	40,500	33.2	8.99		
Gulf		46,600	29,500	31.5	8.55		

Appendix D July 27, 2005 Field Parameters							
Well ID	Depth to Water from TOC (m)	Specific Conductance (µS/cm)	TDS (PPM)	Temp C	pH	Orp	Comments
BIB01	1.243	153,000	108,000	29.3	6.16		
BIB02	1.191	155,000	106,000	31.6	6.18		
BIB03							Dry
BIB04		159,000	110,000	32.6	5.9		
BIB05		158,000	109,000	31.9	5.67		
BIB06							Clogged
BIB07							Clogged
BIB08	1.248	158,000	107,000	29.9	5.69		
BIB09	1.194	160,000	110,000	32.4	6.09		
BIB10							Dry
BIB11		146,000	99,000	30.4	5.73		
BIB12		161,000	112,000	30.5	5.72		
BIB13		165,000	114,000	31.4	5.89		
BIB14		167,000	114,000	32.4	6.05		
BIB15	1.211	149,000	102,000	29.5	5.82		
BIB16	1.205	149,000	102,000	31.5	6.08		
BIB17							Dry
BIB18		153,000	105,000	30.4	5.54		
BIB19		156,000	107,000	30.5	5.42		
BIB20		157,000	108,000	31.2	5.56		
BIB21		151,000	102,000	31.6	5.9		
BIB22	1.181	154,000	106,000	30.2	6.11		
Laguna M.		58,000	36,500	31.1	7.16		
YP01	1.001	77,060	50,060	30.3	7		
YP02	0.880	113,700	76,240	31.5	7.13		
YP03	0.947	120,500	81,200	31.3	7.12		
YP04	0.901	126,400	85,400	31.3	7.38		
YP05	0.832	93,400	61,400	30.7	7.15		
YP06		90,700	59,500	30.9	7.1		
YP07		99,000	65,100	30.5	7.1		
YP08		70,500	45,400	29.9	7.07		
YP09		70,600	45,500	29.2	7.02		
YP10	0.820	88,400	58,000	28.6	7.03		
YP11	0.965	109,800	73,400	31.3	7.07		
YP12							
YP13		98,300	65,000	31.4	7.07		
YP14		135,000	92,000	31.6	6.85		
YP15							
YP16	0.880	60,000	38,300	30.3	7.3		
YP17	0.882	124,000	84,000	30.4	7.04		
YP18		83,300	54,400	30.9	6.8		
YP19		121,500	82,900	30.6	6.84		
YP20		141,000	96,000	29.8	6.9		
YP21		113,000	76,000	29.4	6.9		
YP22	0.854	111,000	74,300	29.3	6.93		
N Pond		76,000	49,000	34.5	8.26		
NE Pond		79,000	51,000	32.0	8.62		
NW Pond		77,000	50,000	31.1	8.45		
SW Pond							Dry
SE Pond							Dry
Laguna M.		73,000	47,000	31.6	8.8		
Gulf		49,000	31,000	30.3	8.33		

Appendix D August 16, 2005 Field Parameters							
Well ID	Depth to Water from TOC (m)	Specific Conductance (µS/cm)	TDS (PPM)	Temp C	pH	Orp	Comments
BIB01	1.289	135,000	91,000	34.2	6.05		
BIB02	1.244	135,000	94,000	34.7	6.09		
BIB03							Dry
BIB04		145,000	100,000	35.7	6.3		
BIB05		147,000	103,000	35.1	5.9		
BIB06							Clogged
BIB07							Clogged
BIB08	1.295	146,000	101,000	32.2	5.76		
BIB09	1.243	144,000	98,000	35.8	5.85		
BIB10							Dry
BIB11		131,000	93,000	34.3	5.45		
BIB12		148,000	102,000	34.4	5.42		
BIB13		150,000	106,000	35.6	5.56		
BIB14		150,000	105,000	36.2	5.51		
BIB15	1.260	137,000	92,000	33.5	5.31		
BIB16	1.242	127,000	86,000	37.1	5.58		
BIB17							Dry
BIB18		134,000	93,000	34.5	5.1		
BIB19		140,000	95,000	34.7	5.16		
BIB20		135,000	93,000	36.1	5.35		
BIB21		128,000	88,000	36.5	5.38		
BIB22	1.233	137,000	94,000	34.2	5.12		
Laguna M.		56,000	36,000	37.9	8.12		
YP01	1.300	74,000	48,000	33.2	6.75		
YP02	1.125	109,000	74,000	33.2	6.87		
YP03	1.138	118,000	80,000	32.7	7.2		
YP04	1.115	124,000	84,000	32.4	7.09		
YP05	1.104	91,000	60,000	32.1	6.89		H2S gas smell
YP06		102,000	68,000	33.0	6.73		H2S gas smell
YP07		98,000	65,000	32.3	6.67		H2S gas smell
YP08		98,000	65,000	31.5	6.82		H2S gas smell
YP09		62,000	39,000	31.2	6.86		H2S gas smell
YP10	1.144	88,000	57,000	30.9	6.82		H2S gas smell
YP11	1.136	103,000	69,000	33.1	6.92		
YP12							Dry
YP13		119,000	80,000	33.3	6.78		
YP14		124,000	84,000	33.4	6.65		
YP15							Clogged
YP16	1.155	59,000	38,000	31.4	7.05		H2S gas smell
YP17	1.136	120,000	82,000	32.7	6.96		
YP18		96,000	63,000	32.9	6.71		
YP19		125,000	84,000	31.8	6.68		
YP20		139,000	95,000	31.2	6.73		
YP21		139,000	95,000	30.9	6.69		
YP22	1.164	114,000	76,000	30.3	6.73		
N Pond		104,000	70,000	36.1	7.91	-162	
NE Pond		98,000	64,000	35.5	8.17	-102	
NW Pond		111,000	74,000	37.0	8.04	-122	
SW Pond							Dry
SE Pond							Dry
Laguna M.		61,000	39,000	37.0	8.47	-97	
Gulf		52,000	34,000	34.4	8.15		

Appendix D September 14, 2005 Field Parameters							
Well ID	Depth to Water from TOC (m)	Specific Conductance (µS/cm)	TDS (PPM)	Temp C	pH	Orp	Comments
BIB01	0.503	127,000	88,000	36.5	6.6		Site flooded with 25-30 cm of ponded rain water
BIB02	0.445	154,000	98,000	34.0	6.3		
BIB03		150,000	102,000	34.0	6.1		
BIB04		146,000	100,000	36.0	6.1		
BIB05		145,000	100,000	36.5	5.9		
BIB06							Clogged
BIB07							Clogged
BIB08	0.516	140,000	96,000	35.0	5.2		
BIB09	0.448	156,000	102,000	34.8	6		
BIB10		71,000	46,000	36.3	6.5		
BIB11		134,000	99,000	36.0	6.3		
BIB12		147,000	101,000	36.3	6.09		
BIB13		147,000	102,000	37.4	6.05		
BIB14		146,000	102,000	36.6	6.1		
BIB15	NA	135,000	92,000	35.9	6.02		
BIB16	0.420	132,000	91,000	35.3	6.35		
BIB17		95,000	63,000	36.5	6.5		
BIB18		138,000	94,000	35.8	6.1		H2S gas smell
BIB19		133,000	91,000	36.4	6.3		
BIB20		132,000	91,000	37.0	6.4		
BIB21		130,000	89,000	35.9	6.35		
BIB22	0.466	141,000	98,000	35.2	5.8		
Laguna M.		53,000	34,000	37.5	8.7		
Ponded Water		1,400	700	38.4	9.16		
YP01	0.709	98,000	65,000	29.3	6.69		Site flooded with 5 cm of ponded rain water
YP02	0.526	120,000	81,000	30.6	6.9		
YP03	0.541	124,000	84,000	30.7	7		
YP04	0.517	126,000	85,000	30.4	6.9		
YP05	0.499	101,000	67,000	30.2	6.9		
YP06		101,000	67,000	31.0	6.7		
YP07		106,000	71,000	31.1	6.77		
YP08		105,000	70,000	30.7	6.78		
YP09		75,000	49,000	30.5	6.8		
YP10	0.554	89,000	59,000	29.9	6.7		
YP11	0.540	116,000	78,000	30.3	6.95		
YP12		114,000	77,000	30.2	7		
YP13		128,000	87,000	30.8	6.73		
YP14		147,000	101,000	31.0	6.54		
YP15		132,000	89,000	31.2	6.85		
YP16	0.543	74,000	48,000	30.6	6.76		
YP17	0.492	125,000	85,000	30.4	7		
YP18		105,000	70,000	31.1	6.8		
YP19		120,000	80,000	31.1	6.6		
YP20		135,000	92,000	31.0	6.94		
YP21		134,000	92,000	31.3	6.6		
YP22	0.575	129,000	88,000	30.6	6.6		
N Pond		42,000	26,000	31.4	7.9		
NE Pond		42,000	26,000	32.7	8		
NW Pond		42,000	26,000	32.0	8		
SW Pond		6,000	3,000	33.0	7.9		
SE Pond		12,000	7,000	32.7	7.9		
Laguna M.		59,000	38,000	27.7	6.84		
Gulf		48,000	30,000	33.0	7.66		
Ponded Water		23,000	14,000	32.3	7.9		

References

Allison, G. B. and Barnes, C. J. 1985. Estimation of evaporation from the normally "dry" Lake Frome in South Australia. Journal of Hydrology. vol 78. p 229-242

Amdurer, M. 1978. Geochemistry, hydrology, and mineralogy of the Laguna Madre Flats, South Texas. Masters Thesis. The University of Texas at Austin. 172 p.

Amdurer, M. and Land, L. S. 1982. Geochemistry, hydrology, and mineralogy of the Sand Bulge area, Laguna Madre Flats, South Texas. Journal of Sedimentary Petrology. vol 52. no 3. p 703-716.

Baker, E. T., 1979, Stratigraphic and hydrogeologic framework of part of the Coastal Plain of Texas, Texas Water Development Board, no. 236, 43 p.

Bear, J. 1988. Dynamics of fluids in porous media. New York: McGraw Hill.

Bejan, A. 1984. Convective heat transfer in porous media. New York: John Wiley.

Berkebile, C. A. and Hay, R. 1995. Phase I groundwater resource investigation at the Padre Island National Seashore – Final report. Texas A&M University – Corpus Christi. Center for Water Supply Studies. report no. TAMU-CC-CWSS-9502. 177 p.

Berkebile, C. A., Hay, R., and Martinez, R. 2001. Phase II groundwater resource investigation at the Padre Island National Seashore – Draft final report. Texas A&M University – Corpus Christi. Center for Water Supply Studies. unpublished report no. TAMU-CC-CWSS-0101. 25 p.

Bowler, J. M. 1986. Spatial variability and hydrologic evolution of Australian lake basins: Analogue for Pleistocene hydrologic change and evaporite formation. Palaeogeography, Palaeoclimatology, Palaeoecology. vol 54. p 21-41.

Boylan, D. M. 1986. The hydrogeologic resources of North Padre Island; Coastal South Texas. Masters Thesis. Baylor University. 143 p.

Carr, J. E., Meyer, W. R., Sandeen, W. M., and McLane, I. R. 1985. Digital models for simulation of ground-water hydrology of the Chicot and Evangeline Aquifers along the Gulf Coast of Texas. Texas Water Development Board. no 289, 100 p.

Cheng, P. 1978. Heat transfer in geothermal systems. In: Advances in Heat Transfer. vol 14. p 1-105.

Combarnous, M. A. and Borries, S. A. 1975. Hydrothermal convection in saturated porous media. Advances in Hydroscience. vol 10. p 231-307.

Cooper, C. A., Glass, R. J., and Tyler, S. W. 1997. Experimental investigation of the stability boundary for double-diffusive finger convection in a Hele-Shaw cell. Water Resources Research. vol 33. no 4. p 517-526.

Cooper, C. A., Glass, R. J., and Tyler, S. W. 2001. Effect of buoyancy ratio on the development of double-diffusive finger convection in a Hele-Shaw cell. Water Resources Research. vol 37. no 9. p 2323-2332.

Davis, R. A., Jr. 1978. Beach sedimentology of Mustang and Padre Islands: A time-series approach. Journal of Geology. vol 86. p 35-46.

Delvin, J. F. 2003. A spreadsheet method of estimating best-fit hydraulic gradients using head data from multiple wells. Ground Water. vol 41. no 3. p 316-320.

Diersch, H.-J.G. and Kolditz, O. 2002. Variable-density flow and transport in porous media: approaches and challenges. Advances in Water Resources. vol 25. p 899-944.

Duffy, C. J. and Al-Hassan, S. 1988. Groundwater circulation in a closed desert basin: Topographic scaling and climatic forcing. Water Resources Research. vol 24. no 10. p 1675-1688.

Elder, J. W. 1967a. Steady free convection in a porous medium heated from below. Journal of Fluid Mechanics. vol 27. part 1. p 29-48.

Elder, J. W. 1967b. Transient convection in a porous medium. Journal of Fluid Mechanics. vol 27. part 3. p 608-623.

Fan, Y., Duffy, C. J., and Oliver, D. S. Jr. 1997. Density-driven groundwater flow in closed desert basins: field investigations and numerical experiments. Journal of Hydrology. vol 196. p 139-184.

Fenstemaker, T., Halihan, T., and Sharp, J. M., Jr. 2001. Using resistivity to detect movements of variable salinity fluids in the barrier island sediments of Padre Island, Texas. Geological Society of America Abstracts with Programs. vol 33. no 6. p A-46.

Fisk, H. N. 1959. Padre Island and Laguna Madre mud flats, south coastal Texas. Second Coastal Geography Conference Proceedings. Baton Rouge, Louisiana. p 103-151.

Frolkovic, P. and Schepper, H. D. 2001. Numerical modeling of convection dominated transport coupled with density driven flow in porous media. Advances in Water Resources. vol 24. p 63-72.

Gebhart, B., Jaluria, Y., Mahajan, R. L., and Sammakia, B. 1988. Buoyancy-induced flows and transport. New York. 971 p.

Hassanizadeh, S. M. and Leijnse, A. 1995. A non-linear theory of high-concentration-gradient dispersion in porous media. Advances in Water Resources. vol 4. p 203-215.

Holzbecher, E. 1998. Modeling density-driven flow in porous media. Berlin: Springer.

Horton, C. W. and Rogers, F. T. 1945. Convective currents in porous medium. Journal of Applied Physics. vol 16. p 367-370.

Land, L. S. 1991. Evidence for vertical movement of fluids, Gulf Coast sedimentary basin. Geophysical Research Letters. vol 18. no 5. p 919-922.

Lapwood, E. R. 1948. Convection in a fluid in a porous medium. Proc. Cambridge Phil. Soc. vol 44. p 508-521.

Leblanc, R. J. and Hodgson, W. D. 1959. Origin and development of the Texas Shoreline. Gulf Coast Assoc of Geological Societies Trans. vol 9, p 197-220.

Leising, J. F., Tyler, S. W., and Miller, W. W. 1995. Convection of saline brines in enclosed lacustrine basins: A mechanism for potassium metosomatism. GSA Bulletin. vol 107. no 10. p 1157-1163.

Long, D. T. and Gudramovics, R. 1983. Major-element geochemistry of brines from the wind tidal flat area, Laguna Madre, Texas. Journal of Sedimentary Petrology. vol 53. no 3. p 797-810.

Lusczynski, R. J. 1961. Head and flow of groundwater of variable density. Journal of Geophysical Research. vol 66. no 12. p 4247-4256.

Narayan, K. A. and Simmons, C. T. 1998. Density induced flow and solute transport below a saline lake bed. In: International Contributions to Hydrogeology. vol 18. p 221-232.

Nield, D. A. 1968. Onset of thermohaline convection in a porous medium. Water Resources Research. vol 1. p 553-560.

Nield, D. A. 1990. The stability of convective flows in porous media. In: Convective heat and mass transfer in porous media. Dordrecht: Kluwer Publishers. p 79-122.

Nield, D. A. and Bejan, A., 1999, Convection in porous media, 2nd ed, Springer, New York, 546 p.

Oltean, C., Ackerer, P., and Bues, M. 1994. Solute transport in 3D laboratory model through a homogeneous porous medium: behavior of dense phase and simulation.

Computational Methods in Water Resources X. Kluwer Academic: Dordrecht. p 521-528.

Oostrom, M., Hayworth, J. S., Dane, J. H., and Güven, O. 1992a. Behavior of dense aqueous phase leachate plumes in homogenous porous media. Water Resources Research. vol 28. no 8. 2123-2134.

Oostrom, M., Dane, J. H., Güven, O., and Hayworth, J. S. 1992b. Experimental investigation of dense solute plumes in an unconfined aquifer model. Water Resources Research. vol 28. no 9. 2315-2326.

Oswald, S. E. and Kinzelbach, W. 2004. Three-dimensional physical benchmark experiments to test variable-density flow models. Journal of Hydrology. vol 290. p 22-42.

Paine, J. G. 1991. Late quaternary depositional units, sea level, and vertical movement along the central Texas coast. PhD Dissertation. University of Texas at Austin. 256 p.

Panda, M. N. and Lake, L. W. 1994. Estimation of single-phase permeability from parameters of particle-size distributions. American Association of Petroleum Geolgists Bulletin. vol 78. p 1028-1039

Pearl, Z., Magaritz, M., and Bendel, P. 1993. Nuclear magnetic resonance imaging of miscible fingering in porous media. Transport in Porous Media. vol 12. p 107-123.

Prasad, A. and Simmons, C. T. 2003. Unstable density-driven flow in heterogeneous porous media: A stochastic study of the Elder [1967b] "short heater" problem. Water Resources Research. vol 39. no 1. p 1007.

Rayleigh, L. 1916. On convection currents in a horizontal layer of fluid when the higher temperature is on the underside. Philosophical Magazine. series 6. vol 32. p 527-546.

Schincariol, R. A. and Schwartz, F. W. 1990. An experimental investigation of variable density flow and mixing in homogeneous and heterogeneous media. Water Resources Research. vol 26. no 10. p 2317-2329.

Schneider, K. J. 1963. Investigation of the influence of free thermal convection on heat transfer through granular material. In: Proc 11th International Congress of Refrigeration. Oxford: Pergamon Press. 11-4. 247-253.

Sellards, E. H., Adkins, W. S., and Plummer, F. B. 1933. The Geology of Texas; Stratigraphy. University of Texas Bureau of Economic Geology. no 3232. 1007 p.

Shafer, G. H. 1968. Groundwater resources of Nueces and San Patricio Counties, Texas. Texas Water Development Board. no 73. 129 p.

Shafer, G. H. and Baker, E. T. 1973. Groundwater resources of Kelberg, Kenedy, and southern Jim Wells Counties, Texas. Texas Water Development Board. no 173. 162 p.

Sharp, J. M., Jr., Fenstemaker, T. R., Simmons, C. T., McKenna, T. E., Dickinson, J. 2001. Potential salinity-driven free convection in a shale-rich sedimentary basin: Example from the Gulf of Mexico basin in south Texas. AAPG Bulletin. vol 85. no 12. p 2089-2110.

Shi M. 2005. Characterizing heterogeneity in low-permeability strata and its control on fluid flow and solute transport by thermalhaline free convection. PhD Dissertation. The University of Texas at Austin. 229 p.

Simmons, C. T. and Narayan, K. A. 1997. Mixed convection processes below a saline disposal basin. Journal of Hydrology. vol 194. p 263-285.

Simmons, C. T., Narayan, K. A., Wooding, R. A. 1999. On a test case for density-dependent groundwater flow and solute transport models: The salt lake problem. Water Resources Research. vol 35. no 12. p 3607-3620.

Simmons, C. T., Fenstemaker, T. R., and Sharp, J. M., Jr. 2001. Variable-density groundwater flow and solute transport in heterogeneous porous media: approaches, resolutions and future challenges. Journal of Contaminant Hydrology. vol 52. p 245-275.

Stewart, M. and Bretnall, R. E. Jr. 1986. Interpretation of VLF resistivity data for ground-water contamination studies. Ground Water Monitoring Review vol 6. no 1, p 71-75.

Tien, C. L. and Vafai, K. 1990. Convective and radiative heat transfer in porous media. Advances in Applied Mechanics. vol 27. p 225-281.

Tyler, S. W., Kranz, S., Parlange, M. B., Albertson, J., Katul, G. G, Cochran, G. F., Lyles, B. A., Holder, G. 1997. Estimation of groundwater evaporation and salt flux from Owens Lake, California, USA. Journal of Hydrology. vol 200. p 110-135.

The University of Texas at Austin Hydrogeology Field Methods Class. 1997. A hydrogeologic investigation of a transect across North Padre Island, Padre Island National Seashore, Kleberg County, Texas. Report to Padre Island National Seashore. 18 p. + appendices.

The University of Texas at Austin Hydrogeology Field Methods Class. 2001. Hydrogeologic characterization of Padre Island National Seashore 28 km south of

Corpus Christi, Texas. Report to Padre Island National Seashore. 41 p. + appendices.

The University of Texas at Austin Hydrogeology Field Methods Class. 2003. A hydrogeologic transect of North Padre Island: Laguna Madre to the Gulf of Mexico along old Bird Island Basin road, Kleberg County, Texas, USA. Report to Padre Island National Seashore. 16 p. + appendices.

The University of Texas at Austin Hydrogeology Field Methods Class. 2005. Hydrogeologic Characterization of Padre Island National Seashore near Corpus Christi, Texas. Report to Padre Island National Seashore. 47 p. + appendices.

Wiese, B. R. and White, W. A., 1980, Padre Island National Seashore: A guide to the geology, natural environments, and history of a Texas barrier island, The University of Texas Bureau of Economic Geology, Guidebook 17, 94 p.

Wood, W. W. 2002. Role of ground water in geomorphology, geology, and paleoclimate of the Southern High Plains, USA. Ground Water, vol 40. no 4. p 438-447.

Wood, M., Simmons, C. T., Hutson, J. L. 2004. A breakthrough curve analysis of unstable density-driven flow and transport in homogeneous porous media. Water Resources Research. vol 40. W03505.

Wooding, R. A. 1957. Steady state free thermal convection of liquid in a saturated permeable medium. Journal of Fluid Mechanics. vol 2. p 273-285.

Wooding, R. A., Tyler, S. W., and White, I. 1997a. Convection in groundwater below an evaporating salt lake: Onset of instability. Water Resources Research. vol 33. no 6. p 1199-1217.

Wooding, R. A., Tyler, S. W., White, I., and Anderson, P. A. 1997b. Convection in groundwater below an evaporating salt lake: Evolution of fingers or plumes. Water Resources Research. vol 33. no 6. p 1219-1228.

This document does not include the vita page from the original.